A Conceptual Framework Describing Mercury Bioavailability to Microbes Through Redox Zones

Benjamin Stenzler

A thesis submitted to the University of Ottawa
in partial fulfillment of the requirements for the
Doctorate in Philosophy Biology
Specialization in Chemical and Environmental Toxicology

Department of Biology
Faculty of Science
University of Ottawa

Abstract

Mercury (Hg) is a global pollutant and potent neurotoxin that is detrimental to the environment and human health. (MeHg). All forms of Hg are toxic, but methylmercury (MeHg) can biomagnify through food webs and become concentrated in food staples such as fish and rice, creating an exposure risk to people. The conversion of Hg to MeHg is mediated by anaerobic microbes, particularly sulfate and iron-reducing bacteria and methanogenic archaea. However, Hg methylation is an intracellular process, and MeHg production is dependent on the bioavailability of inorganic Hg to these microbes. One outstanding knowledge gap in understanding Hg methylation is the nature of bioavailability of inorganic divalent Hg (Hg^{II}). Much research has gone into developing a framework describing how microbes take up Hg for methylation. Still, the framework describing Hg bioavailability processes is not fully developed. The overall objective of my thesis is to address these mechanisms governing Hg^{II} bioavailability to anaerobic microbes.

Hg^{II} bioavailability is determined by its speciation; these are all the different forms and compounds of Hg^{II}. To address the bioavailability of various Hg^{II} species, I used microbial Hg-biosensors. Hg-biosensors are bacterial cells that emit a quantifiable signal when Hg^{II} enters them and let me observe Hg^{II} bioavailability in real-time. The biosensors I developed are the first Hg-biosensors that function without oxygen and let me explore Hg^{II} species and their bioavailability under conditions conducive to methylation. Hg^{II} speciation is spatially and temporally dynamic moving from oxic to anoxic conditions and under various biogeochemical controls. I follow Hg^{II} speciation and bioavailability in my thesis as it transgresses through these conditions. Understanding Hg^{II} bioavailability to complex microbial communities across redox gradients and through dynamic ligand interactions is a missing key component to understanding and predicting MeHg formation.

My results show how altering Hg^{II} speciation can identify novel bioavailability pathways or make it completely inaccessible. My results highlight how microbes can control Hg^{II} bioavailability and the importance of microbial community structure on metal acquisition. First, I resolve pathways for charged inorganic Hg^{II} species through the cell membrane and demonstrate novel pathways for previously unconsidered charged species. Using dissolved organic matter (DOM) originating from various algal species, I show how algae can uniquely control Hg^{II} bioavailability to other organisms. I demonstrate how DOM has emergent properties that can control Hg^{II} bioavailability. Next, I investigated the compounds microbes use to scavenge metals such as iron and copper. I reveal how they could inadvertently interact with Hg^{II} and form new bioavailability pathways. Lastly, I demonstrate how the diffusion of biogenic hydrogen sulfide from an isolated system can make an otherwise non-bioavailable Hg^{II} species rapidly available for microbial uptake. Overall, my thesis expands the framework describing Hg^{II} bioavailability to microbes and potential drivers of Hg methylation in the environment.

Acknowledgments

The first person I would like to acknowledge is my thesis advisor Dr. Alexandre Poulain. You are the best supervisor I could have asked for. I appreciate how you constantly challenged me, pushed me to be a better scientist, and always made time to provide insight and guide my research. Not only are you the best advisor, but you constantly strive to improve the quality of learning of every other student at the university, and I admire that. Thank you for giving me this opportunity.

I would like to thank my committee members and thesis examiners, Dr. Danielle Fortin, Dr. John Chételat, Erik Björn, Laurie Chan, Frances Pick, and Dr. Anh Pham. My research collaborators, Dr. Aaron Hinz, Dr. Vaugn Mangal, Dr. Matti Ruuskanen, Dr. Jeremy Semrau, and Dr. Alan DiSpirito. You allowed me to broaden my research and explore new avenues. I appreciate your feedback and insights.

Thank you to the members of the Poulain lab. Dan, Mija, Martin, Galen, Noemie, Emmanuel, Jess, Rui, and Michelle. Also, and of course, Linda and Dave from the lab lobby. Thank you for listening to my research talks, giving feedback, and making work fun. At first, performing science was just watching test tubes getting gradually cloudier over the course of a day or transferring optically clear fluids into other optically clear fluids to create a matrix of optically clear fluids with something determined mathematically to be in there. Beyond all possible odds, you guys made that an incredibly fun experience and made me excited to come to work each day.

I had the privilege of mentoring the most amazing students. Jessica Gaudet and Rui Zhang, mentoring you two was an amazing experience. You helped guide my thesis, and you both taught me more than I ever could have taught you. I'm proud of all your hard work as scientists and that you are both pursuing your own research interests.

Lastly, I would like to thank my family for their constant support and immutable feedback. Doubtful whether any of it ever veered into the realm of scientific thought, it still remained invaluable and helped me see the bigger picture. Thanks to my mom and dad. Your consistent and seemingly endless support through feeding me marginally palatable food and showing me the apparent effort required to accomplish otherwise seemingly trivial tasks taught me valuable lessons in perspective, expectations, and how to meet people halfway. With hard work and determination taken with an open mind, you will eventually see the superfluous nature of all the little details and just appreciate things. And my brother, Jordan. I am well aware of your interest in science and demystifying the underlying principles governing time, space, and the universe. Accordingly, I don't expect you to read more than the abstract of my thesis. However, in the odd chance there is some inconceivable yet improbable circumstance that would possess you to read this far. For one, I am genuinely concerned that hell just froze over. But also, you're the best brother I could have asked for, and I couldn't have done this without you.

Table of Contents

List of Figures

List of Tables

Abbreviations

[x]	Concentration of compound x
Element(II)	A species of an element with an oxidation state of 2
Element(III)	A species of an element with an oxidation state of 3
AF4	Asymmetrical flow field-flow fractionation
AIC	Akaike information criterion
AMDE	atmospheric mercury depletion events
As	Arsenic
BAL	Dimercaptopropanol
BBM	Bold basal media
Cd	Cadmium
COOH	Carboxylic
Cys	L-cysteine
DDTC	Diethyldithiocarbamate
DFOB	Desferrioxamine B from *Streptomyces pilosus*
DFT	Desferrithiocin
DMSA	Meso-2,3-DimercaptoSuccinic Acid
DOM	Dissolved organic matter
DOC	Dissolved organic carbon
Ent	*Enterobactin from Escherichia coli*
EPS	exopolysaccharides
Fe	Iron
Fe^{II}	Ferrous iron
Fe^{III}	Ferric iron
FbFp	Flavin-based fluorescent protein
FeS	Iron Sulfide
FT ICR MS	Fourier transform ion cyclotron mass spectrometry
GSH	Glutathione
Hg	Mercury
Hg^{II}	divalent Hg species
Hg(II)	divalent Hg species
Hg^0	Elemental Hg
β-HgS	Metacinnabar
$HgS_{(s)}$	Cinnabar
$Hg(SR)_2$	Two thiol coordinated complexes
HSM	High salt media
H_2S	Hydrogen Sulfide
IHSS	International Humic Substances Society
IPCC	International Panel on Climate Change
LB	Lysogeny broth
LMW	Low molecular weight
MB	Methanobactin
MB-OB3b	Methanobactin from *M trichosporium* OB3b
MeHg	Methylmercury
Mn	Manganese

MW	Molecular weight
NA	Nicotianamine
NO_3^-	Nitrate
NMDS	Nonmetric multidimensional scaling
OD_{600}	Optical Density at 600nm
PCA	Principal component analyses
Pen	L-Penicillamine
Pvd	Pyoverdine from *Pseudomonas* sp
SO_4^{2-}	Sulfate
SRFA	Suwannee River Fluvic Acid
TEA	TEA
YFP	yellow fluorescent protein
Zn	Zinc

Chapter 1: Introduction

1.1 Background on Mercury

Mercury (Hg) is a global pollutant and potent neurotoxin that is of concern to natural water resources and human health. The World Health Organization lists Mercury (Hg) as one of the ten leading chemicals of concern (*1*). Hg is unique because it is the only metal that is a liquid at room temperature (25 °C) and can easily evade in its elemental form (Hg^0). Hg^0 is emitted by natural sources (e.g., forest fires, volcanoes, hydrothermal vents) and anthropogenic sources (e.g., artisanal gold mining, fossil fuels (particularly coal-fired power plants), chlorine alkali processing, metal refining, cement production, and waste incineration) (*2*).

Hg^0 has an atmospheric residence time from about six months to a year allowing it to be transported long distances, making it a global pollutant (*3*). Eventually, Hg^0 is oxidized to divalent Hg^{II} that forms water-soluble complexes and can sorb onto particulates and enter aquatic ecosystems through both dry and wet deposition (*4-6*). Once in an ecosystem, Hg^{II} has several fates. It can be reduced back to Hg^0 and emitted back into the atmosphere, sequestered in sediments, or converted to methyl mercury (MeHg), where it becomes an environmental and human health concern (*4-6*).

There are many forms of Hg (e.g., Hg^0, Hg^{2+}, $HgCl_2$, MeHg, etc.), but all are toxic. However, MeHg is of particular concern because it can bioaccumulate and biomagnify through food webs. Hg concentrations in water and air are generally too low to exhibit toxic effects, but Hg in the food web can be orders of magnitude higher than in the environment (*7*). This is highly problematic in food staples such as fish (*8*) and rice (*9*) which can have elevated Hg concentrations of organic Hg (i.e. MeHg). Unlike other forms of Hg, MeHg is readily absorbed

from the GI tract into the body (*10*) and can cause toxic responses, ranging from neurodegenerative (*11*), metabolic (*12*), renal (*13*), to cardiovascular (*14*). MeHg is problematic, that when bound to l-cysteine, mimics the amino acid l-methionine making it a substrate that can cross the blood-brain barrier making it a potent neurotoxin (*15*). Therefore, it is essential to understand what is driving Hg methylation in the environment.

Conversion of Hg to MeHg is primarily mediated by chemotrophic, anaerobic microbes; particularly sulfate and iron-reducing bacteria, and methanogenic archaea (*16*). Hg methylation may also occur abiotically, but abiotic methylation requires environmentally unrealistic conditions and is unlikely to contribute significantly to MeHg in the environment (*17*). Microbes involved in methylation contain the two-gene cluster, *hgcA*, and *hgcB* which encodes a putative corrinoid protein and a ferredoxin (*18*). The presence of this gene cluster and microbes' ability to methylate Hg do not appear to be a detoxification strategy but instead the by-product of one-carbon metabolism and metal homeostasis (*19*). Identifying this gene cluster makes it an ideal tool for identifying Hg methylating microbes and their habitats (*20, 21*). As of writing my thesis, it is unclear why only anaerobic microbes contain the *hgcA* and *hgcB* gene cluster but has contributed to the paradigm that microbial Hg methylation requires the environment to be anoxic.

Anoxic environments conducive to Hg methylation are widespread. Whereas oxygen concentration declines deeper in the water column and sediments, providing ideal habitats for Hg methylation (*22*), micro-anoxic environments are ubiquitous, allowing Hg methylation to occur in biofilms or microbial mats (*23, 24*) and suspended particulate organic matter (*25-27*). More recently, novel sites have been discovered, such as polar snow (*28*), antarctic sea ice (*29*), or in the open ocean water column (*30-32*).

While the *hgcA* and *hgcB* genes and anaerobic conditions are essential to Hg methylation, they do not alone explain the methylation rates observed (*33, 34*). Bravo *et al*., (2020) refer to this as a "biophysicochemical conundrum," where biological, physical, and chemical factors are all driving Hg methylation (*34*) (Figure 1.1). These include Hg fluxes in a system, chemical controls like pH, temperature, redox potential, chemical transformations of Hg, and biological controls such as microbial community structure. Untangling these factors that drive Hg methylation remains a significant knowledge gap in the literature. However, an essential component in Hg methylation is the activity of methylation microbes, where Hg bioavailability is the first step in this process (*33-35*). Therefore, understanding how Hg enters a microbe to become MeHg is critical for determining its fate in the environment and its biomagnification through food webs. My thesis aims to expand the framework of mechanisms governing Hg^{II} bioavailability to anaerobic microbes. When Hg goes from the atmosphere to anoxic conditions where it is methylated, it undergoes various biogeochemical transformations. These affect the chemistry of Hg^{II}, ultimately determining whether microbes can access it. From aerobic, where it is deposited in the environment, to the anoxic conditions, where it is methylated. In my thesis, I develop and optimize tools that can assess Hg bioavailability under controlled environmental conditions that affect both its chemistry and bioavailability. Then I explore mechanisms regulating Hg bioavailability over various environmental redox conditions.

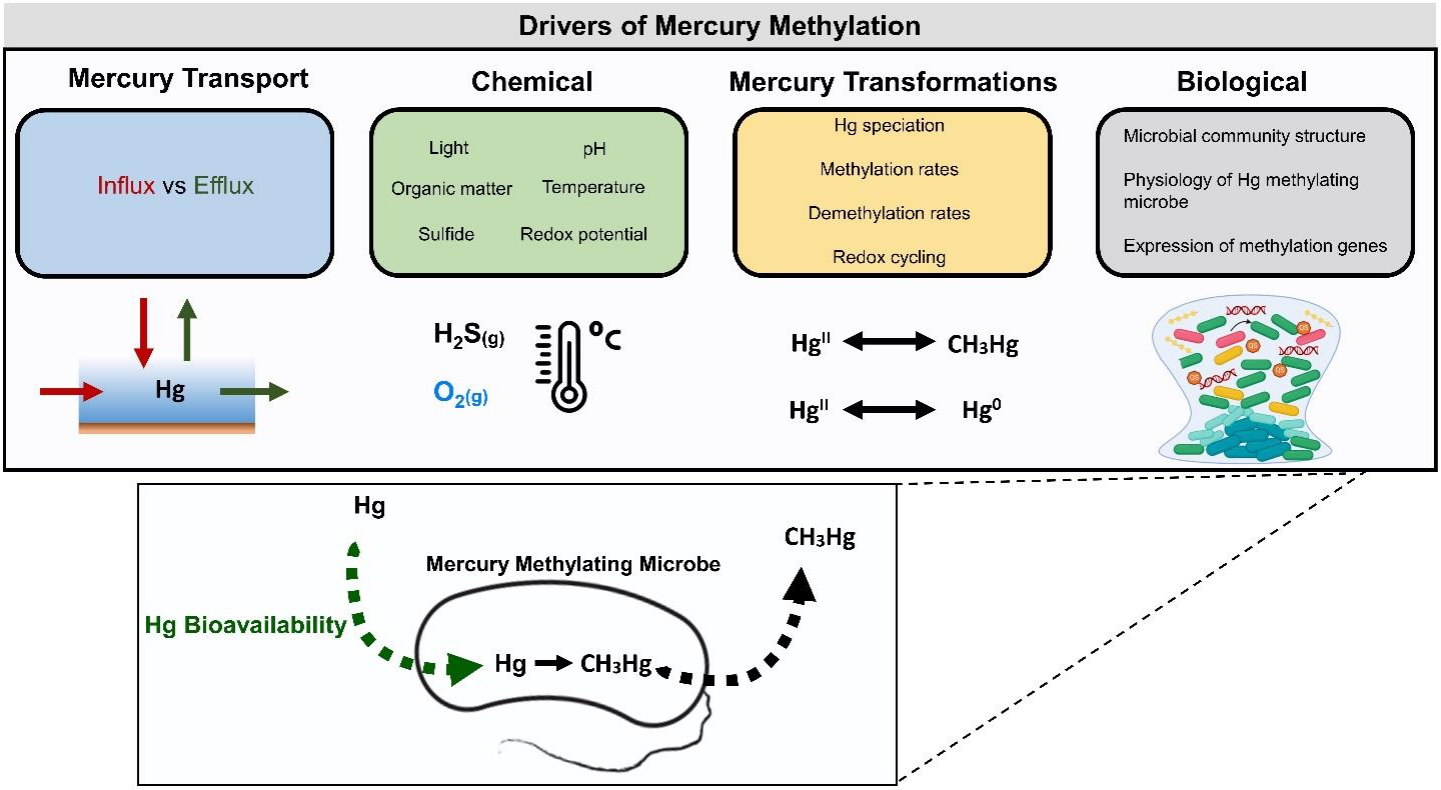

Figure 1.1. Drivers of Mercury methylation in the environment. Hg methylation in the environment is driven by Hg transport, chemical parameters, Hg transformations and biological controls. Hg methylation is facilitated by anaerobic, Hg methylating microbes where bioavailability is the first step. The variables listed are not exhaustive.

1.2 Hg Speciation through aquatic environments

Hg^{II} will never exist as a free ion under conditions that are physiologically relevant to microbes. Its high degree of covalency ensures it is always bound to different ligands. These Hg(II)-ligand complexes are generally referred to as Hg^{II} chemical species (*36*, *37*). Hg^{II} can form with many different ligands (e.g., $HgCl_2$, $Hg(OH)_2$, or $Hg(NH_3)_2^{2+}$), but Hg^{II} has the highest affinity for reduced sulfur-containing ligands like sulfide and thiols. It will typically be found as these species in the environment (e.g., $Hg(cysteine)_2$, $Hg(glutathione)_2$, HgS or $Hg(HS)_2$) (*23*, *38-43*). Hg speciation is dynamic and involves a series of ligand exchanges with ligands of subsequential higher affinities as it transgresses from the atmosphere to anoxic conditions where Hg methylation occurs. Here I discuss a general Hg^{II} speciation pathway through an aquatic system to its most stable form as cinnabar ($HgS_{(s)}$) (Figure 1.2). It is important to note that Hg^{II} has the

potential to be reduced back to Hg^0 at any point during this pathway that can reset the process (*5*, *44-46*).

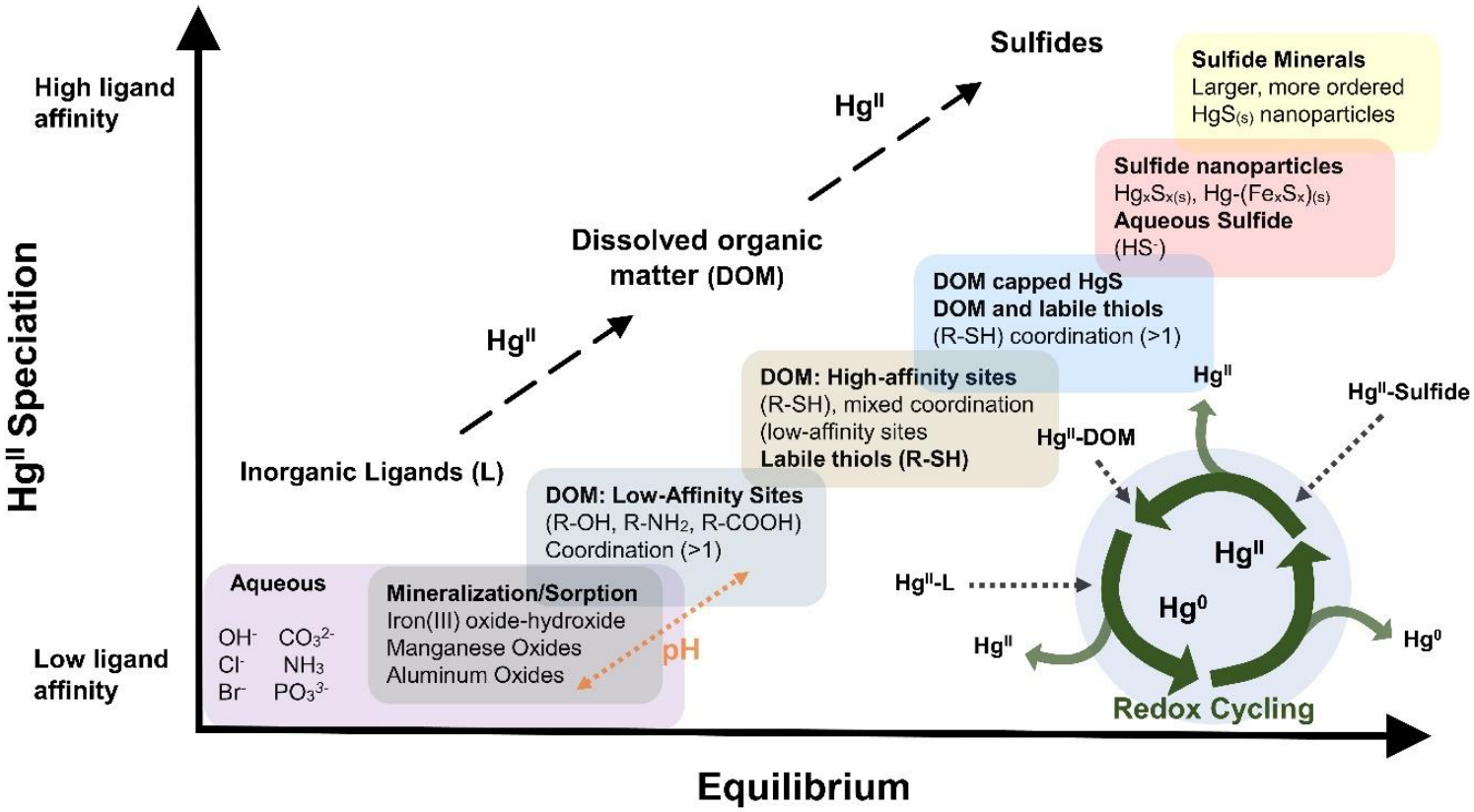

Figure 1.2: Conceptual model of Hg^{II} speciation as it tends towards equilibrium in an aquatic system. Hg^{II} will periodically exchange between ligands of higher and higher affinity, transitioning from inorganic ligands (L) to dissolved organic matter (DOM) and sulfide species. Hg^{II}-sulfide species initially form metastable aqueous species or dissolved nanoparticles. These highly insoluble nanoparticles precipitate, becoming more aggregated and ordered over time. These ligands are grouped in boxes representing ligands with relatively similar affinities for Hg^{II}. Coordination refers to the number of ligands binding to Hg^{II}. The boxes overlapping represents a continuum of ligand affinities. This conceptual model represents neutral pH; however, changes in pH can shift equilibrium Hg^{II} speciation with inorganic ligands and low-affinity sites on DOM. At any point, the equilibrium may be reset by the redox cycling of Hg.

Once Hg^0 is oxidized to Hg^{II} upon entering an aquatic system, the first ligands to control its speciation are inorganic ligands such as halides, especially in arctic and marine systems. Halides, bromine, in particular, have a prominent role in removing Hg from the atmosphere either during

polar springtime atmospheric mercury depletion events (AMDE) (*47*, *48*). While in marine waters, chloride can act as a catalyst for Hg^0 oxidation (*49*). Halides such as chlorides ions can achieve exceedingly high concentrations in environments that are conducive to Hg-methylation, such as polar snow (*28*), Antarctic sea ice (*29*), or in the open ocean water column (*30-32*). With low concentrations of organic ligands (I.e., DOM) and the absence of reduced sulfur moieties, Hg^{II} will form negatively charged Hg(II)-chlorocomplexes (e.g., $HgCl_3^-$, $HgCl_4^{2-}$) (*6*, *50-53*).

Over time ligand exchanges will occur between these halides with dissolved organic matter (DOM). This happens more readily in freshwater systems where Hg may be present as a neutral species (e.g., $HgCl_2$, $Hg(OH)_2$) (*50-52*). DOM is a naturally occurring ligand that is ubiquitous in all natural waters, sediments, and soils. DOM is a complex mixture of heterogeneous materials such carbohydrates, nucleic acids, proteins, lignin, fats, and many other metabolites. These derive from various autochthonous and allochthonous sources (e.g., algae, plants, microbes, decomposition of organic matter). DOM also exhibits many different interactions with Hg^{II} (*39*, *54*, *55*). There are many functional groups present on DOM that interact with Hg (e.g., hydroxyl, amino, carboxyl, and thiols). Hg^{II} may initially bind to low-affinity functional groups such as hydroxyl, amino, and carboxyl, preferring higher coordinations (>1). Over time, ligand exchange occurs so that Hg^{II} will be bound to thiols (*56-58*). Ligand exchanges further occur between single thiol coordination to more favorable coordination by multiple thiols where Hg^{II} is most stable (*39*, *54*, *55*, *57*).

Under reducing conditions where methylation occurs, inorganic sulfides will outcompete DOM and thiols for Hg^{II} and form Hg(II)-sulfide species (*59-61*). Sulfide comes from multiple sources. The most prominent being sulfur-reducing organisms (through dissimilatory SO_4^{2-} reduction pathways) (62-65) or the from mineralization of organic molecules (38, 66). Even in

the absence of H_2S, Hg^{II} bound to thiols on DOM can nucleate Hg(II)-sulfides through the alkylation of metallo-thiolates (*38*). These Hg(II)-sulfides initially form as various dissolved aqueous species or are bound to DOM. Over time, they will aggregate, become more ordered, and crystalline metacinnabar (β-HgS) (*38, 41, 42, 60, 67-74*). Small Hg(II)-sulfides (diameter ~ 4 nm - 200 nm) are a relatively stable endpoint for Hg^{II} (days to weeks) and can travel long distances typically associated with colloidal materials (*60, 61, 73-77*).

The formation of sulfide nanoparticles is not limited to Hg^{II} but occurs with many (non)-metals (notably ferrous iron (Fe^{II})). The prevalence of other sulfide minerals indirectly and significantly affects Hg^{II} speciation. In sediments and soils, (Iron) Fe is orders of magnitude more concentrated (Total [Fe] = 0 – 0.5 mmol/kg (*78*)) than Hg^{II} (Total [Hg] = 0.15 – 0.5 µmol/kg, but can be 2-4 orders of magnitude higher in contaminated soils (*45*)). Fe^{II} readily precipitates with sulfide to form Fe^{II}-sulphides (e.g., mackinawite (FeS)) (*79-83*). This process will either co-precipitate Hg^{II} into the mineral structure or readily sorb almost all the Hg^{II} present to the mineral surface (*79-83*).

The interplay between Fe and Hg in the environment involves coprecipitations, sorption, and redox reactions. Whereas Fe^{II}-sulfides readily sorb and sequester Hg^{II} under sulfidic conditions, under aerobic or more oxidizing conditions, Fe will be present as ferric iron (Fe^{III}). Fe^{III} precipitates as Fe^{III}-oxides; these have large surface areas and can sorb and sequester almost all the Hg^{II} in a system (*84-89*). Hg^{II} is not strictly bound to Fe^{III}-oxides as reductive dissolution of the mineral can liberate Hg^{II}. Reductive dissolution often uses sulfide as a reducing agent, ultimately forming Fe^{II}/Hg^{II}-sulfides (*85, 90-92*).

The interactions with Hg and minerals are not limited to Fe under oxic conditions but also occur with clay minerals, aluminum oxyhydroxides, manganese oxides, and silicates. Hg

will typically adsorb to these minerals on ≡XOH surface groups (where X = Mn, Al, and Si). While the association with these minerals represents a large compartment for the distribution of Hg in a system, the minerals themselves have a relatively weaker affinity for Hg than other environmental ligands (I.e., halides and DOM) (*89, 93*).

1.3 Hg Speciation and Bioavailability

Hg speciation is spatially and temporally dynamic throughout the environment and ultimately determines its bioavailability. The bioavailability of Hg to a microbe is the fraction available for active or passive transport across its cellular membrane. Much work has gone into understanding the mechanisms of Hg bioavailability (*35, 42*). Hg can cross the cell membrane by either active transport or passive diffusion, and the Hg species in part determine this. The current model of Hg bioavailability indicates passive diffusion of Hg(II)-sulfides and Hg^0 and active transport of Hg bound to thiols and other ligands (*35, 42*). Understanding how these Hg species are transported helps us understand the drivers of Hg methylation.

Active transport of Hg^{II} occurs via non-specific metal ion transporters on the inner membrane of a microbial cell (*94-97*). This transport happens through a ligand exchange between the ligand (e.g., thiol or halide) in solution and the transporter (*95, 98*). Ligand exchange does not always readily occur, and in many situations, Hg will not be bioavailable. For instance, high ligand concentrations sequester Hg^{II} and prevent ligand exchange and active transport (*96, 98-103*). Furthermore, some ligands bind Hg so strongly that they are incapable of ligand exchange, such as sorption sites on microbial membranes, some forms of dissolved organic matter, and multidentate low molecular weight thiols (*101, 104-112*).

One of the most notable active transport systems that confer microbial resistance to Hg in the environment is *mer*-based transport. The *mer* operon encodes for a transcription regulator (*MerR*), mercuric reductase (*MerA*), organomercury lyase (*MerB*), a periplasmic Hg^{II} scavenging protein (*MerP*), and a series of inner membrane-spanning transport proteins (MerT). This machinery allows the microbe to efficiently scavenge Hg^{II}, degrade MeHg to Hg^{II} and reduce Hg^{II} to Hg^{0} (*113*). The *mer* operon's transport machinery is incredibly efficient in transporting Hg and allows microbes to access Hg that would otherwise be completely inaccessible (*97*). While widespread, *mer* genes are absent from anaerobes; this transport system is not relevant for methylation (*113*).

Two groups of Hg species diffuse across a membrane passively, Hg^{0} and Hg(II)-sulfides. Hg^{0} can readily diffuse across a membrane and can be oxidized intracellularly (*114-116*). Other neutrally charged low molecular weight Hg species may passively diffuse, but this has yet to be demonstrated (*117*).

Hg(II)-sulfides are one of the most dominant species of Hg in the environment, especially under conditions where it is methylated. Therefore, much work has gone into understanding why these Hg species are bioavailable (*70-74, 79, 117-120*). Dissolved Hg(II)-sulfides aqueous species and small, newly formed Hg(II)-sulfide minerals have been demonstrated to be highly bioavailable. There are limits to passive diffusion of Hg(II)-sulfide species. With enough time and elevated Hg^{II} concentrations, Hg(II)-sulfides will form nanoparticles that will aggregate, be more ordered, and are too large and inaccessible to microbes (*70-74*). Without a means of extraction, Hg^{II} associated with aggregated solid/sorbed phases (e.g., $HgS_{(s)}$, Fe^{II}-sulfides, and including non-sulfidic Fe^{III}-oxide minerals) does not appear to be accessible to microbes (*79, 121-123*).

There is no clear indicator that Hg(II)-sulfides are bioavailable specifically by either active or passive transport as it might be both. To tease this apart, studies have developed experimental designs to discriminate between both active and passive transport. For instance, sequestration of Hg with thiols prevents ligand exchange with a transporter allowing passive diffusion to occur (*118*) or eliminating active transport with proton uncouplers (*120*). A recent study demonstrated how newly formed Hg(II)-sulfides have a high affinity to zinc transporters on the membrane of Hg methylating microbes and how this binding greatly enhanced methylation (*74*).

1.4 Microbial Biosensors and Hg Bioavailability

Hg bioavailability to anaerobic microbes is the first step in the methylation process that is critical for determining its fate in the environment. However, Hg bioavailability to microbes is determined by its speciation. Many mechanistic studies investigating the bioavailability of Hg species under anaerobic conditions deploy methods that focus on i) Hg methylation as an outcome of uptake or ii) ICP-MS mass balance, iii) spectroscopic measurements, and iv) correlations with environmental parameters (69, 73, 74, 95, 119, 120, 132-137). These are useful tools and have advanced the field in many ways. However, insights into the mechanisms of Hg uptake anaerobically so far have been limited due to the lack of biosensing tools capable of evaluating Hg bioavailability anaerobically in real-time.

A useful tool to determine the real-time bioavailability of Hg^{II} are microbial biosensors. These are bacterial cells that emit a quantifiable signal corresponding to intracellular concentrations of a contaminant, in this case, Hg^{II} (*124*). Microbial Hg-biosensors contain gene fusions between the regulatory circuitry of the *mer* operon (including genes encoding for the transcription regulator *MerR* as well as the operator and promoter regions of the operon) and reporting genes (e.g., *lux, gfp, lac* genes). When Hg is present in the cytoplasm, it will bind to

MerR resulting in transcription of the reporting genes and subsequent signal production (*125, 126*). Due to the aerobic restriction of these proteins, Dreper *et al*. (2007) developed a Flavin-based fluorescent protein (FbFp) based on the light oxygen voltage domain of SB2 protein from *P. putida*. This protein can fluoresce in the absence of oxygen (*127*). These conditions are more analogous to environments in which mercury methylation occurs.

In my thesis, I use a non-methylating microbe (*Escherichia coli*). Most microbes in the environment cannot be cultured (*128*) or are not all genetically tractable. *E. coli* are very simple to use, do not generate sulfide without excess cysteine (118), reduce Hg^{II} (129) and allow me to have almost complete and total control of their metabolism and Hg^{II} speciation. A growing body of evidence points to Hg methylation being a syntrophic process where only species are tractable in the lab (*130-133*). Many organisms cannot be studied directly, and model organisms such as *E. coli* provide unique insights into how Hg^{II} can transgress a cell membrane. The biosensors I developed in my thesis can detect Hg^{II} bioavailability within minutes, allowing me to assess the rapid kinetics of Hg transformations before uptake across a range of redox conditions.

1.5 Thesis Framework

The overall objective of my thesis is to understand mechanisms governing Hg bioavailability to anaerobes. My thesis contains methodology chapters (2, 3, and 5) where I developed and optimized tools that can assess Hg^{II} bioavailability in anaerobic microbes. I then apply these tools in 4 data chapters (2, 4, 6 and 7; chapter 2 being both methods and data). Each data chapter addresses Hg^{II} bioavailability with environmental factors indicative of different redox zones. When Hg^{II} is deposited from the atmosphere in an aquatic system, it must go through a series of ligand exchanges to reach anaerobic conditions conducive to methylation. The ligands present are governed mainly by the zones generated by transitions through the redox

ladder, as depicted in figure 1.3. My thesis attempts to create a framework describing Hg bioavailability to microbes throughout various conditions it transgresses to reach Hg methylating microbes.

I will cover the bioavailability associated with Hg^{II} species but not the pathways involving the *mer* operon. While *mer* determinants are widespread in the environment, they are typically not deployed by Hg methylating microbes (*42*), limiting their implications.

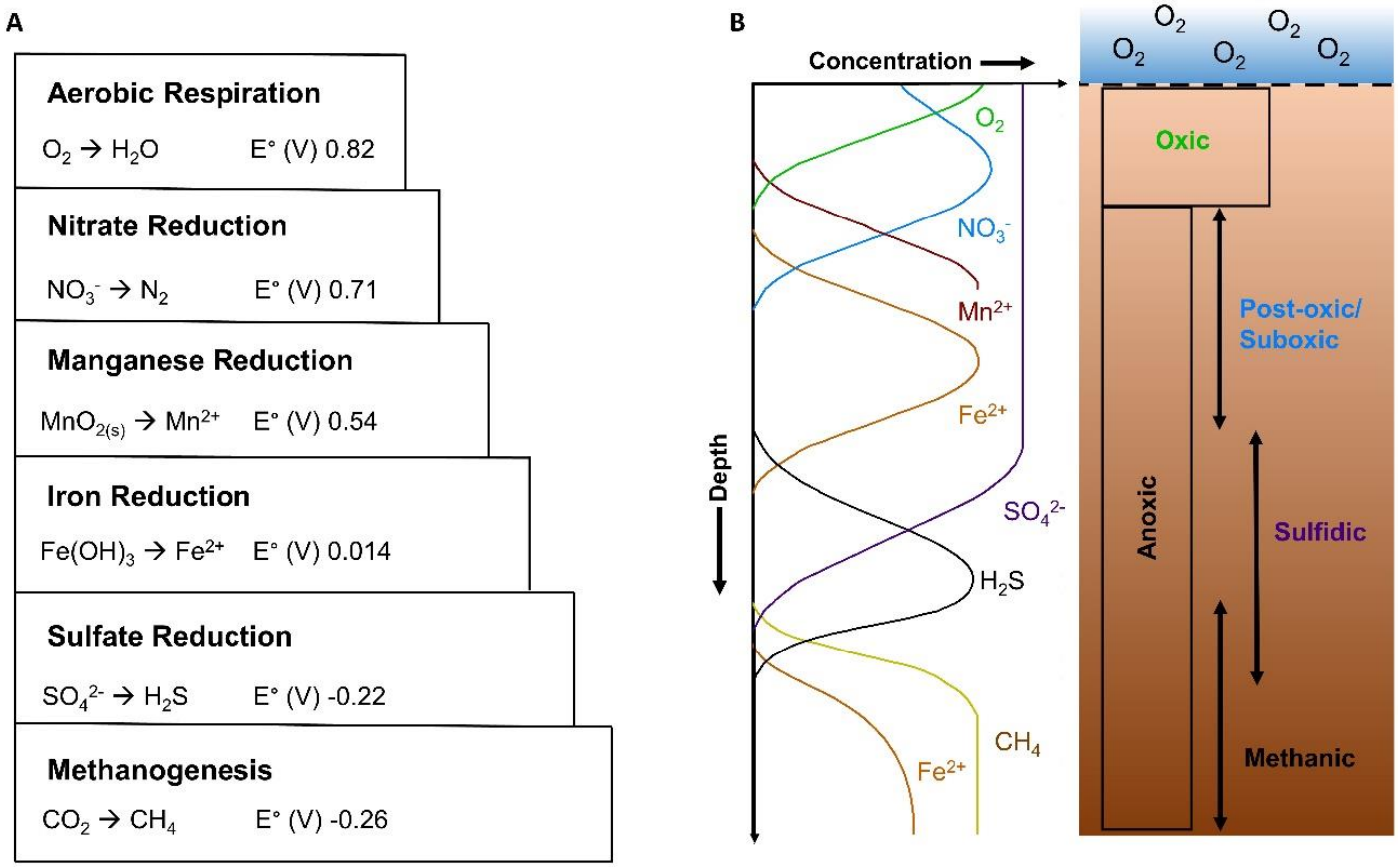

Figure 1.3 The microbial redox ladder and metabolisms associated with Hg methylation. A simplified microbial redox ladder and conceptual changes in concentrations of redox parameters with biogeochemical zonation. **A)** Demonstrated as a staircase, with the most energetically favorable metabolism at the top and least at the bottom. As each terminal electron acceptor (TEA) corresponding to the microbial metabolism is depleted, the next metabolism on the lower stair with a lower reduction potential (E° (V)) will be favored. **B)** Conceptual changes in concentrations of redox parameters with increasing depth from an oxygenated surface adapted from (Appelo and Postma 2004)[*134*]. Redox-specific zones based on (Berner 1981)(*135*): Oxic (O_2 present) and Anoxic (no O_2). Anoxic is further subdivided into Post-oxic/suboxic (depleted concentrations of O_2 and H_2S), Sulfidic (H_2S present), and Methanic (CH_4 present). This zonation is simplified, and further detailed zones are described in (canfield, 2009)(*136*).

1.6 Objectives

The first objective of my thesis in **chapter 2** was to develop a microbial biosensor that could detect Hg anaerobically. This data chapter was published as "Ionic strength differentially affects the bioavailability of neutral and negatively charged inorganic Hg complexes" in *Environmental Science & Technology (137)*. Ideally, I would have used a Hg methylating microbe, but there was no validated methodology to do this when I began my thesis. Therefore, I first created the framework in *E. coli* NEB5α, which served as a tractable reporter chassis. In addition, unlike most Hg methylating microbes, *E. coli* will not generate H_2S as a by-product of its general metabolism in the absence of excess cysteine (118), reduce Hg^{II} (129) or produce MeHg. In addition, very simple and efficient to use. I validated the biosensor using variables, such as halide concentrations and pH, that are simple to model Hg^{II} speciation, which have already been addressed aerobically. I then compared aerobic with the anaerobic (nitrate reduction) data collected in this chapter and pre-existing literature.

Chapter 3 was published as a methods paper in the Journal of Visualized Experiments as "An Anaerobic Biosensor Assay for the Detection of Mercury and Cadmium" (133). This paper provides a detailed methodological approach used in **Chapter 1** for using the biosensor anaerobically and demonstrates how to use the same biosensor to detect cadmium; indeed, the transcription regulator *MerR*, although highly sensitive to Hg, can also respond to cadmium.

In Chapter 4, the next objective was to understand how algae can control Hg bioavailability to other microbes. While halides such as chloride may initially complex Hg^{II} in a system, DOM will ultimately outcompete them for Hg speciation (*50-52*). Algae directly impact Hg methylating microbes and supply labile DOM that affects community structure and

methylation rates (*123, 138-147*). Excreting DOM is an intrinsic property of all algae, and how algal DOM affects Hg^{II} bioavailability remains largely unexplored.

Chapter 4 was published as "Aerobic and Anaerobic Bacterial Mercury Uptake is Driven by Algal Organic Matter Composition and Molecular Weight" in *Environmental Science & Technology* (*148*). To evaluate the role Algal DOM molecular weight (MW) and composition have on Hg bioavailability, I used a multi-pronged approach in collaboration with Vaughn Mangal from Trent University (we are co-first authors on the paper). This study was mainly exploratory to see how specific algal species control Hg^{II} bioavailability to other organisms. We grew and obtained DOM from primary producers of the divisions Chlorophyta (*Scenedesmus obliquus, Chlorella vulgaris, Chlamydomonas reinhardtii*) and Euglenophyta (*Euglena gracilis* and *Euglena mutabilis*). These algal species are common in various aquatic systems and associated with high Hg methylation rates (*149-151*). We then fractionated the DOM based on its molecular weight and then determined how these DOM and their fractions affected HgII bioavailability to the Hg-biosensor. Our next objective was to determine what components of the DOM were interacting with HgII using Fourier transform ion cyclotron mass spectrometry (FT ICR MS). In this chapter, I use the biosensor to show the influence of fresh algal DOM on Hg^{II} bioavailability. This study highlights DOM's emergent property related to how different biomolecules that comprise the complex DOM pool interact to affect metal uptake.

In **Chapter 5**, I expand the capabilities of my anaerobic biosensor to function under highly reduced conditions. Until now the Hg-biosensor I developed was only capable of respiring aerobically ($½O_2 + 2e^- + 2H^+ \rightleftharpoons H_2O$, $E° = 0.82V$) or under nitrate-reducing conditions ($NO_3^- + 2e^- + 2H^+ \rightleftharpoons NO_2^- + H_2O$, $E° = 0.43V$). While I provided a proof of principle that I could create a biosensor that can produce a signal anaerobically, these conditions are still relatively oxidizing

and not conducive to Hg methylating microbes. These redox conditions are ideal for working with inorganic ligands such as halides and DOM. Based on thermodynamics, sulfur, which binds HgII predominantly through strong thiolate/sulfide interactions, should be found in oxidized forms (e.g., SO_4^{2-}). Thiols, for instance, have a very low reduction potential (e.g., (R-S-S-R $+2e^-$ $+2H^+ \rightleftharpoons$ 2RSH, E° ranges typically from -0.289 to -0.383 V but can extend from -0.431 to 0.121V (*152*)). Equilibrium in the environment is seldom reached, and thiols/sulfide will be found under all redox conditions, but working under thermodynamically relevant conditions is ideal. Going forward, I optimize the biosensor to function under more reduced conditions conducive to Hg methylation. By doing so, the reporter systems would be operable in Hg-methylators and indicative of sulfidic and methanogenic zones.

Chapter 5 was published as "Golden Gate Assembly of Aerobic and Anaerobic Microbial Bioreporters" in *Applied and Environmental Microbiology*. In this study, we developed a system for the streamlined construction of microbial biosensors based on Golden Gate assembly. I collaborated with Dr. Aaron Hinz at the University of Ottawa. Aaron developed a suite of genetic tools, including novel destination vectors and genetic parts to construct constitutive and analyte-sensing bioreporters. Then I comprehensively validated the method by measuring signal output and analyte detection dynamics of a broad array of *E. coli* constructs. Using fumarate as an electron acceptor, I calibrated the biosensors to function under highly reduced anoxic conditions (Fumarate $+2e^-$ $+2H^+ \rightleftharpoons$ Succinate, E° = 0.031V). This metabolism is common among microorganisms that carry out environmental Hg methylation (85, 96, 153). Using these biosensors, I demonstrate the quantitative detection of Hg and arsenic aerobically and anaerobically.

In **Chapter 6**, I follow Hg^{II} bioavailability as a Hg^{II} species transgresses post-oxic conditions dominated by thiols into sulfidic environments. Hg methylation in these environments does not occur in simple ligand systems. This chapter shows how thiols interact together to affect Hg^{II} bioavailability. Hg^{II} is in a constant exchange between different thiols, some of these Hg^{II}-thiol species being bioavailable while others are not. The objective of this study was to test if the dynamic equilibrium of competing thiols can facilitate Hg bioavailability (Figure 1.4). This chapter was accepted in *Environmental Microbiology* as "Diffusion of H_2S from thiolated ligand biodegradation rapidly generates bioavailable mercury".

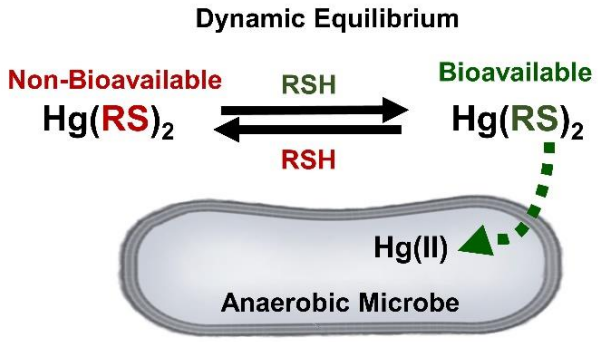

Figure 1.4: The dynamic equilibrium of Mercury and thiols. Hg^{II} forms non-bioavailable thiol complexes ($Hg(SR)_2$) in an equilibrium. The presence of a bioavailable complex may facilitate Hg^{II} bioavailability.

Serendipitously, I discovered how H_2S diffusion can rapidly facilitate Hg^{II} bioavailability. Where trace amounts of biogenic H_2S originating from anaerobic microbial ligand degradation can alter Hg^{II} speciation away from H_2S production site. I show how quickly this process forms bioavailable Hg^{II}-sulphide species from otherwise non-bioavailable ligand.

The objectives of last data chapter of my thesis, **chapter 7**, were explorative, addressing how a wide range of compounds affect Hg^{II} bioavailability. The chapter is divided into two

themes describing this data. First, I showed Hg^{II} bioavailability with compounds associated with iron and other essential metal acquisition. Then I show how emerging contaminants related to the mining industry could affect Hg^{II} bioavailability.

Under post-oxic conditions, ferric iron (Fe^{III}) can become the most favorable TEA. This TEA is also used by Hg-methylating microbes (*85, 154*). Iron forms insoluble Fe^{III}-oxides that readily sorbs and incorporate Hg (*84-89*). It is unclear whether Hg^{II} is directly accessible from these Fe^{III}-oxides (*85, 90-92*), the Fe^{III} is also not accessible due to its insolubility. Many organisms have developed metabolic strategies for breaking apart these oxides to acquire iron. They secrete siderophores that will chelate and dissolve the Fe^{III}. Dissolved Fe^{III}-siderophore complexes are then accessed through siderophore-specific transport pathways. It has been shown that Hg^{II} can use transport systems specific for copper-binding metallophore (methanobactin). For instance, methanotrophs can access Hg^{II} by transporting it as Hg^{II}-methanobactin complex through methanobactin transport pathways (45). If Hg^{II} associated with iron oxides can interact with the siderophores/non-iron specific metallophores, this may provide alternate pathways for microbes to access it.

Chapter 7, "Pathways in metal acquisition affect Hg bioavailability," will soon be submitted for review. The objective of this study was to test whether siderophores, specific and non-specific to iron (metallophores) would affect Hg^{II} bioavailability to a Hg-biosensor. Focusing on siderophores *E. coli* has known transport pathways for (*156*). I selected several of these siderophores/metallophores, that are also widespread in the environment. This chapter shows the unique interactions that specific siderophores have on affecting Hg^{II} bioavailability. I also discuss the implications on how microbes can control Hg^{II} bioavailability to other organisms and the importance of microbial community structure.

The second objective of **chapter 7** was to investigate how several emerging contaminants affect Hg^{II} bioavailability. In the previous chapters of my thesis, I investigate how naturally occurring ligands influence Hg^{II} speciation and its bioavailability. However, many ligands in the environment are no longer naturally occurring, and pollutants from the mining industry contribute to Hg contamination and affect Hg-methylation (*156*). Two contaminants I addressed are ethyl xanthate and diethyldithiocarbamate (DDTC). Two contaminants I tested are ethyl xanthate and diethyldithiocarbamate (DDTC). These two contaminants are regularly discharged into the environment and have become an ecological and health concern (*157*). They have a high affinity for metals and metal sulfide ores, and almost nothing is known on how they affect metal bioavailability (*158*). Here, I report on how they affect Hg^{II} bioavailability to the Hg-biosensor and the potential influences of mining contamination on Hg methylation.

1.7 Novelty and Significance

Hg bioavailability to anaerobic microbes is an essential step in producing MeHg that can biomagnify through food webs. My thesis provides a novel framework for biosensors to determine Hg^{II} bioavailability under anoxic conditions. I uncover distinct mechanisms of microbial Hg acquisition in complex ligand systems and how microbial communities can control Hg^{II} bioavailability. This work provides insight into potentially widespread drivers of Hg methylation in the environment.

1.8 References

1. W. H. Organization, Chemicals of public concerns I Mercury. *https://www.who.int/teams/environment-climate-change-and-health/chemical-safety-and-health/health-impacts/chemicals/mercury*.
2. UN-Environment, "Global Mercury Assessment 2018. UN-Environment Programme, Chemicals and Health Branch, Geneva, Switzerland. 59 pp," (2019).

3. V. Shah *et al.*, Improved Mechanistic Model of the Atmospheric Redox Chemistry of Mercury. *Environmental Science & Technology*, (2021).

4. P. A. Ariya *et al.*, Mercury Physicochemical and Biogeochemical Transformation in the Atmosphere and at Atmospheric Interfaces: A Review and Future Directions. *Chemical Reviews* **115**, 3760-3802 (2015).

5. B. A. Branfireun, C. Cosio, A. J. Poulain, G. Riise, A. G. Bravo, Mercury cycling in freshwater systems - An updated conceptual model. *Science of The Total Environment* **745**, 140906 (2020).

6. B. Gworek, O. Bemowska-Kałabun, M. Kijeńska, J. Wrzosek-Jakubowska, Mercury in Marine and Oceanic Waters—a Review. *Water, Air, & Soil Pollution* **227**, 1-19 (2016).

7. R. C. Harris *et al.*, Whole-ecosystem study shows rapid fish-mercury response to changes in mercury deposition. *Proceedings of the National Academy of Sciences* **104**, 16586 (2007).

8. D. Obrist *et al.*, A review of global environmental mercury processes in response to human and natural perturbations: Changes of emissions, climate, and land use. *Ambio* **47**, 116-140 (2018).

9. Z. Tang, F. Fan, S. Deng, D. Wang, Mercury in rice paddy fields and how does some agricultural activities affect the translocation and transformation of mercury - A critical review. *Ecotoxicology and Environmental Safety* **202**, 110950 (2020).

10. Y.-S. Hong, Y.-M. Kim, K.-E. Lee, Methylmercury exposure and health effects. *J Prev Med Public Health* **45**, 353-363 (2012).

11. P. Chen, M. R. Miah, M. Aschner, Metals and Neurodegeneration. *F1000Res* **5**, F1000 Faculty Rev-1366 (2016).

12. A. A. Tinkov *et al.*, Mercury and metabolic syndrome: a review of experimental and clinical observations. *Biometals* **28**, 231-254 (2015).

13. S. E. Orr *et al.*, Potential mechanisms of cellular injury following exposure to a physiologically relevant species of inorganic mercury. *Toxicol Lett* **304**, 13-20 (2019).

14. G. Genchi, M. S. Sinicropi, A. Carocci, G. Lauria, A. Catalano, Mercury exposure and heart diseases. *International journal of environmental research and public health* **14**, 74 (2017).

15. Z. Yin *et al.*, The methylmercury-l-cysteine conjugate is a substrate for the L-type large neutral amino acid transporter. *Journal of neurochemistry* **107**, 1083-1090 (2008).

16. M. Podar *et al.*, Global prevalence and distribution of genes and microorganisms involved in mercury methylation. *Science Advances* **1**, e1500675 (2015).

17. B. Gu, X. Lu, A. Johs, E. M. Pierce, in *Encyclopedia of Water*. pp. 1-18.

18. J. M. Parks *et al.*, The genetic basis for bacterial mercury methylation. *Science* **339**, 1332-1335 (2013).

19. C. Qian *et al.*, Quantitative Proteomic Analysis of Biological Processes and Responses of the Bacterium Desulfovibrio desulfuricans ND132 upon Deletion of Its Mercury Methylation Genes. *PROTEOMICS* **18**, 1700479 (2018).

20. C. C. Gilmour *et al.*, Mercury Methylation by Novel Microorganisms from New Environments. *Environmental Science & Technology* **47**, 11810-11820 (2013).

21. E. Capo *et al.*, A consensus protocol for the recovery of mercury methylation genes from metagenomes. *bioRxiv*, 2022.2003.2014.484253 (2022).

22. A. G. Bravo *et al.*, Extremely elevated methyl mercury levels in water, sediment and organisms in a Romanian reservoir affected by release of mercury from a chlor-alkali plant. *Water Research* **49**, 391-405 (2014).

23. P. Dranguet, V. I. Slaveykova, S. Le Faucheur, *Kinetics of mercury accumulation by freshwater biofilms*. (2018), vol. 14.

24. T. A. Olsen, C. C. Brandt, S. C. Brooks, Periphyton biofilms influence net methylmercury production in an industrially contaminated system. *Environmental Science & Technology* **50**, 10843-10850 (2016).

25. V. L. Ortiz, R. P. Mason, J. E. Ward, An examination of the factors influencing mercury and methylmercury particulate distributions, methylation and demethylation rates in laboratory-generated marine snow. *Mar Chem* **177**, 753-762 (2015).

26. E. M. Sunderland, D. P. Krabbenhoft, J. W. Moreau, S. A. Strode, W. M. Landing, Mercury sources, distribution, and bioavailability in the North Pacific Ocean: Insights from data and models. *Global Biogeochemical Cycles* **23**, (2009).

27. I. Lehnherr, V. L. St. Louis, H. Hintelmann, J. L. Kirk, Methylation of inorganic mercury in polar marine waters. *Nature Geoscience* **4**, 298-302 (2011).

28. C. Larose *et al.*, Springtime changes in snow chemistry lead to new insights into mercury methylation in the Arctic. *Geochimica et Cosmochimica Acta* **74**, 6263-6275 (2010).

29. C. M. Gionfriddo, M. T. Tate, R. R. Wick, Microbial mercury methylation in Antarctic sea ice. **1**, 16127 (2016).

30. D. Cossa *et al.*, The open sea as the main source of methylmercury in the water column of the Gulf of Lions (Northwestern Mediterranean margin). *Geochimica et Cosmochimica Acta* **199**, 222-237 (2017).

31. C. T. Driscoll, R. P. Mason, H. M. Chan, D. J. Jacob, N. Pirrone, Mercury as a Global Pollutant: Sources, Pathways, and Effects. *Environmental Science & Technology* **47**, 4967-4983 (2013).

32. B. Braune *et al.*, Mercury in the marine environment of the Canadian Arctic: Review of recent findings. *Science of The Total Environment* **509–510**, 67-90 (2015).

33. G. A. Christensen *et al.*, Determining the Reliability of Measuring Mercury Cycling Gene Abundance with Correlations with Mercury and Methylmercury Concentrations. *Environmental Science & Technology* **53**, 8649-8663 (2019).

34. A. G. Bravo, C. Cosio, Biotic formation of methylmercury: A bio–physico–chemical conundrum. *Limnology and Oceanography* **65**, 1010-1027 (2020).

35. O. Regnell, C. J. Watras, Microbial Mercury Methylation in Aquatic Environments: A Critical Review of Published Field and Laboratory Studies. *Environmental Science & Technology* **53**, 4-19 (2019).

36. V. I. Slaveykova, K. J. Wilkinson, Predicting the bioavailability of metals and metal complexes: Critical review of the biotic ligand model. *Environmental Chemistry* **2**, 9-24 (2005).

37. T. B. Kinraide, Improved scales for metal ion softness and toxicity. *Environmental Toxicology and Chemistry* **28**, 525-533 (2009).

38. A. Manceau *et al.*, Formation of Mercury Sulfide from Hg(II)–Thiolate Complexes in Natural Organic Matter. *Environmental Science & Technology* **49**, 9787-9796 (2015).

39. V. Liem-Nguyen, U. Skyllberg, E. Björn, Thermodynamic Modeling of the Solubility and Chemical Speciation of Mercury and Methylmercury Driven by Organic Thiols and Micromolar Sulfide Concentrations in Boreal Wetland Soils. *Environmental Science & Technology* **51**, 3678-3686 (2017).

40. V. Liem-Nguyen, U. Skyllberg, K. Nam, E. Björn, Thermodynamic stability of mercury(II) complexes formed with environmentally relevant low-molecular-mass thiols studied by competing ligand exchange and density functional theory. *Environmental Chemistry* **14**, 243-253 (2017).

41. A. Drott, E. Bjorn, S. Bouchet, U. Skyllberg, Refining thermodynamic constants for mercury (II)-sulfides in equilibrium with metacinnabar at sub-micromolar aqueous sulfide concentrations. *Environmental science & technology* **47**, 4197-4203 (2013).

42. H. Hsu-Kim, K. H. Kucharzyk, T. Zhang, M. A. Deshusses, Mechanisms regulating mercury bioavailability for methylating microorganisms in the aquatic environment: a critical review. *Environ Sci Technol* **47**, 2441-2456 (2013).

43. J. B. Fein, Q. Yu, J. Nam, N. Yee, Bacterial cell envelope and extracellular sulfhydryl binding s: Their roles in metal binding and bioavailability. *Chemical Geology*, (2019).

44. D. S. Grégoire, A. J. Poulain, Shining light on recent advances in microbial mercury cycling. *FACETS* **3**, 858-879 (2018).

45. B. Gworek, W. Dmuchowski, A. H. Baczewska-Dąbrowska, Mercury in the terrestrial environment: a review. *Environmental Sciences Europe* **32**, 128 (2020).

46. S. E. Bone, J. R. Bargar, G. Sposito, Mackinawite (FeS) reduces mercury(II) under sulfidic conditions. *Environmental science & technology* **48**, 10681-10689 (2014).

47. T. A. Douglas *et al.*, The fate of mercury in Arctic terrestrial and aquatic ecosystems, a review. *Environmental Chemistry* **9**, 321-355 (2012).

48. S. E. Lindberg *et al.*, Dynamic Oxidation of Gaseous Mercury in the Arctic Troposphere at Polar Sunrise. *Environmental Science & Technology* **36**, 1245-1256 (2002).

49. M. Yamamoto, Stimulation of elemental mercury oxidation in the presence of chloride ion in aquatic environments. *Chemosphere* **32**, 1217-1224 (1996).

50. H. Zhong, W.-X. Wang, Controls of Dissolved Organic Matter and Chloride on Mercury Uptake by a Marine Diatom. *Environmental Science & Technology* **43**, 8998-9003 (2009).

51. U. Skyllberg, Chemical speciation of mercury in soil and sediment. *Environmental chemistry and toxicology of mercury*, 219-258 (2012).

52. S. Han *et al.*, Mercury Speciation in Marine Sediments under Sulfate-Limited Conditions. *Environmental Science & Technology* **44**, 3752-3757 (2010).

53. G. Liu, Y. Cai, N. O'Driscoll, *Environmental chemistry and toxicology of mercury*. (John Wiley & Sons, 2011).

54. J. Benoit, R. P. Mason, C. Gilmour, G. Aiken, Constants for mercury binding by dissolved organic matter isolates from the Florida Everglades. *Geochimica et cosmochimica acta* **65**, 4445-4451 (2001).

55. C. L. Miller, R. P. Mason, C. C. Gilmour, A. Heyes, Influence of dissolved organic matter on the complexation of mercury under sulfidic conditions. *Environmental Toxicology and Chemistry* **26**, 624-633 (2007).

56. R. T. Drexel, M. Haitzer, J. N. Ryan, G. R. Aiken, K. L. Nagy, Mercury(II) sorption to two Florida Everglades peats: evidence for strong and weak binding and competition by dissolved organic matter released from the peat. *Environ Sci Technol* **36**, 4058-4064 (2002).

57. S. Dunham-Cheatham, B. Mishra, S. Myneni, J. B. Fein, The effect of natural organic matter on the adsorption of mercury to bacterial cells. *Geochimica et Cosmochimica Acta* **150**, 1-10 (2015).

58. C. L. Miller, L. Liang, B. Gu, Competitive ligand exchange reveals time dependant changes in the reactivity of Hg–dissolved organic matter complexes. *Environmental Chemistry* **9**, 495-501 (2012).

59. A. L.-T. Pham *et al.*, Precipitation of nanoscale mercuric sulfides in the presence of natural organic matter: Structural properties, aggregation, and biotransformation. *Geochimica et Cosmochimica Acta* **133**, 204-215 (2014).

60. B. A. Poulin *et al.*, Effects of Sulfide Concentration and Dissolved Organic Matter Characteristics on the Structure of Nanocolloidal Metacinnabar. *Environmental Science & Technology* **51**, 13133-13142 (2017).

61. A. Deonarine, H. Hsu-Kim, Precipitation of Mercuric Sulfide Nanoparticles in NOM-Containing Water: Implications for the Natural Environment. *Environmental Science & Technology* **43**, 2368-2373 (2009).

62. B. B. Jørgensen, A. J. Findlay, A. Pellerin, The Biogeochemical Sulfur Cycle of Marine Sediments. *Frontiers in Microbiology* **10**, (2019).

63. J. V. Mills, G. Antler, A. V. Turchyn, Geochemical evidence for cryptic sulfur cycling in salt marsh sediments. *Earth and Planetary Science Letters* **453**, 23-32 (2016).

64. M. Labrenz *et al.*, Formation of Sphalerite (ZnS) Deposits in Natural Biofilms of Sulfate-Reducing Bacteria. *Science* **290**, 1744 (2000).

65. M. Pester, K.-H. Knorr, M. Friedrich, M. Wagner, A. Loy, Sulfate-reducing microorganisms in wetlands – fameless actors in carbon cycling and climate change. *Frontiers in Microbiology* **3**, (2012).

66. M. Enescu, K. L. Nagy, A. Manceau, Nucleation of mercury sulfide by dealkylation. *Sci Rep* **6**, 39359 (2016).

67. T. Zhang *et al.*, Methylation of mercury by bacteria exposed to dissolved, nanoparticulate, and microparticulate mercuric sulfides. *Environ Sci Technol* **46**, 6950-6958 (2012).

68. L. Si, P. A. Ariya, Photochemical reactions of divalent mercury with thioglycolic acid: formation of mercuric sulfide particles. *Chemosphere* **119**, 467-472 (2015).

69. C. A. Gerbig, C. S. Kim, J. P. Stegemeier, J. N. Ryan, G. R. Aiken, Formation of Nanocolloidal Metacinnabar in Mercury-DOM-Sulfide Systems. *Environmental Science & Technology* **45**, 9180-9187 (2011).

70. Z. Zhang *et al.*, Effects of Extracellular Polymeric Substances on the Formation and Methylation of Mercury Sulfide Nanoparticles. *Environmental Science & Technology* **54**, 8061-8071 (2020).

71. A. M. Graham, G. R. Aiken, C. C. Gilmour, Dissolved Organic Matter Enhances Microbial Mercury Methylation Under Sulfidic Conditions. *Environmental Science & Technology* **46**, 2715-2723 (2012).

72. A. M. Graham, G. R. Aiken, C. C. Gilmour, Effect of Dissolved Organic Matter Source and Character on Microbial Hg Methylation in Hg–S–DOM Solutions. *Environmental Science & Technology* **47**, 5746-5754 (2013).

73. Nashaat M. Mazrui *et al.*, The precipitation, growth and stability of mercury sulfide nanoparticles formed in the presence of marine dissolved organic matter. *Environmental Science: Processes & Impacts* **20**, 642-656 (2018).

74. L. Tian *et al.*, Microbial methylation potential of mercury sulfide particles dictated by surface structure. *Nature Geoscience* **14**, 409-416 (2021).

75. G. V. Lowry, S. Shaw, C. S. Kim, J. J. Rytuba, G. E. Brown, Macroscopic and Microscopic Observations of Particle-Facilitated Mercury Transport from New Idria and Sulphur Bank Mercury Mine Tailings. *Environmental Science & Technology* **38**, 5101-5111 (2004).

76. M. O. Barnett *et al.*, Formation of Mercuric Sulfide in Soil. *Environmental Science & Technology* **31**, 3037-3043 (1997).

77. J. L. Guentzel, R. T. Powell, W. M. Landing, R. P. Mason, Mercury associated with colloidal material in an estuarine and an open-ocean environment. *Marine Chemistry* **55**, 177-188 (1996).

78. C. A. J. Appelo, D. Postma, *Geochemistry, groundwater and pollution*. Geochemistry, groundwater and pollution (CRC press, ed. 2, 2004).

79. N. A. Rivera, Jr., P. M. Bippus, H. Hsu-Kim, Relative Reactivity and Bioavailability of Mercury Sorbed to or Coprecipitated with Aged Iron Sulfides. *Environ Sci Technol* **53**, 7391-7399 (2019).

80. H. Y. Jeong, B. Klaue, J. D. Blum, K. F. Hayes, Sorption of mercuric ion by synthetic nanocrystalline mackinawite (FeS). *Environ Sci Technol* **41**, 7699-7705 (2007).

81. H. Y. Jeong, K. Sun, K. F. Hayes, Microscopic and Spectroscopic Characterization of Hg(II) Immobilization by Mackinawite (FeS). *Environmental Science & Technology* **44**, 7476-7483 (2010).

82. J. Liu, K. T. Valsaraj, I. Devai, R. D. DeLaune, Immobilization of aqueous Hg(II) by mackinawite (FeS). *J Hazard Mater* **157**, 432-440 (2008).

83. S. Wolfenden, J. M. Charnock, J. Hilton, F. R. Livens, D. J. Vaughan, Sulfide species as a sink for mercury in lake sediments. *Environ Sci Technol* **39**, 6644-6648 (2005).

84. M. Ganguly, S. Dib, P. A. Ariya, Fast, Cost-effective and Energy Efficient Mercury Removal-Recycling Technology. *Scientific Reports* **8**, 16255 (2018).

85. Y. Si, Y. Zou, X. Liu, X. Si, J. Mao, Mercury methylation coupled to iron reduction by dissimilatory iron-reducing bacteria. *Chemosphere* **122**, 206-212 (2015).

86. K. H. Johannesson, K. Neumann, Geochemical cycling of mercury in a deep, confined aquifer: Insights from biogeochemical reactive transport modeling. *Geochimica et Cosmochimica Acta* **106**, 25-43 (2013).

87. W. Stumm, & Morgan, J. J., *Aquatic Chemistry: Chemical Equilibria and Rates in Natural Waters*. (Wiley, New York, ed. 3rd, 1996).

88. S. Guedron, S. Grangeon, B. Lanson, M. Grimaldi, Mercury speciation in a tropical soil association; Consequence of gold mining on Hg distribution in French Guiana. *Geoderma* **153**, 331-346 (2009).

89. G. Liu, Y. Li, Y. Cai, in *Environmental Chemistry and Toxicology of Mercury*. (2011), pp. 367-387.

90. J. Harris-Hellal, M. Grimaldi, E. Garnier-Zarli, N. Bousserrhine, Mercury mobilization by chemical and microbial iron oxide reduction in soils of French Guyana. *Biogeochemistry* **103**, 223-234 (2011).

91. J. Hellal *et al.*, Mercury mobilization and speciation linked to bacterial iron oxide and sulfate reduction: A column study to mimic reactive transfer in an anoxic aquifer. *Journal of Contaminant Hydrology* **180**, 56-68 (2015).

92. H. A. Wiatrowski *et al.*, Reduction of Hg(II) to Hg(0) by Magnetite. *Environmental Science & Technology* **43**, 5307-5313 (2009).

93. U. Skyllberg, in *Environmental Chemistry and Toxicology of Mercury*. (2011), chap. 7, pp. 219-258.

94. A. Szczuka, F. M. M. Morel, J. K. Schaefer, Effect of Thiols, Zinc, and Redox Conditions on Hg Uptake in Shewanella oneidensis. *Environmental Science and Technology* **49**, 7432-7438 (2015).

95. J. K. Schaefer, A. Szczuka, F. M. M. Morel, Effect of Divalent Metals on Hg(II) Uptake and Methylation by Bacteria. *Environmental Science & Technology* **48**, 3007-3013 (2014).

96. J. K. Schaefer *et al.*, Active transport, substrate specificity, and methylation of Hg(II) in anaerobic bacteria. *Proceedings of the National Academy of Sciences* **108**, 8714-8719 (2011).

97. U. Ndu *et al.*, The use of a mercury biosensor to evaluate the bioavailability of mercury-thiol complexes and mechanisms of mercury uptake in bacteria. *PLoS One* **10**, e0138333 (2015).

98. S. A. Thomas, T. Tong, J.-F. Gaillard, Hg(ii) bacterial biouptake: the role of anthropogenic and biogenic ligands present in solution and spectroscopic evidence of ligand exchange reactions at the cell surface. *Metallomics* **6**, 2213-2222 (2014).

99. J. K. Schaefer, F. M. M. Morel, High methylation rates of mercury bound to cysteine by Geobacter sulfurreducens. *Nature Geosci* **2**, 123-126 (2009).

100. L. Zhao *et al.*, Contrasting Effects of Dissolved Organic Matter on Mercury Methylation by Geobacter sulfurreducens PCA and Desulfovibrio desulfuricans ND132. **51**, 10468-10475 (2017).

101. Y.-R. Liu *et al.*, Effects of Cellular Sorption on Mercury Bioavailability and Methylmercury Production by Desulfovibrio desulfuricans ND132. *Environmental Science & Technology* **50**, 13335-13341 (2016).

102. H. Lin, X. Lu, L. Liang, B. Gu, Cysteine Inhibits Mercury Methylation by Geobacter sulfurreducens PCA Mutant ΔomcBESTZ. *Environmental Science & Technology Letters* **2**, 144-148 (2015).

103. U. Ndu, R. P. Mason, H. Zhang, S. Lin, P. T. Visscher, Effect of inorganic and organic ligands on the bioavailability of methylmercury as determined by using a mer-lux bioreporter. *Applied and Environmental Microbiology* **78**, 7276-7282 (2012).

104. S. A. Thomas, B. Mishra, S. C. B. Myneni, Cellular Mercury Coordination Environment, and Not Cell Surface Ligands, Influence Bacterial Methylmercury Production. *Environmental Science & Technology* **54**, 3960-3968 (2020).

105. B. Mishra *et al.*, Stoichiometry of mercury-thiol complexes on bacterial cell envelopes. *Chemical Geology*, (2017).

106. Y. Song *et al.*, Toward an Internally Consistent Model for Hg(II) Chemical Speciation Calculations in Bacterium–Natural Organic Matter–Low Molecular Mass Thiol Systems. *Environmental Science & Technology* **54**, 8094-8103 (2020).

107. H. Hu *et al.*, Mercury reduction and cell-surface adsorption by geobacter sulfurreducens PCA. *Environmental Science and Technology* **47**, 10922-10930 (2013).

108. X. Yin *et al.*, Synergistic Effects of a Chalkophore, Methanobactin, on Microbial Methylation of Mercury. *Applied and Environmental Microbiology* **86**, e00122-00120 (2020).

109. S. A. Chiasson-Gould, J. M. Blais, A. J. Poulain, Dissolved Organic Matter Kinetically Controls Mercury Bioavailability to Bacteria. *Environmental Science & Technology* **48**, 3153-3161 (2014).

110. Y. Song *et al.*, Thermodynamics of Hg(II) Bonding to Thiol Groups in Suwannee River Natural Organic Matter Resolved by Competitive Ligand Exchange, Hg LIII-Edge EXAFS and 1H NMR Spectroscopy. *Environmental Science & Technology* **52**, 8292-8301 (2018).

111. A. Šípková, J. Száková, A. Hanč, P. Tlustoš, Mobility of mercury in soil as affected by soil physicochemical properties. *Journal of Soils and Sediments* **16**, 2234-2241 (2016).

112. U. Skyllberg, P. R. Bloom, J. Qian, C.-M. Lin, W. F. Bleam, Complexation of Mercury(II) in Soil Organic Matter: EXAFS Evidence for Linear Two-Coordination with Reduced Sulfur Groups. *Environmental Science & Technology* **40**, 4174-4180 (2006).

113. E. Boyd, T. Barkay, The Mercury Resistance Operon: From an Origin in a Geothermal Environment to an Efficient Detoxification Machine. *Frontiers in Microbiology* **3**, (2012).

114. Y. Wang, J. K. Schaefer, B. Mishra, N. Yee, Intracellular Hg(0) Oxidation in Desulfovibrio desulfuricans ND132. *Environmental Science & Technology* **50**, 11049-11056 (2016).

115. M. J. Colombo, J. Ha, J. R. Reinfelder, T. Barkay, N. Yee, Anaerobic oxidation of Hg(0) and methylmercury formation by Desulfovibrio desulfuricans ND132. *Geochimica et Cosmochimica Acta* **112**, 166-177 (2013).

116. H. Hu *et al.*, Oxidation and methylation of dissolved elemental mercury by anaerobic bacteria. *Nature Geoscience* **6**, 751-754 (2013).

117. J. Zhou *et al.*, Modeling of the Passive Permeation of Mercury and Methylmercury Complexes Through a Bacterial Cytoplasmic Membrane. *Environmental Science & Technology* **51**, 10595-10604 (2017).

118. S. A. Thomas, K. E. Rodby, E. W. Roth, J. Wu, J. F. Gaillard, Spectroscopic and Microscopic Evidence of Biomediated HgS Species Formation from Hg(II)-Cysteine Complexes: Implications for Hg(II) Bioavailability. *Environ Sci Technol* **52**, 10030-10039 (2018).

119. S. A. Thomas, P. Catty, J.-L. Hazemann, I. Michaud-Soret, J.-F. Gaillard, The role of cysteine and sulfide in the interplay between microbial Hg(ii) uptake and sulfur metabolism†. *Metallomics* **11**, 1219-1229 (2019).

120. J. An *et al.*, Mercury Uptake by Desulfovibrio desulfuricans ND132: Passive or Active? *Environmental Science & Technology* **53**, 6264-6272 (2019).

121. S. Jonsson *et al.*, Mercury methylation rates for geochemically relevant HgII species in sediments. *Environmental science & technology* **46**, 11653-11659 (2012).

122. S. Jonsson *et al.*, Differentiated availability of geochemical mercury pools controls methylmercury levels in estuarine sediment and biota. *Nature communications* **5**, 1-10 (2014).

123. V. Liem-Nguyen *et al.*, Effects of Nutrient Loading and Mercury Chemical Speciation on the Formation and Degradation of Methylmercury in Estuarine Sediment. *Environmental Science and Technology* **50**, 6983-6990 (2016).

124. J. R. Van Der Meer, S. Belkin, Where microbiology meets microengineering: design and applications of reporter bacteria. *Nature Reviews Microbiology* **8**, 511-522 (2010).

125. L. D. Rasmussen, R. R. Turner, T. Barkay, Cell-density-dependent sensitivity of a mer-lux bioassay. *Applied and Environmental Microbiology* **63**, 3291-3293 (1997).

126. T. Barkay, R. R. Turner, L. D. Rasmussen, C. A. Kelly, J. W. Rudd, Luminescence facilitated detection of bioavailable mercury in natural waters. *Methods in molecular biology (Clifton, N.J.)* **102**, 231-246 (1998).

127. T. Drepper *et al.*, Reporter proteins for in vivo fluorescence without oxygen. *Nature biotechnology* **25**, 443-445 (2007).

128. A. D. Steen *et al.*, High proportions of bacteria and archaea across most biomes remain uncultured. *The ISME Journal* **13**, 3126-3130 (2019).

129. D. S. Grégoire, N. C. Lavoie, A. J. Poulain, Heliobacteria Reveal Fermentation As a Key Pathway for Mercury Reduction in Anoxic Environments. *Environmental Science & Technology* **52**, 4145-4153 (2018).

130. H. S. Bae, F. E. Dierberg, A. Ogram, Syntrophs dominate sequences associated with the mercury methylation-related gene hgcA in the water conservation areas of the Florida Everglades. *Appl Environ Microbiol* **80**, 6517-6526 (2014).

131. S. Roth *et al.*, Nutrient Inputs Stimulate Mercury Methylation by Syntrophs in a Subarctic Peatland. *Frontiers in Microbiology* **12**, (2021).

132. R.-Q. Yu, J. R. Reinfelder, M. E. Hines, T. Barkay, Syntrophic pathways for microbial mercury methylation. *The ISME Journal* **12**, 1826-1835 (2018).

133. A. G. Bravo *et al.*, Geobacteraceae are important members of mercury-methylating microbial communities of sediments impacted by waste water releases. *The ISME journal* **12**, 802-812 (2018).

134. C. A. J. Appelo, D. Postma, *Geochemistry, groundwater and pollution*. (CRC press, 2004).

135. R. A. Berner, A new geochemical classification of sedimentary environments. *Journal of Sedimentary Research* **51**, 359-365 (1981).

136. D. E. Canfield, B. Thamdrup, Towards a consistent classification scheme for geochemical environments, or, why we wish the term 'suboxic' would go away. *Geobiology* **7**, 385-392 (2009).

137. B. R. Stenzler, A. Hinz, M. O. Ruuskanen, A. J. Poulain, Ionic strength differentially affects the bioavailability of neutral and negatively charged inorganic Hg complexes. *Environ Sci Technol*, (2017).

138. K. Toming *et al.*, Contributions of autochthonous and allochthonous sources to dissolved organic matter in a large, shallow, eutrophic lake with a highly calcareous catchment. *Limnology and Oceanography* **58**, 1259-1270 (2013).

139. L. Lambertsson, M. Nilsson, Organic material: the primary control on mercury methylation and ambient methyl mercury concentrations in estuarine sediments. *Environmental science & technology* **40**, 1822-1829 (2006).

140. A. Drott, L. Lambertsson, E. Björn, U. Skyllberg, Importance of Dissolved Neutral Mercury Sulfides for Methyl Mercury Production in Contaminated Sediments. *Environmental Science & Technology* **41**, 2270-2276 (2007).

141. M. Kim, S. Han, J. Gieskes, D. D. Deheyn, Importance of organic matter lability for monomethylmercury production in sulfate-rich marine sediments. *Science of The Total Environment* **409**, 778-784 (2011).

142. W. L. Lázaro, J. R. D. Guimarães, A. R. Ignácio, C. J. Da Silva, S. Díez, Cyanobacteria enhance methylmercury production: a hypothesis tested in the periphyton of two lakes in the Pantanal floodplain, Brazil. *Science of the Total Environment* **456**, 231-238 (2013).

143. W. L. Lázaro, S. Díez, C. J. da Silva, Á. R. A. Ignácio, J. R. D. Guimarães, Seasonal changes in peryphytic microbial metabolism determining mercury methylation in a tropical wetland. *Science of The Total Environment* **627**, 1345-1352 (2018).

144. S. Gentès, J. Taupiac, Y. Colin, J.-M. André, R. Guyoneaud, Bacterial periphytic communities related to mercury methylation within aquatic plant roots from a temperate freshwater lake (South-Western France). *Environmental Science and Pollution Research* **24**, 19223-19233 (2017).

145. E. B. Graham *et al.*, Oligotrophic wetland sediments susceptible to shifts in microbiomes and mercury cycling with dissolved organic matter addition. *PeerJ* **6**, e4575-e4575 (2018).

146. A. G. Bravo *et al.*, Molecular composition of organic matter controls methylmercury formation in boreal lakes. *Nature Communications* **8**, 1-9 (2017).

147. G. A. Christensen *et al.*, Carbon Amendments Alter Microbial Community Structure and Net Mercury Methylation Potential in Sediments. *Applied and environmental microbiology* **84**, e01049-01017 (2018).

148. V. Mangal, B. R. Stenzler, A. J. Poulain, C. Guéguen, Aerobic and Anaerobic Bacterial Mercury Uptake is Driven by Algal Organic Matter Composition and Molecular Weight. *Environmental Science & Technology* **53**, 157-165 (2019).

149. M. Leclerc, D. Planas, M. Amyot, Relationship between Extracellular Low-Molecular-Weight Thiols and Mercury Species in Natural Lake Periphytic Biofilms. *Environ Sci Technol* **49**, 7709-7716 (2015).

150. S. Dasgupta, J. Fang, S. S. Brake, S. T. Hasiotis, L. Zhang, Biosynthesis of sterols and wax esters by Euglena of acid mine drainage biofilms: Implications for eukaryotic evolution and the early Earth. *Chemical Geology* **306-307**, 139-145 (2012).

151. I. Krohn-Molt *et al.*, Metagenome survey of a multispecies and alga-associated biofilm revealed key elements of bacterial-algal interactions in photobioreactors. *Applied and environmental microbiology* **79**, 6196-6206 (2013).

152. A. Mirzahosseini, B. Noszál, Species-Specific Standard Redox Potential of Thiol-Disulfide Systems: A Key Parameter to Develop Agents against Oxidative Stress. *Scientific Reports* **6**, 37596 (2016).

153. R.-Q. Yu, J. R. Reinfelder, M. E. Hines, T. Barkay, Mercury Methylation by the Methanogen Methanospirillum hungatei. *Applied and Environmental Microbiology* **79**, 6325-6330 (2013).

154. S. Han *et al.*, Sulfide and iron control on mercury speciation in anoxic estuarine sediment slurries. *Marine Chemistry* **111**, 214-220 (2008).

155. R. Hider, X. Kong, Chemistry and biology of siderophores. *Natural product reports* **27**, 637 (2010).

156. C. S. Eckley *et al.*, The assessment and remediation of mercury contaminated sites: A review of current approaches. *Sci Total Environ* **707**, 136031-136031 (2020).

157. R. Dixit *et al.*, Bioremediation of Heavy Metals from Soil and Aquatic Environment: An Overview of Principles and Criteria of Fundamental Processes. *Sustainability* **7**, 2189-2212 (2015).

158. P. Bararunyeretse, Y. Zhang, H. Ji, Molecular Biology-Based Analysis of the Interactive Effect of Nickel and Xanthates on Soil Bacterial Community Diversity and Structure. *Sustainability* **11**, (2019).

Chapter 2: Ionic strength differentially affects the bioavailability of neutral and negatively charged inorganic Hg complexes

Benjamin Stenzler, Aaron Hinz, Matti Ruuskanen & Alexandre J. Poulain*

Biology Department, University of Ottawa, 30 Marie Curie, Ottawa, ON, K1N 6N5, Canada.

*Corresponding author: Alexandre J. Poulain

E-mail address: apoulain@uottawa.ca

Telephone: 1-613-562-5800 ext. 2373

"*A modified version of this chapter was originally published as:* Stenzler, B., Hinz, A., Ruuskanen, M., & Poulain, A. J. (2017). Ionic strength differentially affects the bioavailability of neutral and negatively charged inorganic Hg complexes. *Environmental science & technology*, *51*(17), 9653-9662.] Copyright [2017] American Chemical Society."

Direct link: https://pubs.acs.org/doi/10.1021/acs.est.7b01414

N.B. Supporting information for this chapter can be found in **Appendix B**

2.1 Abstract

Mercury (Hg) bioavailability to bacteria in marine systems is the first step toward its biomagnification in food webs. These systems exhibit high salinity and ionic strength that will both alter Hg speciation and properties of the bacteria cell walls. The role of Hg speciation on Hg bioavailability in marine systems has not been teased apart from that of ionic strength on cell wall properties, however. We developed and optimized a whole-cell Hg bioreporter capable of functioning under aerobic and anaerobic conditions and exhibiting no physiological limitations of signal production to changes in ionic strength. We show that ionic strength controls the bioavailability of Hg species, regardless of their charge, possibly by altering properties of the bacterial cell wall. The unexpected anaerobic bioavailability of negatively charged halocomplexes may help explain Hg methylation in marine systems such as the oxygen-deficient zone in the oceanic water column, sea ice or polar snow.

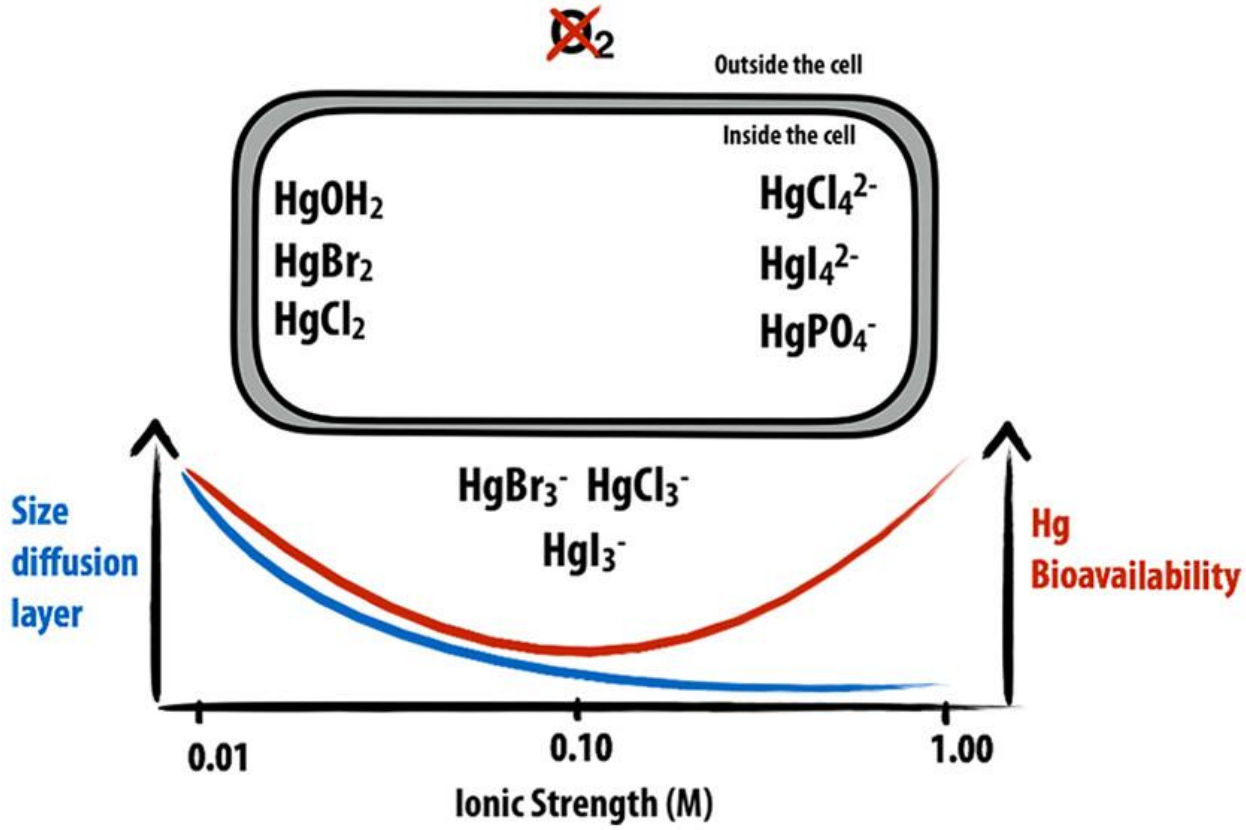

2.2 Introduction

Mercury (Hg) is a global pollutant and its bioavailability to Hg methylating bacteria is the first step toward its biomagnification through food webs [1]. Hg methylation requires (i) the species of mercury to be bioavailable [2-6] and (ii) for the cell to be physiologically capable of methylating mercury [7-9]. Mercury never exists as a free ion under microbial physiologically relevant conditions due to its high degree of covalency [10-12,] and understanding how its speciation in solution affects uptake is important to predict its fate in microbial systems.

As marine ecosystems host some of the largest food webs on the planet, it is important to understand how Hg can enter microbial cells at the high ionic strength representative of

seawater; indeed, ionic strength plays a major role in the ability of metal complexes to interact with microbial cell walls and yet, very few studies have specifically addressed the role of ionic strength on Hg uptake.

Whereas it is widely accepted that mercury is methylated under sulfidogenic conditions where sulfide and dissolved organic matter (DOM) will control its speciation [13], recent studies have shown that mercury could be methylated in polar environments such as snow [14], Antarctic sea ice [15] or in the open ocean water column [16-18]. Such environments can exhibit low oxygen concentrations and host anaerobic metabolisms but not necessarily host conditions conducive to sulfate reduction [19]; they do exhibit high chloride concentrations, however. At these low DOM and sulfide concentrations, especially for that in seawater, Hg is predicted to also exist as negatively charged mercury chlorocomplexes [13,20-23].

Chloride complexation can decrease the bioavailability of mercury with $HgCl_3^-$ and $HgCl_4^{2-}$ species postulated to be incompatible with Hg uptake when investigated aerobically [2,24]. It is predicted that these negatively charged species are unlikely to be relevant for biological uptake in the open ocean as concentrations of reduced thiols, an important ligand for mercury, vastly outnumber [Hg^{II}] [25], although this remains to be empirically tested. Furthermore, studies have shown that high levels of total (i.e., μM range) and bioavailable mercury can be observed in marine systems, such as after atmospheric mercury depletion events (AMDE), typically observed during springtime [26,27]. During AMDE and subsequently, during snowmelt, high levels of Hg^{II} often coexist with high concentrations of halides and other major ions, particularly over sea ice. The bioavailability of mercury during this spring period of greater productivity and vulnerability for polar ecosystems remains to be further assessed. In marine environments, the most abundant anaerobic mercury methylators (i.e., sulfate-reducing bacteria) require elevated ionic strength for

optimal physiological activity where these negatively charged Hg-chloride species are also be predicted to be present [8]. Marine environments also exhibit elevated sulfate concentrations that are known to increase methylation rates as sulfate is used directly by sulfate-reducing bacteria as a terminal electron acceptor to produce energy [9,28].

Clearly, there is a need to clarify the role of halides in general and chloride in particular as a key ligand in marine systems and decouple it from the effect that ionic strength can have on mercury bioavailability under anoxic conditions.

Current Hg biosensing approaches that are employed to evaluate the bioavailability of Hg species either depend on the presence of oxygen as a cofactor to produce a signal or are not viable under highly saline conditions (>0.3 M), making anaerobic detection of Hg bioavailability at salinity relevant to that of seawater where methylation happens [4,5,29]. Hg methylation is an anaerobic process and mechanistic studies investigating Hg uptake focused on (i) methylation as an outcome of uptake or (ii) ICP-MS mass balance [9,30-33]. Our insights into the mechanisms of Hg uptake anaerobically have been very limited due to the unavailability of biosensing tools capable of evaluating Hg bioavailability anaerobically.

In this study, we developed an oxygen-independent bioreporter for mercury that can operate from fresh to highly saline conditions. We discuss the role of ionic strength on Hg uptake, the relevance of considering anionic Hg complexes as bioavailable species, and propose a mechanism for the role of increasing salinity on Hg uptake.

2.3 Material and Methods

2.3.1 Plasmids and Bacterial Strains

The development of an anaerobic Hg bioreporter was made possible through flavin-based fluorescent proteins (FbFP) that can produce a fluorescent signal irrespective of the presence of oxygen. The PpFbFP gene for fluorescent protein as described in Drepper et al. (2007) [34] was commercially synthesized by Genscript, USA, fused to the *merR* gene, and cloned into pUC57 as pUC57merR-Pp (**A,** Genetic Constructs). To obtain a constitutive reporter of the protein, the PpFbFP gene sequence was amplified and ligated to a synthetic constitutive promoter (BBa_J23106 from the Registry of Standard Biological Parts) (generated by custom gene synthesis, Integrated DNA Technologies) in plasmid pUC19 to obtain pUC19AH206-Pp (**A,** Genetic Constructs). Expression of the PpFbFP genes are under the direct control of *merR*, a transcription regulator that is activated by intracellular Hg whereas a constitutive strain will express the PpFbFP protein regardless of the presence of Hg. The vectors pUC57merR-Pp and pUC19AH206-Pp were transformed into *Escherichia coli* NEB 5α and selected/maintained by growth in LB plate cultures in the presence of 210 μg mL^{-1} ampicillin, resistance to which is specified in pUC57/pUC19. Cells were grown in LB broth until logarithmic phase and resuspended into 50% glycerol solution at −80 °C for storage.

2.3.2 Aerobic and Anaerobic Bioassays

For both aerobic and anaerobic bioassays, all pipetting and manipulations of the exposure media were performed in an anaerobic chamber (97% $N_{2\,(g)}$ and 3–4% $H_{2\,(g)}$). Hg was diluted from a 5 μM stock solution prepared in 0.2 M HNO_3 (aerobically, final NO_3^- in exposure being 0.2 mM) or 8 μM stock solution in 0.2 M H_2SO_4 (anaerobically) to a 250 nM working solution in a 7 mL Teflon standard vial. The Hg stock concentrations were verified weekly using an MA-3000

mercury analyzer. Hg was added to exposure media (**A,** Media Recipes) and allowed to equilibrate in solution with its corresponding treatments for 1 h in 7 mL Teflon standard vials, prior to the addition of cells. Anaerobically, the exposure was optimized using 0.2 mM [NO_3^-] as a limiting electron acceptor. For all experiments, Hg concentration was set to 5 nM (i.e., as an intermediate value in the linear range of our calibration curve, Figure 2.1). For aerobic assays, once all preparations were completed, all the treatments were removed from the anaerobic chamber and were left to aerate on the benchtop prior to the addition of cells; anaerobic assays remained in the chamber. After 1 h, 100 μL of a cell stock solution was added to the exposure media. The protocols to grow *E. coli* NEB 5α aerobically and anaerobically to obtain a cell stock solution are detailed in the Supporting Information (**A,** Growth Protocols). After the addition of cells, all treatments in the Teflon standard vials were transferred to a 96 well nonbinding surface black plate with optically clear bottom for exposure in triplicate at 37 °C. Anaerobic fluorescence was measured using a Synergy HTX plate reader with a fluorescence excitation of 440/40 nm and an emission of 500/27 nm whereas aerobic fluorescence was measured using the Tecan Infinite Pro plate reader with a fluorescence excitation of 450/10 nm and an emission of 500/20 nm. OD_{600} was monitored in the plate readers to evaluate cell growth throughout the assay. Because PpFbFP does not absorb or emit at 600 nm and we did not expect it to skew the signal. For both aerobic and anaerobic assays, we set the plate readers to continuous shaking between measurements to prevent cell sedimentation. Details regarding the fluorescent calculations to appropriately design experimental templates are outlined in the **Appendix A** (**A,** Fluorescent Calculations).

2.3.3 Development of Exposure Media

One of the major limitations of phosphate buffers used in previous Hg bioassays is the inability to expose cells to divalent metals in association with Hg or alter the pH of the solution without changing Hg speciation. Phosphate will precipitate divalent metals in low concentrations, and through this process to also coprecipitate mercury [24,35-38]. However, chelating agents such as cysteine and EDTA make these metals soluble in the presence of phosphate [12,30] but will consequently alter Hg speciation. After calculating the solubilities of these metals based on a typical phosphate buffer for mercury exposure (Table **A2**), we designed an exposure solution using β-glycerophosphate that can be used as a source of phosphorus by bacterial cells while avoiding the precipitation of divalent metals [39,40]. Furthermore, the exposure medium allows for Hg to exist as $Hg(OH)_2$ over a wide range of pH (at 37 °C) allowing us to test for the influence of Hg adsorption on cell surface (Figure **A1**), while keeping its speciation constant. We used MOPS as a buffering agent, which does not form complexes either with Hg or with several other metals [41] at [MOPS] ≤ 100 mM [42], allowing us to eventually expand this bioassay protocol to other metals.

2.3.4 Thermodynamic Modeling

All thermodynamic modeling was performed using PHREEQC [43] with the thermoddem data set [44] for its extensive attention to Hg-chloride and Hg-phosphate speciation, while also correcting for temperature and ionic strength; all the data and calculation used can be found in Table **A1**: Thermodynamic Modeling. The database was modified to include the formation of $Hg(NH_3)_x^{+2}$, $HgBr_x^{2-x}$, HgI_x^{2-x}, $HgSO_4$ and $Hg(NO_3)_x^{2-x}$ complexes using data from the NIST 46 data set [45]. To appropriately calculate ionic strength, the database was modified to include the acid dissociation constants of MOPS and β-glycerophosphate [46]. There are currently no stability

constants available for Hg-β-glycerophosphate, but we predict based on Figure **A6** that this complex is unlikely to form relative to Cd and Zn.

2.3.5 Assays Over a Range of Halide and Phosphate Concentrations and Increasing Ionic Strength

We first tested the bioavailability of a full range of Hg-chloride species up to the chloride concentration of seawater; Hg species were determined by using a predictive Hg thermodynamic model [added NaCl] = 550 mM (Figure **A2)** under anaerobic and aerobic conditions.

Second, to decouple the role of chloride from that of ionic strength, we also changed the species of Hg according to phosphate, bromide and iodide gradients. Phosphate, bromide and iodide were used as an alternative inorganic anionic ligands. Sodium phosphate was prepared as a 1 M standard buffered at pH 6.7 (using a combination of Na_2HPO_4 and NaH_2PO_4 salts) to account for the dilution pH increase of phosphate buffer (all pH's in final exposure media were ca. 7). Sodium bromide and sodium iodide standard solutions were both prepared and stored anaerobically.

In a series of additional experiments, ionic strength in the exposure media was also increased through the addition of Na_2SO_4, which is not predicted to change Hg speciation, pH or provide any metabolic advantages or toxicity toward the cells. Na_2SO_4 was added as either a 2.5 or 1 M stock solution to the exposure medium while controlling for the Hg species being present as either neutral or negatively charged species. In all cases, Hg was allowed to equilibrate in exposure media in the 7 mL Teflon Vials for 1 h prior to the addition of cells.

2.3.6 Metal Competition with Zinc and Manganese

To test for the possibility of similar transport pathways for $Hg(OH)_2$ and negatively charged species predicted to form at high salinity, competition experiments were performed using Zinc (Zn) and Manganese (Mn). Indeed, Zn^{II} was used as a known competitor for Hg^{II} transport [12,30,47], whereas Mn^{II} was used as a nontoxic alternative to Zn, while maintaining a high affinity for the Zn transport systems in *E. coli* [48]. $ZnSO_4$ and $MnSO_4$ were prepared as standard solutions anaerobically in 10 mM H_2SO_4 (irrespective of the serial dilution). Metal competition was performed in exposure media with 0 or 550 mM added NaCl.

2.3.7 Influence of pH on Hg Bioavailability

Exposure media allowed to test for the role of pH while maintaining Hg speciation constant in solution (Figure **A1**). We titrated exposure media to the predicted pH using either 2.5 M NaOH or 5 M H_2SO4. The pH of the exposure medium amended with cells was also experimentally measured throughout the experiment to account for the cells' buffering capacity and to determine the actual exposure pH. Unfortunately, we did not test for the role of pH aerobically because pH did not remain constant over the 20 h exposure time required to monitor its effect on Hg uptake aerobically.

2.3.8 Optimization of the Bioassay Conditions

Anaerobically, we determined that a fluorescent end point could be efficiently achieved within few hours by limiting the concentration of our electron acceptor ($NO3^-$) (Figure **A5**) of which the biosensor was calibrated using 0.2 mM (Figure 2.1). By using the same fluorescence end point in both Hg-inducible and constitutive strains, we can effectively account for cell viability under anaerobic conditions and normalize our response signal accordingly (Figure 2.1). For all of our assays, we chose [Hg] = 5 nM as it was always within the linear range of the biosensor

response. As nitrate is the limiting highest energy-providing constituent in our bioreporter system, we anticipate that this protocol will also allow to evaluate the bioavailability of Hg in the presence of labile organic matter ligands that could be used as a source of energy by the bacteria.

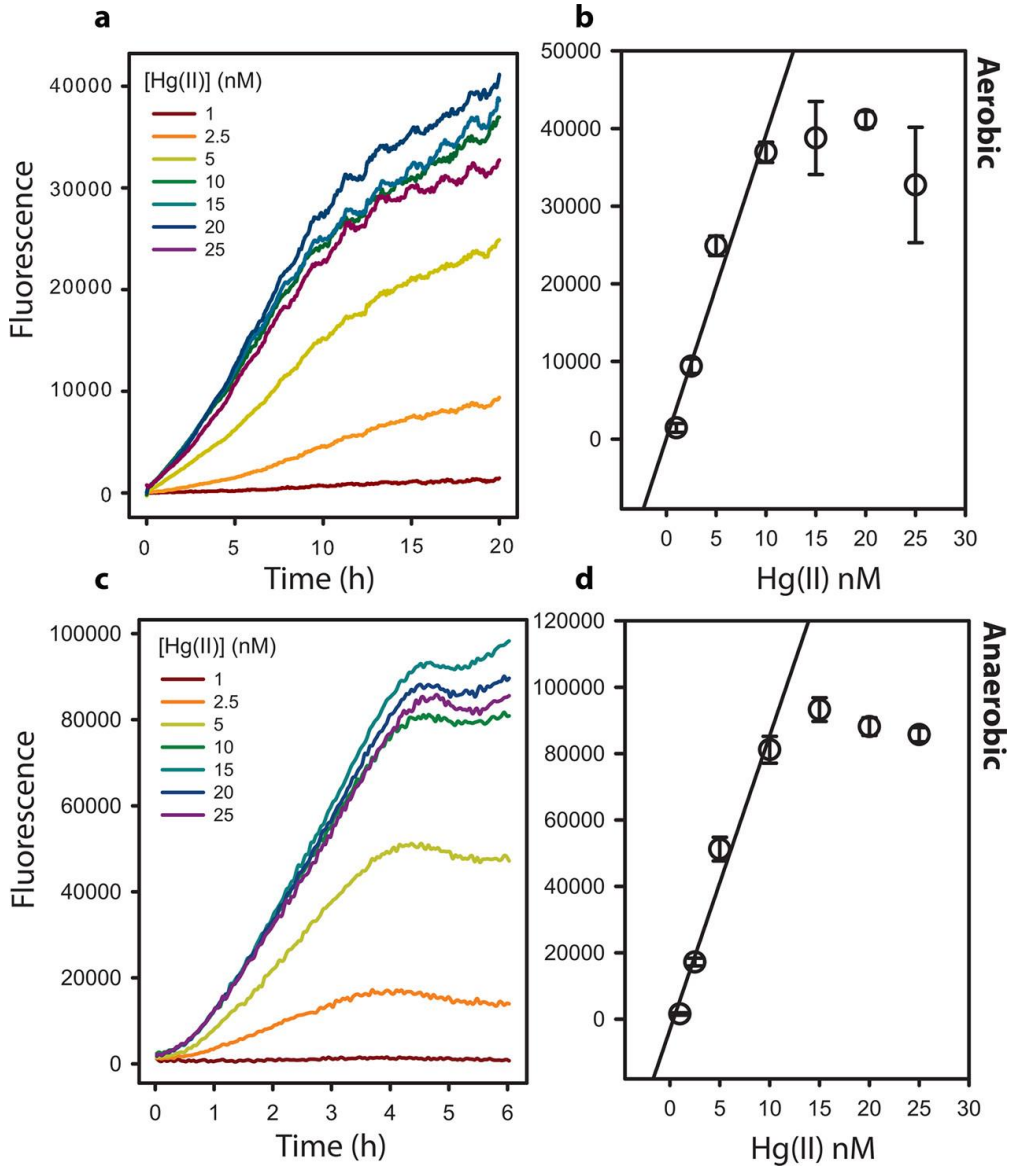

Figure 2.1: Calibration of Hg biosensor aerobically and on NO_3^-. reduction Fluorescence measured as fluorescence units ±1 SD emitted by *E. coli* NEB5α harboring the pUC57merR-Pp (Inducible strain) over time with the addition of Hg (0–25 nM) under aerobic (a, b) and anaerobic (c, d) conditions. [NO_3^-] was set to 0.2 mM. Fluorescence was the average of 3 technical replicates at 37 °C in exposure media. Hg speciation was 97% $Hg(OH)_2$, and 3% $Hg(NH_3)_2^{2+}$. Anaerobically (c,d) is a representation of 4 biological replicates and aerobically (a, b) of 4 biological replicates.

2.4 Results and Discussion

2.4.1 Bioavailability of Negatively Charged Chlorocomplexes

Chloride is a ubiquitous anion in the environment that complexes Hg^{II} but also contributes to the ionic strength of solution. We first tested the bioavailability of a range of Hg-chloride complexes that naturally occur. The bioreporter host, E. coli DH5α, has very high basal salt tolerance [49] and a strain constitutively expressing fluorescence did not exhibit limitations on signal production throughout the chloride gradient tested (Figure 2.2). Under anaerobic conditions, increasing chloride concentrations decreased Hg bioavailability up to [NaCl] = 150 mM, corresponding to the dominance of the $HgCl_3^-$ species (Figure 2.2, Figure **A2**). By further increasing NaCl concentrations up to the chloride concentration of seawater (550 mM), we observed an increase in bioavailability, corresponding to the dominance of $HgCl_4^{2-}$ (Figure 2.2). Increasing chloride concentration beyond 150 mM NaCl did not lead to an increase in aerobic Hg uptake (Figure 2.2).

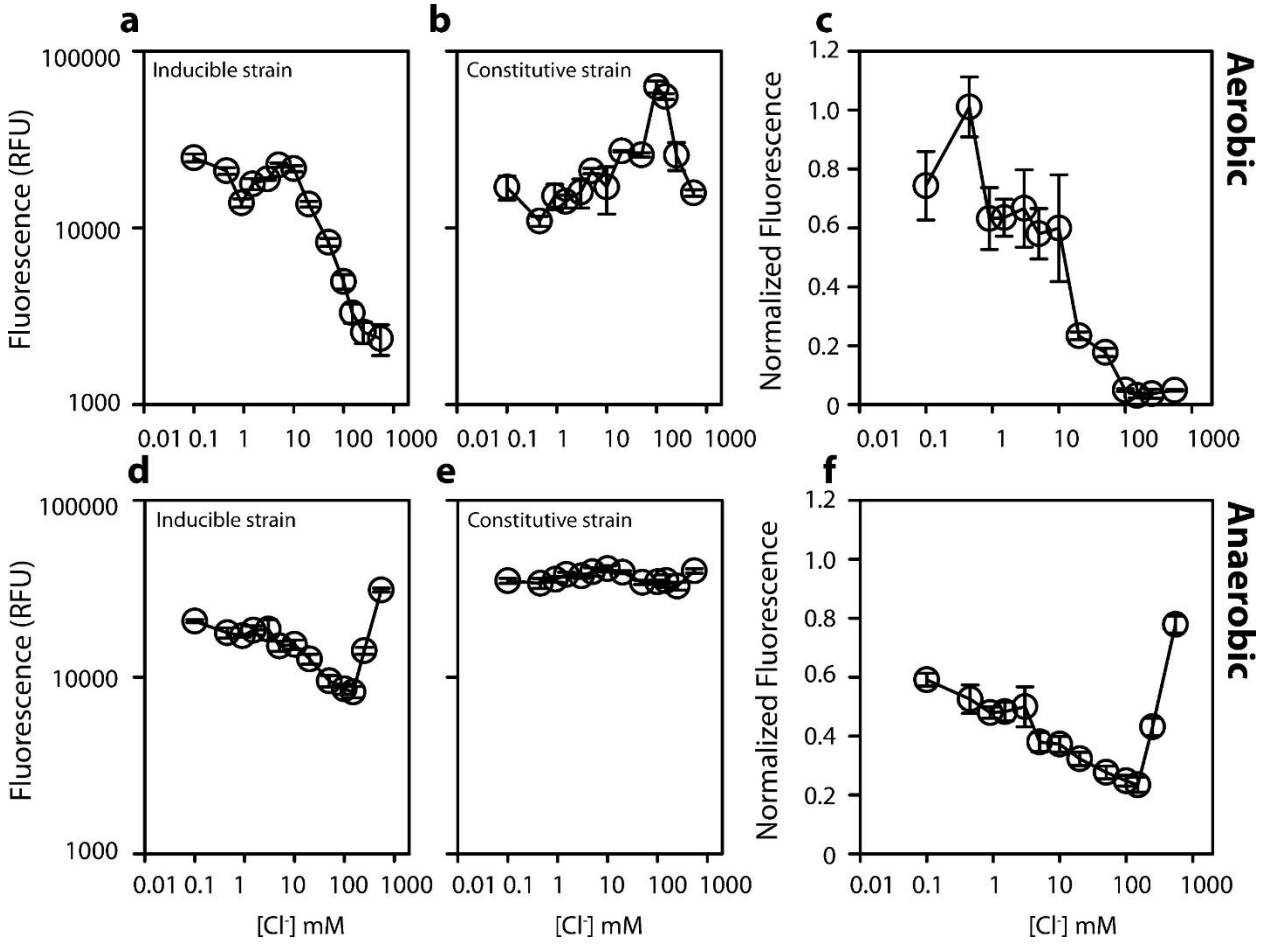

Figure 2.2: Chloride influence Hg bioavailability aerobically and anaerobically. complexation influences Maximum fluorescence measured as relative fluorescence units ±1 SD emitted by *E. coli* NEB5α harboring pUC57merR-Pp (Inducible strain, a and d) normalized (c and f) to the maximum fluorescence ±1 SD emitted by *E. coli* NEB5α harboring pUC19AH206-Pp (Constitutive strain, b and e) over a gradient of chloride (0.1–550 mM) under aerobic (a–c) and anaerobic (d–f) conditions. Chloride was added as NaCl, [Hg] was set to 5 nM and [NO_3^-] was set to 0.2 mM. Fluorescence was the average of 3 technical replicates at 37 °C in exposure media. Anaerobically is a representation of 3 biological replicates and aerobically of 2 biological replicates.

The enhanced Hg bioavailability with increasing ionic strength that we observed anaerobically differs from previous aerobic reports [2,50] and with our own data presented here. We suspect that membrane permeability and the nature of transporters involved in Hg uptake by *E. coli* are differentially affected under aerobic and anaerobic conditions [51,52] contrasting with previous reports with *Shewanella* [30], supporting the necessity to develop an anaerobic biosensor to evaluate Hg bioavailability in anoxic environments.

However, our results are consistent with previous experiments conducted with a known anaerobic methylator, *Desulfovibrio desulfuricans*, where increasing the salinity (NaCl) from 0.02 to 0.5 M, increased methylation rates [8]. In this latter study, enhanced methylation rates were attributed to the halophilic nature of the bacterium, suggesting that it required high salinity to be physiologically active for optimal Hg methylation. As *E. coli* is only halotolerant and not a halophile, it is unlikely that the increased Hg uptake was solely due to an improvement of the physiological state of the cell.

It has recently been reported that Hg^{II} can enter bacterial cells through Zn transporters [12,30,47]. To test whether negatively charged complexes predicted to be present in solution at high [Cl^-] would also enter the cells via Zn^{II} transporters, we performed competition experiments in a system that controlled for both neutral and negatively charged Hg species. At [NaCl] = 0 mM, we observed a decrease in the bioavailability of neutrally charged mercury species ($Hg(OH)_2$) in the presence of Zn^{II} and Mn^{II}, up to concentrations of 1 μM (Figure 2.3a). This data is in agreement with previous reports using Geobacter sulfurreducens and suggest that Hg^{II} and Zn^{II} compete at a transport site; our study also indicates that Mn^{II}, in addition to Zn^{II}, may compete at a transport site for Hg^{II} uptake. Due to Zn^{II} toxicity in our exposure medium at [Zn^{II}] > 1 μM (Figure 2.3a), we solely relied on Mn^{II} as a competitor at high salinity (Figure 2.3b). We

observed that at [NaCl] = 0 M, Hg^{II} uptake ($Hg(OH)_2$) was almost completely inhibited at [Mn^{II}] > 10 μM. However, at [NaCl] = 0.55 M, (coexistence of ca. 30% $HgCl_3^-$ and ca. 60% $HgCl_4^{2-}$), Mn^{II} did not negatively affect Hg bioavailability; an increase was even observed (Figure 2.3b). This data provides evidence that neutral Hg species and negatively charged chlorocomplexes such as $HgCl_4^{2-}$ have distinct mechanisms of transport into the cell. The biouptake of inorganic anions is not an issue for microbes. For instance, the trace element molybdenum (mostly present as MoO_4^{2-}) is essential for nearly all organisms and forms the catalytic center of a large variety of enzymes, particularly for anaerobic metabolism [53]. Further studies should aim at determining which anionic transporters are involved in Hg^{II} uptake.

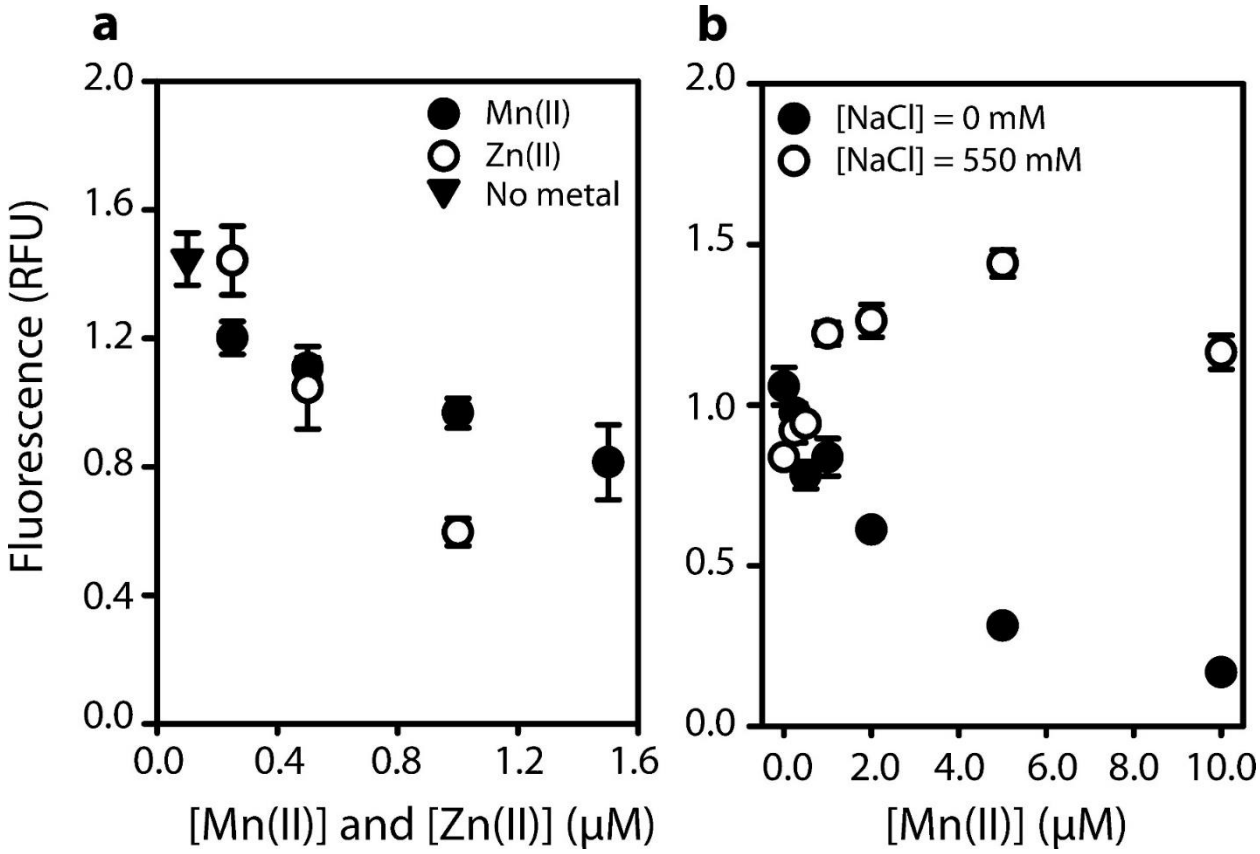

Figure 2.3. Zinc and Manganese competition on Hg bioavailability. Maximum fluorescence measured as relative fluorescence units ±1SD emitted by *E. coli* NEB5α harboring pUC57merR-Pp pUC57merR-Pp (inducible strain) normalized to the maximum fluorescence emitted by *E. coli* NEB5α harboring pUC19AH206-Pp (constitutive strain) (a) with the addition of Mn(II) and Zn (0–1.5 µM) under anaerobic conditions (b) with the addition of Mn(II) (0–10 µM) with and without 550 mM NaCl under anaerobic conditions. Chloride was added as NaCl, Mn(II) was added as $MnSO_4$ in 10 mM H_2SO_4, Zn was added as $ZnSO_4$ in 10 mM H_2SO_4 [Hg] was set to 5 nM and [NO_3^-] was set to 0.2 mM. Fluorescence was the average of 3 technical replicates at 37 °C in exposure media. This is a representation of 3 (a) and 2 (b) biological replicates.

2.4.2 Ionic Strength and Halide Concentrations Control Hg Species Bioavailability

As chloride concentrations increase, so does the ionic strength. This increase can affect Hg bioavailability in multiple ways, by affecting Hg speciation, but also by altering the biophysical and chemical properties of the cell wall. Changes in ionic strength influence all aspects of solutions but one notable influence on bacteria is how ionic strength affects the electrostatic

double layer surrounding the cell. This double layer is a universal feature of all bacterial surfaces, typically exhibiting negative surface potentials under neutral to basic pH (especially for *E. coli*) [54,55]. This negative potential forces a distribution of ions (positively charged being attracted and negatively charged being repelled) partly explaining why negatively charged Hg complexes are thought to be poorly bioavailable [2,56] through the process of anion-exclusion [57,58]. Our results indicate that anion-exclusion is likely not occurring for $HgCl_4^{2-}$; as such, we developed a series of experiments to dissociate ionic strength, anion-exclusion, and specific halides effects from the bioavailability of neutral and negatively charged Hg species.

It is well documented that increases in ionic strength severely compress the double layer of bacterial cells, from nanometers, at low ionic strength, to that of only a few ångströms at the ionic strength of seawater [59-61]. Beyond salt concentrations of 100–150 mM, the Debye screening length is <1 nm in all biological systems [61,62]. Under these conditions, electrostatic forces lose their dominance and processes fall into the domain of ion-specificity [61-63]. As such, at high ionic strength, the electrostatic double layer on the cell will be much less discriminative of charges and should allow enhanced uptake of anions.

In the next series of experiments, we tested the bioavailability of negatively charged Hg halides (Hg–Cl, Hg–Br, and Hg–I) as well as $HgPO_4^-$ because this species will exhibit different functional chemistry than a Hg-halide. Changing the ionic strength with halide or phosphate salts simultaneously alters Hg speciation and properties of the cell wall, making it difficult to tease apart the relative importance of these variables on Hg bioavailability. To adjust ionic strength without the confounding effects on Hg speciation, we used Na_2SO_4, which has a minimal impact on Hg speciation. Under these conditions, we tested the role of increasing ionic strength on the

bioavailability of neutral ($Hg(OH)_2$, $HgCl_2$, $HgBr_2$) and negatively charged ($HgPO_4^-$, $HgCl_3^-$, $HgCl_4^{2-}$, HgI_3^-, HgI_4^{2-}) species.

As ionic strength increased using phosphate and sulfate salts, we first observed a marked decrease in the bioavailability of $Hg(OH)^2$ and $HgPO_4^-$, up to $[SO_4^{2-}]$ = 50 mM (I = 171 mM) or $[PO_4^{3-}]$ = 5 mM (I = 54 mM) (Figure 2.4a). With increasing concentrations of phosphate in the media, speciation is favored toward the formation of $HgPO_4^-$ species (Figure **A3**). Beyond I = 200–300 mM, the bioavailability of both $Hg(OH)_2$ and $HgPO_4^-$ markedly increased. We observed the same enhanced uptake of $HgPO_4^-$ when ionic strength was controlled using SO_4^{2-}, independently of PO_4^{3-} levels (Figure 2.4c).

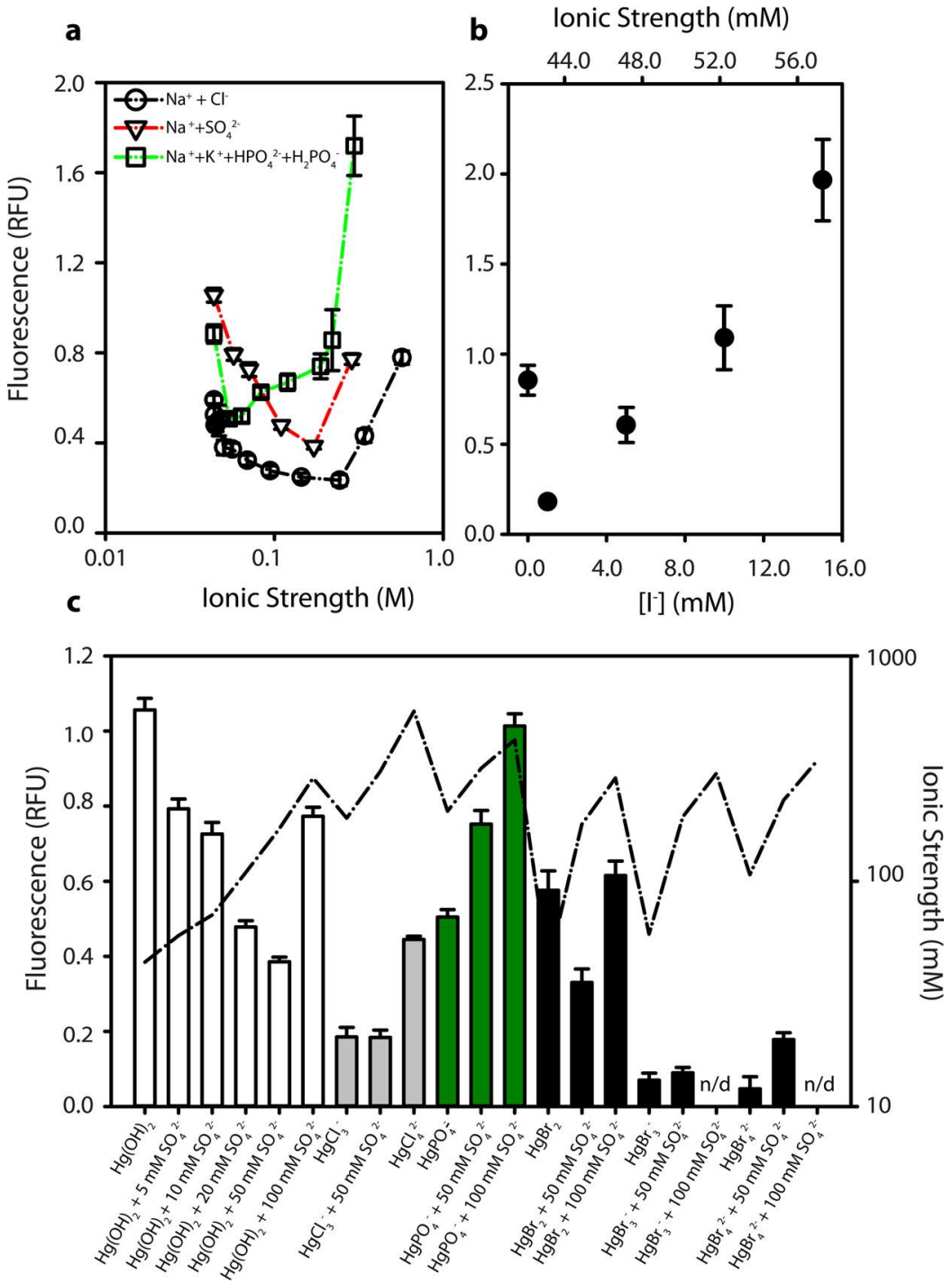

Figure 2.4: Ionic Strength and Iodide dynamically affect Hg bioavailability. Maximum fluorescence measured as relative fluorescence units ±1SD emitted by *E. coli* NEB5α harboring pUC57merR-Pp pUC57merR-Pp (inducible strain) normalized to the maximum fluorescence emitted by *E. coli* NEB5α harboring pUC19AH206-Pp (constitutive strain) (a) over an ionic strength gradient of induced by NaCl, Na_2SO_4 and $Na_{1.61}H_{1.39}PO_4$ under anaerobic conditions (b) over a gradient of I^- (0–15 mM) under anaerobic conditions or (c) with the specified Hg species distribution over variable ionic strengths (dot-dash line) under anaerobic conditions. Sulfate was added as Na_2SO_4, chloride as NaCl, bromide as NaBr, iodide as NaI and phosphate was added as sodium phosphate buffer for a final pH of 7. [Hg] was set to 5 nM and [NO_3^-] was set to 0.2 mM. Fluorescence was the average of 3 technical replicates at 37 °C in exposure media. This is a representation of 3 biological replicates.

We also tested for the bioavailability of Hg bromide and iodide species (Figure 2.4b,c). We first observed that the addition of $[SO_4^{2-}]$ = 50 mM (I = 179 mM) and $[SO_4^{2-}]$ = 100 mM (I = 287 mM) to neutral $HgBr_2$ species mirrored what we observed with $Hg(OH)_2$ (Figure 2.4c), with the greatest bioavailability at the highest $[SO_4^{2-}]$; note that in the presence of bromide, constitutive fluorescence emission by live cells declined as $[SO_4^{2-}]$ increased (data not shown). We previously showed that $HgCl_4^{2-}$ was more bioavailable than $HgCl_3^-$ (Figure 2.2f and Figure 2.4a) and observed the same trend for iodocomplexes (Figure 2.4b) but not for bromocomplexes (Figure 2.4c and Figure **A4**). Hg speciation rapidly changed with small increments in iodide addition and Hg iodocomplexes bioavailability rapidly increased with very little changed in ionic strength (Figure 2.4b). Changing the ionic strength while controlling for distribution of $HgCl_3^-$ or $HgBr^{3-}$ did not result in any change in bioavailability. Note that $HgCl_3^-$, HgI_3^-, $HgBr_3^-$ and $HgBr_4^{2-}$ were the least bioavailable species observed in this study, regardless of ionic strength.

These results suggest that increasing ionic strength differentially affects uptake of neutral and negatively charged Hg species, but not only as result of the compression of the double layer. The effect of ionic strength on Hg bioavailability is complex: on one end it might enable some negatively charged complexes to approach the cell membrane likely by limiting anionic-exclusion but on the other end, it also appears to temporarily limit the bioavailability of neutral Hg species. Increasing cation concentrations as ionic strength increases reduce the swelling of the LPS layer, forming a compressed structure around the cell with a high positive charge density [64-67]. These combined effects have been shown to inhibit the bioavailability of metals that remained positively charged in solution [54,64,68]. Contrary to many metals, Hg will never exist as a free cation in solution. Toxic (soft) metals that form inner-sphere sorption bonds (with N- or S-donor ligands) also exhibit decreased sorption with increasing ionic strength, not because of

electrostatic interactions, but instead through competition with the background electrolyte, changes in metal activity or decreasing access to the transport site [66]. We attempted to quantify the amount of Hg species sorbed onto the cell wall at varying ionic strength to assess whether the extent of sorption was related to the amount of bioavailable Hg. We observed that sorption of $Hg(OH)_2$ to the cell surface increased by 20% with the addition of 100 mM SO_4^{2-} (Figure **A7**); we also observed that the least sorption was observed when $HgCl_3^-$ is predicted to form (ca. 25% sorbed) and that no differences were observed between $Hg(OH)_2$ and $HgCl_4^{2-}$, which sorbed to the same extent on the cell wall (ca. 40% sorbed). These data support that sorption may be a first step in the uptake of Hg^{II}, most likely by localizing Hg near transport sites. This is also consistent with $HgCl_3^-$ having the lowest bioavailability relative to $HgCl_4^{2-}$ and $Hg(OH)_2$. That being said, it is likely that not all cell wall moieties behave conservatively with respect to Hg binding as ionic strength increases, and further detailed sorption studies are warranted to evaluate to which moieties do neutrally or negatively charged Hg species bind.

2.4.3 Changes in pH Alter Cell Wall Properties and Control Hg Bioavailability

Finally, we induced compression of the electrical double layer while only minimally affecting ionic strength (without the addition of the background electrolyte) by decreasing the pH; a decrease in pH shifts the overall charge of the cell (from −50 to −30 mV (pH 9 to 4) specific for *E. coli* [69]) affecting the double layer size but also protonates functional sites [54,63]. Over the pH gradient, Hg speciation was kept constant as the neutrally charged $Hg(OH)_2$ (Figure **A1**).

At the high pH (8.7) and low ionic strength tested, soft ligands such as amines are predominantly deprotonated and we can predict that they will irreversibly bind neutral Hg species via inner-sphere complexes formation, preventing their uptake; indeed, this is the pH at which Hg bioavailability was the lowest (Figure 2.5a,c). When pH decreased from 8.7 to 5, Hg

bioavailability increased by an order of magnitude while exhibiting little effect on the signal production of the constitutive reporter (Figure 2.5b). These results are in line with previous experiments performed with *E. coli* anaerobically [5]. As pH decreases, cell wall functional groups will become protonated, such as carboxyl ($1.7 < pK_a < 4.7$), phosphate ($6.1 < pK_a < 6.8$) and amine ($9 < pK_a < 13$) [54]. These functional sites, particularly carboxyl and phosphate, have been shown to reversibly sorb Hg on membranes [42,70,71]. Although protons usually compete with divalent metals for binding sites onto the cell membrane [54], this is not the case for $Hg(OH)_2$, which sorption onto these cell wall functional groups actually increases as pH decreases (from 10 to 4) [67,70]. To maximize uptake, it is most likely that sorption is reversible (e.g., onto carboxylic and phosphonate groups). Indeed, irreversible binding of Hg onto sulfhydryl groups is independent of the cell surface's pH [70] and is expected to immobilize Hg^{II} onto the cell wall [72].

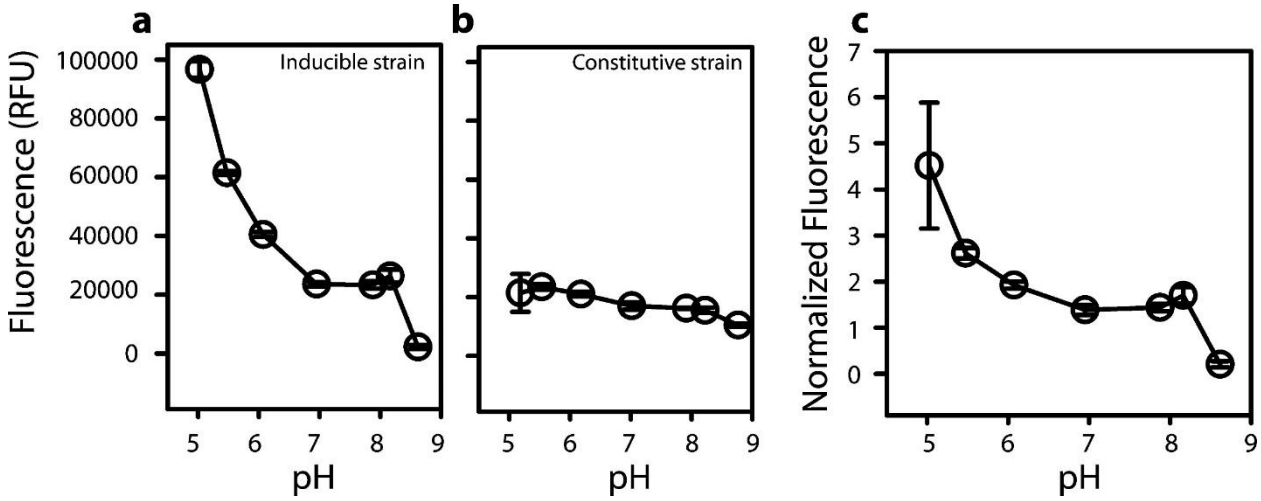

Figure 2.5: Influence of pH on Hg bioavailability. Maximum fluorescence measured as relative fluorescence units ±1 SD (c) emitted by *E. coli* NEB5α harboring pUC57merR-Pp (inducible strain, a) normalized to the maximum fluorescence emitted by *E. coli* NEB5α harboring pUC19AH206-Pp (constitutive strain, b) over a pH gradient (≈5–8.7) under anaerobic conditions. pH was adjusted through the addition of H_2SO_4 or NaOH and was monitored using a pH probe after the addition of cells, [Hg] was set to 5 nM and [NO_3^-] was set to 0.2 mM. Fluorescence was the average of 3 technical replicates at 37 °C in exposure media. This is a representation of 2 biological replicates.

Our work with the biosensor shows that Hg bioavailability increases under conditions that promote Hg sorption onto the cell wall, as supported by other studies [5]. Together, these data suggest that reversible binding of Hg onto the cell wall is an important, but not necessary, step in Hg uptake. This reversible binding may contribute to the formation of an extracellular pool of bioavailable Hg that can become accessible to transporters, as previously shown by studying the fractionation of stable Hg isotopes in the presence of microbial cells [73].

Several processes affect Hg uptake, including (i) transport through the double layer, (ii) the ability to reversibly sorb to the membrane and (iii) ability of the transporter to internalize the Hg complex. What our results show is that both electrostatic interactions and changes in the biophysical properties of the bacterial cell wall affect Hg uptake. We posit that increasing ionic strength favors access of Hg complexes to the bacterial membrane, either because (i) it limits

electrostatic repulsion of anions, (ii) reveals previously unavailable paths toward transport sites enabling facilitated uptake or (iii) allows access to regions of the lipid bilayer that offer a preferential route for passive diffusion.

2.4.4 Extending to the Environment

Our results revealed the bioavailability of negatively charged mercury complexes and also the importance to consider the ionic strength in affecting membrane properties in controlling Hg species uptake, regardless of their charge. Our findings contribute to explain why recent studies have shown that mercury could be methylated in polar environments such as snow [14], Antarctic sea ice [15] or in the open ocean water column [16-18], where chloride ions can compete with organic ligands for Hg complexation [74]. Such environments can exhibit low oxygen and high chloride concentrations and host anaerobic metabolisms but not necessarily conditions conducive to sulfate reduction [19]. Whereas sulfate reducers are arguably the most metabolically efficient mercury methylators, significant methylation can occur with other microbial guilds; Hg methylation is expected to increase, should environmental conditions favor Hg uptake. This is important because the open sea methylation in the water column is as important, if not more, than benthic methylation with respect to accumulation in ocean fish [75]. To improve modeling efforts of Hg bioaccumulation in marine systems, we suggest that it is important to consider the bioavailability of negatively charged Hg complexes.

2.5 Acknowledgments

We thank members of the Poulain Lab for insightful feedbacks. We acknowledge the comments of anonymous reviewers which contributed to improve the quality of this work. An Early Researcher Award from the Province of Ontario and a Discovery Grant and an accelerator

supplement from the Natural Sciences and Engineering Research Council of Canada to A.J.P.

funded this study.

2.6 References

1. Futsaeter, G.; Wilson, S. The UNEP Global Mercury Assessment: Sources, Emissions and Transport E3S Web of Conferences **2013**, 1, 36001 DOI: 10.1051/e3sconf/20130136001

2. Barkay, T.; Gillman, M.; Turner, R. R. Effects of dissolved organic carbon and salinity on bioavailability of mercury Appl. Environ. Microbiol. **1997**, 63 (11) 4267– 4271

3. Ndu, U.; Mason, R. P.; Zhang, H.; Lin, S.; Visscher, P. T. Effect of inorganic and organic ligands on the bioavailability of methylmercury as determined by using a mer-lux bioreporter Appl. Environ. Microbiol. **2012**, 78 (20) 7276– 7282 DOI: 10.1128/AEM.00362-12

4. Golding, G. R.; Kelly, C. A.; Sparling, R.; Loewen, P. C.; Rudd, J. W. M.; Barkay, T. Evidence for facilitated uptake of Hg(II) by Vibrio anguillarum and Escherichia coli under anaerobic and aerobic conditions Limnol. Oceanogr. **2002**, 47 (4) 967– 975 DOI: 10.4319/lo.2002.47.4.0967

5. Golding, G. R.; Sparling, R.; Kelly, C. A. Effect of pH on intracellular accumulation of trace concentrations of Hg(II) in Escherichia coli under anaerobic conditions, as measured using a mer-lux bioreporter Appl. Environ. Microbiol. **2008**, 74 (3) 667– 675 DOI: 10.1128/AEM.00717-07

6. Chiasson-Gould, S. A.; Blais, J. M.; Poulain, A. J. Dissolved Organic Matter Kinetically Controls Mercury Bioavailability to Bacteria Environ. Sci. Technol. **2014**, 48 (6) 3153– 3161 DOI: 10.1021/es4038484

7. Compeau, G.; Bartha, R. Sulfate-reducing bacteria: principal methylators of mercury in anoxic estuarine sediment Appl. Environ. Microbiol. **1985**, 50 (2) 498– 502

8. Compeau, G. C.; Bartha, R. Effect of salinity on mercury-methylating activity of sulfate-reducing bacteria in estuarine sediments Appl. Environ. Microbiol. **1987**, 53 (2) 261– 265

9. Gilmour, C. C.; Henry, E. A.; Mitchell, R. Sulfate stimulation of mercury methylation in freshwater sediments Environ. Sci. Technol. **1992**, 26 (11) 2281– 2287 DOI: 10.1021/es00035a029

10. Slaveykova, V. I.; Wilkinson, K. J. Predicting the bioavailability of metals and metal complexes: Critical review of the biotic ligand model Environmental Chemistry **2005**, 2 (1) 9– 24 DOI: 10.1071/EN04076

11. Kinraide, T. B. Improved scales for metal ion softness and toxicity Environ. Toxicol. Chem. **2009**, 28 (3) 525– 533 DOI: 10.1897/08-208.1

12. Schaefer, J. K.; Szczuka, A.; Morel, F. M. M. Effect of Divalent Metals on Hg(II) Uptake and Methylation by Bacteria Environ. Sci. Technol. **2014**, 48 (5) 3007– 3013 DOI: 10.1021/es405215v

13. Liu, G.; Cai, Y.; O'Driscoll, N. Environmental chemistry and toxicology of mercury; John Wiley & Sons: Hoboken, NJ, 2011.

14. Larose, C.; Dommergue, A.; De Angelis, M.; Cossa, D.; Averty, B.; Marusczak, N.; Soumis, N.; Schneider, D.; Ferrari, C. Springtime changes in snow chemistry lead to new insights into mercury methylation in the Arctic Geochim. Cosmochim. Acta **2010**, 74 (22) 6263– 6275 DOI: 10.1016/j.gca.2010.08.043

15. Gionfriddo, C. M.; Tate, M. T.; Wick, R. R. Microbial mercury methylation in Antarctic sea ice Nat. Microbiol. **2016**, 1 (10) 16127 DOI: 10.1038/nmicrobiol.2016.127

16. Cossa, D.; Durrieu de Madron, X.; Schäfer, J.; Lanceleur, L.; Guédron, S.; Buscail, R.; Thomas, B.; Castelle, S.; Naudin, J.-J. The open sea as the main source of methylmercury in the water column of the Gulf of Lions (Northwestern Mediterranean margin) Geochim. Cosmochim. Acta **2017**, 199, 222– 237 DOI: 10.1016/j.gca.2016.11.037

17. Driscoll, C. T.; Mason, R. P.; Chan, H. M.; Jacob, D. J.; Pirrone, N. Mercury as a Global Pollutant: Sources, Pathways, and Effects Environ. Sci. Technol. **2013**, 47 (10) 4967– 4983 DOI: 10.1021/es305071v

18. Braune, B.; Chételat, J.; Amyot, M.; Brown, T.; Clayden, M.; Evans, M.; Fisk, A.; Gaden, A.; Girard, C.; Hare, A.; Kirk, J.; Lehnherr, I.; Letcher, R.; Loseto, L.; Macdonald, R.; Mann, E.; McMeans, B.; Muir, D.; O'Driscoll, N.; Poulain, A.; Reimer, K.; Stern, G. Mercury in the marine environment of the Canadian Arctic: Review of recent findings Sci. Total Environ. **2015**, 509–510, 67– 90 DOI: 10.1016/j.scitotenv.2014.05.133

19. Gilmour, C. C.; Podar, M.; Bullock, A. L.; Graham, A. M.; Brown, S. D.; Somenahally, A. C.; Johs, A.; Hurt, R. A.; Bailey, K. L.; Elias, D. A. Mercury Methylation by Novel Microorganisms from New Environments Environ. Sci. Technol. **2013**, 47 (20) 11810– 11820 DOI: 10.1021/es403075t

20. Zhong, H.; Wang, W.-X. Controls of Dissolved Organic Matter and Chloride on Mercury Uptake by a Marine Diatom Environ. Sci. Technol. **2009**, 43 (23) 8998– 9003 DOI: 10.1021/es901646k

21. Skyllberg, U. Chemical speciation of mercury in soil and sediment Environmental chemistry and toxicology of mercury **2012**, 219– 258 DOI: 10.1002/9781118146644.ch7

22. Han, S.; Narasingarao, P.; Obraztsova, A.; Gieskes, J.; Hartmann, A. C.; Tebo, B. M.; Allen, E. E.; Deheyn, D. D. Mercury Speciation in Marine Sediments under Sulfate-Limited Conditions Environ. Sci. Technol. **2010**, 44 (10) 3752– 3757 DOI: 10.1021/es903112m

23. Gworek, B.; Bemowska-Kałabun, O.; Kijeńska, M.; Wrzosek-Jakubowska, J. Mercury in Marine and Oceanic Waters—a Review Water, Air, Soil Pollut. **2016**, 227 (10) 1– 19 DOI: 10.1007/s11270-016-3060-3

24. Daguené, V.; McFall, E.; Yumvihoze, E.; Xiang, S.; Amyot, M.; Poulain, A. J. Divalent Base Cations Hamper HgII Uptake Environ. Sci. Technol. **2012**, 46 (12) 6645– 6653 DOI: 10.1021/es300760e

25. Swarr, G. J.; Kading, T.; Lamborg, C. H.; Hammerschmidt, C. R.; Bowman, K. L. Dissolved low-molecular weight thiol concentrations from the U.S. GEOTRACES North Atlantic Ocean zonal transect Deep Sea Res., Part I **2016**, 116, 77– 87 DOI: 10.1016/j.dsr.2016.06.003

26. Douglas, T. A.; Loseto, L. L.; MacDonald, R. W.; Outridge, P.; Dommergue, A.; Poulain, A.; Amyot, M.; Barkay, T.; Berg, T.; Chetelat, J.; Constant, P.; Evans, M.; Ferrari, C.; Gantner, N.; Johnson, M. S.; Kirk, J.; Kroer, N.; Larose, C.; Lean, D.; Nielsen, T. G.; Poissant, L.; Rognerud, S.; Skov, H.; Sørensen, S.; Wang, F.; Wilson, S.; Zdanowicz, C. M. The fate of mercury in Arctic terrestrial and aquatic ecosystems, a review Environmental Chemistry **2012**, 9 (4) 321– 355 DOI: 10.1071/EN11140

27. Lindberg, S. E.; Brooks, S.; Lin, C. J.; Scott, K. J.; Landis, M. S.; Stevens, R. K.; Goodsite, M.; Richter, A. Dynamic Oxidation of Gaseous Mercury in the Arctic Troposphere at Polar Sunrise Environ. Sci. Technol. **2002**, 36 (6) 1245– 1256 DOI: 10.1021/es0111941

28. Johnson, W. P.; Swanson, N.; Black, B.; Rudd, A.; Carling, G.; Fernandez, D. P.; Luft, J.; Van Leeuwen, J.; Marvin-DiPasquale, M. Total- and methyl-mercury concentrations and methylation rates across the freshwater to hypersaline continuum of the Great Salt Lake, Utah, USA Sci. Total Environ. **2015**, 511, 489– 500 DOI: 10.1016/j.scitotenv.2014.12.092

29. Golding, G. R.; Kelly, C. A.; Sparling, R.; Loewen, P. C.; Barkay, T. Evaluation of mercury toxicity as a predictor of mercury bioavailability Environ. Sci. Technol. **2007**, 41 (16) 5685– 92 DOI: 10.1021/es070138i

30. Szczuka, A.; Morel, F. M. M.; Schaefer, J. K. Effect of Thiols, Zinc, and Redox Conditions on Hg Uptake in Shewanella oneidensis Environ. Sci. Technol. **2015**, 49 (12) 7432– 7438 DOI: 10.1021/acs.est.5b00676

31. Graham, A. M.; Bullock, A. L.; Maizel, A. C.; Elias, D. A.; Gilmour, C. C. Detailed assessment of the kinetics of Hg-cell association, Hg methylation, and methylmercury degradation in several Desulfovibrio species Applied and environmental microbiology **2012**, 78 (20) 7337– 7346 DOI: 10.1128/AEM.01792-12
32. Graham, A. M.; Aiken, G. R.; Gilmour, C. C. Dissolved Organic Matter Enhances Microbial Mercury Methylation Under Sulfidic Conditions Environ. Sci. Technol. **2012**, 46 (5) 2715– 2723 DOI: 10.1021/es203658f

33. Zhang, T.; Kim, B.; Levard, C.; Reinsch, B. C.; Lowry, G. V.; Deshusses, M. A.; Hsu-Kim, H. Methylation of mercury by bacteria exposed to dissolved, nanoparticulate, and microparticulate mercuric sulfides Environ. Sci. Technol. **2012**, 46 (13) 6950– 8 DOI: 10.1021/es203181m

34. Drepper, T.; Eggert, T.; Circolone, F.; Heck, A.; Krauß, U.; Guterl, J.-K.; Wendorff, M.; Losi, A.; Gärtner, W.; Jaeger, K.-E. Reporter proteins for in vivo fluorescence without oxygen Nat. Biotechnol. **2007**, 25 (4) 443– 445 DOI: 10.1038/nbt1293

35. Oliva, J.; De Pablo, J.; Cortina, J.-L.; Cama, J.; Ayora, C. Removal of cadmium, copper, nickel, cobalt and mercury from water by Apatite II: Column experiments J. Hazard. Mater. **2011**, 194, 312– 323 DOI: 10.1016/j.jhazmat.2011.07.104

36. Dunham-Cheatham, S.; Rui, X.; Bunker, B.; Menguy, N.; Hellmann, R.; Fein, J. The effects of non-metabolizing bacterial cells on the precipitation of U, Pb and Ca phosphates Geochim. Cosmochim. Acta **2011**, 75 (10) 2828– 2847 DOI: 10.1016/j.gca.2011.02.030

37. Martinez, R. J.; Beazley, M. J.; Sobecky, P. A. Phosphate-Mediated Remediation of Metals and Radionuclides Adv. Ecol. **2014**, 2014, 1 DOI: 10.1155/2014/786929

38. Kim, Y.; Lee, Y. J. Characterization of mercury sorption on hydroxylapatite: Batch studies and microscopic evidence for adsorption J. Colloid Interface Sci. **2014**, 430, 193– 199 DOI: 10.1016/j.jcis.2014.05.028

39. Hurdebise, Q.; Tarayre, C.; Fischer, C.; Colinet, G.; Hiligsmann, S.; Delvigne, F. Determination of Zinc, Cadmium and Lead Bioavailability in Contaminated Soils at the Single-Cell Level by a Combination of Whole-Cell Biosensors and Flow Cytometry Sensors **2015**, 15 (4) 8981– 8999 DOI: 10.3390/s150408981

40. Selim, H. M. Phosphate in Soils: Interaction with Micronutrients, Radionuclides and Heavy Metals; CRC Press: Boca Raton, FL, 2015; Vol. 2.

41. Ferreira, C. M. H.; Pinto, I. S. S.; Soares, E. V.; Soares, H. M. V. M (Un)suitability of the use of pH buffers in biological, biochemical and environmental studies and their interaction with metal ions-a review RSC Adv. **2015**, 5 (39) 30989– 31003 DOI: 10.1039/C4RA15453C

42. Delnomdedieu, M.; Boudou, A.; Georgescauld, D.; Dufourc, E. J. Specific interactions of mercury chloride with membranes and other ligands as revealed by mercury-NMR Chem.-Biol. Interact. **1992**, 81 (3) 243– 269 DOI: 10.1016/0009-2797(92)90081-U

43. Parkhurst, D. L. a. Description of input and examples for PHREEQC version 3–a computer program for speciation, batch-reaction, one-dimensional transport, and inverse geochemical calculations; U.S. Department of the Interior, U.S. Geological Survey: Reston, VA, 2013.

44. Blanc, P.; Lassin, A.; Piantone, P.; Azaroual, M.; Jacquemet, N.; Fabbri, A.; Gaucher, E. C. Thermoddem: A geochemical database focused on low temperature water/rock interactions and waste materials Appl. Geochem. **2012**, 27 (10) 2107– 2116 DOI: 10.1016/j.apgeochem.2012.06.002

45. Smith, R.; Martell, A.; Motekaitis, R. NIST standard reference database 46. NIST Critically Selected Stability Constants of Metal Complexes Database, Version 8; National Institute of Standards and Technology: Gaithersburg, MD, 2004.

46. Goldberg, R. N.; Kishore, N.; Lennen, R. M. Thermodynamic quantities for the ionization reactions of buffers J. Phys. Chem. Ref. Data **2002**, 31 (2) 231– 370 DOI: 10.1063/1.1416902

47. Schaefer, J. K.; Rocks, S. S.; Zheng, W.; Liang, L.; Gu, B.; Morel, F. M. M. Active transport, substrate specificity, and methylation of Hg(II) in anaerobic bacteria Proc. Natl. Acad. Sci. U. S. A. **2011**, 108 (21) 8714– 8719 DOI: 10.1073/pnas.1105781108

48. Porcheron, G.; Garénaux, A.; Proulx, J.; Sabri, M.; Dozois, C. M. Iron, copper, zinc, and manganese transport and regulation in pathogenic Enterobacteria: correlations between strains, site of infection and the relative importance of the different metal transport systems for virulence Front. Cell. Infect. Microbiol. **2013**, 3, 90 DOI: 10.3389/fcimb.2013.00090

49. Joshi, A.; Dang, H. Q.; Vaid, N.; Tuteja, N. Isolation of high salinity stress tolerant genes from Pisum sativum by random overexpression in Escherichia coli and their functional validation Plant Signaling Behav. **2009**, 4 (5) 400– 412 DOI: 10.4161/psb.4.5.8387

50. Solovyev, A.; Kuncova, G.; Demnerova, K. Whole-cell optical biosensor for mercury — operational conditions in saline water Chemical Papers **2015**, 69 (1) 183– 191 DOI: 10.1515/chempap-2015-0009

51. Salmon, K.; Hung, S. P.; Mekjian, K.; Baldi, P.; Hatfield, G. W.; Gunsalus, R. P. Global gene expression profiling in Escherichia coli K12: The effects of oxygen availability and FNR J. Biol. Chem. **2003**, 278 (32) 29837– 29855 DOI: 10.1074/jbc.M213060200

52. Salmon, K. A.; Hung, S. P.; Steffen, N. R.; Krupp, R.; Baldi, P.; Hatfield, G. W.; Gunsalus, R. P. Global gene expression profiling in Escherichia coli K12: Effects of

oxygen availability and ArcA J. Biol. Chem. **2005**, 280 (15) 15084– 15096 DOI: 10.1074/jbc.M414030200

53. Schwarz, G.; Mendel, R. R.; Ribbe, M. W. Molybdenum cofactors, enzymes and pathways Nature **2009**, 460 (7257) 839– 847 DOI: 10.1038/nature08302

54. Macek, T. Microbial Biosorption of Metals; Springer Netherlands: Dordrecht, The Netherlands, 2011.

55. Walker, S. L.; Redman, J. A.; Elimelech, M. Role of Cell Surface Lipopolysaccharides in Escherichia c oli K12 Adhesion and Transport Langmuir **2004**, 20 (18) 7736– 7746 DOI: 10.1021/la049511f

56. Boyd, E. S.; Yu, R. Q.; Barkay, T.; Hamilton, T. L.; Baxter, B. K.; Naftz, D. L.; Marvin-DiPasquale, M. Effect of salinity on mercury methylating benthic microbes and their activities in Great Salt Lake, Utah Sci. Total Environ. **2017**, 581-582, 495– 506 DOI: 10.1016/j.scitotenv.2016.12.157

57. Bresler, E. Anion Exclusion and Coupling Effects in Nonsteady Transport Through Unsaturated Soils: I. Theory1 Soil Science Society of America Journal **1973**, 37 (5) 663– 669 DOI: 10.2136/sssaj1973.03615995003700050013x

58. Hassanin, M.; Kerek, E.; Chiu, M.; Anikovskiy, M.; Prenner, E. J. Binding Affinity of Inorganic Mercury and Cadmium to Biomimetic Erythrocyte Membranes J. Phys. Chem. B **2016**, 120 (50) 12872– 12882 DOI: 10.1021/acs.jpcb.6b10366

59. Poortinga, A. T.; Bos, R.; Norde, W.; Busscher, H. J. Electric double layer interactions in bacterial adhesion to surfaces Surf. Sci. Rep. **2002**, 47 (1) 1– 32 DOI: 10.1016/S0167-5729(02)00032-8

60. Salgın, S.; Salgın, U.; Bahadır, S. Zeta potentials and isoelectric points of biomolecules: the effects of ion types and ionic strengths Int. J. Electrochem. Sci. **2012**, 7, 12404– 12414

61. Spitzer, J.; Poolman, B. The role of biomacromolecular crowding, ionic strength, and physicochemical gradients in the complexities of life's emergence Microbiology and Molecular Biology Reviews **2009**, 73 (2) 371– 388 DOI: 10.1128/MMBR.00010-09

62. Salis, A.; Ninham, B. W. Models and mechanisms of Hofmeister effects in electrolyte solutions, and colloid and protein systems revisited Chem. Soc. Rev. **2014**, 43 (21) 7358– 7377 DOI: 10.1039/C4CS00144C

63. Trefalt, G.; Behrens, S. H.; Borkovec, M. Charge Regulation in the Electrical Double Layer: Ion Adsorption and Surface Interactions Langmuir **2016**, 32 (2) 380– 400 DOI: 10.1021/acs.langmuir.5b03611

64. Jeworrek, C.; Evers, F.; Howe, J.; Brandenburg, K.; Tolan, M.; Winter, R. Effects of Specific versus Nonspecific Ionic Interactions on the Structure and Lateral Organization of Lipopolysaccharides Biophys. J. **2011**, 100 (9) 2169– 2177 DOI: 10.1016/j.bpj.2011.03.019

65. Martinez, R. E.; Smith, D. S.; Kulczycki, E.; Ferris, F. G. Determination of Intrinsic Bacterial Surface Acidity Constants using a Donnan Shell Model and a Continuous pKa Distribution Method J. Colloid Interface Sci. **2002**, 253 (1) 130– 139 DOI: 10.1006/jcis.2002.8541

66. Borrok, D. M.; Fein, J. B. The impact of ionic strength on the adsorption of protons, Pb, Cd, and Sr onto the surfaces of Gram negative bacteria: testing non-electrostatic, diffuse, and triple-layer models J. Colloid Interface Sci. **2005**, 286 (1) 110– 126 DOI: 10.1016/j.jcis.2005.01.015

67. Ledin, M.; Pedersen, K.; Allard, B. Effects of pH and Ionic Strength on the Adsorption of Cs, Sr, Eu, Zn, Cd and Hg by Pseudomonas Putida Water, Air, Soil Pollut. **1997**, 93 (1–4) 367– 381 DOI: 10.1007/BF02404767

68. Plazinski, W. Binding of heavy metals by algal biosorbents. Theoretical models of kinetics, equilibria and thermodynamics Adv. Colloid Interface Sci. **2013**, 197–198, 58– 67 DOI: 10.1016/j.cis.2013.04.002

69. Zhao, W.; Liu, X.; Huang, Q.; Walker, S. L.; Cai, P. Interactions of pathogens Escherichia coli and Streptococcus suis with clay minerals Appl. Clay Sci. **2012**, 69, 37– 42 DOI: 10.1016/j.clay.2012.07.003

70. Dunham-Cheatham, S.; Farrell, B.; Mishra, B.; Myneni, S.; Fein, J. B. The effect of chloride on the adsorption of Hg onto three bacterial species Chem. Geol. **2014**, 373, 106– 114 DOI: 10.1016/j.chemgeo.2014.02.030

71. Delnomdedieu, M.; Allis, J. W. Interaction of inorganic mercury salts with model and red cell membranes: Importance of lipid binding sites Chem.-Biol. Interact. **1993**, 88 (1) 71– 87 DOI: 10.1016/0009-2797(93)90085-D

72. Liu, Y.-R.; Lu, X.; Zhao, L.; An, J.; He, J.-Z.; Pierce, E. M.; Johs, A.; Gu, B. Effects of Cellular Sorption on Mercury Bioavailability and Methylmercury Production by Desulfovibrio desulfuricans ND132 Environ. Sci. Technol. **2016**, 50 (24) 13335– 13341 DOI: 10.1021/acs.est.6b04041

73. Janssen, S. E.; Schaefer, J. K.; Barkay, T.; Reinfelder, J. R. Fractionation of Mercury Stable Isotopes during Microbial Methylmercury Production by Iron- and Sulfate-Reducing Bacteria Environ. Sci. Technol. **2016**, 50 (15) 8077– 8083 DOI: 10.1021/acs.est.6b00854

74. Lamborg, C. H.; Fitzgerald, W. F.; Skoog, A.; Visscher, P. T. The abundance and source of mercury-binding organic ligands in Long Island Sound Mar. Chem. **2004**, 90 (1) 151–163 DOI: 10.1016/j.marchem.2004.03.014

75. Mason, R. P.; Choi, A. L.; Fitzgerald, W. F.; Hammerschmidt, C. R.; Lamborg, C. H.; Soerensen, A. L.; Sunderland, E. M. Mercury biogeochemical cycling in the ocean and policy implications Environ. Res. **2012**, 119, 101– 117 DOI: 10.1016/j.envres.2012.03.013

Chapter 3: An Anaerobic Biosensor Assay for the Detection of Mercury and Cadmium (video article)

Benjamin R. Stenzler[1], Jessica Gaudet[1], Alexandre J. Poulain[1]

Biology Department, University of Ottawa, 30 Marie Curie, Ottawa, ON, K1N 6N5, Canada.

*Corresponding author: Alexandre J. Poulain

E-mail address: apoulain@uottawa.ca

Telephone: 1-613-562-5800 ext. 2373

A modified version of this chapter was originally published as: Stenzler, B.R., Gaudet, J., Poulain, A.J. An Anaerobic Biosensor Assay for the Detection of Mercury and Cadmium. *J. Vis. Exp.* (142), e58324, doi:10.3791/58324 (2018).

Direct link: https://www.jove.com/v/58324/an-anaerobic-biosensor-assay-for-the-detection-of-mercury-and-cadmium

Keywords: Environmental Sciences, Issue 142, Biosensor, Mercury, Cadmium, Anaerobic, Bioavailability, Metal Speciation

3.1 Abstract

Mercury (Hg) bioavailability to microbes is a key step to toxic Hg biomagnification in food webs. Cadmium (Cd) transformations and bioavailability to bacteria control the amount that will accumulate in staple food crops. The bioavailability of these metals is dependent on their speciation in solution, but more particularly under anoxic conditions where Hg is methylated to toxic monomethylmercury (MeHg) and Cd persists in the rhizosphere. Whole-cell microbial biosensors give a quantifiable signal when a metal enters the cytosol and therefore are useful tools to assess metal bioavailability. Unfortunately, most biosensing efforts have so far been constrained to oxic environments due to the limited ability of existing reporter proteins to function in the absence of oxygen. In this study, we present our effort to develop and optimize a whole-cell biosensor assay capable of functioning anaerobically that can detect metals under anoxic condition in quasi-real time and within hours. We describe how the biosensor can help assess how chemical variables relevant to the environmental cycling of metals affect their bioavailability. The following protocol includes methods to (1) prepare Hg and Cd standards under anoxic conditions, (2) prepare the biosensor in the absence of oxygen, (3) design and execute an experiment to determine how a series of variable affects Hg or Cd bioavailability, and (4) to quantify and interpret biosensor data. We show the linear ranges of the biosensors and provide examples showing the method's ability to distinguish between metal bioavailability and toxicity by utilizing both metal-inducible and constitutive strains.

Video Link: The video component of this article and **Table of Materials** can be found at and https://www.jove.com/video/58324/

3.2 Introduction

Mercury (Hg) is a global pollutant and its bioavailability to Hg methylating microbes is the first step towards its biomagnification through food webs and its possible neurotoxic effects in human and wildlife[1]. It is currently thought that microbial Hg methylation is an intracellular process that requires: i) the species of Hg to be bioavailable [2-7] and ii) for the cell to be physiologically capable of methylating Hg [8-10]. Cadmium (Cd) bioaccumulates in organisms, but does not biomagnifies in foodwebs and is widely used in industrial and commercial processes that commonly cause acute exposures in people and the environment[11]. Although microbes play several key roles in the fate of Hg in the environment, most studies on Cd geochemistry and ecotoxicology focus on microbial eukaryotes[12]. Consumption of agricultural crops (*e.g.*, rice) is the main source of direct exposure to cadmium; in this case, the bioavailability of Cd to microbes of the rhizosphere directly influences the amount plants can accumulate[13].

Hg transport pathways are complex and possibly involve an active transport step[14]. When a transporter is involved, recent work suggested that Hg^{II} uses a Zn^{II} or Mn^{II} transporter[7,15-17]. Whereas Cd^{II} is hypothesized to be accidentally transported into the cytosol through divalent metal transport pathways (particularly Mn^{II} or Zn^{II}), mechanisms of Cd^{II} transport inside the cells remain speculative, and no Cd-specific transport pathway has been identified[13,18]. Regardless of the nature of the transporters involved, three mechanistic factors ultimately determine the ability of metals to enter a cell: i) the metal speciation in solution[2,6,15-23], ii) the biophysiochemical properties of the cell membrane [17, 24-31], and iii) the ability for the metal to access a transport site[7,32]. Cd and Hg are unlikely to exists as free ions under microbial physiologically relevant conditions due to their high affinity for Dissolved Organic Matter (DOM), chelating contaminants (*e.g.*, EDTA), or reduced sulfur moieties[33-35] (Cd^{II} can exist as a free ion or form ion-pairs in the

absence of these ligands). There is a lack of efficient methods in determining how these metal species are bioavailable under conditions relevant to their fate in the environment. For instance, Hg is methylated under anaerobic conditions[14], and both cadmium and Hg are soft metals (or class B cations), requiring that their speciation be investigated under conditions that maintain the integrity of reduced sulfur groups.

Microbial biosensors are bacterial cells that emit a quantifiable signal in response to the intracellular concentrations of a metal, in this case Hg or Cd. As such, they are ideal tools to understand how metals enter a cell[36], provided that exposure conditions are carefully controlled for. Hg biosensors typically contain gene fusions between the regulatory circuitry of the *mer*-operon (including genes encoding for the transcription regulator MerRas well as the operator and promoter regions of the operon), and reporting genes (*e.g., lux, gfp, lac* genes). When mercury is present in the cytoplasm, it will bind to MerR, resulting in transcription of the reporting genes and subsequent signal production[19,37]. Specific Cdbiosensors are usually designed using the *cadC, cadAC, zntA* or *zntR* encoded transcription regulators[38], but it is worth noting that MerR has a lower, yet quantifiable affinity to Cd[5]. Due to aerobic restriction of most commonly used luminescent or fluorescent reporter proteins, until recently microbial biosensors remained unable to offer insights into the biotransformation of metals under anoxic conditions. This makes anaerobicdetection of metals bioavailability very difficult over a range of conditions relevant to their environmental fate, specifically in the presence of redox sensitive ligands (*e.g.*, sulfide and thiols) [4-5,39].

To alleviate the methodological hurdle of live imaging in the absence of oxygen, Drepper *et al.* (2007) have developed a flavin-based fluorescent protein (FbFp), based on light oxygen voltage domain of SB2 protein from *P. putida*. This protein family is able to fluoresce in the

absence of oxygen[40]. Building on the work of Drepper *et al.*, our lab designed an anaerobic biosensor allowing for the study of Hg bioavailability under oxic and anoxic conditions and over a wide range of salinity [17]. In the current paper, we describe how to prepare and use the biosensor to test environmental variables' influence on Hg or Cd bioavailability. Although we developed the biosensor for Hg^{II}, we chose to perform experiments with Cd^{II} as a means to draw the reader's attention to the fact that biosensors may also respond to multiple stressors that are likely to co-occur in environmental matrices; in this case Cd^{II} was investigated because it is known to bind to the transcriptional regulator MerR[5]. Here, we show representative calibration and functional linear ranges with respect to either metal. We also give an example when the biosensor's results are conclusive (Mg^{II} and Mn^{II} on Hg bioavailability) and inconclusive (Zn^{II} on Hg bioavailability).

3.3 Protocol

(1) Growth Media and Exposure Media Preparation

1. To make 250 mL of **growth medium**:

    1. Note: If **trace elements #1 solution** and **trace elements #2 solution** are already prepared, skip to step 1.1.5.

    Prepare **trace elements #1 solution** in a clean volumetric flask (200 mL) to contain the final molarities of 1.5 x 10^{-3} M Na_2MoO_4, 6.5 x 10^{-4} M Na_2SeO_4, 5 x 10^{-3} M H_3BO_3, and 0.1 M NaOH.

    CAUTION: Strong bases (NaOH) are corrosive. Make sure when weighing the reagents to ensure that the final molarity represents the key trace elements; Mo, Se, and B.

    2. Under a sterile field, filter sterilize using a 0.22 µm polyethersulfone syringe filter in a clean/sterile plastic/Polytetrafluoroethylene (PTFE) bottle.

    3. Prepare **trace elements #2 solution** in a clean volumetric flask (200 mL) to contain the final molarities of 0.01 M $MnSO_4$, 5 x 10^{-4} M $ZnSO_4$, 3.25 x 10^{-3} M $CoCl_2$, 6.25 x 10^{-3} M $NiCl_2$, and 0.1 M H_2SO_4.

    CAUTION: Strong acids (H_2SO_4) are corrosive. Make sure when weighing the reagents to ensure that the final molarity represents the key trace elements; Mn, Zn, Co, and Ni.

4. Under a sterile field, filter sterilize using a 0.22 µm polyethersulfone syringe filter in a clean glass bottle.

5. Under a sterile field, in a clean/sterile glass bottle (250 mL minimum); add 200 mL ultrapure water, 42.5 mL of M9 Minimal Salts (5x; see **Table of Materials**), 2.5 mL of 2 M Glucose, 125 µL of 2 M $MgSO_4$, 1200 µL of 0.6 M Thiamine HCl from a frozen (-20 ˚C) aliquot, 1.25 mL of 4 M $NaNO_3$, 770 µL of 0.075 M L-leucine/ L-isoleucine/ valine solution, 250 µL **trace elements #1**, 250 µL **of trace element#2**, and 250 µL of 0.01 M EDTA sodium salt.

Note: All reagents in step 1.1.5 should be prepared prior and filter sterilized using a 0.22 µm polyethersulfone syringe filter. Ultrapure water may be sterilized using an autoclave.

6. Take the glass bottle now containing solution from step 1.1.5., loosely cap it and cycle it through the **anaerobic chamber** air lock.

7. In the **anaerobic chamber**, add 15 µL of 0.225 M $FeSO_4$ in 0.2 M H_2SO_4, cap bottle tightly, and shake until all white precipitates disappear.

Note: All reagents in step 1.1.7 should be prepared prior and filter sterilized using a 0.22 µm polyethersulfone syringe filter. Store the 0.225 M $FeSO_4$ in 0.2 M H_2SO_4 in the **anaerobic chamber**.

8. Remove cap from bottle, wait 1 minute for air to exchange, replace the cap from bottle, and then shake vigorously. Repeat this step once.

9. Fasten cap tightly onto the bottle, remove from **anaerobic chamber**, and store bottle in fridge (4 ˚C) until use.

10. Growth medium should be remade once a week by repeating steps 1.1.5 to 1.1.9.

2. To make 100 mL of **exposure medium** in 2 x 50 mL conical sterile polypropylene centrifuge tubes:

Note: We recommend that **exposure medium** be prepared on the day of the **exposure assay** to minimize the risk of contamination, however it can be made in advance and stored in the fridge.

1. In the **anaerobic chamber**, to each 50 mL centrifuge tube add 42 mL of anaerobic ultrapure water, 350 µL of 1 M Sodium Beta- Gylcerophosphate from a frozen (-20 ˚C) aliquot, 2 mL of 1 M MOPS free acid, 50 µL of 1 M $(NH_4)_2SO_4$, 125 µL of 2 M Glucose, 300 µL of 2.5 M KOH, and 200 µL of 2.5 M NaOH.

Note: All reagents in step 1.2.1 should be prepared prior and filter sterilized using a 0.22 µm polyethersulfone syringe filter. Ultrapure water may be heat sterilized using an autoclave. 2.5 M NaOH and 2.5 M NaOH must be stored in plastic/PTFE bottles. All reagents listed must be stored in the **anaerobic chamber** except Sodium Beta-Gylcerophosphate, which is to be stored in a (-20 ˚C) freezer. In general, it is good

practice to leave all plastic or glass parts and containers for several days in the anaerobic chamber to ensure that no traces of oxygen remain.

2. Cap the 50 mL centrifuge tubes, shake well, and remove a 10 mL aliquot to measure the pH. The measured pH of this exposure media must always measure **7.00 ± 0.02 at 25 ˚C**. If the pH does not measure within this range, readjust the volume of added 2.5 M KOH to correct for this.

Note: Never titrate the solution to correct for the pH with a pH probe. pH probes represent a source of contamination for the **exposure medium**. The pH must always be a product of the added reagents in step 1.2.1.

3. Prepare a 5-10 mM $NaNO_3$ stock solution and leave in **anaerobic chamber** to be used during the time of the **exposure assay**. Note: It is easier to dilute a more concentrated primary $NaNO_3$ standard as opposed to making a 5-10 mM $NaNO_3$ primary standard.

(2) Preparation of Mercury and Cadmium Standards.

1. Preparing a 4-8 µM Mercuric (Hg^{II}) solution in 0.2 M H_2SO_4.

1. Prepare a Hg^{2+} standard by making a millimolar (1-10 mM) $HgCl_2$, $HgNO_3$ or $HgSO_4$ solution in 0.2 M H_2SO_4.

CAUTION: Mercury is highly toxic and H_2SO_4 is corrosive. Operate in fume hoods with all required personal protective equipment.

2. In a PTFE bottle, dilute standard from 2.1.1. into 0.2 M H_2SO_4 to obtain a concentration within the range of 4-8 µM Hg^{2+}. Note: The acid used must be analytical grade H_2SO_4.

3. The Hg concentration from 2.1.2 should be validated using a mercury analyzer (see **Table of Materials**). Note: Other methods for validating the Hg concentration may be used.

2. Preparing a 10 µM Cd^{II} solution in 10 mM H_2SO_4.

1. Prepare a primary standard of $CdCl_2$ (10-50 mM range for accurate weighing of powder) in 0.1 M H_2SO_4.

2. In a series of serial dilutions in clean acid rinsed 20 mL borosilicate glass vials with black phenolic screw caps with PTFE faced rubber liners, dilute the standard from 2.2.1 to 10 µM Cd^{2+}. Ensure that the concentration of H_2SO_4 in every subsequent serial dilution remains 10 mM.

(3) Preparation of the Biosensor for Anaerobic Exposure Assay.

1. Plate the mercury inducible biosensor (E. coli NEB5α harboring PUC57merR-PpFbFp) and the constitutively expressed biosensor (E. coli NEB5α harboring PUC19Balch-PpFbFp) from -80 ˚C cryostock onto Lysogeny Broth plates containing 120 ug/mL ampicillin. See our previously published work for details on the production of these biosensors[17].

2. At 4:30-5 PM, inoculate a culture in 10 mL of LB (+ amp) and grow overnight.

Note: Starting from a plate it takes **2 days** to prepare the anaerobic culture for the **exposure assay** (*i.e.,* a culture started on Monday afternoon (4:30-5 PM) will be ready for the **exposure assay** at around noon on Wednesday). The following steps are the required microbiological techniques necessary to prepare the cultures on the day of the **Exposure assay**.

1. Take one colony from the plate culture and add to 10 mL Lysogeny Broth (LB) with **21 µL** of a 100 mg/mL stock solution of ampicillin sodium salt (final concentration is 210 ug/mL amp) in a sterile culture tube.

2. Place the culture into an incubator/shaker and grow overnight at +37 ˚C with shaking at 220 rpm.

3. The next morning at 9-10 AM, resuspend the culture and grow anaerobically throughout the day (20% inoculum).

1. Bring the culture from the incubator (step 3.2.1) and the **growth medium** (step 1.1.9) into the **anaerobic chamber**.

2. Add 8 mL of fresh **growth medium** and ampicillin (210 µg/mL) into a sterile Balch tube.

3. Collect 2 mL of the overnight grown culture and transfer into a 2 mL Microcentrifuge tube. Centrifuge at 10,000 RCF step for 90 seconds, dump supernatant and resuspend in **2 mL** of fresh **growth medium**. Add the resuspended culture to the Balch tube containing 8 mL of fresh **growth medium** and ampicillin.

4. Using sterile technique, carefully place a rubber stopper on the Balch tube. Remove from the **anaerobic chamber** and place in an incubator/shaker and grow anaerobically until 3-5 PM at +37 ˚C with shaking at 220 rpm.

4. Between 3 and 5 PM, perform a 1% anaerobic inoculum into fresh **growth medium** and grow overnight.

1. Bring the Balch tube (step 3.3.4) into the **anaerobic chamber** along with **growth medium**. Add **100 µL** of the culture to 10 mL of fresh **growth medium** (1% inoculum) with amp (210 ug/mL amp) in a sterile Balch tube.

2. Using sterile technique, carefully place a rubber stopper on the Balch tube. Remove from the **anaerobic chamber**, place in an incubator/shaker, and grow overnight at +37 ˚C with shaking at 220 rpm.

5. Between 9 and 10 AM, resuspend the culture to grow anaerobically throughout the day (20% inoculum).

1. Bring the culture from the incubator (step 3.4.1) and the **growth medium** (step 1.1.9) into the **anaerobic chamber**.

2. Add 8 mL of **growth medium** and ampicillin (210 ug/mL amp) into a sterile Balch tube.

3. Collect 2 m of the overnight grown culture and transfer into a 2 mL Microcentrifuge tube. Centrifuge at 10,000 x g for 90 seconds, dump supernatant, and resuspend in **2 mL** of fresh **growth medium**. Add the resuspended culture to the Balch tube containing 8 mL of fresh **growth medium** and ampicillin.

4. Using sterile technique, carefully place a rubber stopper on the Balch tube. Remove from chamber and place in an incubator/shaker and grow anaerobically at +37 ˚C with shaking at 220 rpm.

6. Monitor the growth of the culture using a spectrophotometer (step 3.5.4) until an **OD_{600} of 0.6** is reached. Be sure to vortex culture prior to each OD reading.

Note: This step takes 3-4 hours, and the **exposure medium** (step 1.2) should be prepared during this time as well as the **exposure assay** (step 4.1).

7. Stop the growth when the culture reaches an **OD_{600} of 0.6 (±0.1)** (3-4 hours expected growth).

1. Bring tube in the **anaerobic chamber** (step 3.6) and transfer culture into 2 x **2 mL** Microcentrifuge tubes. Centrifuge at 10,000 x g for 90 seconds, dump supernatant, and resuspend in 2 x **2 mL** of fresh **exposure medium**.

2. Repeat washing step 3.7.1. once to remove any trace of the **growth medium**.

8. Combine both microcentrifuge tubes of cell culture (step 3.7) into a 7 mL PTFE standard vial to obtain **Biosensor Stock** to be used in the **Exposure Assay** (step 4).

Note: Be sure to mix the **Biosensor Stock** by thoroughly yet gently pipetting back and forth prior to use. The method may be paused here for up to an hour.

(4) Preparation of the Biosensor for Anaerobic Exposure Assay.

1. Designing a plate layout.

Note: Be sure to have all pipetting values calculated and stocks prepared prior to starting the **exposure assay.** How to properly design an experiment and what controls to include is detailed in the text. In addition, the experiment should not be started if there is oxygen in the anaerobic chamber indicated on the anaerobic monitor.

1. Design the plate layout according to a 96 well template. To run experiments in technical replicates of 3, this will allow for 32 different treatments, which is best represented by a 4 x 8 grid to set up vials (see **Figure 3.1**).

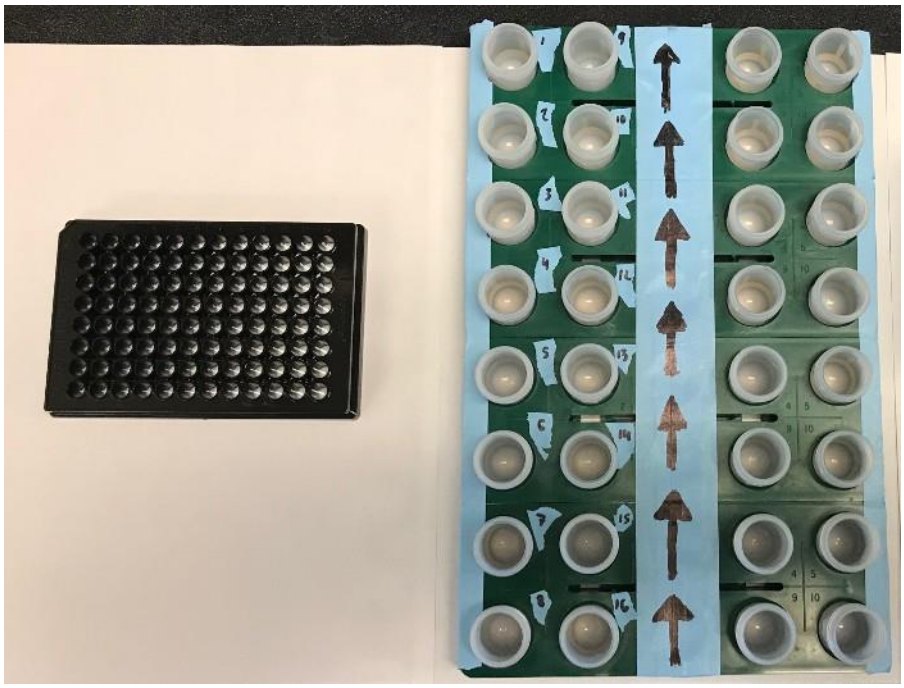

Figure 3.1: Grid of vials containing biosensor to be transferred into a plate. A 96 well plate (left) and a corresponding 4 x 8 grid containing PTFE vials (right) to be transferred to the plate.

Note: When testing for the role of a variable on Hg uptake with the **mercury inducible biosensor;** two treatments are required for each variable: the **treatment** (biosensor + Hg + variable + nitrate) and its **treatment blank** (biosensor + variable + nitrate). When testing for the role of a variable on the physiology of the cell using the **constitutive biosensor,** two treatments are required for each variable: the **treatment** (biosensor + Hg + variable + nitrate) and **treatment blank** (biosensor + variable + Hg). Mercury may be replaced with Cadmium. Hg or Cd will become the variable when performing a calibration curve. The **constitutive** and **inducible** biosensors do not need to be run at the same time (in the same plate layout). A template example for the plate layout and corresponding 4 x 8 grid when testing a concentration range of magnesium (variable)is provided in **Table 3.1**).

Table 3.1: An example plate layout for using the biosensor to test Hg bioavailability (5 nM) over a gradient of Magnesium (0-10 mM)

	1	2	3	4	5	6	7	8	9	10	11	12
a	Hg induced biosensor + Hg + Nitrate + 0 mM Mg			Hg induced biosensor + Nitrate + 0 mM Mg			Constitutive biosensor + Hg + Nitrate + 0 mM Mg			Constitutive biosensor + Hg + 0 mM Mg		
b	Hg induced biosensor+ Hg + Nitrate + 0.1 mM Mg			Hg induced biosensor + Nitrate + 0.1 mM Mg			Constitutive biosensor+ Hg + Nitrate + 0.1 mM Mg			Constitutive biosensor + Hg + 0.1 mM Mg		
c	Hg induced biosensor + Hg + Nitrate + 1 mM Mg			Hg induced biosensor + Nitrate + 1 mM Mg			Constitutive biosensor + Hg + Nitrate + 1 mM Mg			Constitutive biosensor + Hg + 1 mM Mg		
d	Hg induced biosensor + Hg + Nitrate + 10 mM Mg			Hg induced biosensor + Nitrate + 10 mM Mg			Constitutive biosensor + Hg + Nitrate + 10 mM Mg			Constitutive biosensor + Hg + 10 mM Mg		
e												

2. Set up the 4 x 8 grid according to the assay plate layout.

1. Place 7 mL PTFE standard vials in the tray.

Note: PTFE vials should be acid washed/heat sterilized prior to use. Vials should only be handled by manipulating the outside of the vial.

2. To each vial, add the exposure medium volume corresponding to each treatment.

Note: In an exposure with a total volume of 2,000 µL (2 mL), the added **exposure medium** will be: **exposure medium** µL = 2,000 µL –**treatment (blank)** µL. (*e.g.*, exposure medium µL = 2,000 – 100 µL (biosensor) – 40 µL (nitrate) – 100 µL (Hg) – 100 µL (variable (*e.g.*,$MgSO_4$)) = 1660 µL). Be sure that the volume added of the tested variable does not exceed 5% (100 µL) of the final volume.

3. To each vial, add the corresponding volume of the solution of the chemical variable to be tested according to the plate layout.

4. From step 1.3, add nitrate to each vial so that the final concentration is **200 µM** (40-80 µL). Exclude this step for **constitutivebiosensor treatment blanks**.

5. From step 2.1 or 2.2, add Hg (**5 nM** when testing for a variable) or Cd (**300 nM** when testing for a variable) to the vials according to the plate layout. Exclude this step for **mercury inducible biosensor treatment blanks**.

1. When using Hg, take the **4-8 µM** stock and shake well. Dilute the solution in **exposure medium** in a 7 mL PTFE vial to **100-250nM** to make a working Hg solution. From this working solution add Hg to the required vials. In this case a calibration curve of Hg ranging from 0 to 12.5 nM.

Note: When testing for a variable's effect on Hg or Cd bioavailability, make sure that the [Hg] or [Cd] remains constant across all treatments. When adding Hg or Cd, be sure to use one pipette tip but never touch the exposure medium in the vials.

3. Shake in an orbital motion manually.

Note: The experiment may be paused now depending on the time required for Hg or Cd to speciate in solution. If left for more than an hour, place PTFE caps on the PTFE vials to prevent evaporation/contamination.

4. Gently pipette **Biosensor Stock** back and forth to ensure homogeneity. Add 100 µL of **Biosensor Stock** to each vial. Shake orbitally manually.

5. Prepare the plate reader to warm up to read with the following criteria: Temperature at **37˚C**, kinetic run for **10 hours** with reads every 2.5-5 minutes with orbital shaking in between reads,

and fluorescence measurements with a **fluorescence excitation of 440 nm** and an **emission of 500 nm**.

6. Pipette **200 µL** from each PTFE vials in the 4 x 8 grid into the corresponding wells of the 96 well plate (Black, 96-Well Clear-Bottom Nonbinding Surface Microplates). Pipette back and forth 5 times before transferring each 200 µL.

Note: Instead of discarding the pipette tip, leave the pipette tip in the PTFE vial to keep track of pipetting progress.

7. Place the 96 well plate into the tray of the plate reader, then place the lid on the 96 well plate and begin the assay.

3.4 Results and Quantifying the Data

(4)

1. The fluorescence of each **treatment** at each time point must be corrected for each individual well noise and blanked to the **treatment blank.**

    1. The fluorescence for each time point (t) of each **treatment** (**T**) must be translated to account for the initial fluorescence (t0) of the first time point of each well, then averaged across the 3 **treatments** replicates (r_1-r_3)**.** This treatment average must then be blanked to the average **treatment blank** (**TB**) translated in the same manner (Equation 1).

$$\textit{Fluorescence}\ (t) = \textit{average}(\mathbf{T}_{r1(t)} - \mathbf{T}_{r1(t0)}, \mathbf{T}_{r2(t)} - \mathbf{T}_{r2(t0)}, \mathbf{T}_{r3(t)} - \mathbf{T}_{r3(t0)}) - \textit{average}(\mathbf{TB}_{r1(t)} - \mathbf{TB}_{r1(t0)}, \mathbf{TB}_{r2(t)} - \mathbf{TB}_{r2(t0)}, \mathbf{TB}_{r3(t)} - \mathbf{TB}_{r3(t0)}) \quad (1)$$

Note: This should be made as a spreadsheet function. Proper propagation of error should also be calculated for each time point.

2. Graph the corrected fluorescence of each **treatment** as a function of time

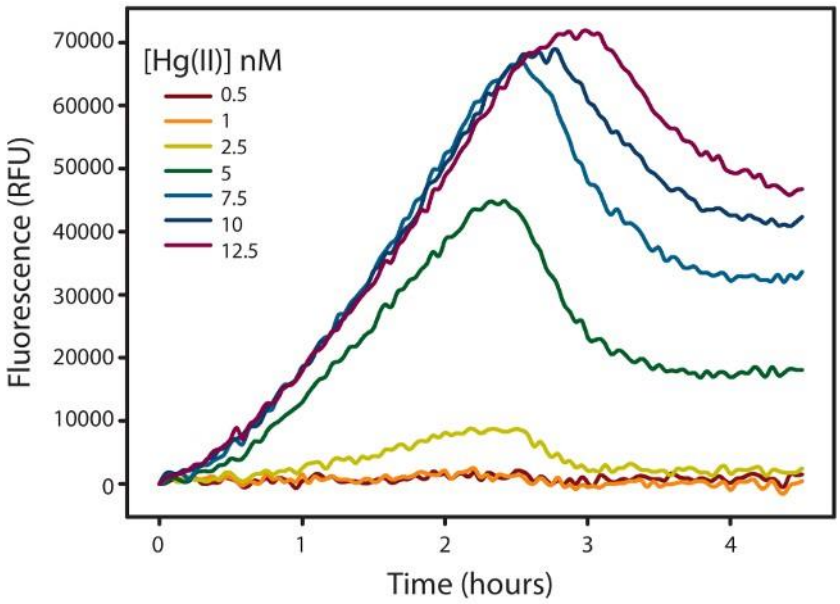

Figure 3.2: Corrected fluorescence data as a function of time. Fluorescence measured as relative fluorescence units (RFU) emitted by *E. coli* NEB5α harboring the pUC57merR-Pp (Inducible strain) over time with the addition of Hg^{II} (0-12.5 nM) under anaerobic conditions. Fluorescence was the average of 3 technical replicates at 37 ˚C.

Note: There is no 0 nM Hg value on the graph, and all other Hg concentrations have been blanked to the 0 nM Hg as a **treatment blank**. Therefore, 0 nM Hg represents the x axis and any positive fluorescence represents fluorescence from Hg given any variable. It is optional to not blank the fluorescence in this manner, but the fluorescent curves will give misleading fluorescence curves if the variable tested has background fluorescence (*i.e.*, dissolved organic matter itself will fluoresce and if there is no treatment blank containing just cells and the dissolved organic matter, increasing dissolved organic matter concentration will increase the fluorescent signal).

3. Quantify the fluorescence peak. A quantifiable fluorescence peak will typically occur after 2.5-4 hours, representing the energy expended from the consumption of all 200 µM nitrate as a terminal electron acceptor. This peak should be quantified and represents the final fluorescence value of that specific **treatment**.

Note: In the event no fluorescence peak is observed (*i.e.*, no Hg bioavailability), the fluorescence of **treatment** at the time point of the fluorescence peak of the control (*i.e.*, no added variable or 5nM Hg) should be quantified. Alternatively, if there is fluorescence induction in the treatment, but fluorescence does not produce a well defined peak, there is likely contamination of a higher affinity electron acceptor such as O_2 and measures should be taken to remove traces of oxygen from all solutions and the experiment must be performed again.

(4) Representative Results.

Once the fluorescence peaks have been quantified according to step 5.3, the result of the fluorescence peaks can be graphed according to the variable concentration illustrating how that variable affects the relative bioavailability of either Hg or Cd. For example, the calibration curve of fluorescence over [Hg^{II}] from **Figure 3.2** will yield the inducible data presented in **Figure 3.3A**. For Hg^{II} calibration, the curve will always contain 3 components for the Hg-inducible strain; a threshold response of about 1-2 nM Hg^{II} before fluorescence signal production is linearly proportional to [Hg^{II}], the linear range where **5 nM Hg^{II}** will reliably always be in the center of that range, and a plateau where increasing [Hg^{II}] will no longer increase fluorescence signal. No change in signal production on the constitutive strain shows that toxicity from [Hg^{II}] does not affect signal production. For Cd^{II} in **Figure 3.3B**, there are always 2 components for the inducible strain; a linear range where **200-300 nM Cd^{II}** will reliably always be in the center of the linear range and a plateau. A decrease in fluorescence signal with increasing [Cd^{II}] shows that higher Cd concentrations are toxic to the cells and can explain a decrease in the inducible fluorescence production after the plateau at 1000 nM Cd^{II}. Therefore, when testing Hg or Cd bioavailability with respect to an environmental variable, we suggest using **5 nM for Hg^{II}** and **300 nM for Cd^{II}**.

In some instances, signal production can be properly attributed to Hg or Cd bioavailability, but in other cases, signal production can be affected by variation in the physiological state of the biosensor cell host (*e.g.*, the metal of interest or environmental conditions tested are toxic). In **Figure 3.4A**, 5 nM Hg bioavailability was tested over a gradient of Zn (0-10 µM). In both Hg-

inducible and constitutive strains, there is a similar decrease in signal with increasing Zn concentrations. Therefore, one cannot discriminate whether the signal results from lowered bioavailability or is a result of Zn toxicity. In Figure 3.4B and 4C, 5nM Hg bioavailability was tested over a gradient of MgII (0-10 mM) and MnII (0-10 µM). Increasing MgII and MnII concentrations decreased the fluorescence signal of the inducible strain. On the other hand, the constitutive strain did not show a decrease in fluorescence with increasing MgII and MnII concentrations (MgII and MnII are beneficial for the cells in the production of the FbFp, as demonstrated by an increase in the fluorescence signal). This demonstrates that the cells are viable and the fluorescence decrease of the Hg-inducible strain results from a decrease in Hg bioavailability. This data emphasizes how important it is for all biosensor assays to also provide constitutive measurements of overall cell fitness.

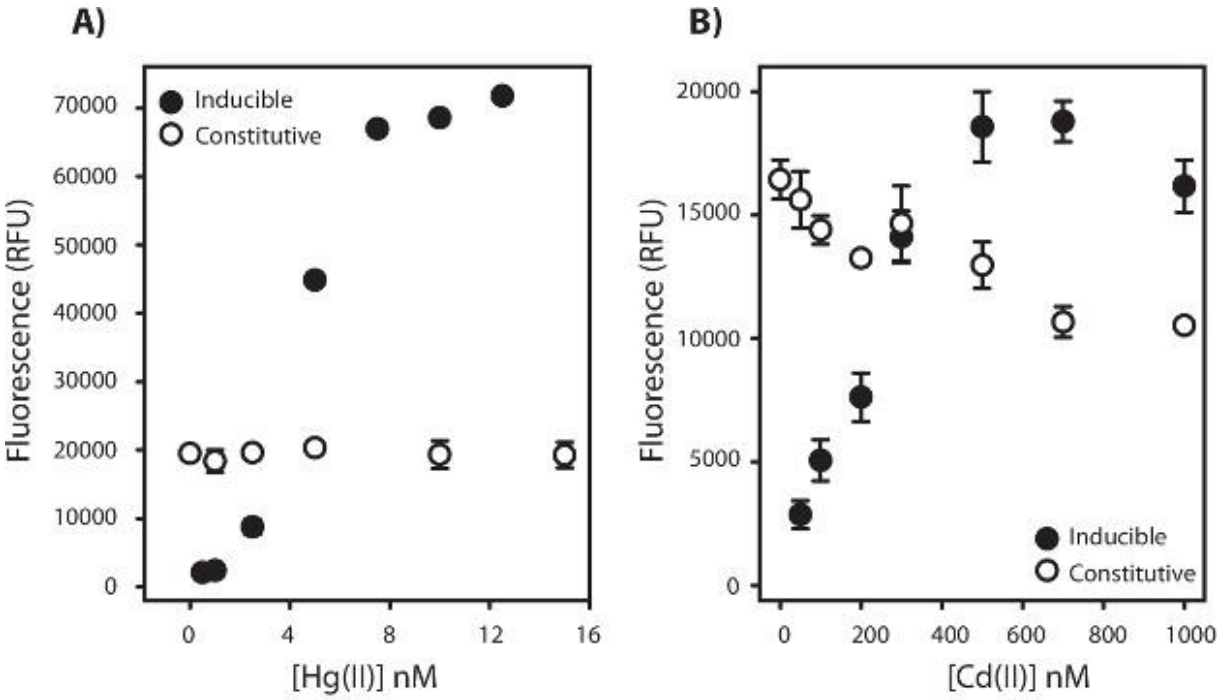

Figure 3.3: Linear ranges of the biosensor with Mercury and Cadmium. Maximum fluorescence measured as relative fluorescence units (RFU) ± 1 Standard Deviation emitted by *E. coli* NEB5α harboring the pUC57merR-Pp (Hg-Inducible) and pUC19Balch-Pp (Constitutive) with the addition of **A)** Hg^{II} (0-15 nM) and **B)** Cd^{II} (0-1,000 nM) under anaerobic conditions. Fluorescence was the average of 3 technical replicates at 37˚C.

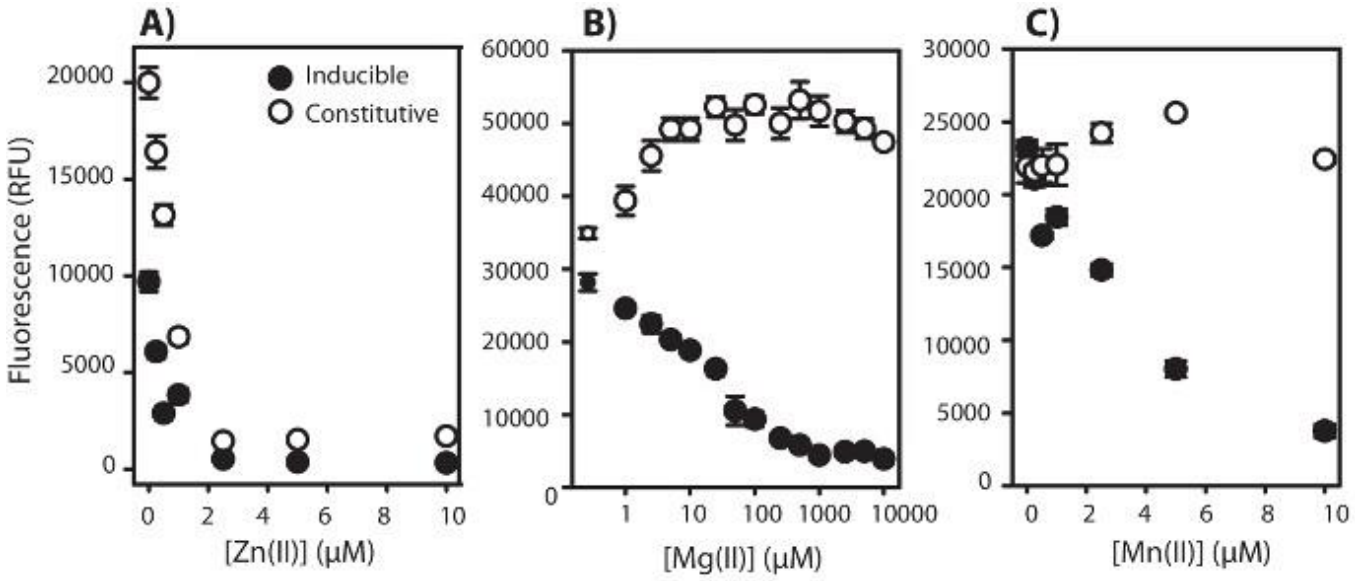

Figure 3.4: Example of an inconclusive result with Zinc and a conclusive result with Magnesium and Manganese. Maximum fluorescence measured as relative fluorescence units (RFU) ± 1 Standard Deviation emitted by *E. coli* NEB5α harboring the pUC57merR-Pp (Hg-Inducible) and pUC19Balch-Pp (Constitutive) with the addition of **A)** Zn^{II} (0-10 µM), **B)** Mg^{II} (0-10 mM), and **C)** Mn^{II} (0-10 µM) under anaerobic conditions. [Hg^{II}] was set to 5 nM for all treatments and fluorescence was the average of 3 technical replicates at 37 ˚C.

3.5 Discussion

Microbial biosensors are useful tools to identify mechanisms by which metals are interacting with microbes. Here, we describe a method that can anaerobically quantify Hg^{II} and Cd^{II} bioavailability to a Gram-negative host cell (*E. coli*) and give a quantifiable result within a few hours. One of the major strengths of this protocol is that it allows extensive control of metal speciation in the exposure medium by avoiding strong binding ligands or components that may lead to metal precipitation. Metal speciation has been modelled and tested in this exposure medium using PHREEQC[17], however other metal speciation software may be deployed. In the case of no added ligands, Hg speciation is expected to be present as 97% $Hg(OH)_2$ and 3% $Hg(NH_3)^{2+}$, while Cd speciation will be present as 59% Cd-β-Glycerophosphate, 25% Cd^{2+}, and 16% $CdSO_4$. Using a simple thermodynamic modeling software, the user can design exposure

media and test for the bioavailability of the metal of interest. In addition, the biosensor host cell (*E. coli* NEB5α) is viable over a wide range of pH (5-8.5) and NaCl concentration (0-0.55 M)[17].

Hg methylation is an anaerobic process, and the protocol outlined in this study does not have a requirement for oxygen, allowing for more accurate description of anaerobic metabolism on metal bioavailability. This is important because the presence of oxygen alters gene expression profiles[48,49] and hence, potential transport pathways; therefore this method presents an advantage over currently exising aerobic alternatives. The biosensing construct presented here can potentially be used with other anaerobic hosts that may be more relevant for mercury methylation(*e.g., Geobacter, Desulfovibrio*), but maybe less tractable than *E. coli*. One current limitation of the approach presented here is that our limit of detection has not yet reached pM levels, contrary to existing aerobic systems[4,19,37]. It is however important to note that to achieve these low detection limits several steps need to be taken[44]: i) ligand addition is required to ensure that Hg remains in solution and does not adsorb onto the microbial cell wall (Hg will be irreversible bound to cell surface thiols preventing its bioavailability[25,27]; see the threshold response for Hg in **Figure 3.3A**), ii) modifications to cell density, or iii) modify the genetic construct to include transport proteins of the *mer*-operon (namely *merT* and *merP*), increasing Hg flux inside the cell[50,51]. These modifications would be beneficial in detecting low concentrations of Hg, but not necessarily ideal when assessing environmentally relevant situations. Whereas previous cadmium biosensors primarily exist as a "proof of principle", they were designed in complex media that do not allow the investigator to assess the role of speciation on bioavailability[41-44].

The biosensor is an incredibly useful tool in determining mechanisms in which metal species are bioavailable. Because the host organism is not a Hg-methylator, it may only be used

to develop a model for how Hg may enter Gram-negative bacteria and not a definitive rationale for how Hg-methylators acquire Hg. Other methods exist for determining Hg bioavailability, such as methylation, as an outcome of uptake or the use of a mass balance approach[10,15,20,45-46]. That being said, the method presented here offers the advantage of quasi real time bioavailability data in viable cells. We do not recommend that this method be used to quantify total Hg or Cd levels in an environmental matrix. Despite the proposed use of biosensors to determine metal concentrations in the environment[36], many more readily available standard methods are available such as ICP-MS, FAAS (for Cd analysis) or Cold vapor atomic absorption spectroscopy (for Hg analysis). The biosensor can however be used

to determine if a given environmental matrix has the potential to enhance or hamper bioavailability; this is achieved by performing standard additions.

The pH of the exposure media may be altered to anywhere within the range of 5 and 8.5, provided the MOPS Free acid (buffer) is exchanged with an alternate free acid of a buffer with the appropriate pKa (please see list of appropriate buffers (Ferreira *et al.* (2015)[47]) and adjusted with KOH to the appropriate pH when making the exposure media. In addition, the method is not limited to Hg and Cd, but could be extended to other metals using other transcription regulators.

The exposure assay may be modified to explore the influence of other electron acceptors such as O_2 and fumarate on Hg or Cd bioavailability. Minor modifications to the method to utilize both O_2 and fumarate as electron acceptors are available upon request.

In summary we would like to emphasize the following points: **I)** It is imperative that the concentrations of Cd or Hg stocks are known in step 2, as these will be used to calibrate the

biosensor. **II)** On the exposure day, the growth of cells must be stopped at an OD_{600} of 0.6 (± 0.1) and that care is taken when resuspending the cell cultures, as the biosensor is calibrated to this cell density. **III)** Lastly, it is important that the exposure medium is made meticulously on the exposure day. To ensure the success of the protocol, multiple cultures should be grown simultaneously (to circumvent the possibility of growth failure) and the growth medium should be remade weekly (to circumvent the metastability of the media and possible contamination). It should also be noted that biological replicates (multiple cell cultures) express variability when it comes to signal production. Although the fluorescent responses may vary from culture to culture, the fluorescent trends in response to a given variable should remain the same throughout numerous biological replicates.

3.6 Acknowledgments

We would like to thank comments from two anonymous reviewers as well members of the Poulain Lab for insightful discussion on the development of the anaerobic biosensor. An Early Researcher Award from the Province of Ontario and a Discovery Grant and an accelerator supplement from the Natural Sciences and Engineering Research Council of Canada to A.J.P. funded this study.

3.7 References

1. Futsaeter, G., & Wilson, S. The UNEP Global Mercury Assessment: Sources, Emissions and Transport. *E3S Web of Conferences.* **1**, 36001, (2013).

2. Barkay, T., Gillman, M., & Turner, R. R. Effects of dissolved organic carbon and salinity on bioavailability of mercury. *Applied and Environmental Microbiology.* **63** (11), 4267-4271, (1997).

3. Ndu, U., Mason, R. P., Zhang, H., Lin, S., & Visscher, P. T. Effect of inorganic and organic ligands on the bioavailability of methylmercury as determined by using a mer-lux bioreporter. *Applied and Environmental Microbiology.* **78** (20), 7276-7282, (2012).

4. Golding, G. R. *et al.* Evidence for facilitated uptake of Hg(II) by Vibrio anguillarum and Escherichia coli under anaerobic and aerobic conditions. *Limnology and Oceanography.* **47** (4), 967-975, (2002).

5. Golding, G. R., Sparling, R., & Kelly, C. A. Effect of pH on intracellular accumulation of trace concentrations of Hg(II) in *Escherichia coli* under anaerobic conditions, as measured using a mer-lux bioreporter. *Applied and Environmental Microbiology.* **74** (3), 667-675, (2008).

6. Chiasson-Gould, S. A., Blais, J. M., & Poulain, A. J. Dissolved Organic Matter Kinetically Controls Mercury Bioavailability to Bacteria. *Environmental Science & Technology.* **48** (6), 3153-3161, (2014).

7. Schaefer, J. K., Szczuka, A., & Morel, F. M. M. Effect of Divalent Metals on Hg(II) Uptake and Methylation by Bacteria. *Environmental Science & Technology.* **48** (5), 3007-3013, (2014).

8. Compeau, G., & Bartha, R. Sulfate-reducing bacteria: principal methylators of mercury in anoxic estuarine sediment. *Applied and Environmental Microbiology.* **50** (2), 498-502, (1985).

9. Compeau, G. C., & Bartha, R. Effect of salinity on mercury-methylating activity of sulfate-reducing bacteria in estuarine sediments. *Applied and Environmental Microbiology.* **53** (2), 261-265, (1987).

10. Gilmour, C. C., Henry, E. A., & Mitchell, R. Sulfate stimulation of mercury methylation in freshwater sediments. *Environmental Science & Technology.* **26** (11), 2281-2287, (1992).

11. Rani, A., Kumar, A., Lal, A., & Pant, M. Cellular mechanisms of cadmium-induced toxicity: a review. *International Journal of Environmental Health Research.* **24** (4), 378-399, (2014).

12. Liu, F., Fortin, C., & Campbell, P. G. C. Can freshwater phytoplankton access cadmium bound to low-molecular-weight thiols? *Limnology and Oceanography.* **62** (6), 2604-2615, (2017).

13. Shahid, M., Dumat, C., Khalid, S., Niazi, N. K., & Antunes, P. M. C. in *Reviews of Environmental Contamination and Toxicology Volume 241*.(ed Pim de Voogt) 73-137, Springer International Publishing (2017).

14. Hsu-Kim, H., Kucharzyk, K. H., Zhang, T., & Deshusses, M. A. Mechanisms regulating mercury bioavailability for methylating microorganisms in the aquatic environment: a critical review. *Environmental Science and Technology.* **47** (6), 2441-2456, (2013).

15. Szczuka, A., Morel, F. M. M., & Schaefer, J. K. Effect of Thiols, Zinc, and Redox Conditions on Hg Uptake in *Shewanella oneidensis. Environmental Science and Technology.* **49** (12), 7432-7438, (2015).

16. Schaefer, J. K. *et al.* Active transport, substrate specificity, and methylation of Hg(II) in anaerobic bacteria. *Proceedings of the National Academy of Sciences of the United States of America.* **108** (21), 8714-8719, (2011).

17. Stenzler, B. R., Hinz, A., Ruuskanen, M. O., & Poulain, A. J. Ionic strength differentially affects the bioavailability of neutral and negatively charged inorganic Hg complexes. *Environmental Science and Technology.* (2017).

18. Sigel, A. *Cadmium: From Toxicity to Essentiality.* Dordrecht : Springer Netherlands : Imprint: Springer (2013).

19. Barkay, T., Turner, R. R., Rasmussen, L. D., Kelly, C. A., & Rudd, J. W. Luminescence facilitated detection of bioavailable mercury in natural waters. *Methods in Molecular Biology (Clifton, N.J.).* **102**, 231-246, (1998).

20. Zhang, T. *et al.* Methylation of mercury by bacteria exposed to dissolved, nanoparticulate, and microparticulate mercuric sulfides. *Environmental Science and Technology.* **46** (13), 6950-6958, (2012).

21. Ndu, U., Mason, R. P., Zhang, H., Lin, S., & Visscher, P. T. Effect of inorganic and organic ligands on the bioavailability of methylmercury as determined by using a mer-lux bioreporter. *Applied and Environmental Microbiology.* **78** (20), 7276-7282, (2012).

22. Moreau, J. W. *et al.* The Effect of Natural Organic Matter on Mercury Methylation by Desulfobulbus propionicus 1pr3. *Frontiers in Microbiology.* **6** (1389), (2015).

23. Schaefer, J. K., & Morel, F. M. M. High methylation rates of mercury bound to cysteine by Geobacter sulfurreducens. *Nature Geoscience.* **2** (2), 123-126, (2009).

24. Dunham-Cheatham, S., Farrell, B., Mishra, B., Myneni, S., & Fein, J. B. The effect of chloride on the adsorption of Hg onto three bacterial species. *Chemical Geology.* **373**, 106-114, (2014).

25. Dunham-Cheatham, S., Mishra, B., Myneni, S., & Fein, J. B. The effect of natural organic matter on the adsorption of mercury to bacterial cells. *Geochimica et Cosmochimica Acta.* **150**, 1-10, (2015).

26. Mishra, B., Shoenfelt, E., Yu, Q. *et al.* Stoichiometry of mercury-thiol complexes on bacterial cell envelopes. *Chemical Geology.* **464**, 137-146, (2017).

27. Sara Anne, T., Qing, M., & Jean-François, G. Probing changes in Hg(II) coordination during its bacterial uptake. *Journal of Physics: Conference Series.* **712** (1), 012078, (2016).

28. Macek, T. *Microbial Biosorption of Metals.* Springer Netherlands (2011).

29. Ledin, M., Pedersen, K., & Allard, B. Effects of pH and Ionic Strength on the Adsorption of Cs, Sr, Eu, Zn, Cd and Hg by Pseudomonas Putida. *Water, Air, and Soil Pollution.* **93** (1-4), 367-381, (1997).

30. Daughney, C. J., & Fein, J. B. The effect of ionic strength on the adsorption of H+, Cd2+, Pb2+ and Cu2+ by Bacillus subtilis and Bacillus licheniformis: A surface complexation model. *Journal of Colloid and Interface Science.* **198** (1), 53-77, (1998).

31. Borrok, D. M., & Fein, J. B. The impact of ionic strength on the adsorption of protons, Pb, Cd, and Sr onto the surfaces of Gram negative bacteria: testing non-electrostatic, diffuse, and triple-layer models. *Journal of Colloid and Interface Science.* **286** (1), 110-126, (2005).

32. Daguené, V. *et al.* Divalent Base Cations Hamper HgII Uptake. *Environmental Science & Technology.* **46** (12), 6645-6653, (2012).

33. Turner, D. R. Speciation and cycling of arsenic, cadmium, lead and mercury in natural waters. *Lead, Mercury, Cadmium and Arsenic in the Environment.* 175-186, (1987).

34. Liu, G., Cai, Y., & O'Driscoll, N. *Environmental Chemistry and Toxicology of Mercury.* John Wiley & Sons (2011).

35. North, A. E., Sarpong-Kumankomah, S., Bellavie, A. R., White, W. M., & Gailer, J. Environmentally relevant concentrations of aminopolycarboxylate chelating agents mobilize Cd from humic acid. *Journal of Environmental Sciences.* **57**, 249-257, (2017).

36. Van Der Meer, J. R., & Belkin, S. Where microbiology meets microengineering: design and applications of reporter bacteria. *Nature Reviews Microbiology.* **8** (7), 511-522, (2010).

37. Rasmussen, L. D., Turner, R. R., & Barkay, T. Cell-density-dependent sensitivity of a mer-lux bioassay. *Applied and Environmental Microbiology.* **63** (8), 3291-3293, (1997).

38. Magrisso, S., Erel, Y., & Belkin, S. Microbial reporters of metal bioavailability. *Microbial Biotechnology.* **1** (4), 320-330, (2008).

39. Golding, G. R., Kelly, C. A., Sparling, R., Loewen, P. C., & Barkay, T. Evaluation of mercury toxicity as a predictor of mercury bioavailability. *Environmental Science and Technology.* **41** (16), 5685-5692, (2007).

40. Drepper, T. *et al.* Reporter proteins for *in vivo* fluorescence without oxygen. *Nature biotechnology.* **25** (4), 443-445, (2007).

41. Kumar, S., Verma, N., & Singh, A. K. Development of cadmium specific recombinant biosensor and its application in milk samples. *Sensors and Actuators B: Chemical.* **240**, 248-254, (2017).

42. Yoon, Y. *et al.* Simultaneous detection of bioavailable arsenic and cadmium in contaminated soils using dual-sensing bioreporters. *Applied and Environmental Microbiology.* **100** (8), 3713-3722, (2016).

43. Kang, Y., Lee, W., Jang, G., Kim, B. G., & Yoon, Y. Modulating the sensing properties of Escherichia coli-based bioreporters for cadmium and mercury. *Applied and Environmental Microbiology.* **102** (11), 4863-4872, (2018).

44. Hynninen, A., Tõnismann, K., & Virta, M. Improving the sensitivity of bacterial bioreporters for heavy metals. *Bioengineered Bugs.* **1** (2), 132-138, (2010).

45. Graham, A. M., Bullock, A. L., Maizel, A. C., Elias, D. A., & Gilmour, C. C. Detailed assessment of the kinetics of Hg-cell association, Hg methylation, and methylmercury degradation in several Desulfovibrio species. *Applied and Environmental Microbiology.* **78** (20), 7337-7346, (2012).

46. Graham, A. M., Aiken, G. R., & Gilmour, C. C. Dissolved Organic Matter Enhances Microbial Mercury Methylation Under Sulfidic Conditions. *Environmental Science & Technology.* **46** (5), 2715-2723, (2012).

47. Ferreira, C. M. H., Pinto, I. S. S., Soares, E. V., & Soares, H. M. V. M. (Un)suitability of the use of pH buffers in biological, biochemical and environmental studies and their interaction with metal ions-a review. *RSC Advances.* **5** (39), 30989-31003, (2015).

48. Salmon, K., Hung, S. P., Mekjian, K., Baldi, P., Hatfield, G. W., & Gunsalus, R. P. Global gene expression profiling in Escherichia coli K12: the effects of oxygen availability and FNR. *Journal of Biological Chemistry.* **278** (32), 29837-29855, (2003).

49. Salmon, K. A., Hung, S. P., Steffen, N. R., Krupp, R., Baldi, P., Hatfield, G. W., & Gunsalus, R. P. Global Gene Expression Profiling in Escherichia coli K12 effects of oxygen availability and ArcA. *Journal of Biological Chemistry.* **280** (15), 15084-15096, (2005).

50. Larose, C., Dommergue, A., Marusczak, N., Coves, J., Ferrari, C. P., & Schneider, D. Bioavailable mercury cycling in polar snowpacks. *Environmental Science & Technology.* **45** (6), 2150-2156, (2011).

51. Omura, T., Kiyono, M., & Pan-Hou, H. Development of a specific and sensitive bacteria sensor for detection of mercury at picomolar levels in environment. *Journal of Health Science.* **50** (4), 379-383, (2004).

Chapter 4: Aerobic and Anaerobic Bacterial Mercury Uptake is Driven by Phytoplankton Organic Matter Composition and Molecular Weight

Mangal V[a$]., Stenzler B.R.[b$]., Poulain A.J.[b*]., Guéguen C[c*].

[a] Environmental and Life Sciences Graduate program, Trent University, 1600 West Bank Drive Peterborough ON, Canada, K9J 7B8

[b] Biology Department, University of Ottawa, 30 Marie Curie, Ottawa ON, Canada, K1N 6N5

[c] Chemistry Department, Trent University, 1600 West Bank Drive Peterborough ON, Canada, K9J 7B8

[*] Corresponding authors; celinegueguen@trentu.ca; apoulain@uottawa.ca

[$]authors contributed equally to this work

Direct link: https://pubs.acs.org/doi/10.1021/acs.est.8b04909

N.B. Supporting information for this chapter can be found **in Appendix B**

4.1 Abstract

The biological mobilization of mercury (Hg) into microbes capable of Hg methylation is one of the limiting steps in the formation of the neurotoxin methylmercury (MeHg). Although algal dissolved organic matter (DOM) has been associated with increased MeHg production, the relationship between bacterial Hg uptake and algal DOM remains unexplored. In this study, we aimed to address how the quantity and quality of DOM, freshly harvested from several algae, affected the bacterial uptake of Hg with the use of a biosensor capable of functioning both aerobically and anaerobically. We combined biosensor measurements with high-resolution mass spectrometry and field-flow fractionation to elucidate how DOM composition and molecular weight influenced microbial Hg uptake. We showed that freshly harvested DOM from Chlorophyte and *Euglena mutabilis* strongly inhibited aerobic and anaerobic Hg uptake, whereas DOM harvested from *Euglena gracilis* did not exhibit this same pronounced effect. Once fractionated, we found that amino acids and polyamines, most abundant in *Euglena gracilis* DOM, were positively correlated to increase Hg uptake, suggesting that these molecules are potentially underappreciated ligands affecting Hg bioavailability. As water quality is affected by eutrophication, algal community assemblages will change, leading to variations in the nature of autochthonous DOM released in aquatic systems. Our results highlight that variations in the emergent properties of DOM originating from varying algal species can have a profound effect on bacterial Hg uptake and thus methylation.

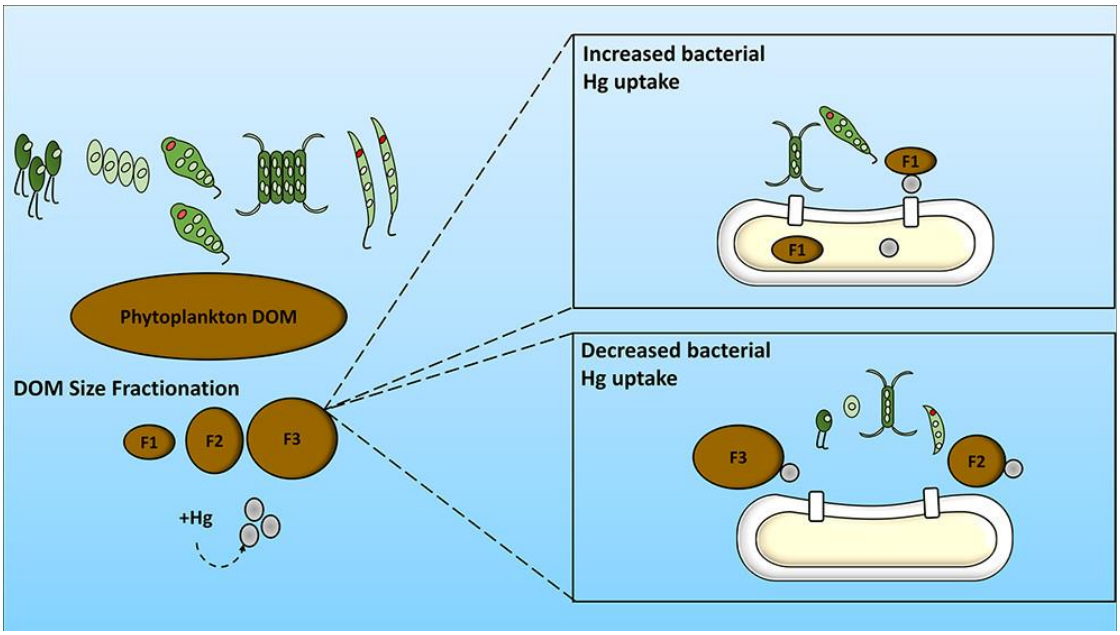

4.2 Introduction

Mercury (Hg) is a naturally occurring element, and its mobilization through anthropogenic mining extractions and fossil fuel combustion has led to increased Hg and methylmercury (MeHg) concentrations in aquatic and terrestrial ecosystems. The biomagnification of MeHg in food webs can result in neurodegenerative disorders, ultimately affecting humans and wildlife.[1–3] Conversion of inorganic Hg to MeHg is predominantly a microbially mediated process most notably performed by chemotrophic, anaerobic microbes.[4] Hg methylation is predicted to mostly occur in anoxic sediments, but alternative sites conducive to MeHg production have been identified in environments with enhanced photo-synthetic activity and dynamic redox interfaces such as chlorophyl maximum layers in polar marine waters,[5,6] sea ice,[7,8] or periphytic biofilms [9–11]. Because Hg methylation is thought to be an intracellular process,[12] these recent discoveries emphasize the need to assess how phototrophic primary producers can impact microbial Hg uptake in oxic and hypoxic environments.

Mercury (Hg) is a naturally occurring element and its mobilization through anthropogenic mining extractions and fossil fuel combustion has led to increased mercury (Hg) and methylmercury (MeHg) concentrations in aquatic and terrestrial ecosystems. The biomagnification of MeHg in food webs can result in neurodegenerative disorders, ultimately affecting humans and wildlife [1-3]. Conversion of inorganic Hg to MeHg is predominately a microbially mediated process most notably performed by chemotrophic, anaerobic microbes [4]. Hg methylation is predicted to mostly occur in anoxic sediments, but alternative sites conducive to MeHg production have been identified in environments with enhanced photosynthetic activity and exhibiting dynamic redox interfaces such as chlorophyll maximum layers in polar marine waters [5-6], sea ice [7-8], or periphytic biofilms [9-11]. Because Hg methylation is thought to be an intracellular process [12], these recent discoveries emphasize the need to assess how phototrophic primary producers can impact microbial Hg uptake in oxic and hypoxic environment

Studies investigating the role of primary producers on Hg methylation face the challenge of distinguishing their direct involvement as methylators from the indirect role they have in supplying nutrients to chemotrophic MeHg producers [13-15]. There is currently very little support, however, for phototrophs participating directly in Hg methylation [16]. It is most likely that primary producers affect Hg^{II} methylation by (i) providing a substrate that affects the activity of Hg methylating microbes [17-19], (ii) releasing methylating compounds that would abiotically methylate Hg^{II} (e.g., CH3Cl/Br/I or dimethylsulfoniopropionate) [20], and/or (iii) releasing chemical ligands that can affect the uptake of Hg^{II} by methylators [11].

A necessary and rate limiting step in Hg methylation is the uptake of Hg to methylating microbes. Hg bioavailability is dependent on its chemical speciation, and in aquatic ecosystems, dissolved organic matter (DOM) is one of the most important metal binding ligands [21,22]. Hg

bioavailability depends on DOM concentrations [23-25], molecular composition [26-28], and molecular weight [29]. More recently, studies have shown that DOM can also exert ecological controls on Hg methylation by affecting anaerobic microbial community structures [18,29]. DOM is heterogeneous, complex, and varies in concentration and composition across aquatic systems. Although allochthonous DOM transported to lakes can represent a significant proportion of the measured DOM in eutrophic freshwaters, microorganism-derived autochthonous DOM is typically more labile, exhibiting rapid turnover rates that can significantly impact lake ecosystem functions [30]. Ongoing warming and changing aquatic nutrient loading from agricultural practices [31] affect algal assemblages in freshwater and marine systems, ultimately impacting the quality of DOM [32]. Furthermore, increased anthropogenic pressures on aquatic systems can lead to eutrophication [33], which can affect primary producer communities by selecting for more competitive and resilient species [34]. Due to the inherent variability of DOM, characterization of DOM−Hg interactions is difficult [35,36]. Therefore, a multipronged analytical approach addressing not only DOM quantity and quality but also accounting for Hg bioavailability is essential to support efforts required to predict and improve management of Hg pollution. A link between algal DOM and increased MeHg concentrations has been established [18, 19, 27], yet we still do not understand the mechanisms by which this occurs. To address these missing links, our study focuses on the role that algal DOM has on microbial Hg uptake; one of the initial step of Hg methylation.

In this study, we harvested and fractionated DOM produced by a diverse set of primary producers of the divisions Chlorophyta (*Scenedesmus obliquus*, *Chlorella vulgaris*, *Chlamydomonas reinhardtii*) and Euglenozoa (*Euglena gracilis* and *Euglena mutabilis*). These algal species are common in a diverse array of aquatic systems including biofilms associated with high Hg methylation rates [11,37,38]. To understand how algal DOM impacts microbial Hg

uptake, we used a unique combination of analytical techniques including asymmetrical flow field-flow fractionation (AF4) to separate DOM based on molecular weight [39-41] and high-resolution mass spectrometry (Fourier transform ion cyclotron resonance mass spectrometry) to gather DOM compositional information [42], while assessing aerobic and anaerobic bacterial Hg uptake using a flavin-based whole cell biosensor [43]. Our study offers novel insights into the complexity of algal DOM and how it can affect the fate of Hg in aquatic ecosystems.

4.3 Materials and Methods

4.3.1 Phytoplankton Growth and Sample Preparation

We axenically cultured a total of five phytoplankton species including *Scenedesmus obliquus (S. obliquus), Chlorella vulgaris* (*C. vulgaris*), *Chlamydomonas reinhardtii* (*C. reinhardtii), Euglena gracilis* (*E. gracilis*) and *Euglena mutabilis* (*E.mutabilis*), obtained from the Canadian Phycological Culture Center (Waterloo, Canada). All phytoplankton were grown at 21°C at a 16:8 light/dark cycle. Bold basal media (BBM) was used to culture *Chlorella vulgaris* and *Scenedesmus obliquus*, high salt media (HSM) for *Chlamydomonas reinhardtii*, and Hutner media for both *Euglena gracilis* and *Euglena mutabilis* [39,44]. Once cultures were in mid exponential growth at 1.0 x 10^6 cells determined by cell hemocytometer counts, DOM was extracted by filtering through a 0.2µm Whatman filter. In addition to phytoplankton DOM, a Suwannee River Fluvic Acid (SRFA) standard obtained from the International Humic Substances Society (IHSS) was used. Both SRFA and phytoplankton DOM were stored at 4°C in the dark for subsequent DOC analyses, fractionation and high-resolution mass spectrometry.

4.3.2 Asymmetrical Flow Field-Flow Fractionation (AF4) and DOC Analysis

To test for the role of the various size fractions of the DOM pool on Hg bioavailability, we performed a gentle separation of DOM based on molecular weight using asymmetrical flow field-flow fractionation (AF4) [41]. The AF2000 Focus fractionation system from Postnova Analytics coupled to a multichannel online spectrophotometer diode array detector (Shimadzu SPDM20A) and fraction collector (Varian ProStar 701) equipped with a 300 Da polyether sulfonate (PES, Postnova Analytics) was used to separate and isolate DOM based on molecular weight [40]. The axial, focus, and cross-flow settings were 0.25, 2.2, and 2.45 mL min^{-1}, respectively [39]. A calibration solution of macromolecular proteins was utilized to separate algal DOM and SRFA based on molecular weight. A 2 mL portion of 5 $mg{\cdot}C{\cdot}L^{-1}$ of SRFA and algal DOM was injected into a 300 μL sample loop. Fractions were collected during the elution step at 1 min intervals, over the course of 3 min, to acquire three distinct molecular weight groups using a fraction collector. Fraction 1 (F1) comprised of low molecular weight DOM (F1:300−500 Da), fraction 2 (F2) consisted of medium molecular weight material (F2:500−1000 Da), and the final third fraction comprised of the largest molecular weight material (F3:1000−2000 Da) (Figure B1). Fractions were not collected below 300 Da, due to the membrane molecular weight cutoff of the AF4, and above 2000 Da due to the low abundance of DOM. During fractionation, the eluent was adjusted by using ultrapure water, NaOH, and HCl to modify pH and a concentrated NaCl solution to match the conductivity of the injected algal DOM samples.

DOC concentrations were measured using a Shimadzu total organic carbon analyzer (TOC-VCPH) (Figure B2). Calibration curves were run with a minimum of 5 concentration standards (prepared gravimetrically) of potassium hydrogen phthalate in ultrapure UV-oxidized water.

4.3.3 Aerobic and Anaerobic Bioassays

Both aerobic and anaerobic bioassays were conducted as per Stenzler et al. (2017) [43]. Two *Escherichia coli* biosensors were used; one was a Hg inducible biosensor (*E. coli* NEB5α harboring the pUC57merR-Pp plasmid) where the production of a flavin based fluorescent protein (FbFP) was under the control of MerR [the transcription regulator of the *mer* operon]. The other was a constitutive biosensor (*E. coli* NEB5α harboring the pUC19AH206-Pp plasmid), which expressed the FbFP irrespective of the presence of Hg. Experiments with both biosensors were performed in parallel to control for the effect of the conditions tested on cell health. From a −80 °C cryostock, cells were grown and selected on lysogeny broth (LB) agar plates exposed to 210 μg mL^{-1} ampicillin and grown at 37 °C. Colonies were selected from the plate and grown in LB before being transferred (an)aerobically in the growth medium described in Stenzler et al. (2017) [43]. Growth was monitored until an optical density at 600 nm (OD600) of 0.6 was reached. Cell growth was subsequently halted by resuspension in the (an)aerobic exposure medium; this was used as a cell stock in the following bioassay.

All pipetting and exposures were conducted in an anaerobic chamber (97% N_2 (g) and 3−4% H_2 (g)). Assays were mixed in a 7 mL Teflon vial along with exposure medium and either unfractionated DOM, at increasing concentrations for bulk assays, or AF4 fractions normalized to 1 mg L^{-1} carbon for molecular weight assays in both aerobic and anaerobic settings. Hg was diluted from an 8 μmol L^{-1} stock solution of $HgSO_4$ to a final concentration of 5 nmol L^{-1} in the Teflon vials to equilibrate with the DOM. After equilibrating, aerobic samples were removed from the anaerobic chamber and aerated under a sterile field. Both aerobically or anaerobically, 100 μL of the cell stock was added to the Teflon vials and immediately transferred to a 96-well plate to be measured at 37 °C on a Tecan Infinite Pro plate reader at fluorescence 450 ± 10 nm

and emission wavelengths of 500 ± 20 nm for aerobic assays. Anaerobic fluorescence was measured in the anaerobic chamber on a Synergy HTX plate reader at a fluorescence excitation of 440/40 mm and an emission fluorescence at 500/ 27 nm. Analytical triplicates were conducted on plate readers, and biological duplicates or triplicates were performed for both aerobic and anaerobic assays. A constitutive bacterial strain was also grown, that emits fluorescence replicates (n = 2 or 3) irrespective of the presence of Hg [45], and exposed to comparable DOM concentrations and fractions to explore the role of DOM on E. coli's ability to emit fluorescence. These values were normalized to the inducible strain results. To compare biological replicates, bioassay results were also normalized to the 5 nmol L^{-1} control fluorescence.

4.3.4 Fourier Transform Ion Cyclotron Mass Spectrometry

A 7T Bruker SolariX XR Fourier transform ion cyclotron resonance mass spectrometer (FT ICR MS) (Billerica, Massachusetts) equipped with an electrospray ionization (ESI) source and a ParaCell ICR cell was used to characterize DOM composition on a molecular level at high throughput for environmental metabolomics [47]. All samples were mixed to a 60:40 MeOH/ultrapure H_2O ratio and diluted to 1 mg L^{-1} carbon at pH 2 using HCl. Prior to injection, a NaTFA tuning mix was used to externally and internally calibrate the sample using three lock masses (i.e., 248.9603, 656.8848, and 928.8344 *m*/*z*). DOM samples were analyzed in negative ESI mode at a capillary voltage of 4500 V, continuous injection rate of 120 μL h^{-1}, and a 0.5 s ion accumulation time to acquire 200 coadded scans in adsorption mode. For each DOM sample, biological duplicates were acquired and only common peaks between replicates were conserved for further analysis.

Peak and formula assignment were conducted using Bruker Compass DataAnalysis (v4.2) with a mass tolerance of ±1 ppm and a relative intensity threshold of 0.1%. MeOH, ultrapure H_2O, and media blanks were all subtracted from algal DOM samples prior to further analysis. The coupling of FT ICR MS to Cytoscape and MetaNetter2 plugins allowed for the visualization of 105 different transformations encompassing essential amino acids, enzymes, functional groups, and biogenic metal chelating molecules in complex networks [47-49]. Elemental formula and *m*/*z* values were exported to Cytoscape (Version 3.6.0) equipped with the MetaNetter 2 application to visualize HRMS *m*/*z* interactions and transformations within mass spectra [47-49]. User defined chemical interactions (transformations) were then incorporated to allow for the calculation of exact mass differences between the two *m*/*z* peaks within ±1 ppm error.

4.3.5 Statistical Analyses

A student *t* test was applied to evaluate the effect of increasing DOM concentrations on Hg bioavailability. To evaluate the effect of fractionation on Hg uptake, a nonmetric multidimensional scaling (NMDS) analysis was conducted using a Euclidian dissimilarity measure in PAST statistical software v3.0 [50]. Bioassay results from all fractionated and unfractionated samples at 1 $mg \cdot C \cdot L^{-1}$ in both aerobic and anaerobic conditions were considered. Clusters were based on significant differences ($p < 0.05$; t test) and validated by a hierarchical cluster analysis using a Euclidian dissimilarity measure where distinct clusters were defined at a 0.35 cutoff (or at least 65% similarity in composition) (Figure B3). To assess significant differences between bioassay concentration gradients and fractionated material, after testing for normality, a one-way ANOVA was conducted at a confidence interval of 95%. Principal component analyses (PCA) based on correlation were also conducted for F1, F2, and F3 fractions

to evaluate how the composition of algal DOM changed after fractionation. Across all three PCAs, 64.3, 62.8, and 68.4% of the total explained variance were explained for F1, F2, and F3, respectively. To address compositional differences between Cytoscape derived transformations, a two-way hierarchical cluster analysis and a Spearman's correlation heatmap were conducted using the online tool Heatmapper [51]. Finally, model II regression models were conducted to evaluate the relationship between normalized Hg uptake fluorescence values and the number of Cytoscape transformations. An Akaike information criterion (AIC) test was applied to ensure the strength of the predicted models generated for nonlinear regressions in RStudio (v.1.0153).

4.4 Results and Discussion

4.4.1 Effect of DOM Concentration on Mercury Uptake

We first compared the effect of freshly harvested biogenic DOM to the well characterized SRFA. The addition of SRFA (up to 5 ppm) decreased Hg uptake by 83.7 ± 1.3% and 65.2 ± 3.7%, under oxic and anoxic conditions, respectively (Figure B4 A,B), in line with previous bioassays 24. Under both oxic and anoxic conditions, DOM harvested from the *Chlorophyta C. reinhardtii, C. vulgaris, S. obliquus* and one *Euglenozoa* species (*E. mutabilis*) decreased Hg uptake by >90% ($p < 0.001$) at [DOM] = 1 ppm (Figure 4.1). Moreover, as little as [DOM] = 0.1 ppm decreased Hg uptake by 50–90%, depending on the DOM source. Of the three Chlorophyta tested, C. reinhardtii was the least effective at reducing Hg bioavailability at low [DOM] (<0.5 ppm; Figure 4.1 B,G). These results are in stark contrast with those obtained using DOM from *E. gracillis*. Although an inhibitory effect was observed, it was to a lesser extent than what was observed for other algae. In this case, the inhibitory effect on Hg bioavailability ranged from 48 to 68% under both aerobic and anaerobic conditions, respectively (Figure 4.1 E,J). We speculate

that these differences in Hg uptake may stem from different strategies that algae have developed to cope with toxic metals. Indeed, Chlorophyta and *E. mutabilis* rely on exopolysaccharides (EPS) to limit interactions between the cell and toxic metals [52-54] and such properties have been used for bioremediation purposes in the past [55]. *E. gracilis* has been shown to internalize and reduce Hg^{II} to Hg^{0} [56]; this strategy may have alleviated the need for *E. gracilis* cells to rely on EPS production as a means to protect themselves against toxic metals.

Clearly, the ability of the exudates produced by these diverse phototrophs to affect Hg uptake is species dependent. All species used here were grown autotrophically prior to harvesting their DOM, but some of the organisms are capable of heterotrophic growth (e.g., *C. reinhardtii*, *E. mutabilis*, and *E. gracilis*). Although we did not test for the role of carbon metabolism (autotrophy vs heterotrophy) on the nature of the DOM produced, this is something that should be the focus of further investigations.

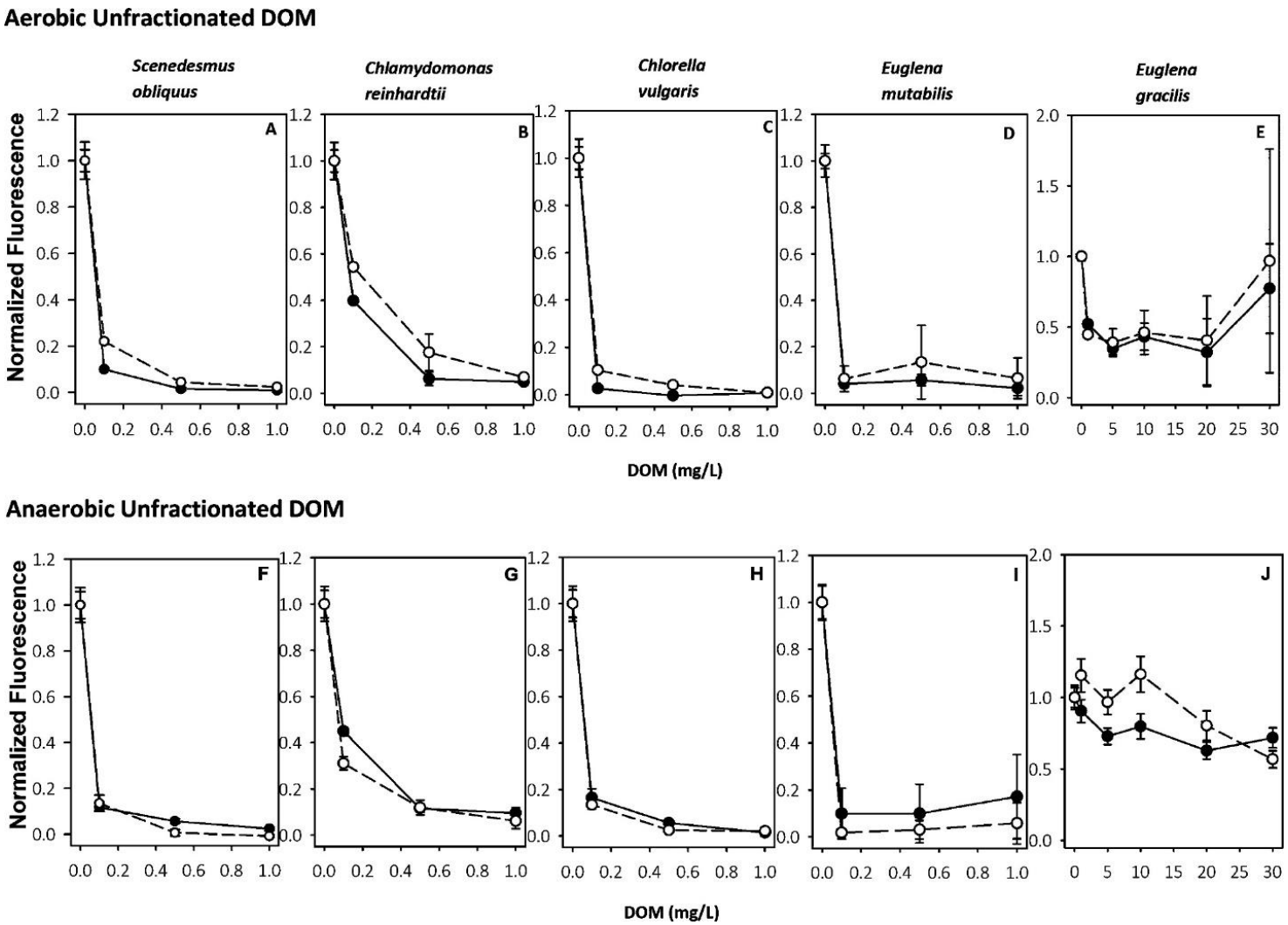

Figure 4.1. Hg bioavailability with unfractionated algal DOM. Aerobic (A–E) and anaerobic (F–J) bioassays with increasing DOM concentrations from algal cultures of *S. obliquus* (A, F), *C. reinhardtii* (B, G), *C. vulgaris* (C, H), *E. mutabilis* (D, I), and *E. gracilis* (E, J) where $n = 3$. Normalized fluorescence (RFU) with increasing concentrations DOM (mg/L). The experiment was performed at 37 ˚C in an anaerobic exposure medium (pH 7).

4.4.2 Effect of DOM size fractions on Hg uptake

The complex and heterogeneous nature of DOM makes it subject to compositional changes depending on environmental conditions 42. The process of fractionating SRFA resulted in more bioavailable Hg relative to the unfractionated material under both aerobic and anaerobic conditions (Figure B4 C,D). NMDS analysis with Euclidian dissimilarity measure was used to tease apart how AF4 fractionation affected microbial Hg uptake relative to unfractionated algal DOM normalized to 1 mg·C·L–1 (Figure 4.2 and Figure B5). Using this approach, three significant clusters were observed. The first cluster (Figure 4.2 A) includes size fractions leading

to a decrease in Hg uptake (73%) comparable to unfractionated material ($p > 0.05$); these fractions included mostly large size fractions (F3) from the Chlorophyta species and *E. mutabilis*. The second cluster (Figure 4.2 B) includes mainly F1 and F2 fractions of Chlorophyta. The third cluster includes *E. gracilis* and *S. obliquus* DOM fractions shown to enhance Hg uptake (50.1% for all E. gracilis fractions and 25.4% for S. obliquus fractions) (Figure 4.2 C) ($p < 0.05$). *E. mutabilis* DOM led to minimal changes to Hg uptake after fractionation, as all treatments regardless of fractionation or the presence of oxygen led to an inhibitory effect on Hg uptake (first cluster, Figure 4.2 A).

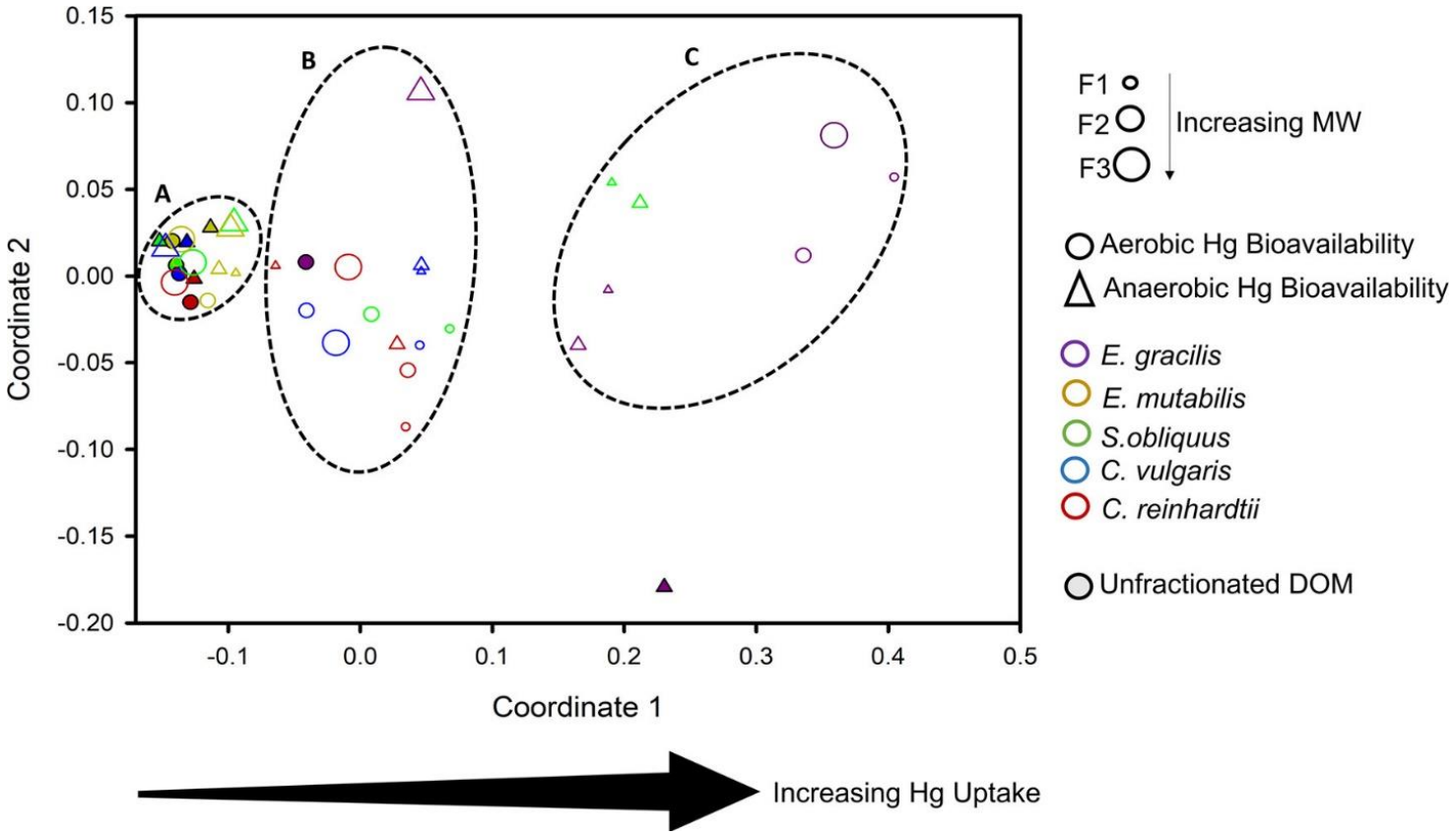

Figure 4.2. NMDS using a Euclidian measure analysis portraying the effect of algal DOM fractionation and Hg uptake. Clusters (**A**, **B**, and **C**) were defined at a 0.35 cutoff (or at least 65% similarity in composition) (Figure B3). Circles represent aerobic assays whereas triangles represent anaerobic bioassays with the size of each symbol corresponding to the molecular weight fraction with smallest circle = F1, medium circle = F2, and large circle = F3. Colors correspond to algal taxa where purple is *E. gracilis*, yellow is *E. mutabilis*, green is *S. obliquus*,

blue is *C. vulgaris*, and red is *C. reinhardtii*. Filled symbols outline unfractionated DOM and dashed lines show significant clustering

While 1 mg·C·L^{-1} of unfractionated DOM from all algae significantly ($p < 0.05$) inhibited Hg bioavailability, the process of fractionation led to an overall increase in Hg uptake in all algae tested, except for *E. mutabilis*. From a biological perspective, unfractionated DOM can act as a dense physical barrier surrounding the bacterial cell walls that can also sequester Hg [57]. The process of fractionation can lead to increased interactions between metals and the cell wall, and fractionation has been shown to enhance metal toxicity [58]. This is likely due to fractionation leading to exposure of heteroatoms that can participate in metal binding and to a more fluid continuum of molecules surrounding the bacteria. The presence of this continuum may facilitate Hg access to the cell wall and possibly its uptake, via a series of ligand exchange.

4.4.3 Algal Dissolved Organic Matter Composition

The transformational differences in algal DOM composition determined via Cytoscape network analysis were evaluated using a Spearman's correlation heatmap and a two-way cluster analysis 47,49 (Figure B6). Three distinct clusters were found along the horizontal axis of the heatmap suggesting similarities in DOM composition based on algal taxa. Specifically, the first cluster (Figure B6 A) is composed of all euglenoid bulk and fractions, except for *E. mutabilis* F3. The second cluster (Figure B6 B) is mainly composed of chlorophyte F1 and F2 fractions, whereas the final cluster (Figure B6 C) consisted of chlorophyte unfractionated DOM and higher molecular weight fractions (F2 and F3). Euglenoid DOM was distinct from chlorophyte DOM with significantly greater proportions of polyamine, cytosine, glutamine, serine, and lysine transformations ($p < 0.05$; Figure B6 A). Transformations indicative of glutamine isomers were the most abundant, and were especially expressed in *E. gracilis* DOM. The F1 and F2 fractions of E. mutabilis were comparable to E. gracilis fractions; however, *E. mutabilis* fractions were

comprised of a greater number of ketol and glyoxylate transformations. Hydrogenation transformations suggestive of highly unsaturated, aliphatic material minimal in double bonds were also abundant in euglenoid DOM.

Although intrinsic differences in algal DOM exist between taxa, the process of fractionation also led to compositional differences within each DOM fraction. Three PCAs were generated for transformations found across F1–F3 (Figure B7 A–C) to reveal how transformations were distributed across AF4 fractions. Euglenoid and chlorophyte DOM were found in two distinct regions of the PCA: positive PC1 and PC2 values for euglenoids and positive PC1 and negative PC2 for chlorophytes in all AF4 fractions. The proximity of the algal vectors was reduced within each algal class as molecular weight increased, suggesting greater similarity in DOM composition within euglenoid and chlorophyte algae in higher molecular weight fractions than that in smaller size fractions. Specifically, the F1 fraction of *E. gracilis* was influenced by acetylation (−H) and glutamine transformations and the F1 fraction of E. mutabilis comprised condensation/dehydration, lysine, and polyamine transformations. *S. obliquus* had contributions from glycine, secondary amines, and ethyl transformations, and *C. reinhardtii* was abundant in many potential Hg chelating transformations such as cysteine or ketol. Tertiary amines, C2H, and isoprene transformations were found in *C. vulgaris* F1. *C. vulgaris* and *C. reinhardtii* F2 samples were more similar where hydroxylation and pyrophosphate was found in *C. vulgaris* F2, and secondary amines, isoprene, and glyoxylate transformations were found in *C. reinhardtii*. *S. obliquus* and *E. gracilis* DOM were found to contain amino acids, energy rich trisaccharides, and sugar isomers that can be favorable sources of energy for bacteria. Finally, all chlorophytes F3 samples were impacted by ketol transformations providing Hg with an electronegative binding site that may account for the overall reduction in Hg uptake across all

chlorophyte F3 samples. *E. mutabilis* F3 DOM was mainly influenced by C_2H_2 addition, suggesting homologous DOM, whereas glutamine and glyoxylate transformations remained abundant in *E. gracilis* F3 DOM. Overall, the process of fractionation led to variable proportions of DOM compounds within each fraction, with more variability in DOM composition at lower molecular weight fractions and less variability at higher DOM fractions.

4.4.5 Relationship between Microbial Hg uptake and Phytoplankton DOM Composition

To identify which biogenic compounds were most likely altering Hg uptake, spectral networks were used to visualize molecular transformations abundant in euglenoid DOM against normalized aerobic and anaerobic Hg uptake data (Figure 4.3). Significant positive relationships were found with aerobic Hg uptake, for glutamine and serine, and with anaerobic Hg uptake for cytosine, glutamine, and polyamine transformations. Given the importance of sulfur functional groups on Hg speciation [59,60], three sulfur containing biogenic isomers including cysteine, methionine, and glutathione were identified; however, they were found at greater proportions in Chlorophyta DOM rather than in Euglenoid DOM (Figure B6).

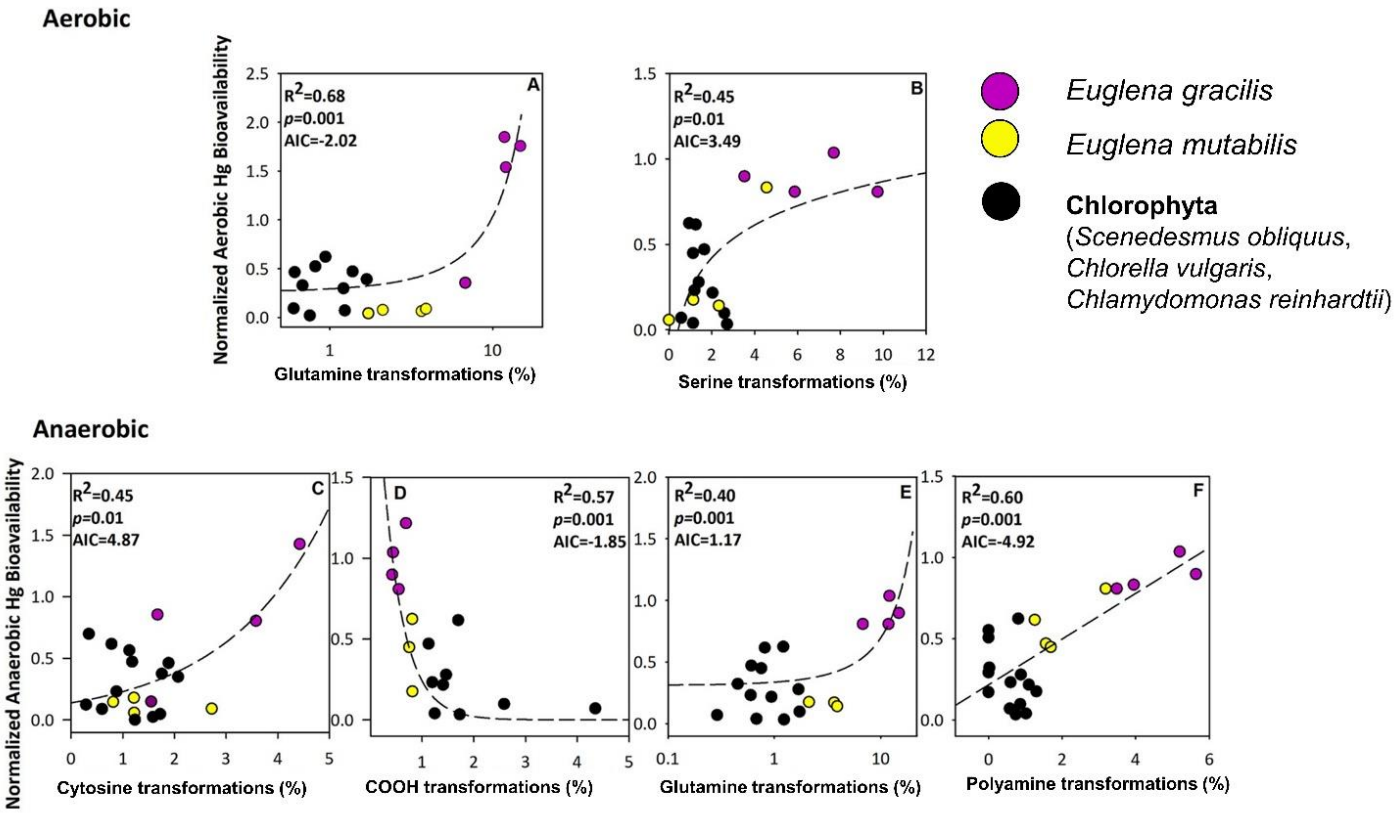

Figure 4.3. Relationships between algal functional groups and Hg bioavailability. Significant model II regression models outlining relationships between Hg bioavailability the percent relative abundance of recorded molecular transformations determined by FTIR-MS. Aerobic bioavailability and the biomolecules C5H10N2O3 (glutamine; A) and C3H7NO3 (serine; B) isomers. Anaerobic Hg bioavailability and biomolecules are also expressed for C4H5N3O (cytosine; C), COOH functional groups (D), C5H10N2O3 (glutamine; E), and C5H14N2 (polyamine; F) isomers. Both euglenoids are highlighted where yellow corresponds to points corresponding to *E. mutabilis* and purple highlights the points influenced by *E. gracilis*.

Amino acids such as glutamine (Figure 4.3 A,E; AIC = −2.02 and 1.17, respectively) or serine (Figure 4.3 B; AIC = −3.49) are essential nutrients for microbial biosynthetic pathways [61-63] as they are important primary amide donors during the biosynthesis of nucleotides [64,65]. Cytosine (Figure 4.3 C; AIC = 4.87) is one of the essential nucleotides involved in the formation of DNA and plays a role in cytidine triphosphate (CTP) formation, an important metabolic cofactor. Soft metals such as Hg and silver (Ag) have been shown to form metal complexes with cytosine and thymine [66-68]. It is possible that the binding of Hg to these amine compounds facilitates its accidental transport inside the cell [62,65]. That being said, we cannot rule out the

possibility that these compounds only facilitate the transfer of Hg from solution, through the diffusion boundary layer, to yet unidentified transport sites.

Carboxylic (COOH) transformations were exponentially and negatively correlated with anaerobic Hg uptake ($R2 = 0.57$, $p = 0.001$, AIC = −1.85; Figure 4.3 D). An increase in COOH transformations in DOM yielded an exponential decrease in Hg uptake irrespective of algal or euglenoid taxa (data not shown). Euglenoid DOM yielded the lowest proportion of COOH transformation (0.41–0.80%) whereas Chlorophyte DOM ranged from 0.69 to 4.34%. Carboxylic acid functional groups are usually associated with higher molecular weight DOM fractions and can have a strong affinity for divalent Hg through the chelate effect, resulting in complexes that are unlikely to pass through biological membranes [69]. These functional groups have been identified in C. vulgaris and C. reinhardtii EPS as being responsible for the rapid removal of Hg from solution [70-71], further supporting the binding and scavenging role of larger, less bioavailable, multidentate DOM complexes [58-60].

Polyamine transformations were positively related to anaerobic Hg uptake ($R2 = 0.60$, $p = 0.001$, AIC = −4.92; Figure 4.3 F) in both euglenoid species containing the highest proportion of polyamine transformations, with the strongest influence from *E. gracilis*. The high degree of affinity of Hg for polyamines, the multitude of microbial uptake systems for polyamines [72-75], and the fact that these systems have been reported to facilitate cation transport [76] suggest that polyamine transport represents an underappreciated uptake pathway for Hg. Indeed, in addition to being part of biogenic algal DOM, polyamine compounds such as cadaverine and putrescine are typically produced during the anaerobic fermentative breakdown of amino acids from dead organisms possibly offering a novel route for Hg uptake in anoxic soils and sediments.

Although we observed enhanced Hg uptake in the presence of discrete DOM size fraction when compared to bulk DOM, we did not observe an enhancement of uptake when compared to no DOM controls. This data highlights a very important emergent property of DOM related to how different biomolecules that comprise the complex DOM pool interact to affect metal uptake. To the best of our knowledge, the role of such emergent properties of DOM on Hg bioavailability remains poorly understood. The process of DOM fractionation led to more variable DOM in lower molecular weight fractions whereas similar DOM compositions were observed at higher molecular weight fractions within euglenoids and chlorophyta. The presence of ketol transformations conserved in F3 among all chlorophyta sheds light into the limited Hg uptake of F3 in both aerobic and anaerobic conditions, as most Hg may be complexed to the abundant oxygen heteroatoms present in large molecules.

4.4.6 Environmental Implications

Using a multipronged approach, we show that DOM from diverse primary producers differentially affect microbial Hg uptake. We propose that amino acids and polyamine biomolecules present in algal DOM are potentially underappreciated ligands involved in enhanced microbial Hg uptake. Our data fits in a broader context where eutrophication, one of the greatest threats to the health of water bodies worldwide, may contribute to conditions that increase Hg bioavailability while also creating conditions optimal for Hg methylation [77]. While unfractionated bulk mixtures of chlorophyte DOM inhibit bacterial Hg uptake, processes leading to fractionation of algal DOM, such as photo or microbial degradation, may trigger periods of increased microbial Hg uptake. Increasing anthropogenic nutrient loading combined with a warming climate stimulate primary production and increase concentrations of autochthonous DOM [78]. One extreme consequence of a stimulation of primary production is eutrophication that

causes ecosystem degradation and anoxia. Eutrophication also often leads to shifts in primary producer community structure [79]. Euglenoids and other mixotrophic algae thrive in water or in sediments of eutrophic and hypertrophic aquatic ecosystems [35], suggesting that their increasing abundance under warming conditions may alter Hg bioavailability. Additional work is required to determine the environmental drivers of phytoplankton assemblage in a warming climate and how such drivers will affect primary producer dynamics potentially releasing biogenic compounds controlling the fate of Hg.

4.5 Acknowledgements

We thank the members of the Guéguen and Poulain laboratories for discussions and insights when preparing this manuscript. We would also like to thank Antoine Perroud for his assistance with DOC analyses, Dr. Chad Cuss for his assistancewith flow field-flow fractionation, and Dr. Naomi Stock for her help with high-resolution mass spectrometry. Special thanks to the Editor and two anonymous reviewers for their insights and feedback to strengthen the manuscript. This study was funded by the Canada Research Chairs program (CG), the Natural Sciences and Engineering Research Council of Canada (AJP, CG, VM), an Early Researcher Award from the Province of Ontario (AJP), and the Canadian Foundation for Innovation, (CG and AJP). Funding was also provided by the W. Garfield Weston Doctoral Award for Northern Research (VM).

4.6 References

1. Pirrone, N.; Cinnirella, S.; Feng, X.; Finkelman, R. B.; Friedli, H. R.; Leaner, J.; Mukherjee, A. B.; Stracher, G. B.; Streets, D. G.; Telmer, K. Global mercury emission to the atmosphere from anthropogenic and natural sources. *Atmos. Chem. Phys.* **2010**, ***10***, 5951– 5964, DOI: 10.5194/acp-10-5951-2010
2. Streets, D. G.; Zhang, Q.; Wu, Y. Projections of global mercury emissions in 2050. *Environ. Sci. Technol.* **2009**, ***43***, 82983– 2988, DOI: 10.1021/es802474j

3. Driscoll, C. T.; Mason, R. P.; Chan, H. M.; Jacob, D. J.; Pirrone, N. Mercury as a global pollutant: Sources, Pathways and Effects. *Environ. Sci. Technol.* **2013**, ***47***, 4967– 4983, DOI: 10.1021/es305071v

4. Hintelmann, H. Organomercurials. Their formation and pathways in the environment. *Met. Ions Life Sci.* **2010**, ***7***, 365– 401, DOI: 10.1039/9781849730822-00365

5. Lehnherr, I.; St. Louis, V.; Hintelmann, H.; Kirk, J. L. Methylation of inorganic mercury in polar marine waters. *Nat. Geosci.* **2011**, ***4***, 298– 302, DOI: 10.1038/ngeo1134

6. Soerensen, A. L.; Jacob, D. J.; Schartup, A. T.; Fisher, J. A.; Lehnherr, I.; St. Louis, V.; Heimburger, L. E.; Sonke, J. E.; Krabbenhoft, D. P.; Sunderland, E. M. A mass budget for mercury and methylmercury in the Arctic Ocean. *Glob. Biogeochem. Cycles.* **2016**, ***30*** (4), 560– 575, DOI: 10.1002/2015GB005280

7. Heimbürger, L. E.; Sonke, J.; Cossa, D.; Point, D.; Lagane, C.; Laffont, L.; Galfond, B. T.; Nicolaus, M.; Rabe, B.; van der Loeff, M. R. Shallow methylmercury production in the marginal sea ice zone of the central Arctic Ocean. *Sci. Rep.* **2015**, ***5*** (10318), 1– 6, DOI: 10.1038/srep10318

8. Gionfriddo, C. M.; Tate, M. T.; Wick, R. R.; Schultz, M. B.; Zemla, A.; Thelen, M. P.; Schofield, R.; Krabbenhoft, D. P.; Holt, K. E.; Moreau, J. W. Microbial mercury methylation in Antarctic sea ice. *Nat. Microbiol.* **2016**, ***1*** (10), 16127, DOI: 10.1038/nmicrobiol.2016.127

9. Dranguet, P.; Le Faucheur, S.; Slaveykova, V. I. Mercury bioavailability, transformations, and effects on freshwater biofilms. *Environ. Toxicol. Chem.* **2017**, ***36*** (12), 3194– 3205, DOI: 10.1002/etc.3934

10. Olsen, T. A.; Brandt, C. C.; Brooks, S. C. Periphyton biofilms influence net methylmercury production in an industrially contaminated system. *Environ. Sci. Technol.* **2016**, ***50***, 10843– 10850, DOI: 10.1021/acs.est.6b01538

11. Leclerc, M.; Planas, D.; Amyot, M. Relationship between extracellular low molecular weight thiols and mercury species in natural lake periphytic biofilms. *Environ. Sci. Technol.* **2015**, ***49***, 7709– 7716, DOI: 10.1021/es505952x

12. Parks, J. M.; Johs, A.; Podar, M.; Bridou, R.; Hurt, R. A.; Smith, S. D.; Tomanicek, S. J.; Qian, Y.; Brown, S. D.; Brandt, C. C.; Palumbo, A. V.; Smith, J. C.; Wall, J. D.; Elias, D. A.; Liang, L. The genetic basis for bacterial mercury methylation. *Science* **2013**, ***339***, 1332– 1335, DOI: 10.1126/science.1230667

13. Lázaro, W. L.; Guimarães, J. R. D.; Ignácio, A. R.; Da Silva, C. J.; Díez, S. Cyanobacteria enhance methylmercury production: a hypothesis tested in the periphyton of two lakes in the Pantanal floodplain, Brazil. *Sci. Total Environ.* **2013**, ***456***, 231– 238, DOI: 10.1016/j.scitotenv.2013.03.022

14. Lázaro, W. L.; Díez, S.; da Silva, C. J.; Ignácio, Á. R. A.; Guimarães, J. R. D. Seasonal changes in peryphytic microbial metabolism determining mercury methylation in a tropical wetland. *Sci. Total Environ.* **2018**, ***627***, 1345– 1352, DOI: 10.1016/j.scitotenv.2018.01.186

15. Gentès, S.; Taupiac, J.; Colin, Y.; André, J. M.; Guyoneaud, R. Bacterial periphytic communities related to mercury methylation within aquatic plant roots from a temperate freshwater lake (South-Western France). *Environ. Sci. Pollut. Res.* **2017**, ***24*** (23), 19223– 19233, DOI: 10.1007/s11356-017-9597-x

16. Franco, M. W.; Mendes, L. A.; Windmoller, C. C.; Moura, K. A. F.; Oliveira, L. A. G.; Barbosa, F.A. R. Mercury methylation capacity and removal of Hg species from aqueous medium by cyanobacteria. *Water, Air, Soil Pollut.* **2018**, ***229*** (127), 1– 12, DOI: 10.1007/s11270-018-3782-5

17. Baines, S. B.; Pace, M. L. The production of dissolved organic matter by phytoplankton and its importance to bacteria: Patterns across marine and freshwater systems. *Limnol. Oceanogr.* **1991**, ***36***, 1078– 1090, DOI: 10.4319/lo.1991.36.6.1078

18. Christensen, G. A.; Somenahally, A. C.; Moberly, J. G.; Miller, C. M.; King, A. J.; Gilmour, C. C.; Brown, S. D.; Podar, M.; Brandt, C. C.; Brooks, S. C.; Palumbo, A. V.; Wall, J. D.; Elias, D. A. Carbon amendments alter microbial community structure and net methylmercury potential in sediments. *Appl. Environ. Microbiol.* **2018**, ***84*** (3), 1– 14, DOI: 10.1128/AEM.01049-17

19. Graham, E. B.; Gabor, R. S.; Schooler, S.; McKnight, D. M.; Nemergut, D. R.; Knelman, J. E. Oligotrophic wetland sediments susceptible to shifts in microbiomes and mercury cycling with dissolved organic matter addition. *PeerJ* **2018**, ***6*** (e4575), 1– 26, DOI: 10.7717/peerj.4575

20. Celo, V.; Lean, D. R. S.; Scott, S. L. Abiotic methylation of mercury in the aquatic environment. *Sci. Total Environ.* **2006**, ***368*** (1), 126– 137, DOI: 10.1016/j.scitotenv.2005.09.043

21. Hsu-Kim, H.; Kucharzyk, K. H.; Zhang, T.; Deshusses, M. A. Mechanisms regulating mercury bioavailability for methylating microorganisms in the aquatic environment: a critical review. *Environ. Sci. Technol.* **2013**, ***47*** (6), 2441– 2456, DOI: 10.1021/es304370g

22. Liu, G., Cai, Y.; O'Driscoll, N. *Environmental chemistry and toxicology of mercury*; John Wiley & Sons: 2011.

23. Moreau, J. W.; Gionfriddo, C. M.; Krabbenhoft, D. P.; Ogorek, J. M.; DeWild, J. F.; Aiken, G. R.; Roden, E. E. The effect of natural organic matter on mercury methylation by *Desulfobulbus propionicus* 1pr3. *Front. Microbiol.* **2015**, ***6*** (1389), 1– 15, DOI: 10.3389/fmicb.2015.01389

24. Chiasson-Gould, S. A.; Blais, J. M.; Poulain, A. J. Dissolved organic matter kinetically controls mercury bioavailability to bacteria. *Environ. Sci. Technol.* **2014**, ***48***, 3153– 3161, DOI: 10.1021/es4038484

25. Graham, A. M.; Bullock, A. L.; Maizel, A. C.; Elias, D. A.; Gilmour, C. C. Detailed assessment of the kinetic of Hg-cell association, Hg methylation, and methylmercury degradation in several *Desulfovibrio* species. *Appl. Environ. Microbiol.* **2012**, ***78*** (20), 7337– 7346, DOI: 10.1128/AEM.01792-12

26. Ortega, S. H.; Catalan, N.; Bjorn, E.; Grontoft, H.; Hilmarsson, T. G.; Bertilsson, S.; Wu, P.; Bishop, K.; Levanoni, O.; Bravo, A. G. High methylmercury formation in ponds fuelled by fresh humic and algal derived organic matter. *Limnol. Oceanogr.* **2018**, ***63***, 544– 553, DOI: 10.1002/lno.10722

27. Bravo, A. G.; Bouchet, S.; Tolu, J.; Bjorn, E.; Mateos-Rivera, A.; Bertilsson, S. Molecular composition of organic matter controls methylmercury formation in boreal lakes. *Nat. Commun.* **2017**, ***8***, 14255– 9, DOI: 10.1038/ncomms14255

28. Graham, A. M.; Aiken, G. R.; Gilmour, C. C. Effect of Dissolved Organic Matter Source and Character on Microbial Hg Methylation in Hg–S–DOM Solutions. *Environ. Sci. Technol.* **2013**, ***47***, 5746– 5754, DOI: 10.1021/es400414a

29. Dieguez, M. C.; Queimalinos, C. P.; Guevara, S. R.; DiPasquale, M. M.; Cardenas, C. S.; Arribere, M. A. Influence of dissolved organic matter character on mercury incorporation by planktonic organisms: An experimental study using oligotrophic water from Patagonian lakes. *J. Environ. Sci.* **2013**, ***25***, 1980– 1991, DOI: 10.1016/S1001-0742(12)60281-2

30. Toming, K.; Tuvikene, L.; Vilbaste, S.; Agasild, H.; Vikk, M.; Kisand, A.; Feldmann, T.; Martma, T.; Jones, R. I.; Noges, T. Contributions of autochthonous and allochthonous sources to dissolved organic matter in a large shallow, eutrophic lake with a highly calcareous catchment. *Limnol. Oceanogr.* **2013**, ***58*** (4), 1259– 1270, DOI: 10.4319/lo.2013.58.4.1259

31. Huertas, E.; Rouco, M.; Lopez-Rodas, V.; Costas, E. Warming will affect phytoplankton differently: evidence through a mechanistic approach. *Proc. R. Soc. London, Ser. B* **2011**, ***278*** (1724), 3534– 3543, DOI: 10.1098/rspb.2011.0160

32. Bopp, L.; Aumont, O.; Cadule, P.; Alvain, S.; Gehlen, M. Response of diatoms distribution to global warming and potential implications: A global model study. *Geophys. Res. Lett.* **2005**, ***32*** (19), 1– 4, DOI: 10.1029/2005GL023653

33. Paerl, H. W.; Gardner, W. S.; Havens, K. E.; Joyner, A. R.; McCarthy, M. J.; Newell, S. E.; Qin, B.; Scott, T. Mitigating cyanobacterial harmful algal blooms in aquatic ecosystems impacted by climate change and anthropogenic nutrients. *Harmful Algae* **2016**, ***54***, 213– 222, DOI: 10.1016/j.hal.2015.09.009

34. Winder, M.; Sommer, U. Phytoplankton response to a changing climate. *Hydrobiologia* **2012**, ***698***, 5– 16, DOI: 10.1007/s10750-012-1149-2

35. Benoit, J. M.; Mason, R. P.; Glimour, C. C.; Aiken, G. R. Constant for mercury binding by dissolved organic matter isolates from the Florida Everglades. *Geochim. Cosmochim. Acta* **2001**, ***65***, 4445– 4451, DOI: 10.1016/S0016-7037(01)00742-6

36. Miller, C. L.; Mason, R. P.; Gilmour, C. C.; Heyes, A. Influence of dissolved organic matter on the complexation of mercury under sulfidic conditions. *Environ. Toxicol. Chem.* **2007**, ***26***

(4), 624– 633, DOI: 10.1897/06-375R.1

37. Dasgupta, S.; Fang, J.; Brake, S. S.; Hasiotis, S. T.; Zhang, L. Biosynthesis of sterols and wax esters by *Euglena* of acid mine drainage biofilms: Implications for eukaryotic evolution and the early Earth. *Chem. Geol.* **2012**, ***306–307***, 139– 145, DOI: 10.1016/j.chemgeo.2012.03.003

38. Krohn-Molt, I.; Wemheuer, B.; Alawi, M.; Poehlein, A.; Gullert, S.; Schmeisser, C.; Pommerening-Roser, A.; Grundhoff, A.; Daniel, R.; Hanelt, D.; Streit, W. R. Metagenome survey of multispecies and alga-associated biofilm revealed key elements of bacterial-algal interactions in photobioreactors. *Appl. Environ. Microbiol.* **2013**, ***79*** (20), 6196– 6206, DOI: 10.1128/AEM.01641-13

39. Mangal, V.; Guéguen, C. Examining concentrations and molecular weights of thiols in microorganism cultures and in Churchill River (Manitoba) using a fluorescent-labeling method coupled to asymmetrical flow field-flow fractionation. *Anal. Bioanal. Chem.* **2015**, ***407*** (15), 4305– 4313, DOI: 10.1007/s00216-015-8599-0

40. Guéguen, C.; Cuss, C. Characterization of aquatic dissolved organic matter by asymmetrical flow field-flow fractionation coupled to UV-Visible diode array and excitation emission matrix fluorescence. *J. Chromatogr. A* **2011**, ***1218*** (27), 4188– 4198, DOI: 10.1016/j.chroma.2010.12.038

41. Reszat, T. N.; Hendry, J. M. Characterizing dissolved organic carbon using asymmetrical flow field flow fractionation with on-line UV and DOC detection. *Anal. Chem.* **2005**, ***77***, 4194– 4200, DOI: 10.1021/ac048295c

42. Kujawinski, E. B.; Freitas, M. A.; Zhang, X.; Hatcher, P. G.; Green-Church, K. B.; Jones, B. R. The application of electrospray ionization mass spectrometry (ESI MS) to the structural characterization of natural organic matter. *Org. Geochem.* **2002**, ***33***, 171– 180, DOI: 10.1016/S0146-6380(01)00149-8

43. Stenzler, B.; Hinz, A.; Ruuskanen, M.; Poulain, A. J. Ionic strength differentially affects the bioavailability of neutral and negatively charged inorganic Hg complexes. *Environ. Sci. Technol.* **2017**, ***51***, 9653– 9662, DOI: 10.1021/acs.est.7b01414

44. Winters, C.; Guéguen, C.; Noble, A. Equilibrium and kinetic studies of Cu (II) and Ni (II) sorption on living *Euglena gracilis*. *J. Appl. Phycol.* **2017**, ***29*** (3), 1391– 1398, DOI: 10.1007/s10811-016-1040-z

45. Drepper, T.; Eggert, T.; Circolone, F.; Heck, A.; Krauss, U.; Guterl, J. K.; Wendorff, M.; Losi, A.; Gartner, W.; Jaeger, K. E. Reporter proteins for in vivo fluorescence without oxygen. *Nat. Biotechnol.* **2007**, ***25***, 443– 445, DOI: 10.1038/nbt1293

46. Viant, M. R.; Sommer, U. Mass spectrometry based environmental metabolomics: a primer and review. *Metabolomics* **2013**, ***9***, 144– 1568, DOI: 10.1007/s11306-012-0412-x

47. Longnecker, K.; Kujawinski, E. B. Using network analysis to discern compositional patterns in ultrahigh-resolution mass spectrometry data of dissolved organic matter. *Rapid Commun. Mass Spectrom.* **2016**, ***30***, 2388– 2394, DOI: 10.1002/rcm.7719

48. Burgess, K. E. V.; Borutzki, Y.; Rankin, N.; Jourdan, F. MetaNetter 2: A Cytoscape plugin for ab initio network analysis and metabolite feature classification. *J. Chromatogr. B: Anal. Technol. Biomed. Life Sci.* **2017**, ***1071***, 68– 74, DOI: 10.1016/j.jchromb.2017.08.015

49. Mangal, V.; Shi, Y. X.; Guéguen, C. Compositional changes and molecular transformations of dissolved organic matter during the arctic spring floods in the lower Churchill watershed (Northern Manitoba, Canada), 2017, **136** (2 151– 165, DOI: 10.1007/s10533-017-0388-8 .

50. Hammer, O.; Harper, D. A. T.; Ryan, P. D. Paleontological statistics software package for education and data analysis. *Palaeontologia Electronica.* **2001**, ***4*** (1), 1– 9

51. Babicki, S.; Arndt, D.; Marcu, A.; Liang, Y.; Grant, J. R.; Maciejewski, A.; Wishart, D. S. Heatmapper: web-enabled heat mapping for all. *Nucleic Acids Res.* **2016**, ***44***, W147–W153, DOI: 10.1093/nar/gkw419

52. Zhou, K.; Hu, Y.; Yang, K. Lin. The role of exopolymeric substances in the bioaccumulation and toxicity of Ag nanoparticles to algae. *Sci. Rep.* **2016**, ***6***, 32998, DOI: 10.1038/srep32998

53. Decho, A. W.; Gutierrez, T. Microbial Extracellular Polymeric Substances (EPSs) in Ocean Systems. *Front. Microbiol.* **2017**, ***8***, 922, DOI: 10.3389/fmicb.2017.00922

54. Gupta, P.; Diwan, B. Bacterial Exopolysaccharide mediated heavy metal removal: a review on biosynthesis, mechanism and remediation strategies. *Biotechnol. Rep.* **2017**, ***13***, 58–71, DOI: 10.1016/j.btre.2016.12.006

55. Zeraatkar, A. K.; Ahmadzadeh, H.; Talebi, A. F.; Moheimani, N. R.; McHenry, M. P. Potential use of algae for heavy metal bioremediation, a critical review. *J. Environ. Manage.* **2016**, ***181***, 817– 831, DOI: 10.1016/j.jenvman.2016.06.059

56. Devars, S.; Aviles, C.; Cervantes, C.; Moreno-Sanchez, R. Mercury uptake and removal by Euglena gracilis. *Arch. Microbiol.* **2000**, ***174*** (3), 175– 80, DOI: 10.1007/s002030000193

57. Koukal; Gueguen, C.; Pardos, M.; Dominik, J. Influence of humic substances on the toxic effects of cadmium and zinc to the green alga Pseudokirchneriella subcapitata. *Chemosphere* **2003**, ***53*** (8), 953– 961, DOI: 10.1016/S0045-6535(03)00720-3

58. Smith, K. S.; Balistrieri, L. S.; Todd, A. S. Using biotic ligand models to predict metal toxicity in mineralized systems. *Appl. Geochem.* **2015**, ***57***, 55– 72, DOI:

10.1016/j.apgeochem.2014.07.005

59. Hesterberg, D.; Chou, J. W.; Hutchinson, K. J.; Sayers, D. E. Bonding of Hg(II) to reduced organic sulfur in humic acid as affected by S/Hg ratio. *Environ. Sci. Technol.* **2001**, ***35*** (13), 2741– 2745, DOI: 10.1021/es001960o

60. Haitzer, M.; Aiken, G. R.; Ryan, J. N. Binding of mercury (II) to dissolved organic matter: The role of the mercury to DOM concentration ratio. *Environ. Sci. Technol.* **2002**, ***36***, 3564– 3570, DOI: 10.1021/es025699i

61. Weiner, J. H.; Heppel, L. A. A binding protein for glutamine and its relation to active transport in *E. Coli*.. *Arch. Biochem. Biophys.* **1971**, ***246***, 6933– 6941, DOI: 10.1016/0003-9861(71)90538-8

62. Forchhammer, K. Glutamine signaling in bacteria. *Front. Biosci., Landmark Ed.* **2007**, ***12***, 358– 70, DOI: 10.2741/2069

63. Schaefer, J. K.; Morel, F. M. M. High methylation rates of mercury bound to cysteine by *Geobacter sulfurreducens*. *Nat. Geosci.* **2009**, ***2***, 123– 126, DOI: 10.1038/ngeo412

64. Prusiner, S.; Stadtman, E. R. *The enzymes of glutamine metabolism*; Academic Press, Inc.: New York, NY, 1973.

65. Tanaka, K. J.; Song, S.; Mason, K.; Pinkett, H. W. Selective substrate uptake: The role of ATP-binding cassette (ABC) transporters in pathogenesis. *Biochim. Biophys. Acta, Biomembr.* **2018**, ***1860***, 866– 877, DOI: 10.1016/j.bbamem.2017.08.011

66. Ono, A.; Cao, S.; Togashi, H.; Tashiro, M.; Fujimoto, T.; Machinami, T.; Miyake, Y.; Okamoto, I.; Tanaka, Y. Specific interactions between silver(I) ions and cytosine-cytosine pairs in DNA duplexes. *Chem. Commun.* **2008**, ***39***, 4825– 4827, DOI: 10.1039/b808686a

67. Yamaguchi; Sebera, J.; Kondo, J.; Komuro, T.; Kawamura, T.; Dairaku, T.; Kondo, Y.; Okamoto, I.; Ono, A.; Burda, J. B.; Kojima, C.; Sychrovsky, V.; Tanaka, Y. The structure of metallo-DNA with consecutive thymine-Hg^{II}-thymine base pairs explains positive entropy for the metallo base pair formation. *Nucleic Acids Res.* **2014**, ***42*** (6), 4094– 4099, DOI: 10.1093/nar/gkt1344

68. Nies, D. H. Microbial heavy-metal resistance. *Appl. Microbiol. Biotechnol.* **1999**, ***51*** (6), 730– 750, DOI: 10.1007/s002530051457

69. Ndu, U.; Mason, R. P.; Zhang, H.; Lin, S.; Visscher, P. T. Effect of inorganic and organic ligands on the bioavailability of methylmercury as determined using a *mer-lux* bioreporter. *Appl. Environ. Microbiol.* **2012**, ***78*** (20), 7276– 7282, DOI: 10.1128/AEM.00362-12

70. Tuzun, I.; Bayramoglu, G.; Yalcin, E.; Basaran, G.; Celik, G.; Arica, M. Y. Equilibrium and kinetic studies on biosorption of Hg(II), Cd(II) and Pb(II) ions onto microalgae

Chlamydomonas reinhardtii. *J. Environ. Manage.* **2005**, ***77*** (2), 85– 92, DOI: 10.1016/j.jenvman.2005.01.028

71. Peng, Y.; Liu, X.; Gong, X.; Li, X.; Liu, Y.; Leng, E.; Zhang, Y. Enhanced Hg(II) Adsorption by Monocarboxylic-Acid-Modified Microalgae Residuals in Simulated and Practical Industrial Wastewater. *Energy Fuels* **2018**, ***32*** (4), 4461– 4468, DOI: 10.1021/acs.energyfuels.7b03094

72. Foti, C.; Giuffre, O.; Lando, G.; Sammartano, S. Interaction of inorganic mercury (II) with polyamines, polycarboxylates and amino acids. *J. Chem. Eng. Data* **2009**, ***54***, 893– 903, DOI: 10.1021/je800685c

73. Halvorson, H. Utilization of single L-amino acids as sole source of carbon and nitrogen by bacteria. *Can. J. Microbiol.* **1972**, ***18***, 1647– 1650, DOI: 10.1139/m72-255

74. Igarashi, K.; Kashiwaqi, K. Polyamine uptake systems in *Escherichia coli*. *Res. Microbiol.* **2001**, ***152***, 271– 278, DOI: 10.1016/S0923-2508(01)01198-6

75. Kurihara, S.; Suzuki, H. Recent advances in bacterial polyamine transport systems. *Polyamines.* **2015**, 171– 178, DOI: 10.1007/978-4-431-55212-3_14

76. Pottosin, I.; Shabala, S. Polyamines control of cation transport across plant membranes: implications for ion homeostasis and abiotic stress signaling. *Front. Plant Sci.* **2014**, ***5*** (154), 1– 16, DOI: 10.3389/fpls.2014.00154

77. Krabbenhoft, D. P.; Sunderland, E. M. Global change and mercury. *Science* **2013**, ***341***, 1457– 1458, DOI: 10.1126/science.1242838

78. Heinsalu, A.; Alliksaar, T.; Leeben, A.; Noges, T. Sediment diatom assemblages and composition of pore-water dissolved organic matter reflect recent eutrophication history of Lake Peipsi (Estonia/Russia). *Hydrobiologia* **2007**, ***584***, 133– 143, DOI: 10.1007/s10750-007-8615-2

79. Hallegraeff, G. M. Ocean climate change, phytoplankton community responses, and harmful algal blooms: a formidable predictive challenge. *J. Phycol.* **2010**, ***46***, 220– 235, DOI: 10.1111/j.1529-8817.2010.00815.x

Chapter 5: Golden Gate Assembly of Aerobic and Anaerobic Microbial Bioreporters

Aaron Hinz[a], Benjamin Stenzler[a], & Alexandre J. Poulain[a#]

[a]Department of Biology, University of Ottawa, Ottawa, Ontario, Canada

[#]**Correspondence:** Dr. Alexandre Poulain

E-mail address: apoulain@uottawa.ca

Direct link: https://journals.asm.org/doi/abs/10.1128/AEM.01485-21

Author Contributions :

A.J.P. supervised the project. A.H designed the method and generated the bioreporters. B.S designed the experiments and protocols to operate the bioreporters. and A.J.P. designed the research and methodologies. A.H, B.S, and A.J.P. performed analyses on the data. A.H, B.S, and A.J.P wrote the paper.

Keywords: bioreporters, Golden Gate assembly, fluorescent proteins, luciferase, flavin-based fluorescent protein, metal biosensors

N.B. Supporting information for this chapter can be found in **Appendix C**.

5.1 Abstract

Microbial bioreporters provide direct insight into cellular processes by producing a quantifiable signal dictated by reporter gene expression. The core of a bioreporter is a genetic circuit in which a reporter gene (or operon) is fused to promoter and regulatory sequences that govern its expression. In this study, we develop a system for constructing novel *Escherichia coli* bioreporters based on Golden Gate assembly, a synthetic biology approach for the rapid and seamless fusion of DNA fragments. Gene circuits are generated by fusing promoter and reporter sequences encoding yellow fluorescent protein, mCherry, bacterial luciferase, and an anaerobically active flavin-based fluorescent protein. We address a barrier to the implementation of Golden Gate assembly by designing a series of compatible destination vectors that can accommodate the assemblies. We validate the approach by measuring the activity of constitutive bioreporters and mercury and arsenic biosensors in quantitative exposure assays. We also demonstrate anaerobic quantification of mercury and arsenic in biosensors that produce flavin-based fluorescent protein, highlighting the expanding range of redox conditions that can be examined by microbial bioreporters.

5.2 Importance

Microbial bioreporters are versatile genetic tools with wide-ranging applications, particularly in the field of environmental toxicology. For example, biosensors that produce a signal output in the presence of a specific analyte offer less costly alternatives to analytical methods for the detection of environmental toxins such as mercury and arsenic. Biosensors of specific toxins can also be used to test hypotheses regarding mechanisms of uptake, toxicity, and biotransformation. In this study, we develop an assembly platform that uses a synthetic biology technique to

streamline construction of novel *Escherichia coli* bioreporters that produce fluorescent or luminescent signals either constitutively or in response to mercury and arsenic exposure. Beyond the synthesis of novel biosensors, our assembly platform can be adapted for numerous applications, including labelling bacteria for fluorescent microscopy, developing gene expression systems, and modifying bacterial genomes.

5.3 Introduction

Microbial bioreporters are living host organisms that produce a quantifiable signal in response to the prevailing environmental conditions (1). By providing access to the inner workings of living cells, experiments with microbial bioreporters have fundamentally contributed to the knowledge of microbial genetics, physiology, and ecology (2–4). In the field of environmental toxicology, bioreporters offer a simple and cost-effective alternative to analytical methods for quantifying toxic chemicals, while conveying crucial biological insights about toxin bioavailability and cellular stress responses (4).

Microbial bioreporters can be categorized based on whether they produce constitutive or inducible signal outputs, also referred to as “light off” or “light on” biosensors. The constitutive “light off” bioreporters emit a continuous signal and are widely used for fluorescent cell labeling and toxicological screening where the signal intensity decreases with the presence of a toxic response (4, 5). In contrast, inducible “light on” bioreporters produce a signal induced by the intracellular presence of a specific analyte or stressor (1, 5). Inducible biosensors are particularly effective at detecting toxic metals and metalloids that bind with high specificity to regulatory proteins (4), and can be far more sensitive, biologically relevant, and practical than other analytical detection methods (6). The potential applications of microbial biosensors are

effectively limitless and include rapid and cheap monitoring of environmental contaminants, assessing their bioavailability, and bioremediation (2, 7–9). Because signal production depends on the bioaccessibility (e.g., access to the cell wall) and bioavailability (e.g., transport across the cell wall) of the analyte (2, 10), biosensors allow researchers to investigate genetic and environmental factors that modulate uptake and transformation of toxins in living cells (11, 12). In addition, biosensors enable the rapid high-throughput screening of environmental samples prior to more costly and in-depth analyses, and can provide an affordable and portable alternative for rapid decision making when analytical support is limited (e.g., in developing countries or remote areas) (4, 13).

The functionality of a bioreporter is determined by promoter sequences that activate expression of a reporter gene (or operon) that produces a quantifiable signal (e.g., green fluorescent protein, luciferase, etc.). Inducible bioreporters can additionally encode regulatory factors that control reporter gene expression in response to a substrate (e.g., the mercury-binding MerR regulator) (14). Bioreporter construction thus involves fusing reporter genes to a promoter and regulatory sequences to create synthetic genetic circuits that are maintained in the host organism on replicating plasmids or integrated into the chromosome (2). The process, however, is often laborious and challenging to scale up, generally relying on traditional molecular cloning methods that involve sequential restriction enzyme digestion, DNA cleanup, and ligation reactions. Synthetic biology methods have emerged as promising alternatives for applications such as DNA assembly (BioBricks, Gibson assembly, Golden Gate assembly, USER fusion, yeast recombination cloning), gene synthesis, and genome editing (MAGE, CRISPR) (15–20). These methods have the potential to vastly increase the efficiency and scale of DNA manipulations but can be challenging for researchers to implement. A major barrier to the

implementation of synthetic biology procedures is the requirement of compatible destination vectors, which often have a limited scope of application. To take full advantage of novel cloning methods, it is necessary to increase the diversity, functionality, and accessibility of destination vectors (21, 22).

In this study, we use Golden Gate assembly, a synthetic biology method that produces seamless DNA fusions (23, 24), to build genetic circuits for bioreporters. The approach relies on Type IIS restriction endonucleases, which in contrast to traditional endonucleases, cleave DNA outside of enzyme recognition sequences. The absence of recognition sequence "scars" in the ligated DNA allows for seamless fusion of DNA fragments in "one-pot" cloning reactions that can be used to rapidly construct multi-fragment assemblies, while eliminating time-consuming intermediate steps (23). We present here a streamlined bioreporter construction platform based on the interchangeable assembly of promoter and reporter gene inserts with novel Golden Gate destination vectors. We validated the method by constructing constitutive bioreporters and analyte biosensors that express fluorescent proteins, bacterial luciferase, and a flavin-based fluorescent protein that is active in both aerobic and anaerobic growth environments. Using a common *E. coli* host strain, we measured the signal strength of constitutive reporters, the detection dynamics of mercury and arsenic biosensors, and optimized anaerobic detection of bioreporters that produce flavin-based fluorescent protein.

5.4 Results and Discussion

5.4.1 Novel Golden Gate destination vectors

We constructed novel destination vectors that accommodate the assembly of promoter-reporter gene fusions in “one-pot” Golden Gate assembly reactions involving the Type IIS restriction enzyme BsaI (Fig. 5.1). Each vector encodes a DNA assembly site, consisting of a *lacZ* cassette bounded by two unique BsaI restriction sites. Digestion of the destination vector produces 4-base pair overhangs (“sticky ends”) available for ligation with the compatible overhangs of digested insert DNA. Notably, the overhang sequences were defined to specify the position and orientation of the ligated fragments within the final construct.

Individual destination vectors vary in functions affecting host range, mobilization, plasmid curing, and chromosomal integration (Table 5.1 and Fig. C1). Basic replicative vectors encode a high-copy number *E. coli* origin of replication (pMB1) (25), an ampicillin resistance cassette, and transcriptional terminators positioned to insulate transcriptional activity originating from insert sequences. Conjugative vectors contain an *oriT* sequence for mobilization into hosts (26, 27). Counter-selectable vectors carry the *sacB* gene for plasmid curing on sucrose media.

Chromosomal modification vectors contain elements for site-specific transposition and two-step chromosomal allelic replacement (28–30).

A secondary Golden Gate assembly site was included in destination vectors to enable replacement of the ampicillin resistance gene with alternative selectable markers. The cloning site features restriction sites for the Type IIS enzyme BbsI and operates independently of the primary BsaI assembly site. Marker exchange at the BbsI site allows vector backbones to be

modified to extend their application to hosts with intrinsic resistance to ampicillin. Furthermore, Golden Gate assembly of multiple DNA inserts at this site can increase versatility by enabling the fusion of selectable marker genes to plasmid elements such as alternative replication origins.

5.4.2 Combinatorial assembly of bioreporters from promoter and reporter gene inserts

The Golden Gate approach is well-suited for bioreporter construction since it enables the seamless fusion of promoter and reporter inserts. Our design strategy required the modification of insert sequences for directed assembly at the BsaI cloning site of destination vectors. The promoter inserts include three constitutive promoters of varying strength and three inducible promoters responsive to arabinose, mercury, or arsenic (Fig. 5.2A). The reporter inserts encode yellow fluorescent protein (YFP), mCherry, a flavin-based fluorescent protein (PpFbFP), and bacterial luciferase. We also modified four antibiotic resistance gene inserts for selectable marker replacement at the secondary BbsI cloning site of destination vectors.

The key modification to insert sequences was the precise addition of BsaI recognition sites and overhang sequences (Fig. 5.2B). These sequences were routinely added to insert sequences during PCR-amplification via 5' sequence extensions to the primers. If necessary, existing Type IIS restriction sites within the insert sequences were altered by site-directed mutagenesis (see Methods). Inserts can be included in assembly reactions either as linear PCR products or from storage vectors, as depicted in Fig. 5.1. During the assembly reaction, defined overhang sequences on the destination vector ligate to complementary overhangs on the promoter and reporter inserts (Fig. 5.2C). Ligation between the promoter and reporter inserts occurs at a position overlapping the start codon of the reporter gene, with the Shine-Dalgarno (SD) sequences for ribosomal binding located in the promoter insert. The consistent use of four-

base pair BsaI overhang sites permits the combinatorial assembly of gene fusions between any pair of promoter and reporter inserts, and novel promoters or reporters can be incorporated by simply adding appropriate BsaI restriction site sequences during insert amplification.

5.4.3 Signal production of constitutive fluorescent and luminescent bioreporters

The continuous signal emitted by constitutive bioreporters can be used to label cells for microscopy or flow cytometry applications or serve as a proxy of cellular health for general toxicity bioreporters. The specific application of a bioreporter depends on type and level of signal production, which can be impacted by the choice of promoter, reporter, and base vector. We compared the signal outputs of constitutive bioreporters expressing fluorescent or luminescent reporter genes paired with each of three constitutive promoters (P_{rrnB}, P_{cons}, and $P_{A1/04/03}$). Signal output was quantified in cell suspension assays (see Methods) and is presented for the fluorescent reporters as fluorescent induction after four hours (Fig. 5.3A-C), during which signal production increased at a linear rate. Peak luminescence was reported for the luciferase reporters (Fig. 5.3D), which exhibited non-linear signal induction (see Fig. C3 for time course curves). Although differences in scaling prevent direct comparisons of values measured for different reporter species, the overall patterns can be compared. Among the fluorescent bioreporters, the $P_{A1/04/03}$ promoter generally had higher fluorescent induction than the P_{cons} and P_{rrnB} promoters (Fig. 5.3A-C), consistent with the strong activity recognized for this promoter (31). Similar promoter rankings were observed for mCherry fusions constructed in multiple Golden Gate destination vectors (pAH1 and pAH1T; see Fig. C1) and two established high-copy number vectors (pUC19 and pUCP19) (25, 32), although the choice of destination vector affected the magnitude of signal production (Fig. 5.3A). Among the flavin-based fluorescent protein (PpFbFP) bioreporters, only the construct with the strong $P_{A1/04/03}$ promoter produced a

higher signal than the "empty vector" control, suggesting that the threshold of PpFbFP detection requires greater gene expression relative to the other fluorescent reporters. Interestingly, the $P_{A1/04/03}$-luciferase bioreporter was genetically unstable, likely due to the energetic burden imposed by the chemiluminescence reaction, while the lower strength promoters produced a robust signal (Fig. 5.3D). Overall, the constitutive fluorescent reporters exhibited similar promoter rankings across reporter types, and these comparisons were aided by the reliably linear increase in signal production during the assay period. In contrast, comparisons of promoter strength for the constitutive luciferase reporters appeared to be confounded by non-linear increases in signal production, different time points for peak luminescence, and genetic instability caused by the fitness cost of the light reaction (Fig. C3A).

5.4.4 Inducible biosensors for quantification of bioavailable mercury and arsenic

We next evaluated biosensors that produce a reporter signal in response to the binding of intracellular mercury (Hg) or arsenic (As) species to cognate transcriptional repressors. We constructed four Hg biosensors containing mCherry, YFP, luciferase, and PpFbFP reporters, and quantified their signal responses following exposure to a gradient of Hg(II) concentrations (Fig. 5.4). Each mercury biosensor produced a dose-dependent response; however, the sensitivity and dynamics of the response depended on the reporter gene. The mCherry and YFP biosensors exhibited linear dose responses between the limit of detection and the maximum concentration tested (1 nM to 20 nM (Fig. 5.4A and 4B)). In contrast, the luciferase and PpFbFP biosensors were more sensitive (0.5 nM detection limit) and exhibited signal plateauing at Hg(II) concentrations greater than 5 nM (Fig. 5.4C and 4D). The luciferase reporter produced greater variation between biological replicates, however.

We constructed a similar set of arsenic biosensors and exposed them to As(V), which is reduced to As(III) under the conditions of the exposure assay (12). The mCherry, YFP, and luciferase reporters exhibited broadly similar response curves between 1 nM and 250 nM, despite some differences in the sensitivity, level of plateauing, and variation between replicates (Fig. 5.5A-C). Surprisingly, the PpFbFP arsenic biosensor had a much higher limit of detection (250 nM) than the other reporters (1-5 nM), resulting in a major shift in its detection range (Fig. 5.5D). This outcome contrasts with that of the mercury-PpFbFP biosensor, which exhibited a detection limit (1 nM) similar to the other mercury biosensors (Fig. 5.4D).

Taken together, these results validate the combinatorial approach to building biosensors from regulatory and reporter insert fragments. Each combination yielded a biosensor producing a distinct dose-response curve, with the choice of reporter gene affecting the sensitivity and the dynamic range of the response. Previously reported Hg and As biosensors vary widely in their ranges of detection with detection limits as low as picomolar concentrations for Hg and low nanomolar concentrations for As and luminescent biosensors typically have much lower detection ranges for both Hg and As (33, 4, 34, 35). However, complementing these ultrasensitive biosensors with others that vary in detection ranges, as described here, offers the ability to detect analytes over wider ranges of concentrations.

5.4.5 Anaerobic detection of flavin-based fluorescent protein bioreporters

Signal production by light-emitting bioreporters usually requires oxygen for either chromophore maturation or as a reactant in the luciferase reaction (36, 37). Flavin-based fluorescent proteins (FbFPs), on the other hand, produce an oxygen-independent fluorescent signal that is triggered by binding between the fluorescent protein and flavin mononucleotide molecules (36, 38).

Therefore, FbFPs can be used to investigate microbial processes under anaerobic conditions in which fluorescent or luminescent bioreporters are typically inactive (11). Signal production by *E. coli* FbFP bioreporters has been demonstrated in cultures undergoing anaerobic respiration with nitrate supplied as terminal electron acceptor (36, 11, 39) but detection in alternative anaerobic growth conditions is less studied. We tested whether the signal was detectable in cultures undergoing anaerobic respiration with fumarate, a highly reduced terminal electron acceptor. In general, preconditioning the *E. coli* cells through several growth cycles was necessary for reliable anaerobic growth and signal production (see Methods). We found that bioreporters expressing PpFbFP from the strong $P_{A1/04/03}$ promoter produced a fluorescent signal during both nitrate and fumarate respiration (Fig. C4). Interestingly, the nature of the carbon source was critical for signal detection during fumarate respiration. Cultures supplied with glucose, glycerol, and pyruvate produced a signal, while those supplied with acetate, ethanol, or lactate did not (Fig. C4B), suggesting that both the nature of the carbon source and its redox state are important to consider when designing biosensor assays.

The successful detection of PpFbFP signal from cells undergoing fumarate respiration expands the range of redox conditions for fluorescent bioreporters into highly reduced anoxic conditions. We next tested whether the PpFbFP biosensors were capable of mercury or arsenic quantification during fumarate respiration, an energy metabolism employed by microorganisms that carry out environmental mercury methylation (40–42). We found that the anaerobic dose-responses to mercury and arsenic exhibited comparable detection dynamics as the aerobic responses (Fig. 5.6). Overall, these results show that *E. coli* flavin-based biosensors are capable of quantifying analytes under anaerobic growth conditions beyond nitrate respiration, offering

opportunities to investigate metal bioavailability and transformation under ecologically relevant culture conditions.

5.5 Conclusions

The aim of this work was to develop a system that applies Golden Gate assembly to molecular cloning applications with a specific focus on bioreporter construction. The advantages of the Golden Gate method are considerable (23, 24). Ligation of multiple DNA segments in a single assembly reaction streamlines cloning procedures and enables the rapid combinatorial assembly of simple or complex gene circuits. Our platform can be incorporated by any research group that carries out traditional restriction-enzyme based cloning in *E. coli*. Furthermore, while the destination vectors were designed for *E. coli* hosts, they can be modified for other bacterial species, as discussed below. New insert sequences can be routinely incorporated by simply encoding sequence extensions in PCR primers (see Fig. 5.3B and Methods), or in custom gene synthesis products. This approach can accommodate numerous applications that require fusing genetic sequences, such as microbial biosensing (6), metabolic pathway engineering (43), and genome editing (30).

Here we outline a proof of concept that the biosensors assembled by our molecular approach can detect and quantify Hg and As over a range of redox gradients. However, analysis of environmental samples can be complicated by factors affecting bioavailability of the analyte to the microbe, such as analyte speciation and composition of the environmental matrix (4) (e.g., a high concentration of Hg in the presence of a strong chelating molecule that inhibits Hg uptake into the bioreporter might not generate a signal). Therefore, investigating these factors will be

crucial for the successful application of whole-cell bioreporters to environmental toxicological monitoring.

Although the bioreporters we evaluated include only those involving *E. coli* replicative plasmids, we present additional vectors that widen the scope of functionalities for bioreporter design and chromosomal modification (Table 5.1 and Fig. C1). Vectors elements supporting conjugative transfer (*oriT*) (26) and counterselection (*sacB*) (44) can be exploited in mobilizable and curable *E. coli* vectors (45). For microbial species that do not support pMB1-based plasmid replication, the vectors can be utilized for chromosomal allelic replacement (*sacB* vectors) (29, 46) or site-specific transposition (mini-Tn7 vectors) (28, 47, 30). In particular, the pR6KT-SacB allelic replacement vector, which has a restrictive R6K origin (48), has been routinely used to generate chromosomal insertions, deletions, or single nucleotide polymorphisms in *E. coli* (unpublished work) and multiple *Pseudomonas* species (30, 49–51).

Finally, modification of the vector backbone sequences can further extend their host ranges. Alternative replicons can be inserted on restriction sites located in the vector backbones to construct shuttle vectors capable of replication in more diverse hosts. In addition, a second Golden Gate assembly site was engineered specifically for substituting selectable marker sequences and can accommodate multi-fragment assemblies that customize destination vectors for specific microbes. For example, sequences for host-specific promoters can be fused to selectable marker genes and alternative replicon sequences in one-pot assembly reactions. Overall, these properties built into the destination vector design provide a flexible framework for increasing the scope of microbial bioreporter and molecular genetic applications.

5.6 Materials and Methods

5.6.1 Media and molecular biology reagents

E. coli cultures were routinely grown at 37 °C in lysogeny broth (LB): 10 g bacto-tryptone, 5 g yeast extract, and 10 g NaCl per liter (52). LB media was supplemented when appropriate with 14 g/l agar (Oxoid), 100-200 μg/ml ampicillin, 30 μg/ml kanamycin, 10 μg/ml gentamicin, 10 μg/ml tetracycline, or 40 μg/ml X-Gal (5-Bromo-4-chloro-3-indolyl β-D-galactopyranoside). Antibiotics and X-Gal were purchased from Sigma-Aldrich.

For the bioreporter suspension assays, cells were grown in LB and Growth Minimal Media (GMM) and exposed in exposure medium. GMM (250 ml) consisted of 43.5ml of Difco^{TM} M9 salts (5x), 20 mM glucose, 15 µl of 0.225 M $FeSO_4$ in 0.2 M H_2SO_4 (stored anaerobically), 125 µl of 2 M $MgSO_4$, 0.5 ml of 0.5 M thiamine HCl from a frozen (-20˚C) aliquot, 10 ml of 1 M Na_2Fumarate, 1.5 ml of 75 mM L-leucine/ L-isoleucine/L-valine, 250 µl of Trace elements #1 and 250 µl of Trace elements #2 solution (as described) (11), and 250 µl of 0.01 M EDTA sodium salt. Media used for anaerobic growth was bubbled under N_2 gas to remove dissolved oxygen, and containers were sealed in an anaerobic chamber. Growth media was not stored longer than 1 week.

Exposure medium consisted of 40 mM MOPS free acid, 7 mM sodium β-glycerophosphate, 1 mM $(NH_4)_2SO_4$, 10 mM glucose, 5 mM NaOH, and 10-15 mM KOH (to adjust the pH to 7) in Milli-Q water. In anaerobic assays, the exposure media contained 5 mM $NaNO_3$ (Nitrate reduction) or 10 mM sodium fumarate (Fumarate reduction). All reagents,

except sodium β-glycerophosphate, were stored anaerobically in the anaerobic chamber. Exposure media was prepared the day it was used.

Fumarate-GMM plates were made by autoclaving 191 ml of Milli-Q water with 3.75 g agar in a sealable borosilicate bottle. The media was bubbled with N_2 while cooling to roughly 60 °C, and the following reagents were quickly added: 43.5 ml of 5X M9 salts, 250 µl of Trace 1 and 2 (as described) (11), 250 µl of 10 mM EDTA, 125 µl of 2 M $MgSO_4$, 10 ml of 1 M sodium fumarate, 15 µl of 0.225 M $FeSO_4$ in 0.1 M H_2SO_4, 0.5 ml of 500 mM thiamine HCl, 1.5 mL of 75 mM leucine/isoleucine/valine solution, 5 ml of 1 M glucose, 250 µl of 100 mg/ml ampicillin. Once reagents were added, the bottle was sealed very tightly and cycled into the anaerobic chamber. Plates were poured anaerobically and used the day they were prepared.

Custom oligonucleotides were purchased from Invitrogen (Thermo Fisher Scientific), and sequences are listed in Table 5.2. Polymerase chain reactions (PCR) were prepared with Phusion High-Fidelity DNA Polymerase (Thermo Fisher Scientific). PCR products were purified with the Wizard SV Gel and PCR Cleanup System (Promega). Plasmid DNA was isolated from bacterial cultures with the QIAprep Spin Miniprep Kit (Qiagen). Restriction endonucleases and T4 DNA ligase were purchased from New England Biolabs. High-fidelity versions of BsaI and BbsI enzymes were used in Golden Gate assembly reactions.

5.6.2 Golden Gate assembly and molecular cloning methods

Golden Gate assembly reactions were prepared as previously described (23, 24). Approximately equimolar amounts (~40 fmol) of destination vector and insert storage vectors were mixed with 1 µl of 10X T4 ligase buffer, 0.5 µl (200 units) of T4 ligase, and 0.5 µl (10 units) of Type IIS enzyme (e.g., BsaI) in a total volume of 10 µl. Reactions were incubated for 2 h at 37 °C, 5 min

at 50 °C, and 5 min at 80 °C. Chemically competent *E. coli* DH5α λpir were transformed with 2 µl of the assembly reactions by the Inoue method (52), and the cells were incubated for 2 h at 37 °C to allow expression of resistance genes. Cells were plated on LB agar supplemented with 100 µg/ml ampicillin and X-Gal. Inserts were validated by colony PCR of white colonies or Sanger sequencing (Genome Quebec, McGill University). Plasmids with the correct series of inserts were isolated and transformed into chemically competent *E. coli* NEB5-alpha cells (New England BioLabs) for quantitative exposure assays.

Traditional restriction enzyme cloning was used in the construction of destination and storage vectors. For these reactions, vector and insert DNA were digested separately for 2 h at 37 °C, purified by spin column, and ligated for 16 h at 16 °C before transformation into *E. coli*. TOPO cloning of purified Phusion PCR products into the pCRBluntII-TOPO vector (Thermo Fisher Scientific) was performed according to the manufacturer's protocol.

5.6.3 Design of Golden Gate assembly sites

Two Golden Gate assembly sites were designed for ligation of reporter gene fusions (BsaI-*lacZ* site) and selectable marker cassettes (BbsI-AmpR site) to destination vectors. The BsaI-*lacZ* site was derived by PCR amplification of *lacZ*α sequences from pUC19 (25) with primers introducing the restriction site sequences (F2-pUC19-BsaI and R2-pUC19-BsaI; Table 5.2). The PCR amplicon was cloned into the BglII and SpeI sites of allelic exchange vector pAH385 (a derivative of pAH79) (49, 53) to form pR6KT-SacB (Table 5.1 and Table C1). In subsequent destination vector designs, the BsaI-*lacZ* site was situated within the mini-Tn7 polylinker (28) (Fig. C2), to provide restriction site options for subcloning inserts into alternative vectors. The BsaI-*lacZ* site was transferred to the mini-Tn7 polylinker by amplifying the BsaI-*lacZ* cloning

site from pR6KT-SacB with primers F-MCS and R-MCS (Table 5.2) and ligating the BbsI-digested product at the BamHI and XhoI sites of the polylinker.

The Golden Gate marker exchange site (BbsI-AmpR) includes a beta-lactamase (*bla*) cassette flanked by inverted BbsI recognition sequences that produces restriction overhangs compatible with selectable marker inserts. The site was created by amplifying the *bla(T720C)* allele (containing a mutation altering an internal BsaI site) with primers F-marker and R-marker (Table 5.2 and Table C2) and incorporating the amplicon into vector backbones during destination vector assembly.

5.6.4 Destination vector constructions

Novel destination vectors were constructed by Golden Gate assembly of multiple PCR amplicons encoding vector functions (e.g., replication origin, selectable markers, and transcriptional terminators) into closed ligation loops. Details on the properties of source and constructed vectors, primer sequences, and amplicons used for vector assemblies are found in Table 5.2 and Supplemental Tables C1 and C2. Intermediate destination vectors containing at minimum the pMB1 replicon and BbsI-AmpR marker exchange site were generated by BsaI-mediated assembly of PCR amplicons listed in Table C2. In a second step, the BsaI-*lacZ* assembly site and surrounding mini-Tn7T polylinker were cloned into the intermediate vectors (see Table C1 for specifics). New functions can be added to or replace existing functions on vector backbones by exploiting standard restriction sites engineered at the fusion junctions between the assembled vector segments. For example, the counterselectable vectors pAH1-SacB and pAH1T-SacB were derived by excising the pMB1 origin from their parent vectors and substituting an amplicon containing pMB1 and *sacB* sequences.

5.6.5 Promoter, reporter, and selectable marker inserts

Inserts compatible with the Golden Gate destination vectors were created by PCR amplification of target sequences from source vectors (Table 5.2 and Tables C1 and C2). Terminal sequence tags of the primer sequences include: 1) six non-specific base pairs at the termini for efficient cleavage near the ends of DNA fragments; 2) an optional standard restriction site for cloning insert segments into long-term storage vectors; 3) a Type IIS recognition sequence (BsaI for bioreporter assembly or BbsI for marker exchange); 4) a defined four-base pair overhang sequence that directs ligation between digested fragments; and 5) an optional standard restriction site for subcloning assembled gene fusions. Consistency in the four-base pair overhang sequences allows for the pairing of any combination of promoter and reporter inserts. Novel inserts can thus be integrated into the assembly platform by using the primer sequences listed in Table C2 as guides. Notably, the fusion junction between promoter and reporter inserts overlaps with the start codon of the reporter gene. Therefore, new promoter inserts must include appropriately distanced ribosome binding sites, and new reporter inserts must be in-frame with the start codon located within the fusion junction.

To avoid interference in assembly reactions, all secondary BsaI (5'-GGTCTC-3') and BbsI (5'-GAAGAC-3') recognition sequences in destination vector and insert sequences were altered. We introduced synonymous mutations at secondary sites using a previously described site-directed mutagenesis method that introduces mutation at ligation junctions during Golden Gate assembly of PCR products (30). Derivatives of pUC19 and pAH79 vectors were constructed that carry a synonymous mutation that alters the internal BsaI site of the beta-lactamase gene: *bla(T720C)*. In addition, the following synonymous nucleotide substitutions were introduced in insert gene sequences: *luxC(A1312C)*, *tetA(C654G)*, and *mCherry(G456A)*.

All amplicons carrying promoter, reporter, and selectable marker sequences were cloned into one or more of the following vectors for long-term storage: pCR-BluntII-TOPO (Invitrogen), pUIC3, pUC19, pEX18Gm, and pEX18Tc (25, 46, 53).

5.6.6 Growth for bioreporter suspension assays

E. coli strains were grown at 37 ˚C and selected with 200 μg/ml ampicillin (unless otherwise stated) in preparation for suspension assays, with no antibiotic used in the suspension assay. For aerobic assays, a single colony was selected from a plate and grown in LB broth over day. Cultures were transferred (1% inoculum) from LB to GMM and grown overnight. The next morning, cultures were transferred (10% inoculum) into fresh GMM and grown to an OD_{600} of 0.6. Cultures were washed twice in exposure media (10,000 RCF for 90 seconds). The cultures were ready for a 1/20 dilution in exposure media for the bioreporter suspension assay.

Anaerobic suspension assays were carried out under both nitrate and fumarate reducing conditions for bioreporters expressing flavin-based fluorescent protein. All anaerobic manipulations of cell cultures were performed in a Coy Vinyl Anaerobic chamber (98% N_2, 1.5% H_2), and anaerobic growth was performed in anaerobic balch tubes. Before growth for the suspension assay, cultures were acclimated to grow in Anaerobic GMM supplemented with 20 mM $NaNO_3$ by culturing for 7-10 days with daily 1% transfers from stationary phase, until an $OD_{600} > 0.6$ was reached. Corresponding cryostocks were made of the nitrate acclimated cultures.

For anaerobic suspension assays performed under nitrate reducing conditions, nitrate-acclimated cultures from cryostocks were plated onto an LB plate with 120 μg/ml ampicillin and grown aerobically. Single colonies were selected and grown aerobically in LB broth overnight.

The following morning, the cultures were resuspended in anaerobic GMM (20% inoculum) supplemented with 20 mM $NaNO_3$ and grown over the day. The cultures were transferred (1% inoculum) to grow overnight, then transferred (20% inoculum) and grown to an OD_{600} of 0.6. Cultures were washed twice in anaerobic exposure media supplemented with 5 mM $NaNO_3$ (10,000 RCF for 90 seconds). The cultures were ready for a 1/20 dilution in exposure media for the bioreporter suspension assay.

The FbFP bioreporter suspension assay was optimized for fumarate reduction using a pUC19 construct with the promoter $P_{A1/O4/O3}$, which produced the highest anaerobic response on NO_3^- (Fig. C4A). This constitutive bioreporter as well as the Hg and As sensing bioreporters were acclimated to grow in anaerobic GMM supplemented with 40 mM Na_2Fumarate by culturing for 7-10 days with daily 1% transfers from stationary phase, until an $OD_{600} > 0.6$ was reached. Corresponding cryostocks were made of the fumarate acclimated cultures. From cryostock, cultures were plated onto fumarate-GMM plates with 100 μg/ml ampicillin and grown in anaerobic plate jars for several days. A single colony was selected and grown in anaerobic GMM supplemented with 40 mM Na_2Fumarate. The following day, cultures were transferred (20% inoculum) and grown to an OD_{600} of 0.6. Cultures were resuspended twice (10,000 RCF for 90 seconds) in anaerobic exposure media supplemented with 10 mM Na_2Fumarate. The cultures were ready for a 1/20 dilution in exposure media for the bioreporter suspension assay.

The bioreporter suspension was optimized for fumarate reduction using a variety of different electron sources that *E. coli* has known metabolism for: acetate, ethanol, glucose, glycerol, lactate and pyruvate (Fig C4B). Glucose was ultimately selected for exposure due to the highest fluorescent induction response. Pyruvate and glycerol also supported signal production,

while acetate, ethanol, lactate, and the “no carbon/electron source” treatment gave no induction response.

5.6.7 Bioreporter suspension assays

Suspension assays were performed in exposure medium using 7 ml standard PTFE vials. Hg was prepared as a 7.2 μM $HgSO_4$ stock in 0.2 M H_2SO_4, the concentration being determined using an MA-3000 Mercury Analyzer. Hg was diluted in exposure medium to a working concentration of 100 nM in PTFE vials before addition to the suspension assay. Arsenic was prepared as 10 mM Na_2HAsO_4 or Na_2AsO_3 standards and was diluted in exposure medium in PTFE vials before addition to the suspension assay. Anaerobic exposure medium was supplemented with 5 mM $NaNO_3$ or 10 mM Sodium Fumarate. After dilution of the corresponding metal(loid) in the exposure medium, bioreporter cells (see “Growth for bioreporter suspension assays”) were added to 1/20 of the suspension assay volume of 2 ml. The suspension assay was transferred in triplicate from the PTFE vials to a 96-well plate (Black, Clear-Bottom, Nonbinding Surface Microplates) and analyzed in a Tecan Infinite F200Pro plate reader (Aerobic) or a Synergy HTX plate reader (Anaerobic).

Readings for fluorescence, luminescence and OD_{600} were taken every five minutes for 20 hours at 37 ˚C. Fluorescence was read for YFP (Ex: 500/20 nm, Em: 520/10 nm), mCherry (Ex: 560/20 nm, Em: 620/10 nm), and PpFbFp (aerobic Ex: 448/70 nm, Em: 500/20 nm; anaerobic Ex: 440/40 nm, Em: 500/27 nm). Fluorescent signal production was reported as fluorescent induction, defined as the amount of signal, measured in relative fluorescent units (RFUs), produced by the cultures during the exposure assay. Fluorescent induction was calculated by subtracting the initial RFU, measured at the start of the assay, from the final RFU, measured

after 4 hours of exposure (or 10 hours for cultures undergoing fumarate respiration). Fluoresent induction increased linearly and no growth (i.e., change in OD_{600}) was observed during the 4 hour (or 10 hour) measurement periods.

In contrast to the fluorescent induction, luminescent signal production did not increase linearly over time and exhibited peak values over the course of the 20 hour exposure assays. Since the timing of peak luminescence varied depending on type of promoter and analyte concentration, we reported peak luminescence instead of luminescence at fixed time points. Constitutive luminescence trends were highly variable between promoters (Fig. C3 A) and in order to compare constitutive promoters, we reported the maximum value within 20 hours. For As inducible luminescence, the maximum initial luminescence peak was quantified within 4-6 hours. For Hg inducible luminescence, luminescent peaks were observed at variable times depending on the Hg concentration (Fig. C3 B) and therefore we reported the maximum value within 20 hours. We observed some growth (changes in OD_{600}) during the 20 hour luminescence assays, but did not normalize the peak luminescence values to OD_{600} since peaks frequently occurred at time points where cell densities were too low to be accurately quantified.

Data availability

Nucleotide sequences of the novel destination vectors and inserts described in this study have been deposited in GenBank under the accession numbers OK148689 to OK148700 and OK165501 to OK165509. Bacterial strains, vectors, and data are available upon reasonable request.

5.7 Acknowledgements

We thank Thien-Fah Mah and Rees Kassen for kindly providing genetic resources and members of the Poulain lab, especially Martin Pothier, for helpful insights and discussions. This work was funded by the Natural Sciences and Engineering Research Council of Canada (NSERC).

5.8 Tables and Figures

Table 5.1. Properties of Golden Gate destination vectors

Plasmid	Description	Golden Gate assembly sites[a]	Selectable markers[b]	Origins[c]	Additional elements[d]
pAH1	*E. coli* vector	BsaI-*lacZ*; BbsI-AmpR	*bla(T720C)*	pMB1	Terminators
pAH1T	Conjugative *E. coli* vector	BsaI-*lacZ*; BbsI-AmpR	*bla(T720C)*	pMB1; *oriT*	Terminators
pAH1-SacB	Counterselectable *E. coli* vector	BsaI-*lacZ*; BbsI-AmpR	*bla(T720C)*; *sacB*	pMB1	Terminators
pAH1T-SacB	Conjugative counterselectable *E. coli* vector	BsaI-*lacZ*; BbsI-AmpR	*bla(T720C)*; *sacB*	pMB1; *oriT*	Terminators
pAH1-Tn7	Mini-Tn7 vector	BsaI-*lacZ*; BbsI-AmpR	*bla(T720C)*; *aacC1*	pMB1	mini-Tn7T-Gm
pAH1T-Tn7	Conjugative mini-Tn7 vector	BsaI-*lacZ*; BbsI-AmpR	*bla(T720C)*; *aacC1*	pMB1; *oriT*	mini-Tn7T-Gm
pR6KT-SacB	Allelic exchange vector	BsaI-*lacZ*	*bla(T720C)*; *tet*; *sacB*	*oriR6K*; *oriT*	None

[a] Sites for replacing *lacZ* marker with insert DNA (BsaI-*lacZ*) or for substituting the ampicillin-resistance gene with an alternative resistance cassette (BbsI-AmpR).

[b] *bla(T720C)*, ampicillin-resistance gene with nucleotide substitution altering an internal BsaI site; *aacC1*, gentamicin-resistance gene; *tet*, tetracycline-resistance gene; *sacB*, sucrose-sensitivity gene.

[c] pMB1, high-copy *E. coli* origin of replication; *oriR6K*, *pir*-dependent origin of replication; *oriT*, origin of conjugative transfer.

[d] Terminators indicates the presence of transcriptional terminators flanking the BsaI-*lacZ* site; mini-Tn7T-Gm is a site-specific transposon (28) with embedded BsaI-*lacZ* assembly site.

Table 5.2. Oligonucleotides used in this study.

Primer name	**Sequence (5' to 3')**[a]	**Restriction sites** [b]
BsaI-lacZ cloning site derivation		
F2-pUC19-BsaI	GCG**AGATCT**GTCGTGAGACCGGTGATGACGGTGAAAACCT	BglII, Inverted BsaI [CGAC]
R2-pUC19-BsaI	GCG**ACTAGT**GCAATGAGACCATTAATGCAGCTGGCACGAC	SpeI, Inverted BsaI [TTGC]
F-MCS	GCGGAAGACT**GGATCCAGATCT**GTCGTGAGACCGGTGAT	BbsI [GATC], BamHI, BglII, Inverted BsaI [CGAC]
R-MCS	GCGGAAGACA**CTCGAG**GCAATGAGACCATTAATGCAGC	BbsI [TCGA], XhoI, Inverted BsaI [TTGC]
Golden Gate destination vector assembly		
F-Marker	GCGGGTCT**CAATTG**TGTCTTCATAGTTAAGCCAGCCCCGAC	BsaI [ATTG], MfeI, Inverted BbsI [AATT]
R-Marker	GCGGGTCTCGCGCCGTCTTCTCACGTTAAGGGATTTTGGTCA	BsaI [CGCC], Inverted BbsI [CGCG]
F-pMB1	GCGGGTCTCT**GGCGCGCC**TTTCGTTCCACTGAGCGTCA	BsaI [GGCG], AscI
R-pMB1	GCGGGTCTC**GGCCGGCCCCATGG**CAAAAGGCCAGGAACCGTA	BsaI [GCCG], FseI, NcoI
F-oriT	GCGGGTCTCTCGGCC**GCGGCCGC**TGGCCTTTTGCTCACATGTTC	BsaI [CGGC], NotI
R-oriT	GCGGGTCTCCTAGCGCTTCCTCGCTCACTGAC	BsaI [TAGC]
F-termT1T2	GCGGGTCTCT**GCTAGC**AAAAAGAGTTTGTAGAAACGCA	BsaI [GCTA], NheI
R-termT1T2	GCGGGTCTCC**GGGCCCGGTACC**GAGTAGGGAACTGCCAGGC	BsaI [GGGC], ApaI, KpnI
F-termT0T1	GCGGGTCTCTGCCC**ATGCAT**GCTTAATTAGCTGAGCTTGGAC	BsaI [GCCC], NsiI
R-termT0T1	GCGGGTCTCA**CAATTG**ATCCCCAATTCGATCGTCCG	BsaI [CAAT], MfeI
R-lacZalpha	GCGGGTCTCA**CAATTG**CTATGCGGCATCAGAGCAGA	BsaI [CAAT], MfeI
F-sacB-pMB1	GCGGGTCTCT**GGCGCGCC**CCTGTAGCGGCGCATTAAG	BsaI [GGCG], AscI
Promoter amplicons		
F-Pconst-term	ACTGCG**AGATCT**GGTCTCAGTCG**CCCGGG**ATCGACACTGCTCGATCCG	BglII, BsaI [GTCG], XmaI
R-Pconst	ACTGCG**ACTAGT**GGTCTCCCATCTAGTATTTCTCCTCTTTACAGT	SpeI, BsaI [CATC]
F-PA10403	ACTGCG**AGATCT**GGTCTCAGTCG**CCCGGG**ACCTCGAGAAAATTTATCAAAAAG	BglII, BsaI [GTCG], XmaI
R-PA10403	ACTGCG**ACTAGT**GGTCTCGCATCCTTAATTTCTCCTCTTTA	SpeI, BsaI [CATC]
F-PrrnB	ACTGCG**AGATCT**GGTCTCAGTCG**CCCGGG**GTTGCGCGGTCAGAAAATTA	BglII, BsaI [GTCG], XmaI
F2-Pbad	ACTGCG**AGATCT**GGTCTCAGTCG**CCCGGG**TACTCCGTCAAGCCGTCAAT	BglII, BsaI [GTCG], XmaI
R2-Pbad	ACTGCG**ACTAGT**GGTCTCGCATCGTGTATACCTCCTGCTAGCCCAAAAAAACGGGTA	SpeI, BsaI [CATC]
F-arsRbs2	GCG**GGATCC**GGTCTCAGTCG**CCCGGG**AGAGCCACCAACTC	BamHI, BsaI [GTCG], XmaI

R-arsRbs2	GCG**TCTAGA**GGTCTCGCATCATGCCTCCCGGATAAAACACA	XbaI, BsaI [CATC]
F-merR	GCG**GGATCC**GGTCTCAGTCG**CCCGGG**AGAACACTATTAGGTGCGTCGA	BamHI, BsaI [GTCG], XmaI
R-merR	GCG**TCTAGA**GGTCTCGCATCCGTTGGCCCTTTTGAATTTGG	XbaI, BsaI [CATC]
Reporter amplicons		
F-yfp	ACTGCG**AGATCT**GGTCTCAGATGCTGAGCAAGGGCGAGGA	BglII, BsaI [GATG]
R-gfpmut3	ACTGCG**ACTAGT**GGTCTCAGCAA**GAATTC**TTTGAAGCTAATTCGATCATGC	SpeI, BsaI, [GCAA], EcoRI
F-PpFbFP	ACTGCG**AGATCT**GGTCTCAGATGATCAACGCAAAACTCCTGC	BglII, BsaI [GATG]
R-PpFbFP	ACTGCG**ACTAGT**GGTCTCAGCAA**GAATTC**GATCCTCGACGCAAGCAAAA	SpeI, BsaI, [GCAA], EcoRI
F-mCherry	ACTGCG**AGATCT**GGTCTCAGATGGGTCATCACCATCACC	BglII, BsaI [GATG]
R-mCherry-Syn	GCGGAAGACTGGTTTTCTTCTGCATTACGGGGCC	BbsI [GTTT]
F-mCherry-Syn	GCGGAAGACGAAAACCATGGGCTGGGAGGC	BbsI [AAAC]
R-mCherry	ACTGCG**ACTAGT**GGTCTCAGCAA**GAATTC**GCAGCCAACTCAGCTTCCA	SpeI, BsaI, [GCAA], EcoRI
F1-lux	GCGGAAGACT**GGATCC**GGTCTCAGATGACTAAAAAAATTTCATTCATTATTAACG	BbsI [GATC], BamHI, BsaI [GATG]
R1-lux	GCGGAAGACGGTCGCATTCCGTCATGAGATCCACC	BbsI [TCGC]
F2-lux	GCGGAAGACATGCGACCGTTGCAACGATTAGTGA	BbsI [GCGA]
R3-lux	GCGGAAGACG**TCTAGA**GGTCTCAGCAA**GAATTC**TTCTCCGAAATCTGGGAGCG	BbsI [CTAG], XbaI, BsaI [GCAA], EcoRI
Selectable marker amplicons		
F-AmpR	GCG**GGATCC**GAAGACA**CAATTG**ATAGTTAAGCCAGCCCCGAC	BamHI, BbsI [AATT], MfeI
R-AmpR	GCG**TCTAGA**GAAGAC**GGCGCGCC**TCACGTTAAGGGATTTTGGTCA	XbaI, BbsI [CGCG], AscI
F-KanR	GCG**GGATCC**GAAGACA**CAATTG**TCATAGCTGTTTCCTGAGGC	BamHI, BbsI [AATT], MfeI
R-KanR	GCG**TCTAGA**GAAGAC**GGCGCGCC**GAAGGTGAGCCAGGTGATT	XbaI, BbsI [CGCG], AscI
F-TetR-Syn	GCGGGTCTCTGTGTTCTTTATCATGCAACTCGTAGGA	BsaI [GTGT]
R-TetR-Syn	GCGGGTCTCAACACAGTCATAAGTGCGGCGAC	BsaI [ACAC]
F-pUIC3-bla	ACTGCGGGTCTCTACCGCGGGACCCACGCTCACCGGCT	BsaI [ACCG]
R-pUIC3-EcoRI	ACTGCGCAGACAAGCTGTGACCGTCT**GAATTC**	EcoRI

[a] BsaI and BbsI recognition sequences are underlined. Other restriction sites recognition sequences are in **bold**. Mutations introduced to alter secondary BsaI or BbsI sites are red and underlined.

[b] Four-base pair overhangs resulting from BsaI or BbsI digestion are in brackets.

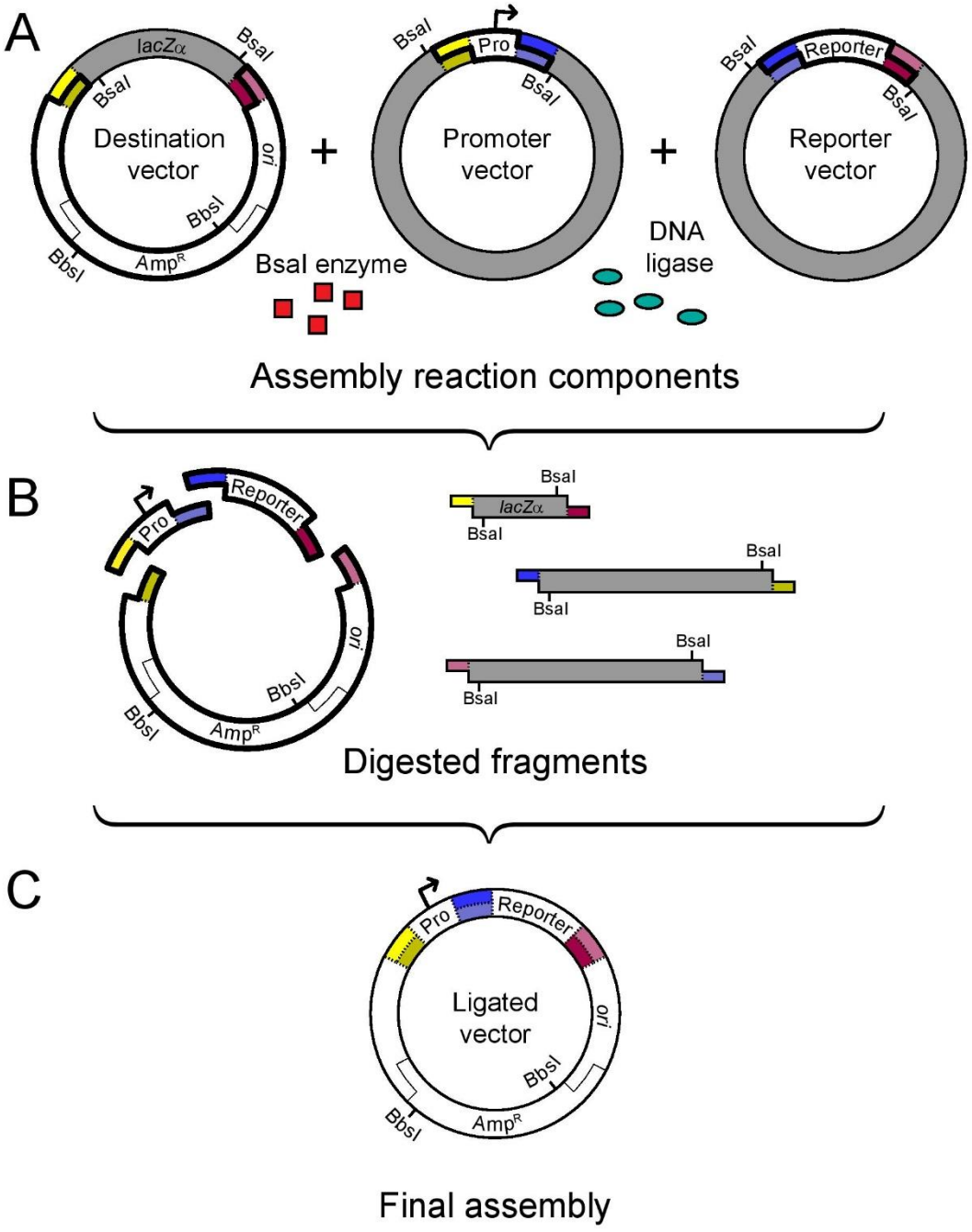

Figure 5.1. Golden Gate assembly of gene fusions into destination vectors. The diagram illustrates a typical "one pot" assembly reaction that produces a promoter-reporter gene fusion in a Golden Gate destination vector. (A) Reaction components include the destination vector, insert storage vectors, BsaI restriction enzyme, and DNA ligase. The positions of recognition sequences (labelled "BsaI") and cleavage sites (colored boxes) are positioned such that recognition sequences are absent from fragments intended for the final assembly (outlined in bold). Thus, the enzyme cleaves away from *lacZα* sequences in the destination vector, and towards the inserts in storage vectors. (B) The sequences of each four-base pair overhang are complementary to those of their intended ligation partner. BsaI recognition sequences are confined to digested fragments excluded from the final construct (gray fill). (C) The assembled vector is resistant to further digestion and lacks *lacZα* sequences, permitting blue-white screening of transformants. Further modifications to the vector backbone (e.g., substitution of the ampicillin resistance (Amp^R) cassette) can be performed at the indicated BbsI restriction sites.

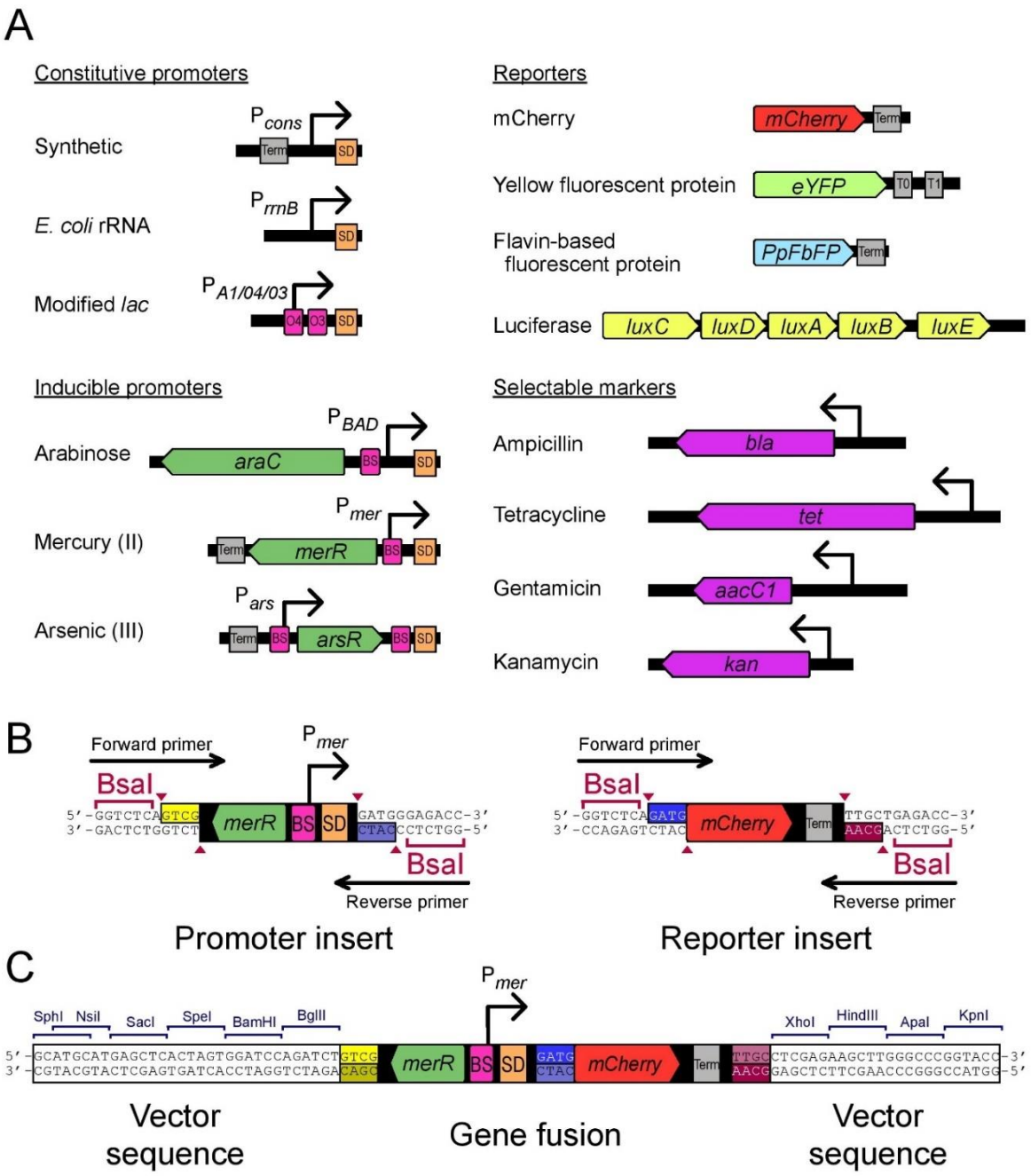

Figure 5.2. Interchangeable promoter and reporter inserts for bioreporter constructions. (A) Constitutive promoters include a medium-strength synthetic promoter (P_{cons}) derived from a combinatorial sequence library (Anderson promoter BBa_J23106; http://parts.igem.org) (54), an *E. coli* ribosomal RNA operon promoter (P_{rrnB}), and a strong modified T7 promoter with O4 and O3 *lac* operator sites ($P_{A1/04/03}$) (31). Inducible promoters responsive to arabinose, mercury, and arsenic are linked to genes encoding their respective analyte-binding transcriptional regulators (11, 12, 55). The locations of regulator binding sites (BS), transcriptional terminators (Term), and Shine-Dalgarno ribosomal binding sites (SD) are indicated. Reporter inserts encode oxygen-dependent (YFP and mCherry) and flavin-dependent (PpFbFP) fluorescent proteins and the bacterial luciferase operon (38, 56, 57). Selectable marker inserts include antibiotic resistance cassettes that can be cloned into the BbsI cloning site of destination vectors. (B) Promoter and reporter inserts were amplified from template sources using primers encoding 5' sequence extensions encoding the BsaI recognition sequence (5'-GGTCTCN-3') followed by the unique four-base pair cleavage site sequence (yellow, blue, and purple boxes). The "sticky end" sequences at the promoter-reporter fusion junction include the start codon (ATG) of the reporter gene. (C) Following assembly in Golden Gate destination vectors, gene fusions can be subcloned into alternative vectors using standard restriction sites.

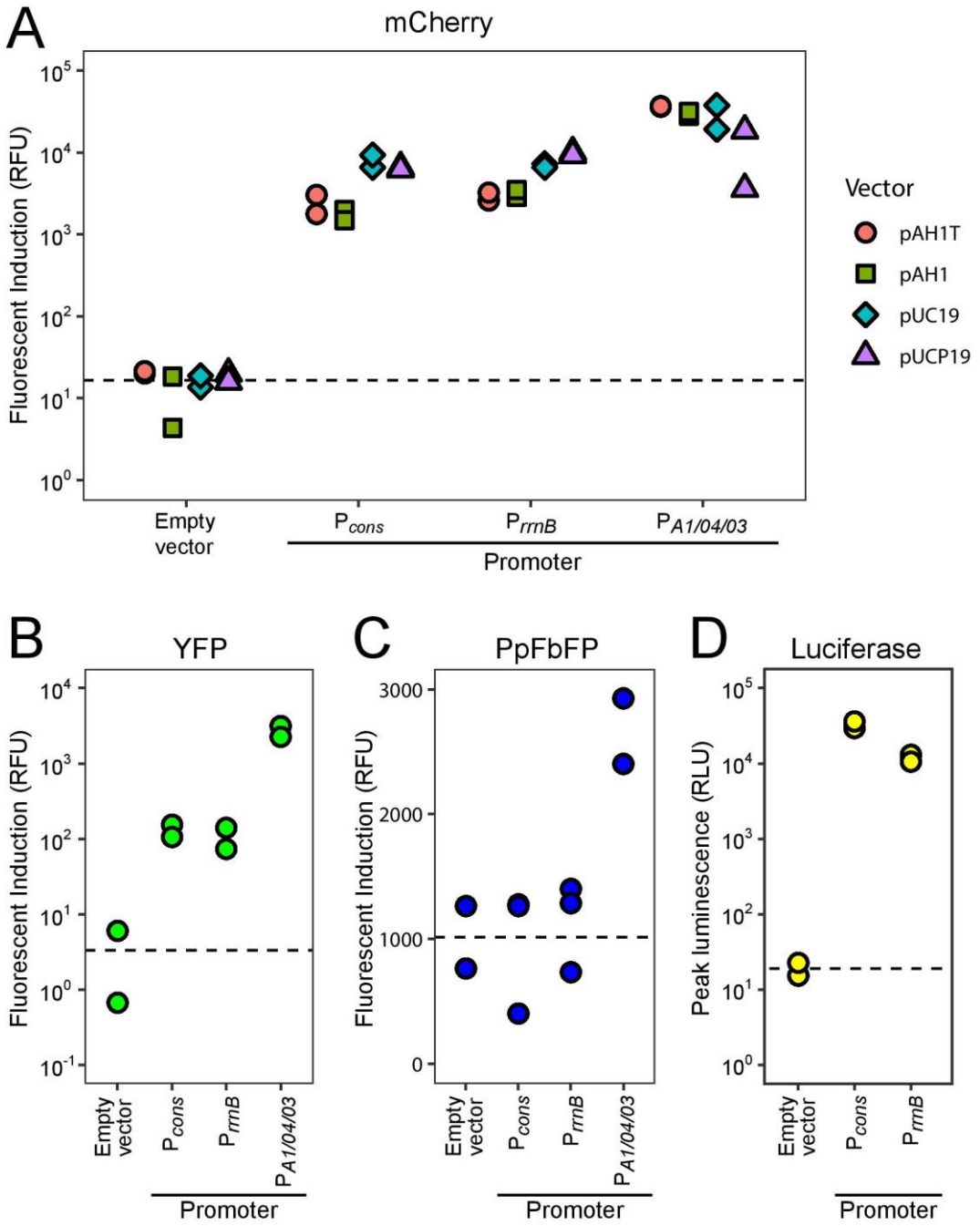

Figure 5.3. Signal output of constitutive bioreporters expressing mCherry, YFP, PpFbFP, and luciferase. Signal output was quantified in aerobic cell suspension assays of *E. coli* NEB5-α harbouring constitutive (A) mCherry, (B) YFP, (C) PpFbFP, or (D) bacterial luciferase gene fusions. mCherry fusions were assembled in two Golden Gate destination vectors (pAH1T and pAH1) and subcloned into two standard high-copy vectors (pUC19 and pUCP19). The remaining bioreporters were constructed with the pAH1T vector. Signal output is presented in relative fluorescence units (RFU) as fluorescent induction at 4 hours or in relative luminescence units (RLU) as peak luminescence over 20 hours (see Materials and Methods). The mean values of three technical triplicates are plotted for at least two independently prepared suspension assays for each bioreporter. Dashed lines indicate the mean background signal for "empty vector" cultures. The relative units should only be compared within each reporter type, since scaling is specific to the filter set combination used for signal detection. The mCherry induction rates were transformed by adding a constant of 15 RFU to allow log-scale plotting of negative values obtained for two "empty vector" controls.

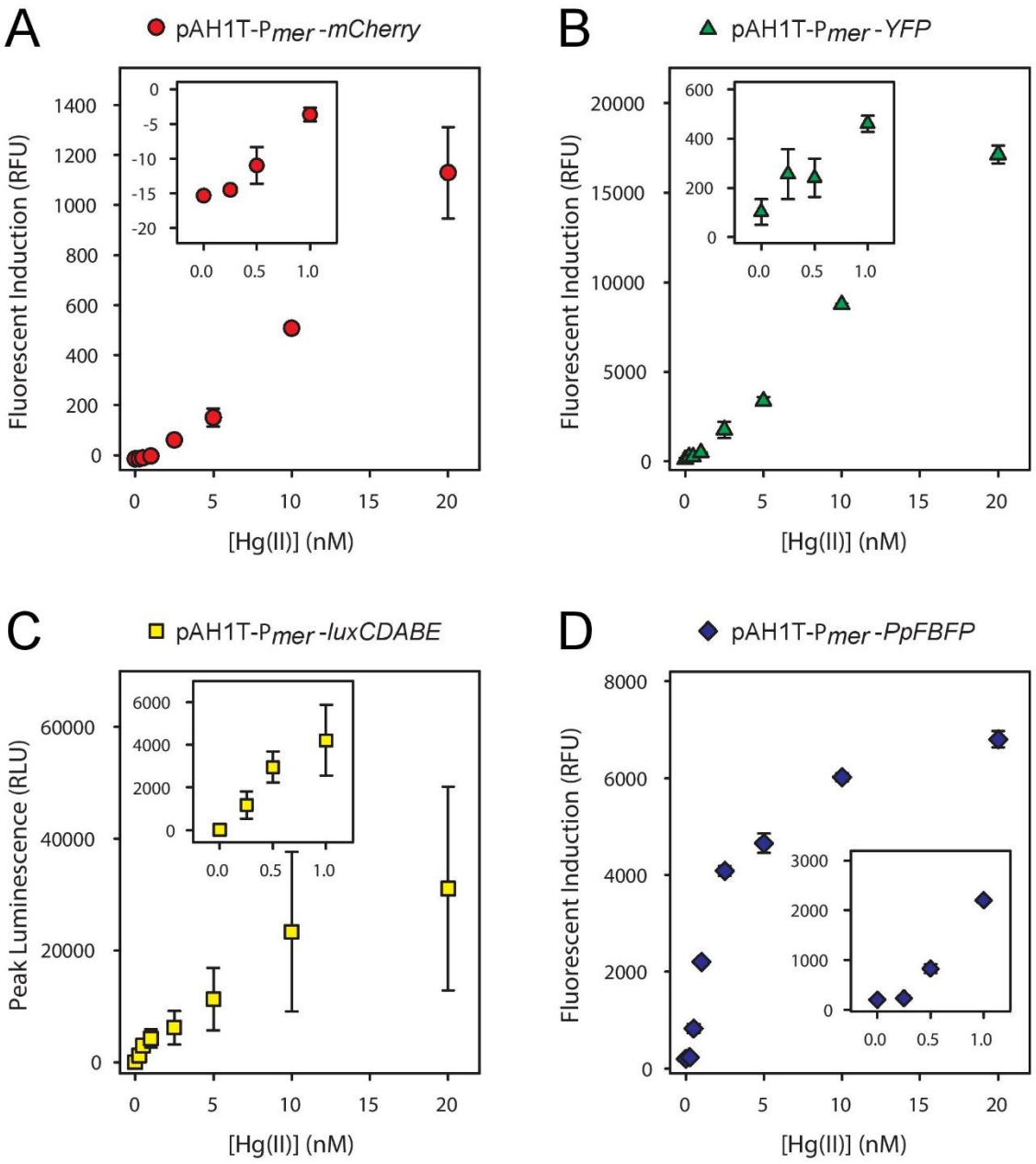

Figure 5.4. Mercury-inducible biosensors. Mercury-inducible biosensors were exposed to $HgSO_4$ concentrations ranging from 0.25 nM to 20 nM. The signal induction at each Hg(II) concentration is presented for (A) mCherry, (B) YFP, (C) luciferase, and (D) PpFbFP reporters. For each reporter, the fluorescent induction at 4 hours (in RFUs) or peak luminescence over 20 hours (in RLUs) is presented as the mean and standard error for two biological replicates (assayed in triplicate). Insets were rescaled to display the responses at the lowest tested mercury concentrations.

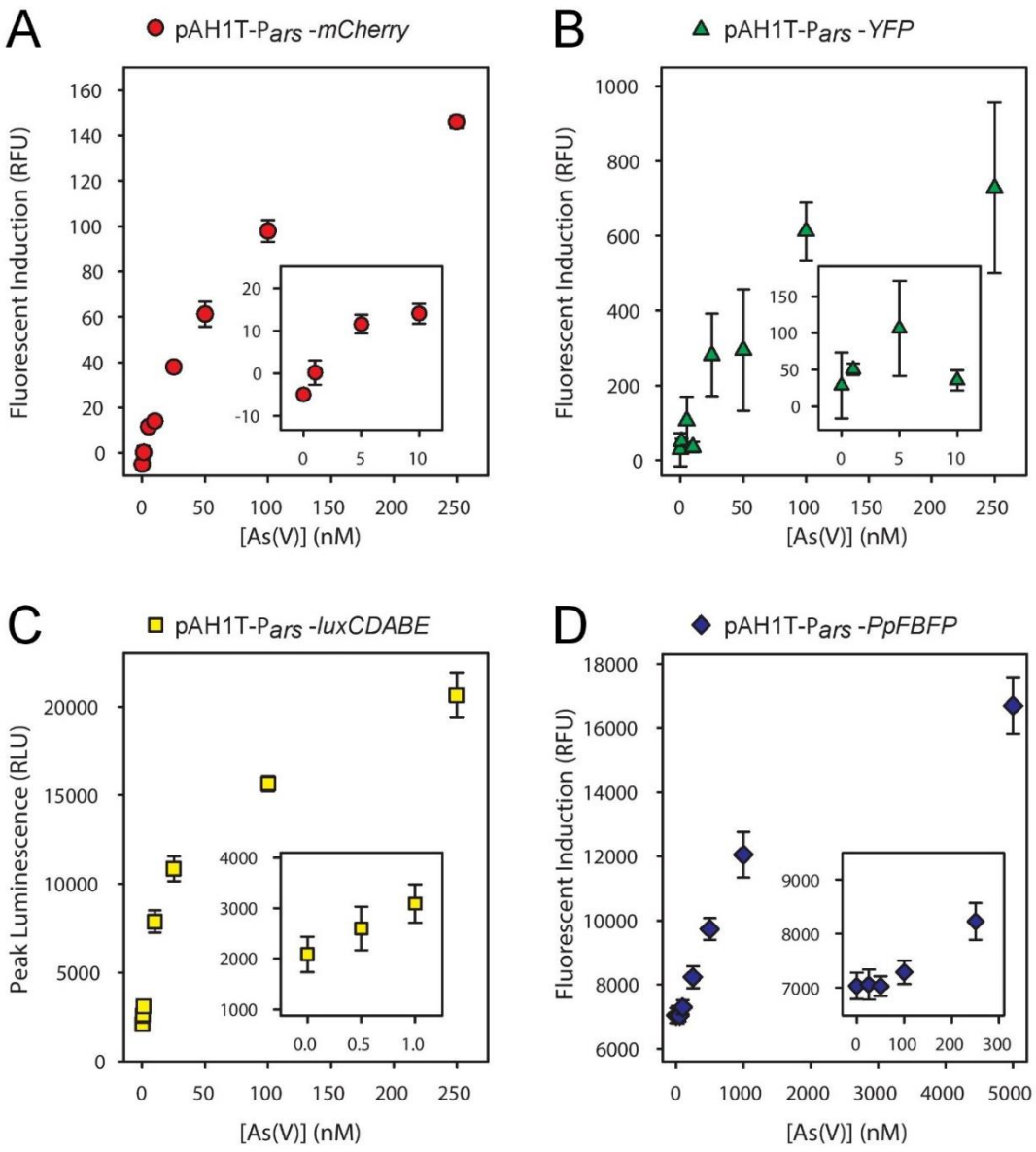

Figure 5.5. Arsenic-inducible biosensors. Arsenic-inducible biosensors were exposed to As(V) concentrations ranging from 0.5 nM to 5000 nM. The signal induction at each As(V) concentration is presented for (A) mCherry, (B) YFP, (C) luciferase, and (D) PpFbFP reporters. For each reporter, the fluorescent induction at 4 hours (in RFUs) or peak luminescence over 3-5 hours (in RLUs) is presented as the mean and standard error for two biological replicates (assayed in triplicate). Insets were rescaled to display the responses at the lowest tested arsenic concentrations.

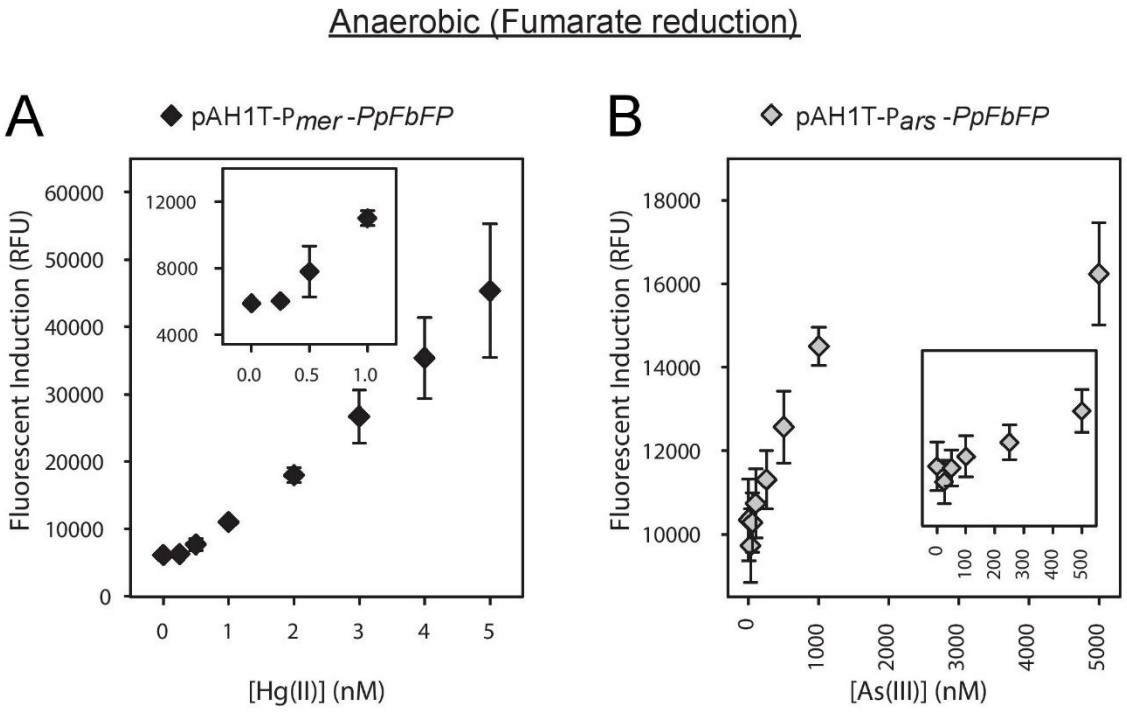

Figure 5.6. Anaerobic quantification of mercury and arsenic during fumarate respiration. PpFbFP biosensors were exposed to (A) mercury or (B) arsenic in anaerobic conditions with fumarate supplied as terminal electron acceptor. The mean fluorescent induction as relative fluorescence units (RFU) at 10 hours and standard error for 3 biological replicates (assayed in triplicate) is presented. Insets were rescaled to display the responses at the lowest analyte concentrations.

5.9 References

1. Daunert S, Barrett G, Feliciano JS, Shetty RS, Shrestha S, Smith-Spencer W. 2000. Genetically Engineered Whole-Cell Sensing Systems: Coupling Biological Recognition with Reporter Genes. Chem Rev 100:2705–2738.

2. Meer JR van der, Belkin S. 2010. Where microbiology meets microengineering: design and applications of reporter bacteria. Nat Rev Microbiol 8:511–522.

3. Leveau JHJ, Lindow SE. 2002. Bioreporters in microbial ecology. Curr Opin Microbiol 5:259–265.

4. Xu T, Close DM, Sayler GS, Ripp S. 2013. Genetically modified whole-cell bioreporters for environmental assessment. Ecol Indic 28:125–141.

5. Ivask A, Rõlova T, Kahru A. 2009. A suite of recombinant luminescent bacterial strains for the quantification of bioavailable heavy metals and toxicity testing. BMC Biotechnol 9:41.

6. Mehrotra P. 2016. Biosensors and their applications – A review. J Oral Biol Craniofacial Res 6:153–159.

7. Su L, Jia W, Hou C, Lei Y. 2011. Microbial biosensors: A review. Biosens Bioelectron 26:1788–1799.

8. Lim JW, Ha D, Lee J, Lee SK, Kim T. 2015. Review of Micro/Nanotechnologies for Microbial Biosensors. Front Bioeng Biotechnol 3:61.

9. Inda ME, Lu TK. 2020. Microbes as Biosensors. Annu Rev Microbiol 74:337–359.

10. Meer JRVD, Tropel D, Jaspers M. 2004. Illuminating the detection chain of bacterial bioreporters. Environ Microbiol 6:1005–1020.

11. Stenzler B, Hinz A, Ruuskanen M, Poulain AJ. 2017. Ionic Strength Differentially Affects the Bioavailability of Neutral and Negatively Charged Inorganic Hg Complexes. Environ Sci Technol 51:9653–9662.

12. Pothier MP, Hinz AJ, Poulain AJ. 2018. Insights Into Arsenite and Arsenate Uptake Pathways Using a Whole Cell Biosensor. Front Microbiol 9:2310.

13. Srinivasan B, Tung S. 2015. Development and Applications of Portable Biosensors. J Lab Autom 20:365–389.

14. Selifonova O, Burlage R, Barkay T. 1993. Bioluminescent sensors for detection of bioavailable Hg(II) in the environment. Appl Environ Microbiol 59:3083–3090.

15. Hughes RA, Miklos AE, Ellington AD. 2011. Chapter twelve - Gene Synthesis: Methods and Applications, p. 277–309. *In* Voigt, C (ed.), Methods in Enzymology. Academic Press.

16. Casini A, Storch M, Baldwin GS, Ellis T. 2015. Bricks and blueprints: methods and standards for DNA assembly. Nat Rev Mol Cell Biol 16:568–576.

17. Shanks RMQ, Caiazza NC, Hinsa SM, Toutain CM, O'Toole GA. 2006. Saccharomyces cerevisiae-Based Molecular Tool Kit for Manipulation of Genes from Gram-Negative Bacteria. Appl Environ Microbiol 72:5027–5036.

18. Geu-Flores F, Nour-Eldin HH, Nielsen MT, Halkier BA. 2007. USER fusion: a rapid and efficient method for simultaneous fusion and cloning of multiple PCR products. Nucleic Acids Res 35:e55.

19. Adli M. 2018. The CRISPR tool kit for genome editing and beyond. Nat Commun 9:1–13.

20. Nyerges Á, Csörgő B, Nagy I, Bálint B, Bihari P, Lázár V, Apjok G, Umenhoffer K, Bogos B, Pósfai G, Pál C. 2016. A highly precise and portable genome engineering method allows

comparison of mutational effects across bacterial species. Proc Natl Acad Sci 113:2502–2507.

21. Silva-Rocha R, Martínez-García E, Calles B, Chavarría M, Arce-Rodríguez A, de las Heras A, Páez-Espino AD, Durante-Rodríguez G, Kim J, Nikel PI, Platero R, de Lorenzo V. 2013. The Standard European Vector Architecture (SEVA): a coherent platform for the analysis and deployment of complex prokaryotic phenotypes. Nucleic Acids Res 41:D666–D675.

22. Shetty RP, Endy D, Knight TF. 2008. Engineering BioBrick vectors from BioBrick parts. J Biol Eng 2:5.

23. Engler C, Kandzia R, Marillonnet S. 2008. A One Pot, One Step, Precision Cloning Method with High Throughput Capability. PLOS ONE 3:e3647.

24. 2013. Synthetic Biology. Humana Press.

25. Yanisch-Perron C, Vieira J, Messing J. 1985. Improved M13 phage cloning vectors and host strains: nucleotide sequences of the M13mpl8 and pUC19 vectors. Gene 33:103–119.

26. Simon R, Priefer U, Pühler A. 1983. A Broad Host Range Mobilization System for In Vivo Genetic Engineering: Transposon Mutagenesis in Gram Negative Bacteria. Bio/Technology 1:784–791.

27. Figurski DH, Helinski DR. 1979. Replication of an origin-containing derivative of plasmid RK2 dependent on a plasmid function provided in trans. Proc Natl Acad Sci U S A 76:1648–1652.

28. Choi K-H, Gaynor JB, White KG, Lopez C, Bosio CM, Karkhoff-Schweizer RR, Schweizer HP. 2005. A Tn 7 -based broad-range bacterial cloning and expression system. Nat Methods 2:443–448.

29. Hmelo LR, Borlee BR, Almblad H, Love ME, Randall TE, Tseng BS, Lin C, Irie Y, Storek KM, Yang JJ, Siehnel RJ, Howell PL, Singh PK, Tolker-Nielsen T, Parsek MR, Schweizer HP, Harrison JJ. 2015. Precision-engineering the Pseudomonas aeruginosa genome with two-step allelic exchange. Nat Protoc 10:1820–1841.

30. Lebeuf-Taylor E, McCloskey N, Bailey SF, Hinz A, Kassen R. 2019. The distribution of fitness effects among synonymous mutations in a gene under directional selection. eLife 8:e45952.

31. Lanzer M, Bujard H. 1988. Promoters largely determine the efficiency of repressor action. Proc Natl Acad Sci 85:8973–8977.

32. Schweizer HP. 1991. Escherichia-Pseudomonas shuttle vectors derived from pUC18/19. Gene 97:109–112.

33. Hansen LH, Sørensen SJ. 2000. Versatile biosensor vectors for detection and quantification of mercury. FEMS Microbiol Lett 193:123–127.

34. Merulla D, Buffi N, Beggah S, Truffer F, Geiser M, Renaud P, van der Meer JR. 2013. Bioreporters and biosensors for arsenic detection. Biotechnological solutions for a world-wide pollution problem. Curr Opin Biotechnol 24:534–541.

35. Zeng N, Wu Y, Chen W, Huang Q, Cai P. 2021. Whole-Cell Microbial Bioreporter for Soil Contaminants Detection. Front Bioeng Biotechnol 9:622994.

36. Mukherjee A, Walker J, Weyant KB, Schroeder CM. 2013. Characterization of Flavin-Based Fluorescent Proteins: An Emerging Class of Fluorescent Reporters. PLOS ONE 8:e64753.

37. Guglielmetti S, Santala V, Mangayil R, Ciranna A, Karp MT. 2019. O2-requiring molecular reporters of gene expression for anaerobic microorganisms. Biosens Bioelectron 123:1–6.

38. Drepper T, Eggert T, Circolone F, Heck A, Krauß U, Guterl J-K, Wendorff M, Losi A, Gärtner W, Jaeger K-E. 2007. Reporter proteins for in vivo fluorescence without oxygen. Nat Biotechnol 25:443–445.

39. Stenzler BR, Gaudet J, Poulain AJ. 2018. An Anaerobic Biosensor Assay for the Detection of Mercury and Cadmium. JoVE J Vis Exp e58324.

40. Schaefer JK, Rocks SS, Zheng W, Liang L, Gu B, Morel FMM. 2011. Active transport, substrate specificity, and methylation of Hg(II) in anaerobic bacteria. Proc Natl Acad Sci U S A 108:8714–8719.

41. Yu R-Q, Reinfelder JR, Hines ME, Barkay T. 2013. Mercury Methylation by the Methanogen Methanospirillum hungatei. Appl Environ Microbiol 79:6325–6330.

42. Si Y, Zou Y, Liu X, Si X, Mao J. 2015. Mercury methylation coupled to iron reduction by dissimilatory iron-reducing bacteria. Chemosphere 122:206–212.

43. Young R, Haines M, Storch M, Freemont PS. 2021. Combinatorial metabolic pathway assembly approaches and toolkits for modular assembly. Metab Eng 63:81–101.

44. Gay P, Le Coq D, Steinmetz M, Berkelman T, Kado CI. 1985. Positive selection procedure for entrapment of insertion sequence elements in gram-negative bacteria. J Bacteriol 164:918–921.

45. Bhatnagar K, Hinz A, Kohlman M, Wong A. 2020. An sRNA Screen for Reversal of Quinolone Resistance in Escherichia coli. G3 Genes Genomes Genet 10:79–88.

46. Hoang TT, Karkhoff-Schweizer RR, Kutchma AJ, Schweizer HP. 1998. A broad-host-range Flp-FRT recombination system for site-specific excision of chromosomally-located DNA sequences: application for isolation of unmarked Pseudomonas aeruginosa mutants. Gene 212:77–86.

47. Choi K-H, Schweizer HP. 2006. mini-Tn7 insertion in bacteria with single attTn7 sites: example Pseudomonas aeruginosa. Nat Protoc 1:153–161.

48. Rakowski SA, Filutowicz M. 2013. Plasmid R6K replication control. Plasmid 69:231–242.

49. Bailey SF, Hinz A, Kassen R. 2014. Adaptive synonymous mutations in an experimentally evolved Pseudomonas fluorescens population. Nat Commun 5:1–7.

50. Melnyk AH, McCloskey N, Hinz AJ, Dettman J, Kassen R. 2017. Evolution of Cost-Free Resistance under Fluctuating Drug Selection in Pseudomonas aeruginosa. mSphere 2:e00158-17.

51. Dench J, Hinz A, Aris-Brosou S, Kassen R. 2020. Identifying the drivers of computationally detected correlated evolution among sites under antibiotic selection. Evol Appl 13:781–793.

52. J. Sambrook, Molecular cloning: a laboratory manual / Joseph Sambrook, David W. Russell. D. W. Russell, L. Cold Spring Harbor, Eds., (Cold Spring Harbor Laboratory, Cold Spring Harbor, N.Y, 2001).

53. Rainey PB. 1999. Adaptation of Pseudomonas fluorescens to the plant rhizosphere. Environ Microbiol 1:243–257.

54. Kelly JR, Rubin AJ, Davis JH, Ajo-Franklin CM, Cumbers J, Czar MJ, de Mora K, Glieberman AL, Monie DD, Endy D. 2009. Measuring the activity of BioBrick promoters using an in vivo reference standard. J Biol Eng 3:4.

55. Guzman LM, Belin D, Carson MJ, Beckwith J. 1995. Tight regulation, modulation, and high-level expression by vectors containing the arabinose PBAD promoter. J Bacteriol 177:4121–4130.

56. Shaner NC, Steinbach PA, Tsien RY. 2005. A guide to choosing fluorescent proteins. Nat Methods 2:905–909.

57. Becher A, Schweizer HP. 2000. Integration-Proficient Pseudomonas aeruginosa Vectors for Isolation of Single-Copy Chromosomal lacZ and lux Gene Fusions. BioTechniques 29:948–952.

Chapter 6: Diffusion of H_2S from thiolated ligand biodegradation rapidly generates bioavailable mercury

Authors

Benjamin R. Stenzler[1], Rui Zhang[1], Jeremy D. Semrau[2], Alan A. DiSpirito[3], and Alexandre J. Poulain[1]*†

Affiliations

[1]Biology Department, University of Ottawa, 30 Marie Curie, Ottawa, ON K1N 6N5, Canada

[2]Department of Civil and Environmental Engineering, University of Michigan, Ann Arbor, MI 48109, USA.

[3]Roy J. Carver Department of Biochemistry, Biophysics and Molecular Biology, Iowa State University, Ames, IA 50011, USA

*Corresponding author. Email: apoulain@uottawa.ca

"This is the accepted version of the following article: [Stenzler, B.R., Zhang, R., Semrau, J.D., DiSpirito, A.A. and Poulain, A.J. (2022), Diffusion of H_2S from anaerobic thiolated ligand biodegradation rapidly generated bioavailable mercury. Environ Microbiol. Accepted Author Manuscript. https://doi.org/10.1111/1462-2920.16078], which has been published in final form at https://sfamjournals.onlinelibrary.wiley.com/doi/abs/10.1111/1462-2920.16078. This article may be used for non-commercial purposes in accordance with Wiley Terms and Conditions for Use of Self-Archived Versions. This article has been modified for thesis dissertation."

N.B. Supporting information for this chapter can be found in **Appendix D**

6.1 Summary

Methylmercury (MeHg) is a potent neurotoxin that biomagnifies through food webs and which production depends on anaerobic microbial uptake of inorganic mercury (Hg) species. One outstanding knowledge gap in understanding Hg methylation is the nature of bioavailable Hg species. It has become increasingly obvious that Hg bioavailability is spatially diverse and temporally dynamic but current models are built on single thiolated ligand systems, mostly omitting ligand exchanges and interactions, or the inclusion of dissolved gaseous phases. In this study, we used a whole-cell anaerobic biosensor to determine the role of a mixture of thiolated ligands on Hg bioavailability. Serendipitously, we discovered how the diffusion of trace amounts of exogenous biogenic H_2S, originating from anaerobic microbial ligand degradation, can alter Hg speciation - away from H_2S production site - to form bioavailable species. Regardless of its origins, H_2S stands as a mobile mediator of microbial Hg metabolism, connecting spatially separated microbial communities. At a larger scale, global planetary changes are expected to accelerate the production and mobilization of H_2S and Hg, possibly leading to increased production of the potent neurotoxin; this work provides mechanistic insights into the importance of co-managing biogeochemical cycle disruptions.

Originality-Significance Statement

This study demonstrates a mechanism in which microbes can liberate mercury from non-bioavailable thiol sinks through the generation and rapid diffusion of gaseous H_2S, making mercury immediately accessible to microbes in neighboring systems.

Keywords: mercury bioavailability, biosensors, sulfide, anoxic, diffusion

6.2 Introduction

Methylmercury (MeHg) is a neurotoxin of concern because it biomagnifies through food webs (Driscoll et al., 2013) and concentrates in food staples such as fish (Obrist et al., 2018) and rice (Tang et al., 2020). MeHg in the environment is produced by anaerobic microbes, particularly sulfate and iron-reducing bacteria and methanogens (Podar et al., 2015). Methylation of divalent mercury (Hg(II)) is an intracellular process, and therefore, Hg-bioavailability to microbes is a critical step (Regnell and Watras, 2019), which, in part, depends on Hg(II) speciation (i.e., the inorganic and organic ligands it is bound to) (Hsu-Kim et al., 2013; Regnell and Watras, 2019). Hg(II) has a high affinity for reduced sulfur (S) moieties ((e.g., $Hg(cysteine)_2$, $Hg(glutathione)_2$, HgS^0 or $Hg(HS)_2{}^0$). These Hg(II) species form with different substrates; low molecular weight thiols, microbial membranes, dissolved organic matter (DOM), and extracellular polymeric substances that form biofilms (Drott et al., 2013; Hsu-Kim et al., 2013; Manceau et al., 2015; Liem-Nguyen et al., 2017a; Liem-Nguyen et al., 2017b; Dranguet et al., 2018; Fein et al., 2019). These Hg(II)-thiol complexes do not uniquely define Hg bioavailability as some Hg(II) species are bioavailable to microbes while others are not (Schaefer et al., 2011; Zhao et al., 2017; An et al., 2019; Yin et al., 2020). Decoupling Hg(II) S-associated speciation from bioavailability in environments where Hg methylation occurs is necessary for modeling environmental constraints on Hg methylation.

The current model describing how Hg species enter microbial cells involves either an active transport of Hg thiol species and/or the passive diffusion of Hg(II)-sulfide complexes (Regnell and Watras, 2019). For Hg(II) species to enter the cell via non-specific metal ion transporters (Schaefer et al., 2011; Schaefer et al., 2014; Ndu et al., 2015; Szczuka et al., 2015), a ligand exchange must occur between the ligand in solution and the transport site on the cell

membrane (Schaefer et al., 2014; Thomas et al., 2014). Thiols create labile Hg(II) species that can shuttle Hg to the transport site, but high concentrations of these thiols sequester Hg(II), preventing its transport across the cell wall (Schaefer and Morel, 2009; Schaefer et al., 2011; Ndu et al., 2012; Thomas et al., 2014; Lin et al., 2015; Liu et al., 2016; Zhao et al., 2017). Furthermore, any levels of multidentate thiol ligands such as sorption sites on microbial membranes, dissolved organic matter, and low molecular weight thiols bind Hg so strongly that they typically inhibit Hg(II) uptake (Hu et al., 2013a; Chiasson-Gould et al., 2014; Liu et al., 2016; Mishra et al., 2017; Song et al., 2018; Song et al., 2020; Thomas et al., 2020; Yin et al., 2020). Under most environmentally relevant conditions, inorganic sulfides will outcompete thiols for Hg(II) speciation and form Hg(II)-sulfide complexes (Deonarine and Hsu-Kim, 2009; Pham et al., 2014; Poulin et al., 2017) typically present as HgS nanoparticles that can be used as substrates for Hg methylation. Newly formed small Hg(II)-sulfides can permeate readily through cytoplasmic membranes (Zhou et al., 2017; Thomas et al., 2018; An et al., 2019; Thomas et al., 2019; Tian et al., 2021). However, given enough time and elevated Hg(II) concentrations, these HgS particles can aggregate and become too large and unavailable to cells (Graham et al., 2012, 2013; Mazrui et al., 2018; Zhang et al., 2020; Tian et al., 2021).

The areas of highest Hg methylation are not simple ligand systems, however. Methylation occurs in (micro)-anoxic zones of microbial ecosystems, such as biofilms or microbial mats (Olsen et al., 2016; Dranguet et al., 2018), the oxycline in water/sediments (Bravo et al., 2014), and in suspended particulate organic matter (Sunderland et al., 2009; Lehnherr et al., 2011; Ortiz et al., 2015). These environments are typically characterized by rapid nutrient turnover across redox gradients. This is the case for rapid and often cryptic sulfur cycling (Pester et al., 2012; Leclerc et al., 2015; Mills et al., 2016; Beulig et al., 2019; Jørgensen et al., 2019; Raven et al.,

2021), such as the transformation of high valences (S(VI); e.g., SO_4^{2-}) and low valence sulfur containing molecules (S(-II); e.g., thiols and H_2S). This process creates localized elevated µM-mM concentrations of thiols and transient H_2S production (Beulig et al., 2019; Jørgensen et al., 2019; Huynh et al., 2020; Raven et al., 2021). Extracellular thiols are generated by almost all forms of life (e.g., microbes, plants, algae, dissolved organic matter (DOM)) (Kawakami et al., 2006; Carrasco-Gil et al., 2011; Yu et al., 2014; Dunham-Cheatham et al., 2015; Mangal et al., 2016; Adediran et al., 2019), and H_2S is primarily produced by sulfur-reducing organisms (through dissimilatory SO_4^{2-} reduction pathways) (Labrenz et al., 2000; Pester et al., 2012; Mills et al., 2016; Jørgensen et al., 2019), but can also result from mineralization of organic molecules (Manceau et al., 2015; Enescu et al., 2016).

The role of thiolated ligands on Hg(II) bioavailability has received a lot of attention, and more recently, an effort has been made to further explore how microbial interactions can alter the fate of Hg(II). Most notably, the interactions between methanotrophic bacteria and Hg-methylating microbes have received much attention. Methanotrophs thrive at the oxic/anoxic interface and have also been shown to control Hg bioavailability to other organisms with production of the chalkophore, methanobactin (MB) (Semrau and Gu, 2020). While MB is secreted by methanotrophs to acquire copper, it has been shown to also interact strongly with Hg(II), altering bioavailability to both methanotrophs (Vorobev et al., 2013) and Hg-methylating microbes (Yin et al., 2020).

Whereas the study of individual ligands is essential to building conceptual models, we need to move away from single ligands to properly model Hg(II) bioavailability in complex microbial systems. Hg(II) speciation is dynamic, involves a series of ligand exchanges, and cannot be assumed to always be at equilibrium. To identify mechanisms underlying the dynamic

nature of Hg bioavailability in methylation sites, our lab has so far mostly focused on anaerobic Hg redox processes (Grégoire and Poulain, 2018; Branfireun et al., 2020) to evaluate whether these reactions can "reset" Hg speciation bound to otherwise poorly bioavailable ligands (e.g., multidentate thiols and DOM). Indeed, newly anaerobically produced Hg^0 may be reoxidized and become available for methylation (Colombo et al., 2013; Hu et al., 2013b) or diffuse away (evade) as a gas. Gases are not limited to the aqueous phase and are essential for Hg transport and cycling in the environment through evasion and deposition (Driscoll et al., 2013). This unique property of Hg emphasizes the importance of including (dissolved) gaseous phases at a scale that is relevant to microbial processes, and not only in global atmospheric models, when attempting to model Hg bioavailability to methylators.

In this study, we used a whole-cell anaerobic Hg-biosensor to determine the role of a mixture of thiolated ligands on Hg(II) bioavailability and serendipitously discovered a role for biogenic H_2S diffusion in controlling Hg(II) bioavailability at a distance. The Hg and sulfur cycles are intrinsically linked, but we have yet to consider the role of diffusive gaseous H_2S in controlling Hg(II) bioavailability. Here, we show how H_2S, either biogenic or added as Na_2S, diffuses away from the solution where it was produced, making an otherwise non-bioavailable Hg(II) species and located at a distance rapidly available for microbial uptake.

6.3 Results and Discussion

6.3.1 Identifying bioavailable and non-bioavailable Hg(II) thiolated species

The first objective was to use a biosensor to determine which thiols, and at what concentrations, control anaerobic Hg(II) bioavailability. The addition of glutathione (GSH), methanobactin from *Methylosinus trichosporium* OB3b (MB-OB3b) and dimercaptosuccinic acid (DMSA) to the

exposure assay completely inhibited the fluorescence response of the Hg-inducible biosensor (μ=0) at 1 μM (0.026 RFU± 0.035, p = 0.131), 5 μM (-0.09 RFU ± 0.02, p = 0.002) and 0.1 μM (-0.003 RFU ± 0.095, p = 0.943) respectively (Fig. 6.1, A, B and C). The addition of these thiols did not inhibit constitutive fluorescence production by the biosensor, showing that a decrease in the inducible fluorescent signal was not associated with a reduction in cell viability under the conditions tested. In fact, the addition of both GSH and the MB from *Methylosinus trisporium* OB3b (MB-OB3b) enhanced the constitutive biosensor's fluorescence up to 1.75 ± 0.37x and 2.30 ± 0.20x that of the control, indicating a physiological benefit to the presence of these thiols (Fig. 6.1 A and B).

By contrast, the addition of penicillamine (Pen), cysteine (Cys), and dimercaprol (BAL) enhanced maximum fluorescence up to 5.13 ± 1.09x (Pen), 1.53 ± 0.60x (Cys), and 3.00 ± 0.70x (BAL) the control (Fig. 6.1 D, E, and F). As ligands concentrations increased, fluorescence eventually decreased but, interestingly, was never completely inhibited – as was observed for GSH, MB-OB3b, and DMSA - even when up to 4 mM of Pen or Cys was added (Fig. 6.1 D, and F). The constitutive biosensor fluorescence response suggests that reduction in Hg-inducible fluorescence may result from physiological stress to excess of these thiols.

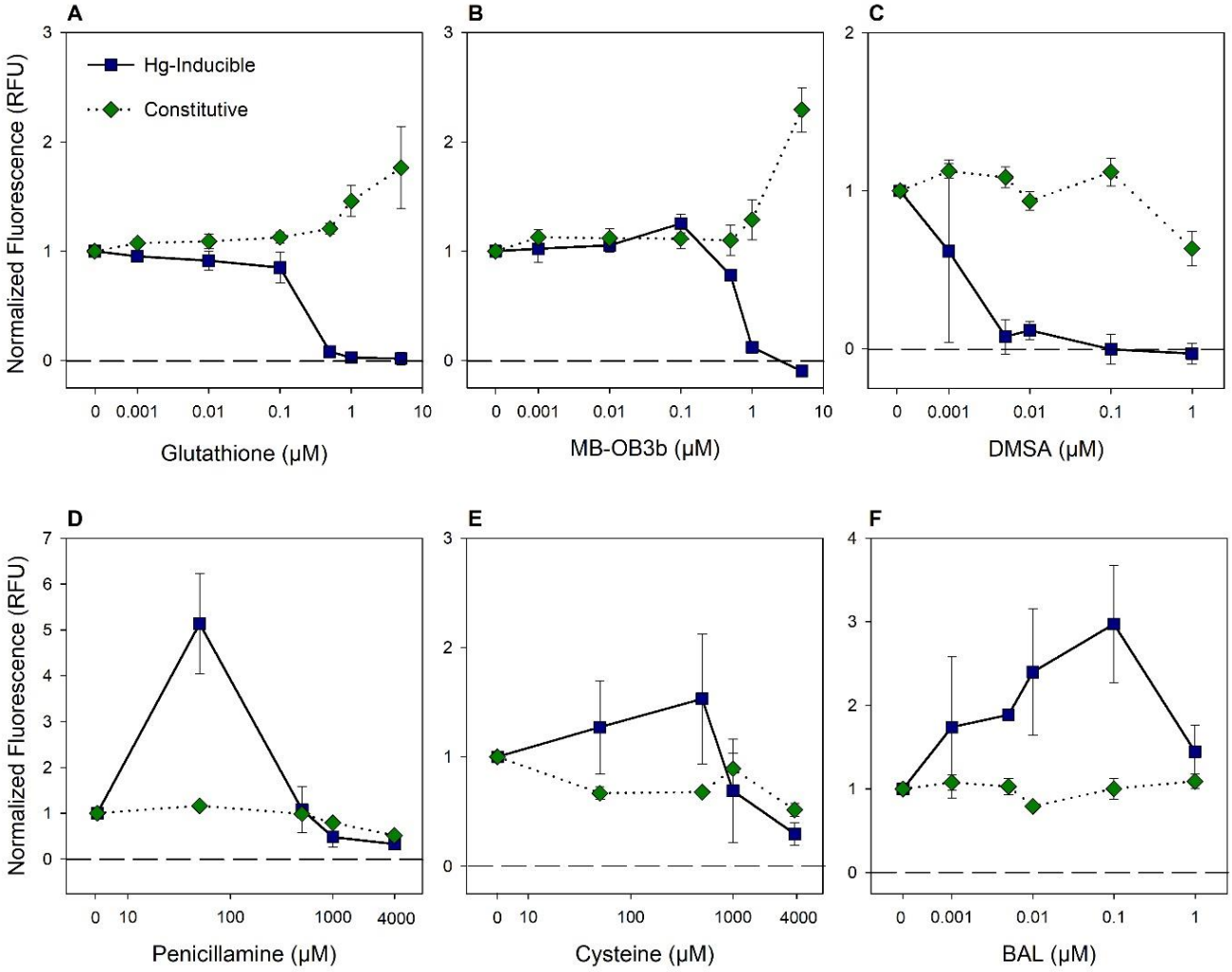

Figure 6.1: Hg(II) bioavailability in the presence of various thiols. Average Normalized Fluorescence measured as relative fluorescence units (RFU) ± 1SD at 10 hours emitted the Hg-Inducible biosensor (*E. coli* NEB5α harboring the pUC57merR-Pp plasmid) and the Constitutive biosensor (*E. coli* NEB5α harboring pUC19AH206-Pp plasmid) with the addition of **A)** glutathione (0-5 μM) **B** methanobactin from *M trichosporium* OB3b (MB-OB3b) (0-5 μM), **C)** DMSA (0-4000 μM), **D)** penicillamine (0-4000 μM), **E)** cysteine (0-4000 μM) and **F)** BAL (0-1 μM). Fluorescence at 10 hours was normalized to the control (0 μM) at 10 hours for each biological replicate (between 3 and 11 biological replicates per point, see Table D1 for further details). [Hg] was set to 2 nM. The experiment was performed at 37 ˚C in an anaerobic exposure medium (pH 7).

Our results support that Hg(II) bioavailability is highly dependent on its speciation. We modeled Hg(II) speciation with and without a representative cell membrane (Fig. 6.2 and Fig. D1) with parameters inferred from (Song et al., 2020). In the absence of a membrane, Hg(II) forms two thiol coordinated complexes with GSH/Pen/Cys (>2:1 [RSH]:[Hg]) over the entire concentration gradients used in the assay (Fig, D1 A, D, and E). Initially, it appears that two thiol coordinated complexes ($Hg(RS)_2$) for GSH/Pen/Cys are highly bioavailable at low ligand

concentration. As ligand concentration increases, bioavailability lowers for each of these thiols and is completely inhibited by GSH. Hg(II) bioavailability is better explained by complexation with the membrane (Fig. 6.2). $Hg(GSH)_2$ is likely not bioavailable since it prevents Hg(II) from forming membrane complexes (Fig. 6.1 A; Fig. 6.2 A). Increasing Pen and Cys concentration initially enhances Hg(II) bioavailability which may be explained by the 1-3% Hg(Mem-RS)(RS) species at 50 µM (Fig. 6.1 D and E; Fig. 6.2 D and E). Further increasing concentration forms 100% $Hg(RS)_2$ species that are still bioavailable but much less. However, as described in the next section, we cannot merely assume that Hg(II) bioavailability with Cys is related to the formation of Hg(II)-Cys complexes.

These results are consistent with the dynamic effects of thiol concentration on Hg(II) bioavailability. Increasing thiol concentrations first enhances bioavailability before higher concentrations decrease it (Regnell and Watras, 2019).

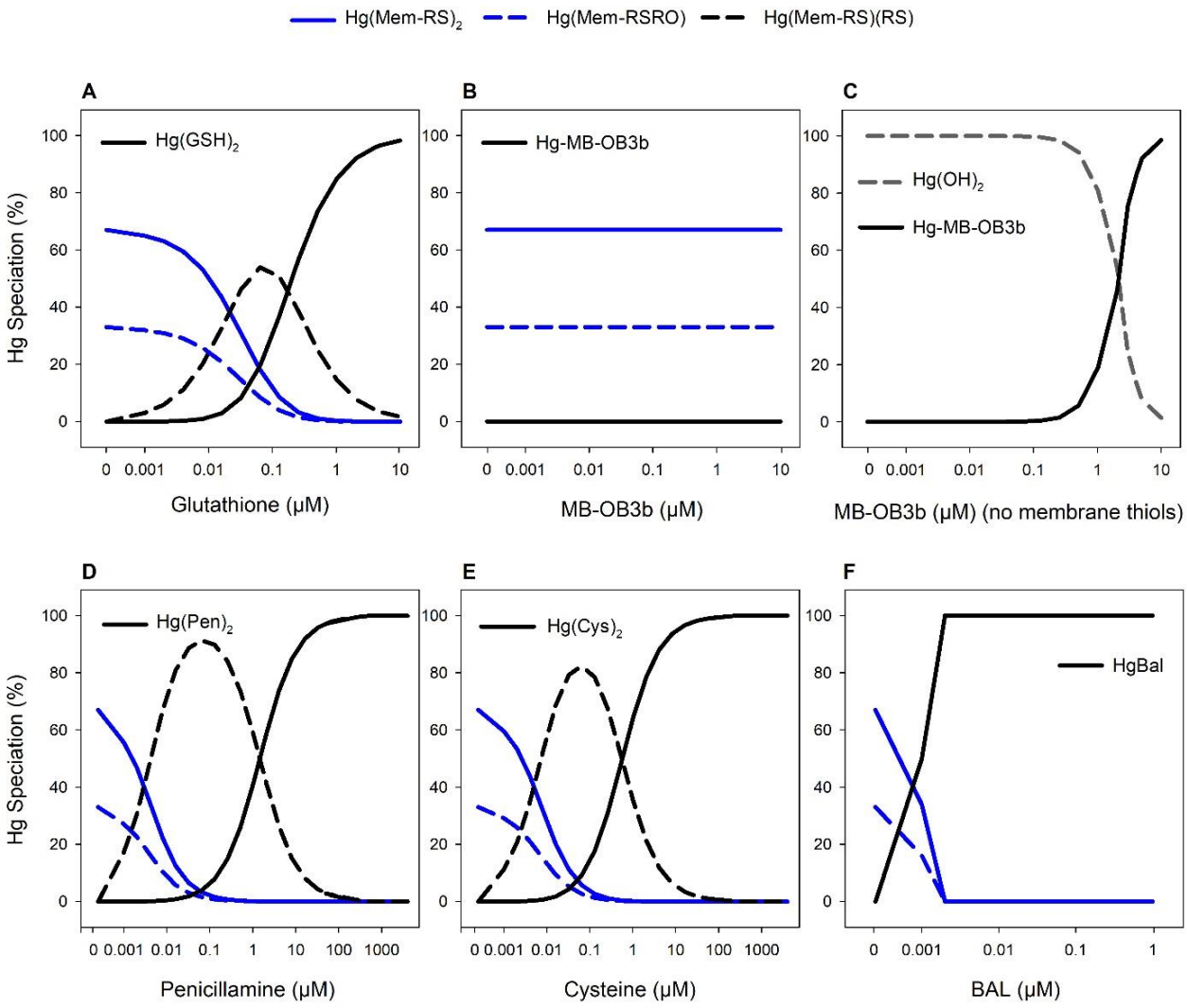

Figure 6.2: Hg(II) species with the addition of various thiols at equilibrium with a cell membrane. Thermodynamic model predicting the Hg speciation (%) with the addition **A)** glutathione (0-10 µM) **B** methanobactin from *M trichosporium* OB3b (MB-OB3b) (0-10 µM), **C)** MB-OB3b (0-10 µM) when no membrane thiols were included in the model, **D)** penicillamine (0-4000 µM), **E)** cysteine (0 -4000 µM) and **F)** BAL (0-1 µM). The models performed at 25˚C. The model contains a representative cell membrane with 1.37 µM thiols. With the membrane, Hg(II) can form two-coordinate thiols bonds between two thiols on the membrane ($Hg(Mem\text{-}RS)_2$), a mixed two-coordinate thiol complex between the membrane and a thiol in solution (Hg(Mem-RS)(RS)), or a one-coordinate thiol complex on the membrane with neighboring O/N functionality (Hg(Mem-RSRO). Models were performed in anaerobic exposure medium (pH 7), and [Hg(II)] was set to 2 nM.

Hg(II) bioavailability with MB-OB3b may also be explained by a lack of complexation with the cell membrane. MB-OB3b cannot compete for Hg(II) (Fig. 6.2 B) when modeled at equilibrium. However, MB-OB3b was allowed to equilibrate with Hg(II) before cells were added to the system. Without membrane thiols competing for Hg(II), changes in Hg(II) speciation with increasing MB-OB3b concentrations follow changes in bioavailability (Fig. 6.1 B and Fig. 6.2 C). Once bound to MB-OB3b, Hg(II) is not likely going to achieve thermodynamic equilibrium in an aqueous solution. Similar observations have been made in an attempt to displace Hg(II) and Au(III) from MB-OB3b and MB from Methylocystis strain SB2 with divalent copper (Cu(II)). Despite having orders of magnitude higher binding constants, in competitive assays, Cu(II) could not displace Hg(II) or Au(III) and even preferentially bound Hg(II) over Cu(II) (Baral et al., 2014; Kalidass et al., 2015). Thermodynamic modeling of aqueous chemical species is typically limited to the assumption of equilibrium; however, sometimes systems cannot achieve equilibrium.

The Hg-MB-OB3b complex may be also be too large, and steric restrictions are preventing ligand exchange with the membrane. Active Hg(II) transport occurs across the inner membrane of a cell (Schaefer et al., 2011; Schaefer et al., 2014; Ndu et al., 2015; Szczuka et al., 2015). *Enterobacteriaceae* have general "unspecific" porins on the outer membrane with a strict cut-off limit on the sizes of molecules that can permeate (600 Da). This is a critical factor in designing antibiotics (Choi and Lee, 2019). MB-OB3b has a molecular weight (MW) of 1154.26 Da (1354.85 Da with Hg(II)). Porin exclusion may also be happening with $Hg(GSH)_2$. Two GSH molecules have a MW 614.63 Da (813.23 Da as ($Hg(GSH)_2$). If this is the reason $Hg(GSH)_2$ and Hg-MB-OB3b are not bioavailable, performing ligand exchanges to form smaller Hg(II) species

may facilitate bioavailability. The other ligands used in this study form Hg(II) complexes with a MW <600 Da.

Lastly, there was a stark contrast in Hg(II) bioavailability with BAL and DMSA (Fig. 6.1 C and F). Although these synthetic molecules are not naturally occurring in the environment, the rationale for using BAL and DMSA in the experimental design was to identify Hg(II) species that would be entirely non-bioavailable to test the ligand exchange hypothesis. Any amount of BAL would completely alter Hg(II) speciation (Fig. 6.2 F; Fig. D1 F). Whereas no stability constants are available for DMSA, we assume, similar to BAL, that any concentration of DMSA (>[Hg(II)] alters speciation entirely. Hg(BAL) species are highly bioavailable, while HgDMSA species have no bioavailability at all. The only notable difference between the two molecules is that DMSA complexes are charged and hydrophilic, and BAL complexes are lipophilic and neutral (Bjørklund et al., 2019). This may be a factor differentiating their bioavailability by passive diffusion of HgBAL. However, assessing the ability of non-naturally occurring ligands to facilitate Hg(II) bioavailability through passive diffusion is beyond the scope of this study.

It is important to note that the models may not fully represent our system's Hg(II) speciation. We used modeling parameters to generally infer how Hg(II) speciation affects its bioavailability. The exact concentrations of thiols on the *E. coli* cell membrane have not been measured. They might be higher or lower than anticipated; this would skew the model. The recommended concentrations of membrane thiols also had an error of 13%. In addition, the constants for Hg(Mem-RS)(Pen) and Hg(Mem-RS)(GSH) complexes have not been measured but inferred from cysteine. These species are likely are forming (Song et al., 2018; Song et al., 2020), but this is yet to be verified experimentally, using a combination of spectroscopic methods.

6.3.2 Thiol Ligand Exchanges and Hg Bioavailability

After identifying the bioavailability of Hg(II) species using single ligands, we proceeded to test how ligand exchange affect Hg bioavailability. Changing Hg(II) speciation from non-bioavailable to bioavailable (e.g., $Hg(GSH)_2 \rightarrow Hg(Pen)_2$) should enhance Hg(II) uptake. We modelled Hg(II) speciation with GSH or MB-OB3b (5µM) with increasing concentrations of Pen or Cys (Fig. D2). By adding 50 and 500 µM of competing ligand we will completely alter the speciation and form bioavailable species (e.g., $Hg(Pen)_2$ and $Hg(Cys)_2$). However, the addition of 50 or 500 µM Pen did not rescue Hg(II) bioavailability in the presence of 5µM GSH or MB-OB3b (Fig. 6.3 A) by forming $Hg(Pen)_2$. The constitutive biosensor data indicated that this was not the result of stress possibly induced by the presence of a combination of ligands. The same observation was made with a combination of Pen and MB-OB3b (Fig. 6.3 A). Altering the speciation to form bioavailable Hg(II) species did not enhance Hg(II) bioavailability. It is possible that ligand exchange did not occur, possibly because of kinetic/modeling constraints, but this is consistent for Hg(II) not being able to be displaced from MB-OB3b (Baral et al., 2014; Kalidass et al., 2015). We did not observe a fluorescence signal developing over 10 hours (Fig. 6.3 A) or 20 hours when we let the experiment last longer (data not shown).

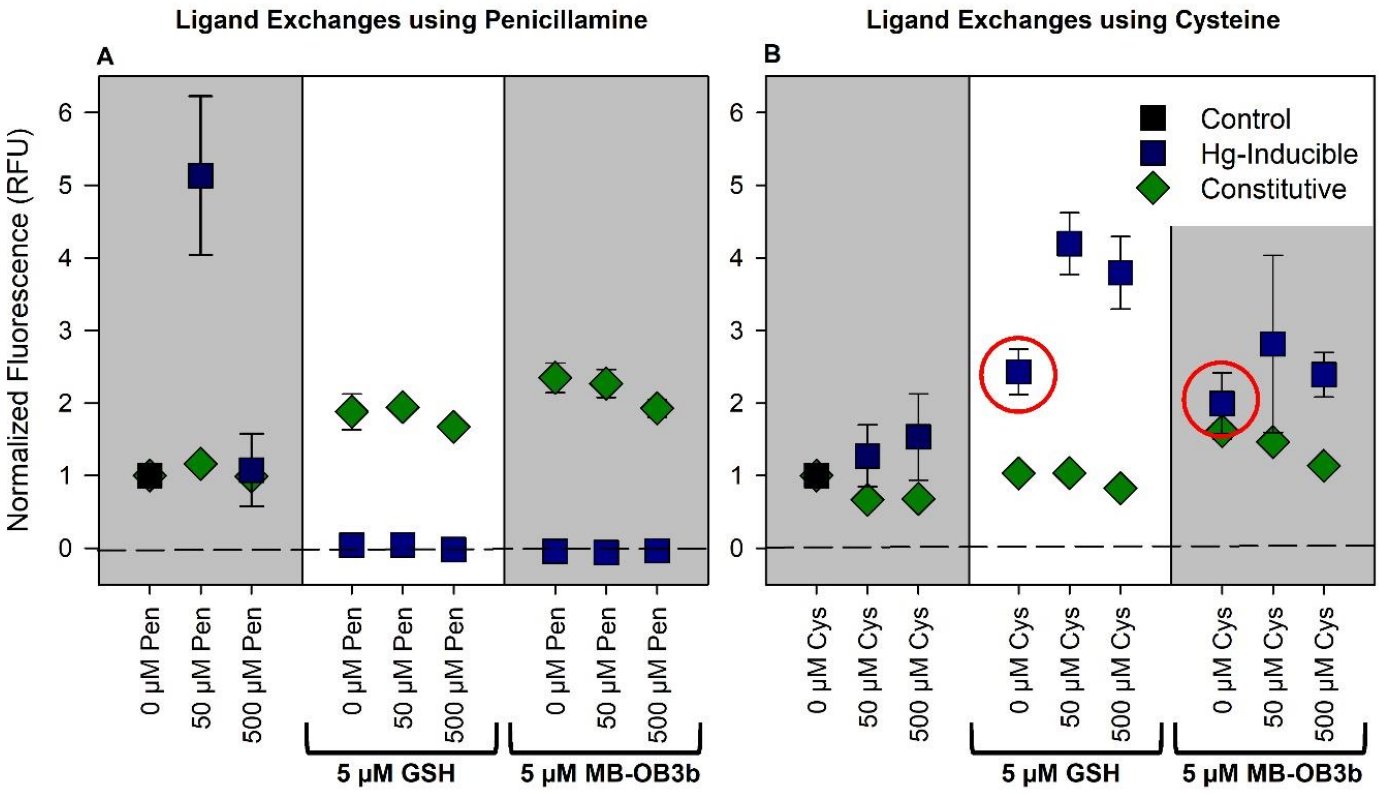

Figure 6.3: Thiol ligand exchanges affect Hg(II) speciation and bioavailability. Average Normalized Fluorescence measured as relative fluorescence units (RFU) ± 1SD at 10 hours by Hg-Inducible biosensor (*E. coli* NEB5α harboring the pUC57merR-Pp plasmid) and the Constitutive biosensor (*E. coli* NEB5α harboring pUC19AH206-Pp plasmid). Measurements were made with the addition of **A**) penicillamine (Pen) (0, 50, or 500 µM) or **B)** cysteine (Cys) (0, 50, or 500 µM), when Hg(II) had already been equilibrated with 5 µM glutathione (GSH) or 5 µM methanobactin from *Methylosinus trichosporium* OB3b (MB-OB3b). Red circles around Hg-Inducible fluorescence highlight unexpected results. Fluorescence at 10 hours was normalized to the control (0 µM) at 10 hours for each biological replicate (between 4-5 biological replicates per point, see Table D1 for further details). The experiments and models were performed in anaerobic exposure medium (pH 7), and [Hg(II)] was set to 2 nM. The experiments were performed at 37 ˚C. The 50, 500 µM Cys and Pen treatments without GSH or MB-OB3b are the same data as Fig. 6.1.

In sharp contrast to the addition of Pen, the addition of Cys had a profoundly different effect on Hg-inducible fluorescent induction (Fig. 6.3 B). This was surprising because Pen is only a methylated analog of Cys. The addition of 50 and 500 µM Cys vastly increased Hg-Inducible fluorescence in both the GSH and MB-OB3b treatments. Initially, we assumed that ligand exchange to form $Hg(Cys)_2$ species made Hg(II) bioavailable. However, the control wells containing no Cys and only Hg(II), GSH, or MB-OB3b (Fig. 6.3 B circled in red) also exhibited

a signal consistent with enhanced bioavailability. These concentrations made Hg(II) non-bioavailable (Fig. 6.1 A and B).

Cys and Pen are differentially metabolized by cells. Microbes exposed to Cys (typically >100 µM) can degrade it to H_2S, ammonia, and pyruvate (Thomas et al., 2018; Thomas et al., 2019). This process is not reported to happen with Pen due to the fact that it is methylated. Therefore, we speculated that the presence of H_2S resulting from cysteine degradation could change Hg(II) speciation in solution to form bioavailable Hg(II)-sulfides (Thomas et al., 2018; Thomas et al., 2019). It takes nM levels of H_2S (>[Hg(II)]) to change Hg(II) speciation and form aqueous Hg(II)-sulfides (e.g., $Hg(HS)_2$ and $Hg(HS)^-$) or facilitate the precipitation of metacinnabar (β-$HgS_{(s)}$) (Fig. 6.4). That is, our modeling shows that at equilibrium, almost any amount of H_2S will begin to facilitate the precipitation β-$HgS_{(s)}$ and form aqueous Hg(II)-sulfides when 2 nM Hg(II) is in the presence of 5 µM GSH/ MB-OB3b or 50 µM Cys (Fig. 6.4 A, B and C). With 500 µM Cys present, it requires a little more H_2S (50-500 nM) to begin forming aqueous Hg(II) sulfides but will only precipitate β-$HgS_{(s)}$ between 100 nM to 50 µM H_2S (Fig. 6.4 D). These Hg(II)-sulfides are likely forming in solution, however it is unclear whether aqueous species, β-$HgS_{(s)}$, or a combination of the two, are bioavailable. The differential metabolism of Cys and Pen to H_2S by microbial cells may explain why Cys but not Pen could make Hg(II) bioavailable with GSH and MB-OB3b.

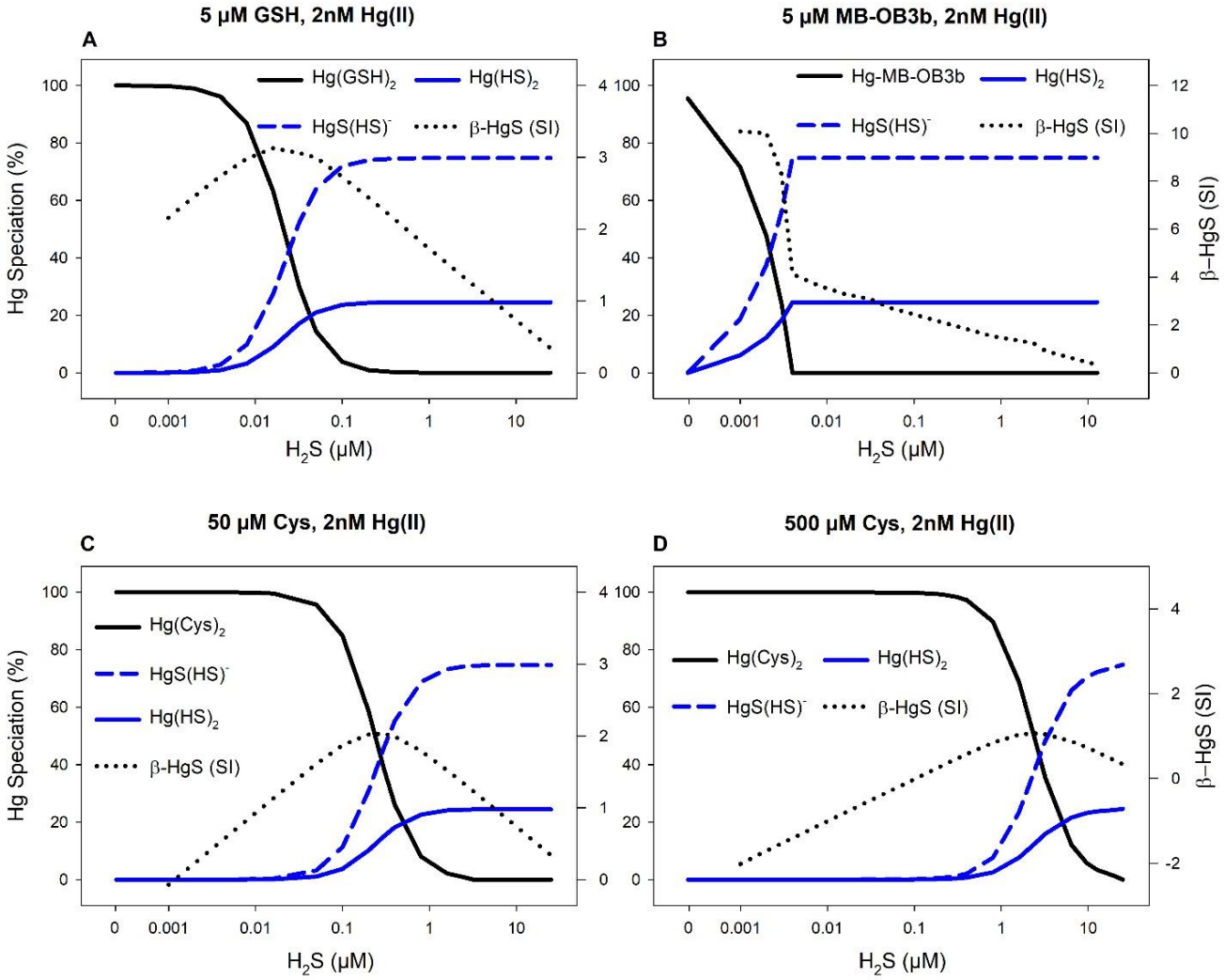

Figure 6.4: Hg(II) species with the addition of H_2S. Thermodynamic model predicting the Hg speciation (%) (left axis) with the addition H_2S (0-25 µM) to **A)** 5 µM glutathione (GSH) **B)** 5 µM methanobactin from *M trichosporium* OB3b (MB-OB3b), **C)** 50 µM Cysteine (Cys), and **D)** 500 µM Cysteine (Cys). The model did not include precipitation but shows a saturation index of metacinnabar (β-HgS (SI) (right axis). Models were performed in anaerobic exposure medium (pH 7) and [Hg(II)] was set to 2 nM. The models performed at 25˚C.

The really surprising result was that the 0 µM Cys treatments that also contained 5 µM GSH or MB-OB3b showed fluorescent induction for the Hg-inducible biosensor (Fig. 6.3 B circled in red) even though no Hg(II) should have been bioavailable at these concentrations (Fig. 6.1 A and B). These experiments were performed in 96-well microplates with lids, but such lids do not hermetically isolate wells from one another. This is notable since the treatments in each panel of Figure 6.3 were performed in the separate 96-well microplates (Fig. D3).

H_2S is unlikely to stay in solution, especially at a neutral pH in a shaking microplate. At a pH 7 (pH of exposure medium), sulfide is present as both 50% HS^- and 50% H_2S species in solution ($H_2S = HS^- + H^+$, pKa =7). While only the H_2S species can diffuse as a gas, proton transfer is incredibly fast, allowing H_2S to readily diffuse to reach equilibrium with its partial pressure above the liquid (Balls and Liss, 1983; Schwarzenbach, 2002). The previous observations led us to test the hypothesis that biogenic H_2S diffusion away from its production well was responsible for the enhanced Hg bioavailability in wells located at a distance. The diffusion of $H_2S_{(g)}$ could remotely affect Hg(II) speciation to form bioavailable Hg(II)-sulfides.

6.3.3 The diffusion of gaseous H_2S makes Hg(II) bioavailable

To test this hypothesis, we first determined the kinetics behind $H_2S_{(g)}$ production and migration in the microplate to determine how much could reasonably affect Hg(II). We measured H_2S, as total dissolved sulfide (operationally measured as S^{2-}), produced by the biosensor in the exposure medium when exposed to 500 µM Cys and Pen (Fig. 6.5 A and B). After 4 hours, we measured 62.69 ± 7.01 µM of H_2S with 500 µM Cys, but H_2S remained below the limit of detection with 500 µM Pen or without any added thiol. In addition, no H_2S was detected with the biosensor metabolizing 5 µM GSH, 5 µM MB-OB3B, 1 µM BAL, or 1 µM DMSA after 4 hours or when left overnight and metabolizing it for 24 hours (Table D2). If trace H_2S was generated from the metabolism of these thiols (below detection), it was insufficient to affect Hg(II) speciation and bioavailability. This data confirmed the differential metabolism of Pen and Cys to H_2S by *E. coli*.

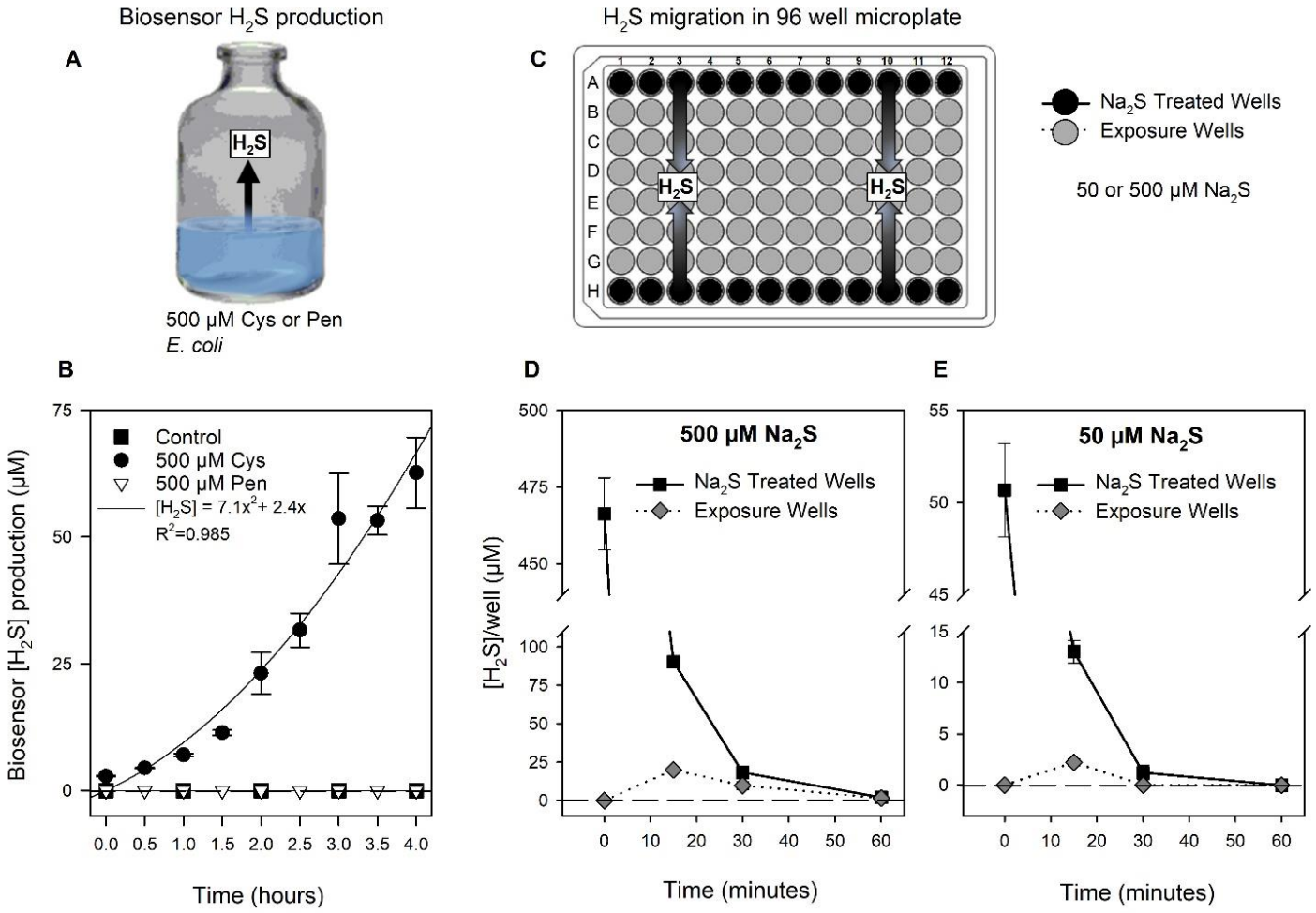

Figure 6.5: H_2S produced by *E. coli* and migration in the 96 well microplate. A) Hydrogen sulfide (H_2S) (µM) produced by the Hg-Inducible biosensor in the presence of either 500 µM cysteine (Cys) or penicillamine (Pen) in anaerobic serum bottles. **B)** The H_2S (µM) ± 1SD over time (hours) in the presence of either 500 µM Cys, 500 µM Pen, or no added thiol (Control). The experiment was performed at 37 ˚C in an anaerobic exposure medium (pH 7) in triplicate. **C)** H_2S migration in the 96 well microplate from Na_2S treated wells (50 or 500 µM Na_2S in exposure medium) to exposure wells containing exposure medium. Average H_2S concentration per well measured as ([H_2S]/well) (µM) ± 1SD in the Na_2S treated wells and exposure wells after 0, 15, 30, and 60 minutes in the microplate reader in plates containing either **D)** 500 or **E)** 50 µM Na_2S. Measurements for each time point were measured in triplicate (3 separate 96 well microplates). Values with concentrations below the detection limit for H_2S (0.34 µM [H_2S]/well) are reported as zero.

H_2S dispersion in the microplate was fast. This was demonstrated by adding 50 or 500 µM Na_2S (in exposure medium buffered at pH=7) in one-quarter of the microplate wells (Fig. 6.5 C). For both 50 or 500 µM Na_2S treatments (Fig. 6.5 D and E), 74-80% of the H_2S evaded the Na_2S treated wells after 15 minutes and >95% after 30 minutes. Within 15 minutes, H_2S was detected in all of the non-treated wells. The non-treated wells contained 2.22 ± 0.35 and 19.88 ±

1.27 µM H_2S/well for microplates with 50 or 500 µM Na_2S, respectively. In the microplates containing 50 µM Na_2S, H_2S was below the limit of detection in the non-treated wells after 30 minutes or 1 hour microplates containing 500 µM Na_2S. For perspective, it took the biosensor about 3 hours (Fig. 6.3 A) to produce 50 µM of biogenic H_2S that would be undetectable in the non-treated wells after 30 minutes (Fig. 6.3 E). Although transient, this [H_2S] in the non-treated wells is predicted to be enough to alter Hg(II) speciation in the presence of GSH or MB-OB3b (Fig. 6.4 A and B).

Our results show it takes several minutes for biogenic H_2S to affect Hg(II) bioavailability remotely and biogenic [H_2S] required to facilitate Hg(II) bioavailablity is likely in the low nanomolar to micromolar range. We estimated the half-life for the diffusion of sulfide from and the plate to be roughly 11-12.5 minutes (Fig. D5 A). Taking into account biogenic H_2S production (metabolizing 500 µM cysteine (Figure 6.5) in remote plate wells, we created a model determining the amount of sulfide that can accumulate in the 96 well microplates (Fig. D5 B). The amount of H_2S remaining in the 96 well microplate is far less than the total amount of H_2S produced due to evasion, reducing the potential H_2S available for diffusion into the plate wells. We also determined the highest [H_2S]/well that would be found in the plate, assuming all of the sulfide was evenly distributed throughout the plate and in the aqueous phase. [H_2S]/well increases from low-mid nanomalor (0-550 nM) over the first hour and steadily increasing into the low micromolar range. We estimate that there is likely less than 50 to 260 nM H_2S in all the wells from biogenic H_2S production between 2.5 to 15 minutes when Hg(II) bioavailability is significant. Still this is more than enough sulfide to affect Hg(II) speciation (Fig 6.4 A and B). These are rough estimates based on our data and limited modelling parameters. Modelling sulfide equilibrium at the air-water interface is subject to many factors (Lahav et al., 2006). The

modelling, however, does support that sustained biogenic production is sufficient to maintain sulfide concentrations throughout the entire microplate.

We then tested whether Cys-induced biogenic production of $H_2S_{(g)}$ (Fig. 6.6 A) or H_2S amended as Na_2S (Fig. 6.6 B), could remotely alter the Hg(II) speciation of bound to refractory thiols in isolated microplate wells not amended with either Cys or Na_2S (Fig. 6.4 A and B). When no H_2S (biogenic or amended as Na_2S) was present in the microplates, there was no fluorescent induction from the Hg-inducible biosensor with 5 µM GSH, 5 µM MB-OB3b, and 1 µM DMSA over 10 hours (Fig. 6.6 C).

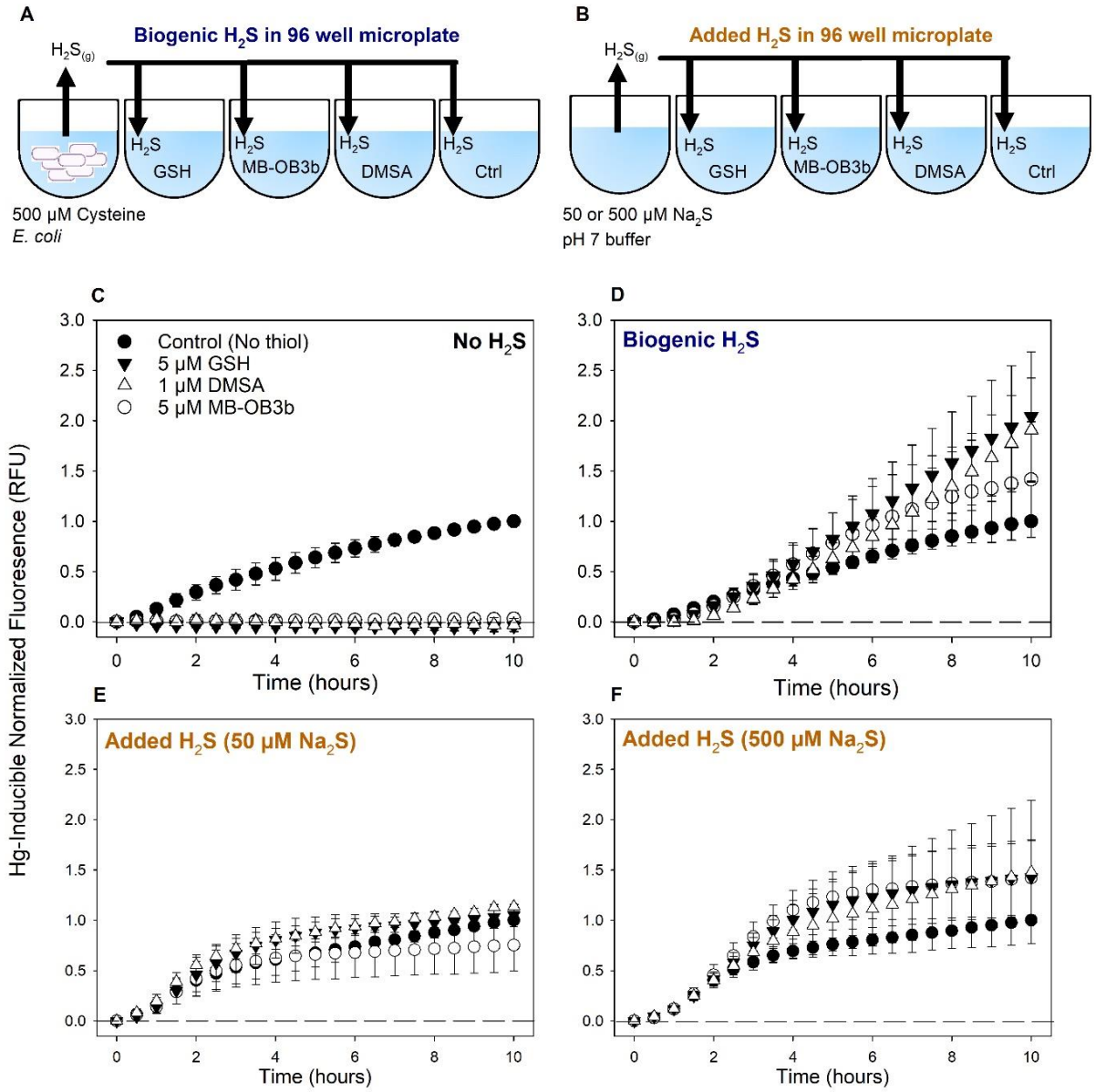

Figure 6.6: Diffusion of both biogenic and added H_2S affect Hg(II) bioavailability in the presence of refractory thiols. A) Biogenic H_2S was generated in the 96 well microplate by the Hg-inducible biosensor (*E. coli* NEB5α harboring the pUC57merR-Pp plasmid) in the presence 500 µM cysteine or **B)** added H_2S in the 96 well microplate was generated by the addition of Na_2S (50 or 500 µM) into exposure medium. Sulfide (H_2S) diffused out of the wells containing H_2S and into wells containing the refractory thiols glutathione (GSH), methanobactin from *M trichosporium* OB3b (MB-OB3b), DMSA, and the Control (CTRL) that had equilibrated with 2 nM Hg(II). ¼ of the wells in the plate were used to generate H_2S. Average Normalized Fluorescence measured as relative fluorescence units (RFU) ± SD over time (hours) from the Hg-Inducible biosensor with the addition of 5 µM GSH, 5 µM MB-OB3b, 1 µM DMSA or no thiol (Control). These experiments were performed when **C)** No H_2S, **D)** Biogenic H_2S, **E)** 50 µM H_2S or **F)** 500 µM H_2S came from ¼ of the plate wells. Fluorescence was normalized to the control (0 µM) at 10 hours for each biological replicate. (For **C**, n = 23 for the control, n = 12 for GSH, n = 13 for MB-OB3b and n = 7 for DMSA. For **D**, n= 12 for the control, n = 8 for GSH and MB-OB3b, and n = 4 for DMSA. For **E**, n= 8 for the control, GSH and MB-OB3b, and n = 4 for DMSA). [Hg] was set to 2 nM. The experiment was performed at 37 ˚C in an anaerobic exposure medium (pH 7).

In the presence of biogenic $H_2S_{(g)}$, every treatment produced a fluorescent response over 10 hours (Fig. 6.6 D). The onset of fluorescence induction in the presence of biogenic H_2S was also dependent on the nature of the thiolated ligand present. Significant induction ($\mu = 0$, $p < 0.05$) was observed after 2.5 minutes (first measurement time, 2.5 minute increments are not shown on graph) for the control and 5 µM GSH, 32.5 minutes for 5 µM MB-OB3b, and 77.5 minutes for 1 µM DMSA. The addition of 50 or 500 µM Na_2S led to faster induction than with biogenic $H_2S_{(g)}$ and also ligand-dependent (Fig. 6.6 E and F). At 50 µM Na_2S added, significant induction ($\mu = 0$, $p < 0.05$) began after 2.5 minutes for the control and 5 µM GSH, and after 5 minutes for 5 µM MB-OB3b and 1 µM DMSA. At 500 µM Na_2S added, significant induction ($\mu = 0$, $p < 0.05$) began after 2.5 minutes for the control, 5 µM GSH, and DMSA, and after 10 minutes for 5 µM MB-OB3b. We note that the induction from biogenic $H_2S_{(g)}$ was delayed, but more sustained than that from $H_2S_{(g)}$ amended as Na_2S; this is likely because cells need some time to metabolize Cys and will continue to produce H_2S long after all the pulse of $H_2S_{(g)}$ from Na_2S addition had dispersed out of solution (Fig D5). There is little lag between H_2S diffusion and a change in Hg bioavailability (2.5 – 10 min for H_2S from Na_2S amendments and 2.5 – 77.5 min for biogenic H_2S). We predict the biogenic H_2S concentrations required to facilitate bioavailability to be roughly <50-700 nM (Fig. D5) (assuming all the sulfide is in solution, evenly distributed throughout the plate). This lag time appears to be ligand-specific, but we lack evidence to evaluate whether it is associated with the strength of Hg-ligand binding. Ligand selectivity may hinder the process of Hg ligand exchange (thiol to sulfide). The addition of any amount of H_2S will completely alter Hg(II) speciation in the control wells in addition to GSH, MB-OB3b, or DMSA. The overlap in increasing Hg-inducible signal observed for all treatments

over the first few hours (Fig. 6.6 D, E, and F) may reflect the fact that Hg(II) speciation is likely the same across all treatments with the addition of H_2S.

Hg(II) bioavailability is likely the result of changes in speciation with sulfide. The exchange from thiols/DOM with sulfide will initially form metacinnabar (β-HgS) but can form more ordered α-HgS over time or under ideal conditions (Manceau et al., 2015; Poulin et al., 2017; Thomas et al., 2018). This formation of β-HgS is rapid and supported by X-ray Absorption Spectroscopy studies that showed the detection of Hg(II)-sulfide nanoparticles within an hour (Manceau et al., 2015; Poulin et al., 2017; Thomas et al., 2018). However, in the presence of far excess ligand (e.g., 1 mM cysteine), only α-HgS will only form (Thomas et al., 2018).

Several studies have shown the central role of sulfide in Hg methylation (Graham et al., 2012, 2013; Zhou et al., 2017; Mazrui et al., 2018; Thomas et al., 2018; An et al., 2019; Thomas et al., 2019; Zhang et al., 2020; Tian et al., 2021). Most recently, Tian *et al*. described the importance of Hg(II)-sulfides as a major driver of MeHg production (Tian et al., 2021). They showed that the crystalline structure formed during the early stage of HgS mineralization binds very favorably to natural ligands (e.g., DOM, and GSH) or cell surfaces, and specifically to zinc transporters (ZnuA). This binding to the cell surface greatly enhanced Hg(II) methylation. The aging of HgS nanoparticles changed their crystal structures, but not their sizes, which decreased Hg(II) binding and methylation. *E. coli s*trains, and especially the K-12 strain we use in our study, express the same zinc transporter (ZnuA) that Tian *et al.* (2021) deployed (The UniProt, 2021), and we posit that a similar binding/uptake sequence was observed with the biosensor, suggesting a common process across microbial species. In our study, we observed the effect of changing Hg(II) speciation from Hg(II)-thiols to Hg(II)-sulfides within a matter of seconds to

minutes. The formation of β-HgS formation may be a facilitating Hg(II) bioavailability. However, it is also possible aqueous Hg(II)-sulfides are also entering the cell through either active or passive transport.

The objective of this study was to investigate the influence of thiol ligand exchanges on Hg(II) bioavailability. We used model ligands to gain a mechanistic understanding of this process. Serendipitously, we reveal the importance of biogenic production of H_2S from ligand degradation and of its diffusion on Hg(II) bioavailability. This study demonstrates the profound and rapid role H_2S has, even far from its production site, on Hg(II) bioavailability, regardless of Hg(II) original speciation.

6.3.4 Environmental Implications

This study demonstrates the importance of including dissolved gaseous phases to better understand microbial Hg transformations. Until now, redox reactions appeared to be the main catalysts to possibly reset Hg speciation where methylation occurs (Grégoire and Poulain, 2018; Branfireun et al., 2020). Here we show how the diffusion of another gas, $H_2S_{(g)}$, can perform a similar process to resetting Hg(II) speciation in allowing microbes to access Hg. H_2S concentrations are normally buffered at equilibrium by ferruginous conditions that can deplete the concentration of H_2S to nM levels through the precipitation of iron(II)-sulfides (Shakeri Yekta et al., 2014) or through microbial metabolisms (Jørgensen et al., 2019). These buffers are not always present or entirely efficient where the slow abiotic oxidation of H_2S allows it to diffuse away from its production site. Thus, (micro)organisms producing H_2S may influence Hg(II) speciation in systems devoid of endogenous H_2S production, prompting us to reevaluate the possible interplay between S and Hg cycling and the conditions governing its bioavailability. When a metal is bound to DOM or present as a sulfide mineral, it is generally assumed that

microbes cannot access it. The transition between these two phases with transient $H_2S_{(g)}$ may play a critical role in allowing microbes to access metals that are often essential catalysts for anaerobic metabolisms.

Global planetary changes are expected to remobilize previously sequestered Hg into the environment and accelerate S cycling. The roughly 793 gigagrams (874,133 tons) of Hg accumulated in the arctic permafrosts for thousands of years is now being released through climate change (Schuster et al., 2018). Combined with novel sources of H_2S produced through progressive eutrophication of aquatic ecosystems (Hinckley et al., 2020) and the mass global emergence of oceanic dead zones (Diaz and Rosenberg, 2008), humans can facilitate new conditions for Hg methylation. Our mechanistic findings suggest that the bioavailability of both sequestered and remobilized Hg will be exacerbated with increased global H_2S production. This will lead to rapid degradation of aquatic habitat quality and the production of more MeHg, a potent neurotoxin affecting the health of humans and wildlife. Whenever possible, co-management of global biogeochemical cycles (here S and Hg) may offer a path to mitigate some of the consequences of these planetary changes.

6.5 Experimental Procedures

6.5.1 Experimental Design

Our study uses microbial biosensors to assess Hg(II) bioavailability as described in our previous (Stenzler et al., 2018). The Hg-biosensor, *Escherichia coli* NEB5α, emits a quantifiable fluorescent signal only when Hg(II) enters the cell. Our biosensor can detect trace levels of Hg(II) (2 nM used in this study) to implicate Hg(II) bioavailability mechanisms in environmentally relevant Hg(II) concenftrations. To address the bioavailability of a certain

Hg(II) species, we add a ligand to an exposure medium containing Hg(II) to form a Hg(II)-ligand complex as determined by thermodynamic modeling. We then combine these fluorescent readings with a constitutive biosensor, that always produces a fluorescent signal independent of Hg(II). Letting us distinguish Hg(II) bioavailability from the biosensor's viability (i.e, if the ligand is killing the biosensor, it would not produce any fluorescent signal and give us a false negative for Hg(II) bioavailability).

The biosensor in our study, *E.. coli* NEB5α, functions anaerobically using fumarate as the terminal electron acceptor. Ideally, we would use a Hg methylating microbe to assess bioavailability, but *E. coli* NEB5α serves the purpose of a Hg reporter system. In addition, unlike most Hg methylating microbes, *E. coli* will not generate H_2S as a byproduct of its general metabolism in the absence of excess cysteine (Thomas et al., 2018) or reduce Hg(II) (Grégoire et al., 2018). Therefore, we can completely dissociate gaseous phases of Hg(II) and H_2S from exogenous sources. Furthermore, fumarate reduction is a metabolism common among Hg(II) methylating microbes (sulfate and iron-reducing bacteria and methanogens) (Schaefer et al., 2011; Yu et al., 2013; Si et al., 2015) and indicative of sulfidic environments.

The purpose of this study was to address the hypothesis that Hg(II) bioavailability can be enhanced by ligand exchange. When Hg(II) is present as a non-bioavailable species, changing the speciation to a bioavailable one by adding a different ligand should enhance its bioavailability. To address this, this study was broken down into three objectives. **1)** We identified which Hg(II)-thiol species were bioavailable and which ones were not. **2)** Test the ligand exchange hypothesis. We equilibrated Hg(II) with thiols that inhibit Hg(II) bioavailability then added thiols that form bioavailable Hg(II) species. **3)** Determine how H_2S diffusion controls

Hg(II) bioavailability to the biosensor. We controlled for the diffusion of H_2S into isolated wells of a 96-well microplate containing non-bioavailable Hg(II) species.

6.5.2 Reagents and chemical preparation

Glutathione (GSH) was purchased from Fisher Scientific Acros Organics Dimercaptopropanol (BAL), Meso-2,3-DimercaptoSuccinic Acid (DMSA) and L-Penicillamine (Pen) were purchased from Alfa Aesar. L-cysteine-free (Cys) base was purchased from MP biomedicals. Methanobactin from *Methylosinus trichosporium* OB3b (MB-OB3b) was isolated and characterized as described in (Bandow et al., 2011). All solutions were prepared anaerobically and in Coy Vinyl Anaerobic chamber (98% N_2, 1.5% H_2), and solvents were $N_{2(g)}$ bubbled to make anaerobic. All thiols except DMSA and BAL were made in anaerobic Milli-Q water. DMSA and BAL were dissolved in anaerobic, 100 % ethanol. All solutions mentioned were stored at -20 °C.

6.5.3 Bacterial Strains and Growth

Biosensors growth and suspension assays were performed as described in (Stenzler et al., 2018). The method was modified to use fumarate as a terminal electron acceptor instead of nitrate. Two microbial biosensors based in *E. coli* NEB5α (DH5α derivative of K12 strain) were deployed; a Hg-Inducible (*E. coli* NEB5α harboring the pUC57merR-Pp plasmid) and a Constitutive biosensor (*E. coli* NEB5α harboring pUC19AH206-Pp plasmid). The expression of a flavin-based fluorescent protein on the plasmids are regulated by the transcriptional regulator of the *mer* operon (*merR*) or a constitutive promoter. All anaerobic manipulations of cell cultures were performed in a Coy Vinyl Anaerobic chamber (98% N_2, 1.5% H_2). Anaerobic growth was performed in anaerobic balch tubes.

For anaerobic growth for suspension assay, *E. coli* biosensors were grown at 37˚C and the plasmids were selected with 200 μg/ml ampicillin (unless otherwise stated), no antibiotic was used in the suspension assay. From -80°C cryostock, the biosensors were plated onto fumarate-GMM plates (SI: fumarate reduction plates for recipe) with 100 μg/ml ampicillin and grown anaerobically in anaerobic plate jars (this took a couple of days). A single colony was selected and grown in anaerobic GMM (SI: Growth Medium for recipe) overnight. The following day, cultures were transferred (20% inoculum) into fresh GMM and grown to an OD_{600} of 0.6. Cultures were resuspended twice in anaerobic exposure medium (SI: Exposure Medium for recipe) supplemented with 10 mM Na_2Fumarate (10,000 RCF for 90 seconds). The cells were ready for a 1/20 dilution into the biosensor suspension assay in exposure medium.

6.5.4 Determination of Biogenic H_2S

The biosensor was prepared as such for the biosensor exposure assay. Instead of performing a 1/20 dilution of the biosensor into the suspension assay, the biosensor was added to a crimped serum bottle with an exposure medium containing no added thiol (Control), 500 μM Pen, 500 μM Cys, 5 μM GSH, 5 μM MB-OB3b, 1 μM BAL, and 1 μM DMSA. The serum bottles were placed in a shaking incubator at 37°C. Every 30 minutes (Pen and Cys) or 1 hour (Control, GSH, MB-OB3B, BAL and DMSA), the 5 mL medium was withdrawn from the serum bottles, filtered through 0.2-micron filters, and the H_2S was operationally quantified as $[S^{2-}]$ (μM) but reported as $[H_2S]$ (μM). Serum bottles were used to limit the evasion of H_2S and get a more accurate quantification of H_2S production that could not be done in a microplate. H_2S was measured using the methylene blue protocol method (Hach protocol Method 8131, USEPA method 376.2, and Standard Method 4500-S2– D for wastewater).

6.5.5 Biosensor suspension assays

Suspension assays were performed inside a Coy Vinyl Anaerobic chamber (98% N_2, 1.5% H_2). Suspension assays were performed in exposure medium using 7 ml standard PTFE vials. Hg(II) was prepared as a 7.2 μM $HgSO_4$ stock in 0.2 M H_2SO_4. The concentration was determined using an MA-3000 Mercury Analyzer. Hg was diluted in exposure medium to a working concentration of 100 nM in PTFE vials before addition to the suspension assay. The added reagents (thiols) to be equilibrated with Hg(II) were added before Hg(II). Hg(II) was added to the exposure medium at a final concentration of 2 nM and set to equilibrate for 30 minutes. Biosensor cells (as prepared from "Bacterial Strains and Growth") were added last as a 1/20 dilution into the suspension assay. The suspension assay was transferred (200 μL) in triplicate from the PTFE vials to a 96 well microplate (Black, 96-Well Clear-Bottom Nonbinding Surface Microplates) and transferred to a Synergy HTX plate reader (present in the anaerobic chamber). All assays that contained Cys or sulfide were performed in their own 96 well microplate.

Non-bioavailable Hg(II) species were identified by increasing thiol concentrations until the fluorescence of the biosensors was inhibited. Each thiol concentration gradient was performed in a separate 96-well microplate. The Hg(II) species were then determined using thermodynamic modelling. In some instances, inhibition was not observed well beyond physiologically relevant conditions (up to 4 mM). Dimercaptopropanol (BAL) and dimercaptosuccinic acid (DMSA) used in this study are not naturally occurring in the environment but contain extremely high affinities for Hg(II) and have found use in chelation therapy. They were investigated in this study as we anticipate they would completely inhibit Hg(II) bioavailability for the first objective.

Several modifications were made to the assay were made to address ligand exchanges and the diffusion of H_2S. Hg(II) was pre-equilibrated with GSH/MB-OB3b before adding Pen/Cys when performing ligand exchanges. For assays that used biogenic H_2S; when performing 1/20 dilution of the biosensor into the suspension assay, it was also added to the exposure medium containing 500 µM Cys. The biosensor/Cys mixture was then added to wells A1-A12 and H1-H12 of the 96 well microplates (1 quarter of the wells) immediately before placing them into the plate reader. To generate added non-biogenic H_2S, Na_2S was diluted from a 200 mM stock to either 50 or 500 µM in exposure medium for added H_2S. Like biogenic H_2S, these were immediately added to 1 quarter of the wells before placing it into the plate reader.

Readings for fluorescence, luminescence, and OD_{600} were taken every 2.5 minutes for 10 hours at 37 ˚C. Shaking continuously between reads. Fluorescence was read for PpFbFp (Excitation: 440 nm, Emission: 500 nm**).** Hg-inducible and constitutive fluorescence were measured at 10 hours. Calculations were performed as described in (Stenzler et al., 2018). All values were then normalized to the no thiol treatment control (2 nM Hg(II)) at 10 hours for each biological replicate in the assay. Biological replicates here are independent cell cultures prepared from a single colony selected from fumarate reduction plates (See "Bacterial Strains and Growth").

6.5.6 Determination of H_2S migration in 96 well microplates

The 96 well microplate plate was divided into 4 sections (Fig. D4); Sulfide treatment (wells A1-A12 and H1-H12), Section 1 (Wells B1-B12 and C1-C12), Section 2 (Wells D1-D12 and E1-E12), and Section 3 (Wells F1-F12 and G1-G12). 200 uL of exposure medium were added to all the wells in Sections 1-3. This was done to obtain enough volume to perform sulfide analysis. Then a concentrated sulfide standard (200 mM Na_2S) was diluted in exposure medium (6 mL, to

avoid Na_2S altering the pH) to a concentration of 50 or 500 µM. These sulfide solutions were added to the sulfide treatment wells. A plate lid was immediately placed on the 96 well microplates and placed in the plate reader. The plate reader ran the biosensor protocol for 15, 30, and 60 minutes before sulfide concentrations in each section were measured. For 0 minutes, the 96 well microplates were not placed in the plate reader. Every measurement for each time point was measured in an independent experiment and performed in triplicate.

Once the experiment was completed, all four sections (4.8 mL per section) were quickly withdrawn and added to 15 mL polypropylene centrifuge tubes containing 5mL of zinc trap solution (1 mM zinc acetate, 1 mM nitrilotriacetic acid, and 5 mM NaOH). Sulfide was measured using the methylene blue protocol method (Hach protocol Method 8131, USEPA method 376.2, and Standard Method 4500-S2– D for wastewater). The results for the sulfide concentration (µM $[H_2S]$/well) for each section individually are reported in Figure D4 (A and B). The sulfide concentration between sections 1-3 appeared to be homogenous, and therefore the average of the three sections are reported in the results as "exposure wells." The limit of detection of H_2S per well to account for the 2.08x dilution required to perform the sulfide measurements was (0.34 µM $[H_2S]$]/well).

6.5.7 Thermodynamic Modelling

All thermodynamic modeling was performed using PHREEQC (Parkhurst, 2013). All equilibrium constants used for calculations can be found in Table D3. All modeling was performed at 25 ˚C, in exposure medium (pH 7), with 2 nM Hg(II). Lack of thermodynamic constants to correct for temperature would make modeling with Hg(II) not be representative of 37˚C in the biosensor assay. Constants for thiols were only obtained from (Liem-Nguyen et al., 2017b; Song et al., 2018; Song et al., 2020) for internal consistency. These studies improve on

the methodology to refine difficult to measure Hg(II)-thiol stability constants by combining liquid chromatography–inductively coupled plasma mass spectrometry, EXAFS spectroscopy measurements, and Density functional theory calculations. These studies also take into account ligand exchanges, single thiol coordinated complexes (Hg(II)-SR), and heterocomplexes (R^1S-Hg-SR^2). The single thiol coordinate complexes represented in the models include coordination with one N/O groups on the same thiol molecule (Song et al., 2018). The stability constants for heterocomplexes were determined to be at least 1.5 log units smaller than the average stability constant for the corresponding two thiol coordinated complexes ($Hg(SR)_2$)(Liem-Nguyen et al., 2017b). Values for Hg(II)-sulfide speciation and metacinnabar (β-HgS(s)) precipitation were obtained from (Drott et al., 2013).

Models were made to include thiol complexation of Hg(II) on a representative cell membrane. All values are reported in Table D3. While no specific thiol site concentrations are measured specifically for *E. coli* used in our study, much work has gone into identifying modeling parameters. Surface thiol concentrations have been determined in *Bacillus*, *Shewanella*, *Pseudomonas*, *Geobacter*, and *Desulfovirbio sp.* (Glazyrina et al., 2010; Yu et al., 2014; Mishra et al., 2017; Song et al., 2020; Thomas et al., 2020). Roughly 5% of the total membrane-bound thiols are close enough to form two thiol coordinate bonds with Hg(II) (Mishra et al., 2017). This coordination has been demonstrated in *E. coli* using X-ray absorption near edge structure (XANES) (Thomas et al., 2014). The total membrane thiol sites recommended for the model are ($Mem\text{-}RS_{tot}$ = 380 ± 50 μmol $g^{-1}C$) (Mishra et al., 2017). Based on the standard conversion from *E. coli* OD_{600} to cell number ($1OD_{600}$ = 8 x 10^8 cells/ml) and *E. coli* dry weight ($3x10^{-13}$g/Cell). Also, assuming 50% TOC factor for dry weight (Mishra et al., 2017). ($0.6OD_{600}$ x 8x 10^8)cells/mL x ($3x10^{-13}$ g/Cell) (dry weight) x 0.5 (TOC content factor) x (380 μmol

thiols)/(gTOC) x 1/20 (dilution factor into assay) x 1000mL/L = 1.37 μM thiols in the assay. 5% (68nM) are capable of forming two thiol coordinated complexes ($Hg(Mem\text{-}RS)_2$) with other membrane functional groups ($Mem\text{-}R^{II}S^-$). All thiols were capable of forming two thiol coordinate complexes between the membrane and a ligand in solution (Hg(Mem-RS)(RS) or a single thiol coordinate complexes between a membrane thiol and a neighboring O/N functionality on the same molecule (Hg(Mem-RSRO). No thermodynamic data was available to form HgMem-RS(Pen)/HgMem-RS(GSH) complexes, and the values were inferred as Cys. These three low molecular weight thiols have similar stability constants with Hg(II) but vary over an order of magnitude ($Hg^{2+} + 2RS^- = Hg(RS)_2$, log k= 38.8, 37.5, 36.9 for GSH, Cys, Pen). While using only the constant for Cys will skew the model. Excluding them from the model will be less realistic since these species are likely to form (Song et al., 2018; Song et al., 2020).

Thermodynamic models were made to evaluate Hg(II) speciation over the gradient of thiols used in the biosensor assays. Models were made with and without the addition of thiols on the membrane. A mixture of $Hg(OH)_2$ and $Hg(NH_3)_x^{2+}$ species would form at 25˚C, but at 37˚C this would shift to ≈98% $Hg(OH)_2$. To simplify these models, $Hg(OH)_2$ and $Hg(NH_3)_x^{2+}$ species were displayed as $Hg(OH)_2$ only.

Thermodynamic models were made to demonstrate Hg(II) speciation shift by performing ligand exchanges. The first set of exchanges were with Cys and Pen to 5 μM MB-OB3b and GSH. Only GSH was modeled with a representative cell membrane. The second set of ligand exchange was with H_2S and only in systems that were determined to contain H_2S; 5 μM MB-OB3b, 5 μM GSH, 50 μM Cys, and 500 μM Cys. Interactions with the membrane were excluded from these models due to limited thermodynamic data between Hg(II)-sulfides and the membrane. Also, we modeled under the assumption that these species were not exchanging with

the membrane. There were no substantial changes (at most, 1%) in speciation distributions in systems with 50 µM and 500 µM Cys with the addition of 5 µM GSH/MB-OB3b, therefore only models of 50 µM Cys and 500 µM Cys are shown. We did not enable precipitation of β-HgS(s) in the models, but its formation is indicated by the Saturation Index (SI). When the saturation index is above 0, the mineral is above saturation and should precipitate.

6.5.8 Statistical Analyses

To assess if Hg(II) bioavailability was completely inhibited by any variable added to the exposure medium, the normalized fluorescence needed to be equal to or less than zero. A two-tailed, one-sample t-test on Normalized Fluorescence (%) was performed (H_0, $\mu = 0$, with a confidence interval of 95%). To determine the time of significant normalized fluorescent induction, normalized fluorescence needed greater than zero. A one-tailed, one-sample t-test on Normalized Fluorescence (%) was performed on every measured time point (2.5 min intervals) (H_0, $\mu = 0$, with a confidence interval of 95%). The time point was reported if every time point after was also significant. Changes in Hg-bioavailability relative to the control were determined with a two-tailed, one-sample t-test on Normalized Fluorescence (%) (H_0, $\mu = 1$, with a confidence interval of 95%). Statistical Analyses were performed in Microsoft Excel.

6.6 References

G.A. Adediran, V. Liem-Nguyen, Y. Song, J.K. Schaefer, U. Skyllberg, and E. Björn (2019) Microbial Biosynthesis of Thiol Compounds: Implications for Speciation, Cellular Uptake, and Methylation of Hg(II). *Environmental Science & Technology* **53**: 8187-8196.

J. An, L. Zhang, X. Lu, D.A. Pelletier, E.M. Pierce, A. Johs et al. (2019) Mercury Uptake by Desulfovibrio desulfuricans ND132: Passive or Active? *Environmental Science & Technology* **53**: 6264-6272.

P.W. Balls, and P.S. Liss (1983) Exchange of H2S between water and air. *Atmospheric Environment (1967)* **17**: 735-742.

N.L. Bandow, W.H. Gallagher, L. Behling, D.W. Choi, J.D. Semrau, S.C. Hartsel et al. (2011) Isolation of Methanobactin from the Spent Media of Methane-Oxidizing Bacteria. *MethEnzymol* **495**: 259-269.

B.S. Baral, N.L. Bandow, A. Vorobev, B.C. Freemeier, B.H. Bergman, T.J. Herdendorf et al. (2014) Mercury binding by methanobactin from Methylocystis strain SB2. *Journal of Inorganic Biochemistry* **141**: 161-169.

F. Beulig, H. Røy, S.E. McGlynn, and B.B. Jørgensen (2019) Cryptic CH4 cycling in the sulfate–methane transition of marine sediments apparently mediated by ANME-1 archaea. *The ISME Journal* **13**: 250-262.

G. Bjørklund, G. Crisponi, V.M. Nurchi, R. Cappai, A. Buha Djordjevic, and J. Aaseth (2019) A Review on Coordination Properties of Thiol-Containing Chelating Agents Towards Mercury, Cadmium, and Lead. *Molecules* **24**.

B.A. Branfireun, C. Cosio, A.J. Poulain, G. Riise, and A.G. Bravo (2020) Mercury cycling in freshwater systems - An updated conceptual model. *Science of The Total Environment* **745**: 140906.

A.G. Bravo, C. Cosio, D. Amouroux, J. Zopfi, P.-A. Chevalley, J.E. Spangenberg et al. (2014) Extremely elevated methyl mercury levels in water, sediment and organisms in a Romanian reservoir affected by release of mercury from a chlor-alkali plant. *Water Research* **49**: 391-405.

S. Carrasco-Gil, A. Alvarez-Fernández, J. Sobrino-Plata, R. Millán, R.O. Carpena-Ruiz, D.L. Leduc et al. (2011) Complexation of Hg with phytochelatins is important for plant Hg tolerance. *Plant Cell Environ* **34**: 778-791.

S.A. Chiasson-Gould, J.M. Blais, and A.J. Poulain (2014) Dissolved Organic Matter Kinetically Controls Mercury Bioavailability to Bacteria. *Environmental Science & Technology* **48**: 3153-3161.

U. Choi, and C.-R. Lee (2019) Distinct Roles of Outer Membrane Porins in Antibiotic Resistance and Membrane Integrity in Escherichia coli. *Frontiers in Microbiology* **10**.

M.J. Colombo, J. Ha, J.R. Reinfelder, T. Barkay, and N. Yee (2013) Anaerobic oxidation of Hg(0) and methylmercury formation by Desulfovibrio desulfuricans ND132. *Geochimica et Cosmochimica Acta* **112**: 166-177.

A. Deonarine, and H. Hsu-Kim (2009) Precipitation of Mercuric Sulfide Nanoparticles in NOM-Containing Water: Implications for the Natural Environment. *Environmental Science & Technology* **43**: 2368-2373.

R.J. Diaz, and R. Rosenberg (2008) Spreading Dead Zones and Consequences for Marine Ecosystems. *Science* **321**: 926.

P. Dranguet, V.I. Slaveykova, and S. Le Faucheur (2018) *Kinetics of mercury accumulation by freshwater biofilms*.

C.T. Driscoll, R.P. Mason, H.M. Chan, D.J. Jacob, and N. Pirrone (2013) Mercury as a global pollutant: sources, pathways, and effects. *Environmental science & technology* **47**: 4967-4983.

A. Drott, E. Bjorn, S. Bouchet, and U. Skyllberg (2013) Refining thermodynamic constants for mercury (II)-sulfides in equilibrium with metacinnabar at sub-micromolar aqueous sulfide concentrations. *Environmental science & technology* **47**: 4197-4203.

S. Dunham-Cheatham, B. Mishra, S. Myneni, and J.B. Fein (2015) The effect of natural organic matter on the adsorption of mercury to bacterial cells. *Geochimica et Cosmochimica Acta* **150**: 1-10.

M. Enescu, K.L. Nagy, and A. Manceau (2016) Nucleation of mercury sulfide by dealkylation. *Sci Rep* **6**: 39359.

J.B. Fein, Q. Yu, J. Nam, and N. Yee (2019) Bacterial cell envelope and extracellular sulfhydryl binding s: Their roles in metal binding and bioavailability. *Chemical Geology*.

J. Glazyrina, E.M. Materne, T. Dreher, D. Storm, S. Junne, T. Adams et al. (2010) High cell density cultivation and recombinant protein production with Escherichia coli in a rocking-motion-type bioreactor. *Microb Cell Fact* **9**: 42.

A.M. Graham, G.R. Aiken, and C.C. Gilmour (2012) Dissolved Organic Matter Enhances Microbial Mercury Methylation Under Sulfidic Conditions. *Environmental Science & Technology* **46**: 2715-2723.

A.M. Graham, G.R. Aiken, and C.C. Gilmour (2013) Effect of Dissolved Organic Matter Source and Character on Microbial Hg Methylation in Hg–S–DOM Solutions. *Environmental Science & Technology* **47**: 5746-5754.

D.S. Grégoire, and A.J. Poulain (2018) Shining light on recent advances in microbial mercury cycling. *FACETS* **3**: 858-879.

D.S. Grégoire, N.C. Lavoie, and A.J. Poulain (2018) Heliobacteria Reveal Fermentation As a Key Pathway for Mercury Reduction in Anoxic Environments. *Environmental Science & Technology* **52**: 4145-4153.

E.-L.S. Hinckley, J.T. Crawford, H. Fakhraei, and C.T. Driscoll (2020) A shift in sulfur-cycle manipulation from atmospheric emissions to agricultural additions. *Nature Geoscience* **13**: 597-604.

H. Hsu-Kim, K.H. Kucharzyk, T. Zhang, and M.A. Deshusses (2013) Mechanisms regulating mercury bioavailability for methylating microorganisms in the aquatic environment: a critical review. *Environ Sci Technol* **47**: 2441-2456.

H. Hu, H. Lin, W. Zheng, B. Rao, X. Feng, L. Liang et al. (2013a) Mercury reduction and cell-surface adsorption by geobacter sulfurreducens PCA. *Environmental Science and Technology* **47**: 10922-10930.

H. Hu, H. Lin, W. Zheng, S.J. Tomanicek, A. Johs, X. Feng et al. (2013b) Oxidation and methylation of dissolved elemental mercury by anaerobic bacteria. *Nature Geoscience* **6**: 751-754.

K. Huynh, V. Liem-Nguyen, C. Feng, R. Lindberg, and E. Björn (2020) Quantification of total concentration of thiol functional groups in environmental samples by titration with monobromo(trimethylammonio)bimane and determination with tandem mass spectrometry. *Talanta* **218**: 121109.

B.B. Jørgensen, A.J. Findlay, and A. Pellerin (2019) The Biogeochemical Sulfur Cycle of Marine Sediments. *Frontiers in Microbiology* **10**.

B. Kalidass, M.F. Ul-Haque, B.S. Baral, A.A. DiSpirito, and J.D. Semrau (2015) Competition between metals for binding to methanobactin enables expression of soluble methane monooxygenase in the presence of copper. *Applied and environmental microbiology* **81**: 1024-1031.

S.K. Kawakami, M. Gledhill, and E.P. Achterberg (2006) Production of phytochelatins and glutathione by marine phytoplankton in response to metal stress 1. *Journal of phycology* **42**: 975-989.

M. Labrenz, G.K. Druschel, T. Thomsen-Ebert, B. Gilbert, S.A. Welch, K.M. Kemner et al. (2000) Formation of Sphalerite (ZnS) Deposits in Natural Biofilms of Sulfate-Reducing Bacteria. *Science* **290**: 1744.

M. Leclerc, D. Planas, and M. Amyot (2015) Relationship between Extracellular Low-Molecular-Weight Thiols and Mercury Species in Natural Lake Periphytic Biofilms. *Environ Sci Technol* **49**: 7709-7716.

I. Lehnherr, V.L. St. Louis, H. Hintelmann, and J.L. Kirk (2011) Methylation of inorganic mercury in polar marine waters. *Nature Geoscience* **4**: 298-302.

V. Liem-Nguyen, U. Skyllberg, and E. Björn (2017a) Thermodynamic Modeling of the Solubility and Chemical Speciation of Mercury and Methylmercury Driven by Organic Thiols and Micromolar Sulfide Concentrations in Boreal Wetland Soils. *Environmental Science & Technology* **51**: 3678-3686.

V. Liem-Nguyen, U. Skyllberg, K. Nam, and E. Björn (2017b) Thermodynamic stability of mercury(II) complexes formed with environmentally relevant low-molecular-mass thiols studied by competing ligand exchange and density functional theory. *Environmental Chemistry* **14**: 243-253.

H. Lin, X. Lu, L. Liang, and B. Gu (2015) Cysteine Inhibits Mercury Methylation by Geobacter sulfurreducens PCA Mutant ΔomcBESTZ. *Environmental Science & Technology Letters* **2**: 144-148.

Y.-R. Liu, X. Lu, L. Zhao, J. An, J.-Z. He, E.M. Pierce et al. (2016) Effects of Cellular Sorption on Mercury Bioavailability and Methylmercury Production by Desulfovibrio desulfuricans ND132. *Environmental Science & Technology* **50**: 13335-13341.

A. Manceau, C. Lemouchi, M. Enescu, A.-C. Gaillot, M. Lanson, V. Magnin et al. (2015) Formation of Mercury Sulfide from Hg(II)–Thiolate Complexes in Natural Organic Matter. *Environmental Science & Technology* **49**: 9787-9796.

V. Mangal, N.L. Stock, and C. Guéguen (2016) Molecular characterization of phytoplankton dissolved organic matter (DOM) and sulfur components using high resolution Orbitrap mass spectrometry. *Anal Bioanal Chem* **408**: 1891-1900.

Nashaat M. Mazrui, E. Seelen, C.K. King'ondu, S. Thota, J. Awino, J. Rouge et al. (2018) The precipitation, growth and stability of mercury sulfide nanoparticles formed in the presence of marine dissolved organic matter. *Environmental Science: Processes & Impacts* **20**: 642-656.

J.V. Mills, G. Antler, and A.V. Turchyn (2016) Geochemical evidence for cryptic sulfur cycling in salt marsh sediments. *Earth and Planetary Science Letters* **453**: 23-32.

B. Mishra, E. Shoenfelt, Q. Yu, N. Yee, J.B. Fein, and S.C.B. Myneni (2017) Stoichiometry of mercury-thiol complexes on bacterial cell envelopes. *Chemical Geology*.

U. Ndu, R.P. Mason, H. Zhang, S. Lin, and P.T. Visscher (2012) Effect of inorganic and organic ligands on the bioavailability of methylmercury as determined by using a mer-lux bioreporter. *Applied and Environmental Microbiology* **78**: 7276-7282.

U. Ndu, T. Barkay, R.P. Mason, A.T. Schartup, R. Al-Farawati, J. Liu, and J.R. Reinfelder (2015) The use of a mercury biosensor to evaluate the bioavailability of mercury-thiol complexes and mechanisms of mercury uptake in bacteria. *PLoS One* **10**: e0138333.

D. Obrist, J.L. Kirk, L. Zhang, E.M. Sunderland, M. Jiskra, and N.E. Selin (2018) A review of global environmental mercury processes in response to human and natural perturbations: Changes of emissions, climate, and land use. *Ambio* **47**: 116-140.

T.A. Olsen, C.C. Brandt, and S.C. Brooks (2016) Periphyton biofilms influence net methylmercury production in an industrially contaminated system. *Environmental Science & Technology* **50**: 10843-10850.

V.L. Ortiz, R.P. Mason, and J.E. Ward (2015) An examination of the factors influencing mercury and methylmercury particulate distributions, methylation and demethylation rates in laboratory-generated marine snow. *Mar Chem* **177**: 753-762.

D.L.a. Parkhurst (2013) *Description of input and examples for PHREEQC version 3--a computer program for speciation, batch-reaction, one-dimensional transport, and inverse geochemical calculations*: Reston, Virginia : U.S. Department of the Interior, U.S. Geological Survey, 2013.

M. Pester, K.-H. Knorr, M. Friedrich, M. Wagner, and A. Loy (2012) Sulfate-reducing microorganisms in wetlands – fameless actors in carbon cycling and climate change. *Frontiers in Microbiology* **3**.

A.L.-T. Pham, A. Morris, T. Zhang, J. Ticknor, C. Levard, and H. Hsu-Kim (2014) Precipitation of nanoscale mercuric sulfides in the presence of natural organic matter: Structural properties, aggregation, and biotransformation. *Geochimica et Cosmochimica Acta* **133**: 204-215.

M. Podar, C.C. Gilmour, C.C. Brandt, A. Soren, S.D. Brown, B.R. Crable et al. (2015) Global prevalence and distribution of genes and microorganisms involved in mercury methylation. *Science Advances* **1**: e1500675.

B.A. Poulin, C.A. Gerbig, C.S. Kim, J.P. Stegemeier, J.N. Ryan, and G.R. Aiken (2017) Effects of Sulfide Concentration and Dissolved Organic Matter Characteristics on the Structure of Nanocolloidal Metacinnabar. *Environmental Science & Technology* **51**: 13133-13142.

M.R. Raven, R.G. Keil, and S.M. Webb (2021) Microbial sulfate reduction and organic sulfur formation in sinking marine particles. *Science* **371**: 178.

O. Regnell, and C.J. Watras (2019) Microbial Mercury Methylation in Aquatic Environments: A Critical Review of Published Field and Laboratory Studies. *Environmental Science & Technology* **53**: 4-19.

J.K. Schaefer, and F.M.M. Morel (2009) High methylation rates of mercury bound to cysteine by Geobacter sulfurreducens. *Nature Geosci* **2**: 123-126.

J.K. Schaefer, A. Szczuka, and F.M.M. Morel (2014) Effect of Divalent Metals on Hg(II) Uptake and Methylation by Bacteria. *Environmental Science & Technology* **48**: 3007-3013.

J.K. Schaefer, S.S. Rocks, W. Zheng, L. Liang, B. Gu, and F.M.M. Morel (2011) Active transport, substrate specificity, and methylation of Hg(II) in anaerobic bacteria. *Proceedings of the National Academy of Sciences* **108**: 8714-8719.

P.F. Schuster, K.M. Schaefer, G.R. Aiken, R.C. Antweiler, J.F. Dewild, J.D. Gryziec et al. (2018) Permafrost Stores a Globally Significant Amount of Mercury. *Geophysical Research Letters* **45**: 1463-1471.

R.P. Schwarzenbach, Gschwend, P.M. and Imboden, D.M. (2002) *Air–Water Exchange. In Environmental Organic Chemistry (eds R.P. Schwarzenbach, P.M. Gschwend and D.M. Imboden). https://doi.org/10.1002/0471649643.ch20*.

J.D. Semrau, and B. Gu (2020) Final Technical Report: Methanotrophic-Mediated Methylmercury Transformation: Characterization of Products, Mechanism, and Environmental Significance. In: University of Michigan.

S. Shakeri Yekta, B.H. Svensson, A. Björn, and U. Skyllberg (2014) Thermodynamic modeling of iron and trace metal solubility and speciation under sulfidic and ferruginous conditions in full scale continuous stirred tank biogas reactors. *Applied Geochemistry* **47**: 61-73.

Y. Si, Y. Zou, X. Liu, X. Si, and J. Mao (2015) Mercury methylation coupled to iron reduction by dissimilatory iron-reducing bacteria. *Chemosphere* **122**: 206-212.

Y. Song, T. Jiang, V. Liem-Nguyen, T. Sparrman, E. Björn, and U. Skyllberg (2018) Thermodynamics of Hg(II) Bonding to Thiol Groups in Suwannee River Natural Organic Matter Resolved by Competitive Ligand Exchange, Hg LIII-Edge EXAFS and 1H NMR Spectroscopy. *Environmental Science & Technology* **52**: 8292-8301.

Y. Song, G.A. Adediran, T. Jiang, S. Hayama, E. Björn, and U. Skyllberg (2020) Toward an Internally Consistent Model for Hg(II) Chemical Speciation Calculations in Bacterium–Natural Organic Matter–Low Molecular Mass Thiol Systems. *Environmental Science & Technology* **54**: 8094-8103.

B. Stenzler, J. Gaudet, and A.J. Poulain (2018) An Anaerobic Biosensor Assay for the Detection of Mercury and Cadmium. *JoVE*: e58324.

E.M. Sunderland, D.P. Krabbenhoft, J.W. Moreau, S.A. Strode, and W.M. Landing (2009) Mercury sources, distribution, and bioavailability in the North Pacific Ocean: Insights from data and models. *Global Biogeochemical Cycles* **23**.

O. Lahav, A. Sagiv, and E. Friedler (2006) A different approach for predicting H2S(g) emission rates in gravity sewers. *Water Research* **40**: 259-266.

A. Szczuka, F.M.M. Morel, and J.K. Schaefer (2015) Effect of Thiols, Zinc, and Redox Conditions on Hg Uptake in Shewanella oneidensis. *Environmental Science and Technology* **49**: 7432-7438.

Z. Tang, F. Fan, S. Deng, and D. Wang (2020) Mercury in rice paddy fields and how does some agricultural activities affect the translocation and transformation of mercury - A critical review. *Ecotoxicology and Environmental Safety* **202**: 110950.

C. The UniProt (2021) UniProt: the universal protein knowledgebase in 2021. *Nucleic Acids Research* **49**: D480-D489.

S.A. Thomas, T. Tong, and J.-F. Gaillard (2014) Hg(ii) bacterial biouptake: the role of anthropogenic and biogenic ligands present in solution and spectroscopic evidence of ligand exchange reactions at the cell surface. *Metallomics* **6**: 2213-2222.

S.A. Thomas, B. Mishra, and S.C.B. Myneni (2020) Cellular Mercury Coordination Environment, and Not Cell Surface Ligands, Influence Bacterial Methylmercury Production. *Environmental Science & Technology* **54**: 3960-3968.

S.A. Thomas, K.E. Rodby, E.W. Roth, J. Wu, and J.F. Gaillard (2018) Spectroscopic and Microscopic Evidence of Biomediated HgS Species Formation from Hg(II)-Cysteine Complexes: Implications for Hg(II) Bioavailability. *Environ Sci Technol* **52**: 10030-10039.

S.A. Thomas, P. Catty, J.-L. Hazemann, I. Michaud-Soret, and J.-F. Gaillard (2019) The role of cysteine and sulfide in the interplay between microbial Hg(ii) uptake and sulfur metabolism†. *Metallomics* **11**: 1219-1229.

L. Tian, W. Guan, Y. Ji, X. He, W. Chen, P.J.J. Alvarez, and T. Zhang (2021) Microbial methylation potential of mercury sulfide particles dictated by surface structure. *Nature Geoscience* **14**: 409-416.

A. Vorobev, S. Jagadevan, S. Baral Bipin, A. DiSpirito Alan, C. Freemeier Brittani, H. Bergman Brandt et al. (2013) Detoxification of Mercury by Methanobactin from Methylosinus trichosporium OB3b. *Applied and Environmental Microbiology* **79**: 5918-5926.

X. Yin, L. Wang, L. Zhang, H. Chen, X. Liang, X. Lu et al. (2020) Synergistic Effects of a Chalkophore, Methanobactin, on Microbial Methylation of Mercury. *Applied and Environmental Microbiology* **86**: e00122-00120.

Q. Yu, J. Szymanowski, S.C.B. Myneni, and J.B. Fein (2014) Characterization of sulfhydryl sites within bacterial cell envelopes using selective site-blocking and potentiometric titrations. *Chemical Geology* **373**: 50-58.

R.-Q. Yu, J.R. Reinfelder, M.E. Hines, and T. Barkay (2013) Mercury Methylation by the Methanogen Methanospirillum hungatei. *Applied and Environmental Microbiology* **79**: 6325-6330.

Z. Zhang, R. Si, J. Lv, Y. Ji, W. Chen, W. Guan et al. (2020) Effects of Extracellular Polymeric Substances on the Formation and Methylation of Mercury Sulfide Nanoparticles. *Environmental Science & Technology* **54**: 8061-8071.

L. Zhao, H. Chen, X. Lu, H. Lin, G.A. Christensen, and E.M. Pierce (2017) Contrasting Effects of Dissolved Organic Matter on Mercury Methylation by Geobacter sulfurreducens PCA and Desulfovibrio desulfuricans ND132. **51**: 10468-10475.

J. Zhou, M.D. Smith, S.J. Cooper, X. Cheng, J.C. Smith, and J.M. Parks (2017) Modeling of the Passive Permeation of Mercury and Methylmercury Complexes Through a Bacterial Cytoplasmic Membrane. *Environmental Science & Technology* **51**: 10595-10604.

6.7 Acknowledgments

We would like to thank Mija Azdajic for providing technical assistance and other members of

the Poulain Lab at the University of Ottawa for providing outstanding moral fiber.

Funding:

This work was funded by an NSERC discovery grant, an Early Researcher Award from the Province of Ontario, and an NSERC Accelerator Grant funding to AJP.

Author contributions:

A.J.P. supervised the project. B.R.S., and A.J.P. designed the research and methodologies. J.D.S., and A.A.D. provided methanobactin samples and, together with R.Z., contributed to the experimental design. B.R.S performed the experiments. R.Z calibrated the biosensor to function on fumarate reduction. B.R.S and A.J.P. performed analyses on the data. B.R.S and A.J.P wrote the paper with contributions from J.D.S., A.A.D.

Competing interests:

The authors declare that they have no known competing interests.

Chapter 7: Pathways in metal acquisition affect Hg bioavailability

Authors

Benjamin R. Stenzler[1], Rui Zhang[1], and Alexandre J. Poulain[1]*†

Affiliations

[1]Biology Department, University of Ottawa, 30 Marie Curie, Ottawa, ON K1N 6N5, Canada

*Corresponding author. Email: apoulain@uottawa.ca

*Corresponding author. Email: apoulain@uottawa.ca

N.B. Supporting information for this chapter can be found in **Appendix D and E**

7.1 Abstract

Methylmercury (MeHg) is a potent neurotoxin that biomagnifies through food webs and which production depends on anaerobic microbial uptake of inorganic mercury (Hg) species. Hg bioavailability is an essential step in forming toxic MeHg but accessing Hg is not always possible. Hg often gets sequestered in insoluble iron oxides, making it inaccessible to organisms. The insolubility of iron also represents a limitation for most organisms because it is an essential nutrient, which bacteria, fungi, and plants compete for. Using siderophores, microbes solubilize iron, making it accessible and bioavailable. The dissolution of these oxides will also affect the fate of the Hg. Siderophores are not only specific to iron but can form complexes with other metals as well. Siderophores are ubiquitous, yet very little is known on how they interact with Hg. In this study, using a whole-cell biosensor and siderophores from several microbial genera, we evaluated how siderophores influenced Hg bioavailability. The siderophores that affected Hg^{II} bioavailability are produced predominantly by Enterobacteriaceae, *Pseudomonas*, and *Streptomyces.* Between 1 and 5000 nM of each siderophore had a unique and dynamic effect on Hg bioavailability. Our study indicates that microbes can inadvertently influence Hg bioavailability to each other by processes related to iron acquisition.

7.2 Introduction

Mercury (Hg) bioavailability to Hg methylating microbes is the first step in the methylation process that forms methylmercury (MeHg) (*1*). MeHg will biomagnify through food webs (*2*) and is a major concern in food staples such as fish (*3*) and rice (*4*). In the environment, Hg methylation occurs in sulfate and iron-reducing bacteria and methanogens (*5*). Divalent mercury

(Hg(II)) has a very high affinity for reduced sulfur species (e.g., thiols and sulfide). Hg(II) is often found as these species (e.g., $Hg(cysteine)_2$, $Hg(glutathione)_2$, HgS or $Hg(HS)_2$) in the environment (*6-12*). These observations are notable in sulfidic conditions or reducing environments in sediments conducive to sulfate reduction or methanogenesis where these species are found (*1, 10*). Still, very little is known of Hg(II) speciation under conditions dominated by other electron acceptors, such as Fe(III).

Iron reducing-microbes are also critical Hg methylating microbes in the environment. The presence of iron(III) oxides has been shown to enhance Hg methylation rates by stimulating microbes using Fe(III) as a terminal electron acceptor (*13, 14*). The role of colloidal oxide minerals on Hg methylation is complex; not only are they used in metabolism, but Hg(II) is readily sorbed and associated with the mineral structures. These compounds have very large surface areas and can extensively sorb and sequester Hg, often in environments depleted of dissolved organic matter (*14-19*).

Several mechanisms have been associated with the release Hg(II) from these colloidal minerals to be accessible to iron reducing-microbes (IRBs); reductive dissolution of the mineral or Hg(II) reduction (*14*, *20-22*). However, most organisms in the environment have also developed unique strategies using siderophores to solubilize these minerals and acquire the iron (Fe) that is otherwise not accessible or available. Almost every microbe, plant, or fungi either secretes siderophores or contains transporters for them. Siderophores are not unique to accessing iron but also can mobilize other metals and are frequently referred to as “metallophores.” Siderophores have a wide range of structures and functions beyond accessing metals, including quorum sensing, metal sequestration, or acting as reducing agents. The importance of

siderophores on microbes' physiology has been covered extensively (*23-27*). However, few studies have addressed how they interact with Hg or affect its bioavailability.

Whereas siderophores have a high affinity towards iron, they can also form complexes with other metals that can possibly be accessed through siderophore-specific pathways (*28, 29*). Still, Hg(II) complexation with siderophores is not usually considered. Hg(II) has been demonstrated to be accidentally transported into methanotrophs through pathways associated with copper uptake, namely via a methanobactin (MB) transport system. MB is a chalkophore produced by some methanotrophs to scavenge copper in the environment, and the MB-copper complex is transported into the cell (*30*). Further studies have demonstrated how MB can influence Hg(II) bioavailability to Hg methylators (*31*). There are many different siderophore transport pathways that microbes use to scavenge metals. It is not known how many siderophores can interact with Hg(II) or how they affect bioavailability.

The general model describing Hg bioavailability to microbes involves either active transport or passive diffusion (*1, 10*). Active transport of Hg(II) into a microbial cell occurs through non-specific metal transporters on the inner membrane (Zn or Mn transporters) (*32-36*). This process happens between a ligand-binding Hg(II) in solution and the transporter (*33, 37*). It is also possible for passive diffusion of Hg across a membrane when present as reduced Hg^0 (*38-41*) or small, neutrally charged freshly formed Hg(II)-sulfide species (*42-50*).

We first used a whole-cell Hg-biosensor hosted in a *E. coli* chassis to investigate the potential for naturally produced siderophores to affect Hg(II) bioavailability. We chose *E. coli* because its metal transport systems are well documented in the literature. Like many Enterobacteriaceae, while not all *E. coli* strains may synthesize a siderophore; they still expresses transport systems for many of them (*51*). We compared Hg(II) bioavailability with siderophores

in which either *E. coli* has known and no reported pathways. Our results highlight how ligands used to acquire essential metals in the environment can influence Hg(II) bioavailability.

7.3 Methodology

7.3.1 Experimental design.

Our study uses microbial biosensors to assess Hg(II) bioavailability when ligands . The Hg-biosensor is a microbe, *Escherichia coli* NEB5α, that emits a quantifiable fluorescent signal only when Hg(II) enters the cell. We then combine these fluorescent readings with a constitutive biosensor, that always produces a fluorescent signal independent of Hg(II). Letting us distinguish Hg(II) bioavailability from the biosensor's viability (i.e, if the ligand is killing the biosensor, it would not produce any fluorescent signal and give us a false negative for Hg(II) bioavailability).

We use four siderophores that *E. coli* has known transport systems for (*51*); Enterobactin (Ent) from *Escherichia coli*, Desferrioxamine B (DFOB) from *Streptomyces pilosus*, Ferrichrome from *Ustilago sphaerogena*, and citrate, a ubiquitous biological metabolite. We also used four siderophores with no reported transport pathways in *E. coli*; Desferrithiocin (DFT) from *Streptomyces pilosus*, Pyochelin (I and II) (Pch) and pyoverdines (Pvd) from *Pseudomonas* sp. Finally, we also used the phytosiderophore nicotianamine (NA). NA is a metal chelating compound ubiquitous to all higher plants used to translocate metals throughout the plant body. While not secreted by microbes, it is a structural analog with similar binding properties to the phytosiderophore deoxymugineic acid that is used to extract iron from soil (*52*). NA and many NA-like metallophores are also used by bacteria to scavenge zinc (*53*). It is also important to note that these experiments were performed under anoxic conditions to emulate that conducive to Hg methylation but also that affect the expression of ferric iron transporters. These transporters

are transcribed from operons; enterobactin (*entA-entD*), ferrioxamine (*fhuACDB*), Ferrichrome (*fhuACDB*), and citrate (*fecABCDE*). These operons are in part regulated by the Ferric Uptake *Regulator* (*fur*) protein (*54*). While anoxic conditions will increase the expression of *fur* (*55*), our system for detecting Hg(II) is in an iron-depleted exposure medium. The Ent operon (*entA-entD)* is still highly expressed under anoxic conditions conducive to fumarate reduction (*56*) or in medium containing µM levels of iron.

In this study, we exposed the biosensor to Hg(II) with siderophores in concentrations covering an order of magnitude. This was to assess the wide range of variability that could be expected in the environment. Very few studies have quantified specific concentrations of each siderophore that would be present in environmental samples. However, data is available to infer concentrations of siderophores, or their analogues, from pure cultures (**Table 7.1**). These concentrations are observed under ideal conditions and may not entirely represent the environment.

The siderophores used in this study are not entirely regulated by iron homeostasis (e.g, iron-replete environments limit their production. While bioavailable iron may reduce the expression of the genes controlling their production, many of these siderophores serve multiple functions independent of acquiring iron (*28, 58*) (**Table 7.1**).

Table 7.1: Siderophores production and relative concentrations of siderophores used in the study and related siderophores. Table describing the siderophore and the notable organisms that produce the siderophore (not exhaustive). Siderophore concentration ranges associated with organisms (i.e., culture production) or environmental samples are reported. Included is whether the presence of iron (Fe) inhibits siderophore production. There are many structural analogs for each siderophore; this table does not differentiate between them.

Siderophore producing organisms	Production affected by Iron.	Concentrations found associated with organisms or required for growth.	Ref

Pyochelin (Pch) Notably *Pseudomonas sp*. But also *Burkholderia cepacia*; *Streptomyces scabies* (*57*)	Enhanced production with 1 uM [Fe(III)]. Lowered but not inhibited by 30 uM[Fe(III)].	1-60 µM in cultures	(*59-61*)
Desferrioxamines (DFO) Notably *Streptomyces sp*. and many Actinobacteria But also *Erwinia sp.* *Vibrio sp*. (*57*)	Enhanced production by 1 uM [Fe(III)]. 25% inhibited by 10 uM. Inhibited by 1 mM iron (under ideal conditions while fermenting)	>0.1µM (required for most syntrophs) 1-240 µM (in cultures) 1.38 - 13.8 µMDFO/hour under ideal conditions while fermenting	(*62-69*)
Pyoverdines (Pvd) *Pseudomonas sp*.	Inhibited by about 8uM [Fe(III)]. However, some strains will continue to produce at 10 uM.	1-325 µM (in cultures)	(*61, 70-73*)
Enterobactin (Ent) Notably *Escherichia sp. Streptomyces sp.* and many Enterobacteriaceae but also *Serratia sp.* (*57*)	Suppressed but not inhibited by 25 µM Fe(III)	1- 91µM (in cultures) It can be lowered to 200nM with excess iron. (in cultures) 50 nmol/kg soil (bulk hydroximates) (*74*)	(*69, 75-77*)
Nicotianamine (NA) All higher plants NA and NA-like metallophores are used by many bacteria/archaea/fungi Notably *Staphylococcus sp.* *Pseudomonas sp.* *Nicotiana. sp* *Neurospora sp.* *Methanothermobacter sp.*	N/A	Typically 3.3 µmol – 200 µmol/kg (dry weight) of plant 2–90 nmol/kg of soil	(*53, 78, 79*)

Lastly, we tested Hg bioavailability in the presence of two dithiocarboxylic acids used extensively in the mining industry as floatation agents; Sodium Ethylxanthate Sodium and Diethyldithiocarbamate (DDTC). The structures of the ligands in the study can be found in

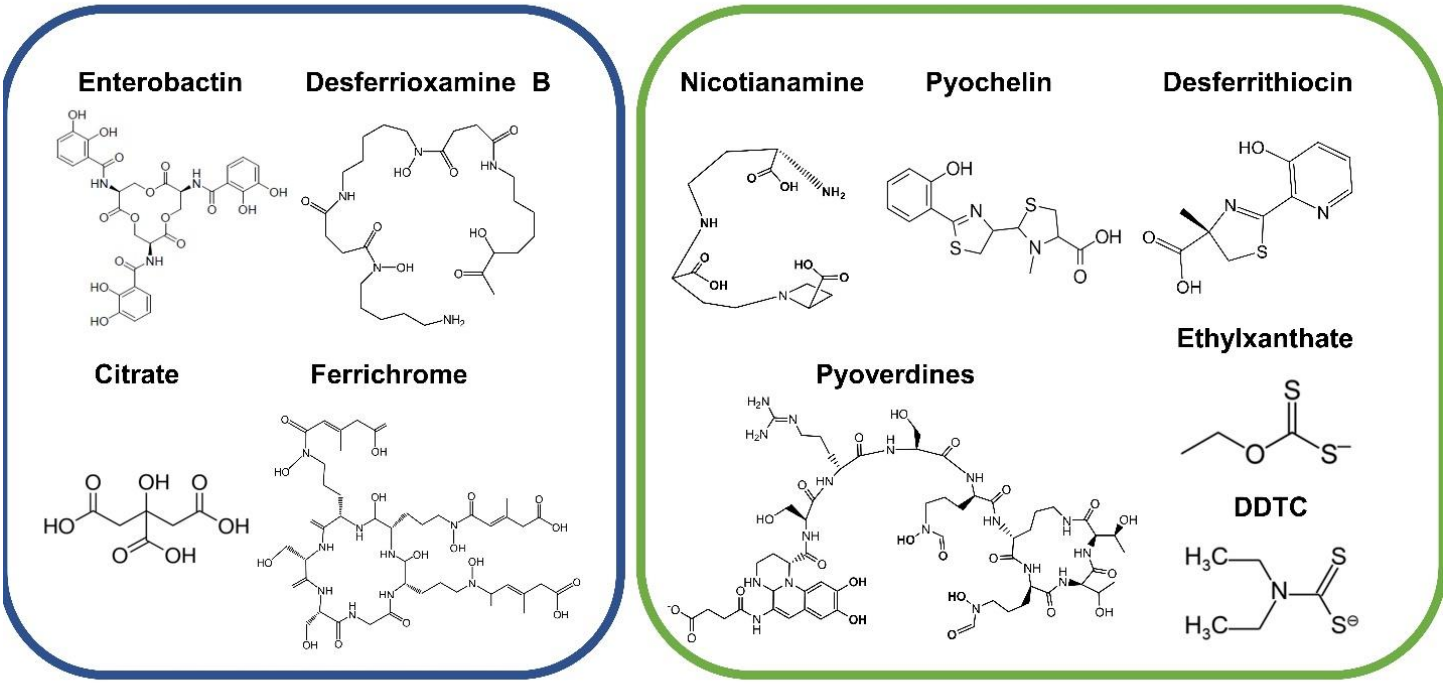

Figure 7.1: Selection of ligands used in the study and their structures. Ligands are grouped into ones that the *E. coli* used in our study has known transport systems for (Blue) and one it does not (Green).

7.3.2 Reagents and chemical preparation

Nicotianamine was purchased from Toronto Research Chemicals (Cat No: A510970), was dissolved in 50% ethanol:water, and serially diluted in water. Sodium Diethyldithiocarbamate

was purchased from Fisher Scientific Company (CAT No: S287100), dissolved in anoxic 100% ethanol, and serially diluted in anaerobic 100% ethanol. Sodium Ethylxanthate purchased from VWR International Co. (Cat No: TCE0195-025G), dissolved in anoxic 100% ethanol and serially diluted in anoxic 100% ethanol. Ferrichrome was purchased from Sigma-Aldrich Canada (Co. CAT No: F8014-1MG), dissolved in water, and serially diluted in water. Desferrioxamine B was purchased from Fisher Scientific Company (Cat No: 2527501GM), dissolved in 50% ethanol:water, and serially diluted in water. Enterobactin was purchased from Sigma-Aldrich Canada Co. Cat No: E3910-1MG), dissolved in ethyl acetate, and serially diluted in anaerobic water. Pyochelin (Pyochelin I and Pyochelin II mixture) was purchased from Toronto Research Chemicals (CAT No: P840365), dissolved in anaerobic DMSO, and serially diluted in anaerobic water. Desferrithiocin was purchased from Sigma-Aldrich Canada Co. (CAT No: SML1289-5MG), dissolved in anaerobic DMSO, and serially diluted in anaerobic water. Pyoverdines was purchased from Sigma-Aldrich Canada Co. (CAT No: P8124-1MG), dissolved in anaerobic DMSO, and serially diluted in anaerobic water. Citrate is dissolved in anaerobic water and serially diluted in anaerobic water. All solutions were stored at -20 °C. All solutions were prepared anaerobically and in Coy Vinyl Anaerobic chamber (98% N_2, 1.5% H_2), and solvents were $N_{2(g)}$ bubbled to make anaerobic.

7.3.3 Bacterial Strains and Growth

Biosensor growth and suspension assays were performed as described in (*80*). The method was modified to use fumarate as a terminal electron acceptor instead of nitrate. Two microbial biosensors hosted in *E. coli* NEB5α (DH5α derivative of K12 strain) were deployed; a Hg-Inducible (*E. coli* NEB5α harboring the pUC57merR-Pp plasmid) and a Constitutive biosensor (*E. coli* NEB5α harboring pUC19AH206-Pp plasmid). The expression of a flavin-based

fluorescent protein on the plasmids are regulated by the transcriptional regulator of the *mer* operon (*merR*) or a constitutive promoter. All anaerobic manipulations of cell cultures were performed in a Coy Vinyl Anaerobic chamber (98% N_2, 1.5% H_2). Anaerobic growth was performed in anaerobic balch tubes.

For the anaerobic suspension assay, *E. coli* biosensors were grown at 37˚C and the plasmids were selected with 200 μg/ml ampicillin (unless otherwise stated), no antibiotic was used in the suspension assay. From -80°C cryostock, the biosensors were plated onto fumarate-GMM plates (**Appendix D** fumarate reduction plates for the recipe) with 100 μg/ml ampicillin and grown anaerobically in anaerobic plate jars (this took a couple of days). A single colony was selected and grown in anaerobic GMM (**Appendix D** Growth Media for recipe) overnight. The following day, cultures were transferred (20% inoculum) into fresh GMM and grown to an OD_{600} of 0.6. Cultures were resuspended twice in anaerobic exposure media (**Appendix D** Exposure Media for recipe).) supplemented with 10 mM Na_2Fumarate (10,000 RCF for 90 seconds). The cells were ready for a 1/20 dilution into the biosensor suspension assay in exposure media.

7.3.4 Biosensor suspension assays

All manipulations were performed inside a Coy Vinyl Anaerobic chamber (98% N_2, 1.5% H_2). Assays were performed in exposure medium using 7 ml standard PTFE vials. Hg(II) was prepared as a 7.2 μM $HgSO_4$ stock in 0.2 M H_2SO_4. The concentration was determined using an MA-3000 Mercury Analyzer. Hg was diluted in exposure medium to a working concentration of 100 nM in PTFE vials before addition to the suspension assay. The added ligands to be equilibrated with Hg(II) were added before Hg(II). The stock concentrations of the ligands added to the suspension assay were made so that the carrier fluid (e.g., ethanol) into the suspension

assay would not exceed 1% of the total volume. Hg(II) was added to the exposure medium at a final concentration of 2 nM and set to equilibrate for 30 minutes. Biosensor cells (**Appendix D** "Bacterial Strains and Growth") were added last as a 1/20 dilution into the suspension assay. The suspension assay was transferred (200 µL) in triplicate from the PTFE vials to a 96 well microplate (Black, 96-Well Clear-Bottom Nonbinding Surface Microplates) and transferred to a Synergy HTX plate reader (present in the anaerobic chamber).

Readings for fluorescence, luminescence, and OD_{600} were taken every 2.5 minutes for 10 hours at 37 ˚C. Shaking continuously between reads. Fluorescence was read for PpFbFp (Excitation: 440 nm, Emission: 500 nm**).** Hg-inducible and constitutive fluorescence were measured at 10 hours. Calculations were performed as described in (*80*). All values were then normalized to the no ligand treatment control (2 nM Hg(II)) at 10 hours for each biological replicate in the assay. Biological replicates here are independent cell cultures prepared from a single colony selected from fumarate reduction plates (**Appendix D** "Bacterial Strains and Growth)

7.4 Results and Discussion

7.4.1 Hg bioavailability and *E. coli* compatible siderophores

The *E. coli* transport pathways for incorporating metal-siderophore complexes in the cell are well documented and typical of gram-negative bacteria. Once a metal is scavenged and bound to a siderophore, this induces a conformational change in the siderophore. This metal-siderophore complex has a high affinity for a specialized transporter on the outer membrane to be transported to the periplasmic space. Here the complex is bound to a periplasmic binding protein that facilitates transport to an ABC-type transporter on the inner membrane (*51*). Using a microbial

Hg-biosensor, we investigated the potential of Hg to use this process using siderophores that are compatible with *E. coli*. The siderophores we selected were enterobactin (Ent) from *Escherichia coli* and Desferrioxamine B (DFOB) from *Streptomyces pilosus*, ferrichrome from *Ustilago sphaerogena*, and citrate.

Of the *E. coli* compatible siderophores, only Ent and DFOB affected Hg(II) bioavailability (Fig. 7.2). 1 nM of Ent enhanced the signal of the Hg-inducible biosensor by 50%. Further increasing the siderophore concentration to 5 µM reduced, but did not inhibit, the signal (Fig. 7.2A). However, the constitutive biosensor only showed an increase in signal increasing concentrations. The addition of any DFOB up to 5 µM reduced the signal of the Hg-inducible biosensor but did not affect constitutive fluorescence (Fig. 7.2 B). The addition of ferrichrome and citrate created a large variation in the fluorescence of the Hg-inducible biosensor (Fig. 7.2 C and D). This variation was observed across 3-6 replicated experiments. While ferrichrome and citrate both significantly enhanced constitutive fluorescence, we cannot conclude how they affect Hg(II) bioavailability due to our inability to control for this large variability.

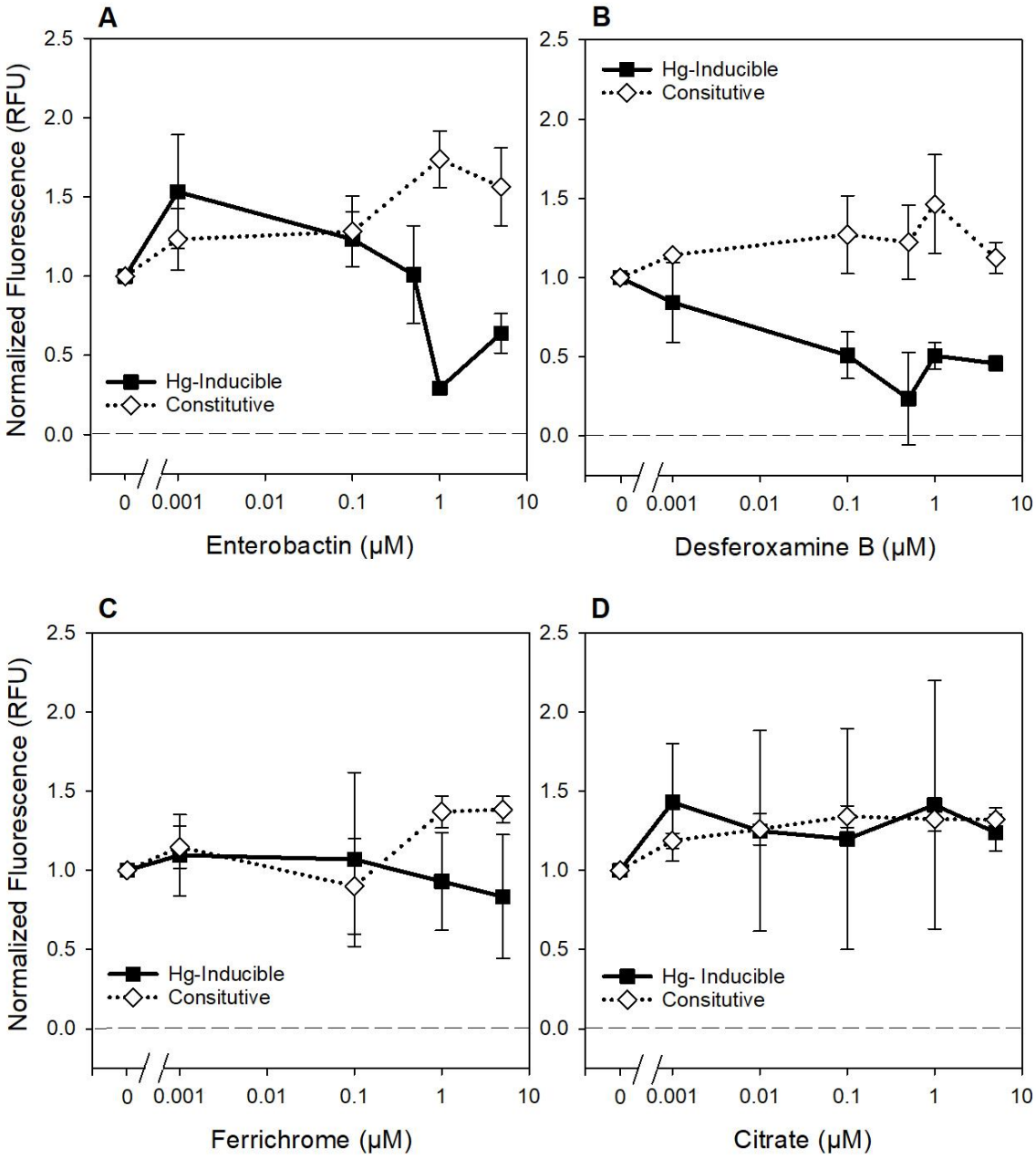

Figure 7.2: Hg(II) bioavailability in the presence of ligands with known transport pathways in *E. coli*. Average Normalized Fluorescence measured as relative fluorescence units (RFU) ± 1SD at 10 hours emitted the Hg-Inducible biosensor (*E. coli* NEB5α harboring the pUC57merR-Pp plasmid) and the Constitutive biosensor (*E. coli* NEB5α harboring pUC19AH206-Pp plasmid) with the addition of **A)** Enterobactin (Ent) (0-5 μM), **B)** Desferrioxamine B (DFOB) (0-5 μM), **C)** Ferrichrome (0-5 μM), **and D)** Citrate (0-5 μM). Fluorescence at 10 hours was normalized to the control (0 μM) at 10 hours for each biological replicate (between 3 and 5 biological replicates per point, see Table E1 for further details). [Hg(II)] was set to 2 nM. The experiment was performed at 37 ˚C in an anaerobic exposure medium (pH 7).

It is surprising to observe that 1 nM Ent greatly enhanced Hg(II) bioavailability. By hijacking parts of the Ent system encoded by the *ent* operon, Hg(II) might have more transport pathways. The concentration of Ent that enhanced uptake was half that of Hg(II) (2nM).

Suggesting that half the Hg(II) may have had alternative transport routes. While Ent may not bind Hg(II) with as high of an affinity as other ligands (e.g, thiols or the cell membrane), we did let Hg(II) and Ent equilibrate before the biosensor cells were added and it is possible that structural or kinetic controls may have prevented an exchange between Hg and a ligand with a stronger binding constant than Ent. In contrast, the decrease of Hg bioavailability in the presence of incrasing concentration of DFOB suggest that the role of siderophore on Hg uptake is complex and controlled by a series of ligand exchanges from solution to the transport site. *E. coli* has different metal ion transporters exhibiting different affinities towards metals and their ligands in solution (*81, 82*). The first step in active transport is often the exchange of the metal between its ligand in solution and the transport site. It remains unclear if Hg(II) is bioavailable through siderophore transport pathways or if these siderophores facilitate/limit uptake through other mechanisms.

Enterobactin (Ent) is the archetypical siderophore produced by many Enterobacteriaceae and *Streptomyces sp*. Enterobacteriaceae are ubiquitous, living in terrestrial and aquatic environments and inside other living organisms (*83*). It is notable as the siderophore with the strongest affinity for Fe(III) (*51*). Few studies have attempted to quantify Ent concentrations in environmental samples, but the molecule is likely to be ubiquitous (*84*). The production of Enterobactin is not limited to acquiring iron and has many functions, including cell signaling and oxidative stress responses (*28*). Enterobacteriaceae are capable of a wide range of anaerobic metabolisms that allow them to survive in Hg-methylating environments. Even under these reducing conditions with bioavailable Fe, Ent expression is not inhibited (**Table 7.1**). The ability of Enterobactin to complex Hg(II) has not been investigated until now but the low Ent

concentrations required to affect Hg(II) bioavailability indicate this process deserves further study.

Actinobacteria, and more specifically *Streptomyces sp.* are the main producers of Desferoxamines (**Table 7.1**) (DFOB used in this study). They are ubiquitous, account for much of the soil microflora community (*84-86*), and are found in aquatic/marine systems (*66, 67*). Feroxamine transport systems are also widespread and necessary for many syntrophic interactions (*65, 87*). No interactions between DFOB and Hg(II) are reported in the literature. However, DFOB does not only bind Fe(III) but has a high affinity for many other divalent metals. It forms strong complexes with soft metals such as Pb(II) and Cd(II), albeit the stability constants are orders of magnitude lower than that of Fe(III) (*64*). While Hg(II) may interact with DFOB and Enterobactin, it remains to be evaluated the extent to which these Hg(II) complexes are compatible with these siderophore transport systems.

7.4.2 Hg bioavailability and *E. coli* incompatible siderophores

The next objective was to compare Hg(II) bioavailability using siderophores that are not compatible with *E. coli* transport systems: Desferrithiocin (DFT), nicotianamine (NA), Pyoverdines (Pyo) from *P. fluorescens*, Pyochelin (Pch) from *P. aeruginosa*. DFT and the phytosiderophore NA had a dynamic influence on Hg bioavailability (Fig. 7.3 A and B) with increasing Hg(II) at discrete concentrations (1 nM for NA and 1 µM for DFT).

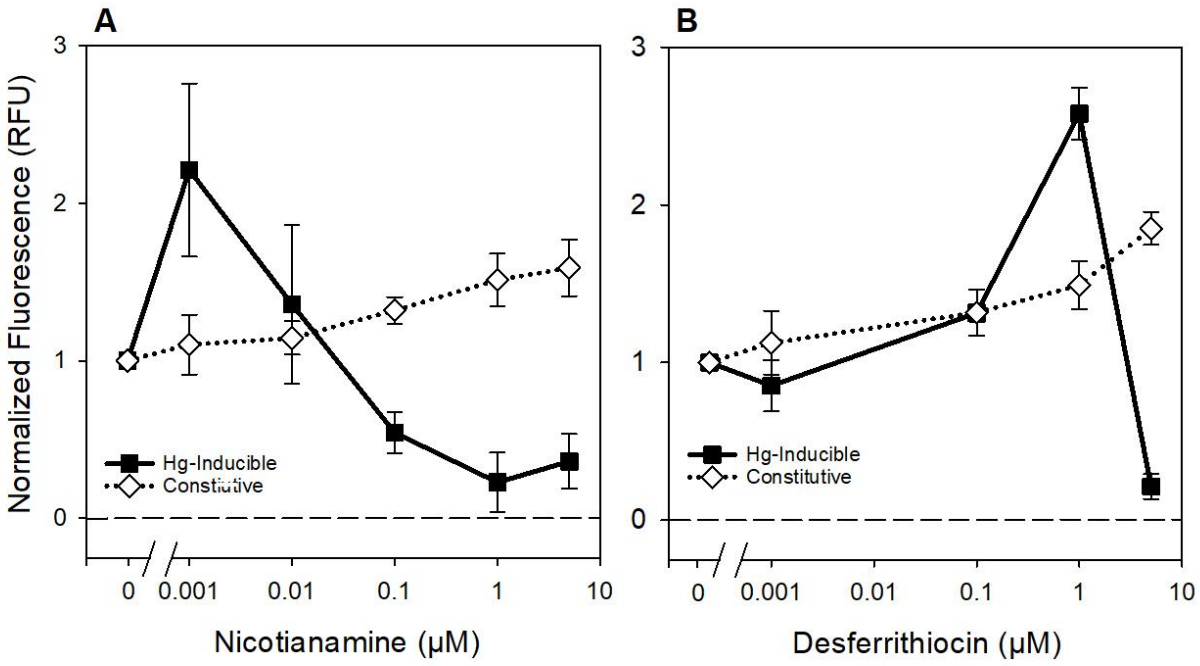

Figure 7.3: Hg(II) bioavailability in the presence of ligands with no known transport pathways in *E. coli*. Average Normalized Fluorescence measured as relative fluorescence units (RFU) ± 1SD at 10 hours emitted the Hg-Inducible biosensor (*E. coli* NEB5α harboring the pUC57merR-Pp plasmid) and the Constitutive biosensor (*E. coli* NEB5α harboring pUC19AH206-Pp plasmid) with the addition of **A)** Nicotianamine (NA) (0-5 μM) and **B)** Desferrithiocin (DFT) (0-5 μM). Fluorescence at 10 hours was normalized to the control (0 μM) at 10 hours for each biological replicate (between 3 and 5 biological replicates per point, see Table E1 for further details). [Hg(II)] was set to 2 nM. The experiment was performed at 37 ˚C in an anaerobic exposure medium (pH 7).

DFT is a siderophore produced by *Streptomyces sp.* but was originally isolated from *Streptomyces antibioticus.* Over the years, it has gathered attention as a potential therapeutic in chelation therapy for Fe(III). DFT and its ferric complexes can diffuse through cell membranes in red blood cells and hepatocytes to extract iron (95-97). However, research into an unmodified molecule has been strained due to its high lipophilicity and toxicity (98). In addition to Fe(III), it has a high affinity for many divalent metals (99). Still, this research is the first to evaluate its interaction Hg(II) and bioavailability.

NA is metallophore ubiquitous in higher plants. It binds to and is essential for iron, copper, nickel, and zinc regulation (*53*). These complexes form strong interactions with divalent metals and can facilitate the transport of Zn^{2+} while simultaneously sequestering Cd^{2+} (*92*).

While notable in plants, NA and NA-like metallophores are used extensively in nature by many bacteria/archaea and fungi to scavenge Zn (*53*) (**Table 7.1**). Interestingly, we observed its effect on Hg(II), where 1 nM can almost double Hg(II) bioavailability (**Fig 7.1a**). There are no reported NA transporters in *E. coli,* and the bioavailability is likely by facilitating ligand exchange with transporters.

We also deployed two siderophores produced by *Pseudomonas* sp. (Pyoverdin, Pyo and Pyochelin, Pch) to acquire iron (*93*). Both had markedly opposing effects on the response of the biosensors. With increasing concentrations of Pch, fluorescent induction of the Hg-inducible and constitutive strain increased (Fig. 7.4 A). With the increasing concentrations of Pvd, fluorescence steadily decreases for both the Hg-inducible and constitutive biosensors (Fig. 7.4 B). Pvd are produced by *Pseudomonas* sp. but are notable in the virulence of *P. aeruginosa*. The toxicity has been shown to inhibit the growth of other microbial species (*94-96*), so it is not surprising it had this effect on the biosensor. On the other hand, Pch can also inhibit the growth and iron bioavailability to microbes that do not have the transport pathways (*60, 97*); this appears not to be the case with Hg (II). Because the Hg-inducible and constitutive biosensors responded similarly to the presence of these ligands, it would be misleading to conclude on their definitive role on Hg bioavailability, but clearly deserves further study

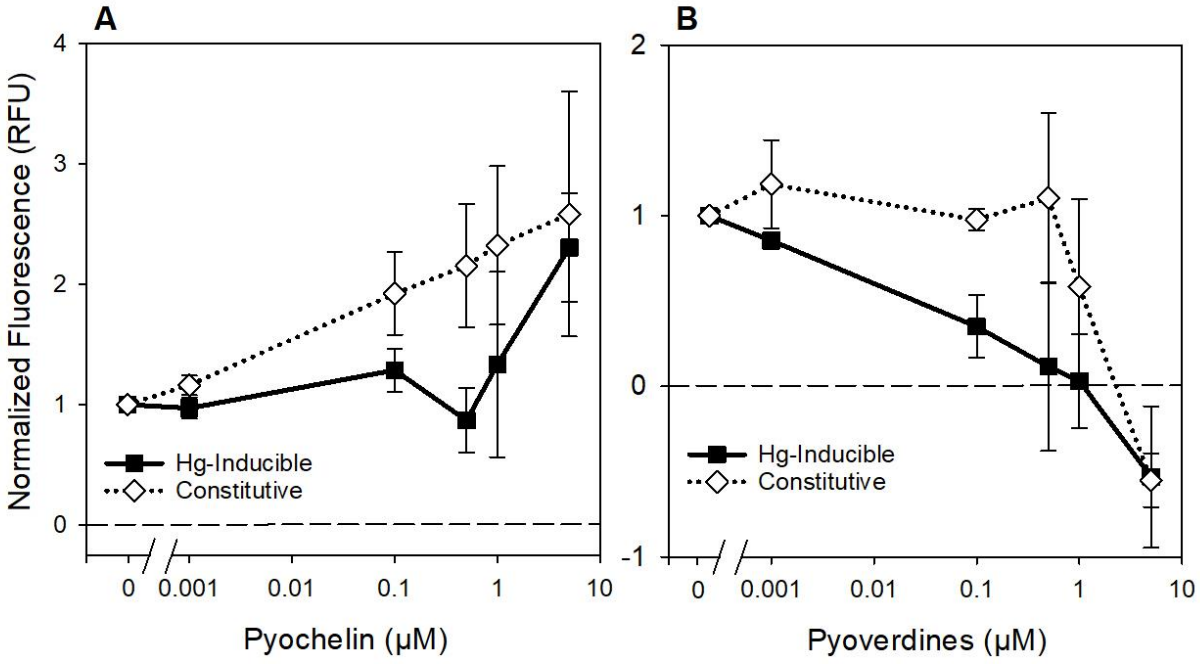

Figure 7.4: Hg(II) bioavailability in the presence of *Pseudomonas* derived ligands with no known transport pathways in *E. coli*. Average Normalized Fluorescence measured as relative fluorescence units (RFU) ± 1SD at 10 hours emitted the Hg-Inducible biosensor (*E. coli* NEB5α harboring the pUC57merR-Pp plasmid) and the Constitutive biosensor (*E. coli* NEB5α harboring pUC19AH206-Pp plasmid) with the addition of **A)** Pyochelin (Pch) (0-5 μM) and **B)** Pyoverdines (Pvd) (0-5 μM). Fluorescence at 10 hours was normalized to the control (0 μM) at 10 hours for each biological replicate (between 3 and 5 biological replicates per point, see Table E1 for further details). [Hg(II)] was set to 2 nM. The experiment was performed at 37 ˚C in an anaerobic exposure medium (pH 7).

Pseudomonas and their siderophores are ubiquitous in the environment and have a role in controlling metal bioavailability (*98*). They also cohabit the same environments with Hg-methylating microbes (e.g., *Geobacter sulfurreducens*), where they can compete for resources and potentially form syntrophic relationships (*99, 100*). Unlike the other siderophores used in this study, Pch and Pvd have had interactions investigated with Hg(II) (*59, 73*). Pch and Pvd showed an affinity to bind 16 metals, including Hg(II). Hg(II) could even compete with Fe(III) for complexation with Pch, unlike Pch. While Hg(II) can form complexes with Pch and Pvd, these complexes could not be transported into the cell using the siderophore transport system, unlike the other metals tested (*59, 73*).

A notable siderophore produced by *Pseudomonas* sp., not used in this study, is PDTC (pyridine-2,6-bis(thiocarboxylic acid)). PDTC is unique among siderophores in that it binds metals with two thiocarboxylate groups, these groups have high affinities for heavy metals such as Cd, Pb, Hg. A study by Cortese et al. (2001) found that PDTC can bind to Hg(II) and form insoluble, uncharged complexes. PDTC eliminated Hg(II) toxicity to 14 of 16 of the microbial strains tested. It was unclear if PDTC was facilitating the formation of HgS(*101*). It would be interesting to test this compound in further studies.

Each of the siderophores tested has a unique role in ecology. Our research emphasizes the importance of microbial community structure and Hg(II) bioavailability. Our results indicate that these siderophores interact with Hg(II) and control its bioavailability. More importantly, we demonstrate how Enterobacteriaceae, *Pseudomonas*, and *Streptomyces*, widely found in nature, can influence Hg(II) bioavailable to other organisms. This work provides a benchmark and rationale for further delving into this research.

7.4.3 Hg bioavailability and Emerging Contaminants

A second objective of this study was to evaluate how synthetic ligands with Hg chelating properties and typically associated with mining activities affected Hg(II) bioavailability. Contamination from mining operations is an ongoing problem that contributes to Hg-methylation from mining wastewaters (*102*). Compounds used to extract metals are regularly discharged (*103*), and there is little if any information on they affect metal bioavailability to microbes (*104*). Using the Hg-biosensor, we give insight into how these compounds affect Hg(II) bioavailability and provide and their role in Hg cycling.

Hg methylation associated with mining operations and wastewaters is an ongoing problem (*102*). Therefore, we investigated common chemicals used in these operations that have become an emerging contaminant in the environment. Ethyl xanthate and DDTC are widely used as floatation agents in the mining industry, where they bind to sulfide minerals and remove them from a slurry. They are also widely used as herbicides or for stabilizing rubber. These chemicals are problematic as they are regularly discharged into the environment and have become an ecological and health concern (*103*). These compounds can alter bacterial community structures in contaminated areas. Still, there is little known about how they affect metal bioavailability (*104*). Although these are not naturally occurring, anthropogenic ligands are not considered in the Hg cycle despite becoming more ubiquitous and problematic every year. Due to their high affinity for metals, investigating their effects on Hg(II) bioavailability was warranted.

Increasing the concentrations of either ethyl xanthate and DDTC (Figure 7.5 A and B) did not inhibit fluorescence of the Hg-inducible biosensor but instead reduced it until a plateau was observed at high micromolar concentrations. Some toxicity was observed with the constitutive biosensors and may partly explain why Hg-inducible fluorescence decreases. These compounds appear to reduce Hg(II) bioavailability at about 1 µM but do not inhibit it, even at concentrations of up to 250 µM.

The studies showing the interaction of xanthate and dithiocarbamates with Hg(II) are limited, and no equilibrium constants are reported that can indicate changes in Hg(II) speciation related to bioavailability. These compounds typically bind metals with 1-2 ligand coordination in aqueous solution depending on ligand concentration, but specific Hg(II) speciation is uncertain. 3-4 coordinate is possible at high ligand concentrations (*105*, *106*). Hg(II) has a high affinity for these compounds and readily displace other metals (*107*). These Hg(II) species are also

incredibly lipophilic, where Hg(dithiocarbamate)$_2$ has an extraction constant (LogK) of 40-41 (*108*). In his thesis dissertation, Gideon (1971) demonstration that xanthates were efficient (98%) at removing divalent Hg and MeHg from water and fractioning it into pure hexane. The binding of Hg(II) to xanthates was so strong that stannous chloride ($SnCl_2$), a powerful reducing agent, could not reduce it to Hg^0 for analysis without degrading the xanthates first (*109*). Ligands that bind Hg so strongly that $SnCl_2$ can not reduce it (e.g., dithiolate ligands such as DMPS) (*110*) have been demonstrated to make Hg(II) non-bioavailable to Hg methylators (*31, 111, 112*) and this is what we observe here with the biosensor. While extensively used in metallurgy, DDTC has found a niche use in medicinal practice. Due to its high lipophilicity, it can readily passively diffuse across cell membranes while chelating metals. This has been shown to be effective at removing nickel from brain tissue (*113*), as a vehicle to facilitate lead uptake into brain tissue in rats (*114*), or transporting nanoparticles into cells (*115*).

In **Chapter 6**, I compared Hg(II) bioavailability with two dithiols (BAL and DMSA) that coordinate Hg(II) similarly but only differ in their lipophilicity (105, 106). We observed high bioavailability of Hg(II) in the presence of lipophilic BAL as opposed to virtually no Hg(II) bioavailability in the presence of hydrophilic DMSA. While proposed that lipophilic Hg(II) complexes may cross a cell membrane through passive diffusion (107), evidence supporting this is scarce. While unlikely to find ligands such as DMPS, BAL, or DMSA in the environment, ethyl xanthate and DDTC represent major contaminants that can alter metal speciation and facilitate transport using novel mechanisms. We hypothesize that at higher concentrations of the dithiocarboxylic acids, passive diffusion of these Hg(II) complexes might occur.

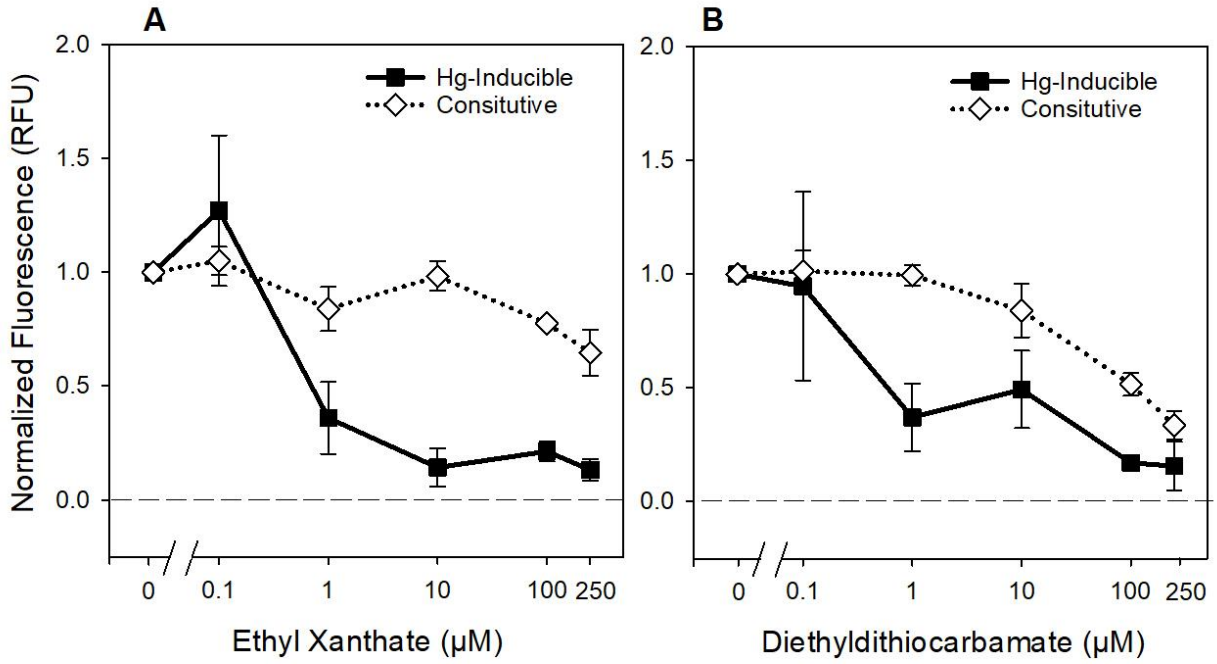

Figure 7.5: Hg(II) bioavailability in the presence of dithiocarboxylic acids. Average Normalized Fluorescence measured as relative fluorescence units (RFU) ± 1SD at 10 hours emitted the Hg-Inducible biosensor (*E. coli* NEB5α harboring the pUC57merR-Pp plasmid) and the Constitutive biosensor (*E. coli* NEB5α harboring pUC19AH206-Pp plasmid) with the addition of **A)** Ethyl Xanthate (0-250 µM) and **B)** Diethyldithiocarbamate (0-250 µM). Fluorescence at 10 hours was normalized to the control (0 µM) at 10 hours for each biological replicate (between 3 and 7 biological replicates per point, see Table E1 for further details). [Hg(II)] was set to 2 nM. The experiment was performed at 37 ˚C in an anaerobic exposure medium (pH 7).

7.5 References

1. O. Regnell, C. J. Watras, Microbial Mercury Methylation in Aquatic Environments: A Critical Review of Published Field and Laboratory Studies. *Environmental Science & Technology* **53**, 4-19 (2019).

2. R. C. Harris *et al.*, Whole-ecosystem study shows rapid fish-mercury response to changes in mercury deposition. *Proceedings of the National Academy of Sciences* **104**, 16586 (2007).

3. D. Obrist *et al.*, A review of global environmental mercury processes in response to human and natural perturbations: Changes of emissions, climate, and land use. *Ambio* **47**, 116-140 (2018).

4. Z. Tang, F. Fan, S. Deng, D. Wang, Mercury in rice paddy fields and how does some agricultural activities affect the translocation and transformation of mercury - A critical review. *Ecotoxicology and Environmental Safety* **202**, 110950 (2020).

5. M. Podar *et al.*, Global prevalence and distribution of genes and microorganisms involved in mercury methylation. *Science Advances* **1**, e1500675 (2015).

6. A. Manceau *et al.*, Formation of Mercury Sulfide from Hg(II)–Thiolate Complexes in Natural Organic Matter. *Environmental Science & Technology* **49**, 9787-9796 (2015).

7. V. Liem-Nguyen, U. Skyllberg, E. Björn, Thermodynamic Modeling of the Solubility and Chemical Speciation of Mercury and Methylmercury Driven by Organic Thiols and Micromolar Sulfide Concentrations in Boreal Wetland Soils. *Environmental Science & Technology* **51**, 3678-3686 (2017).

8. V. Liem-Nguyen, U. Skyllberg, K. Nam, E. Björn, Thermodynamic stability of mercury(II) complexes formed with environmentally relevant low-molecular-mass thiols studied by competing ligand exchange and density functional theory. *Environmental Chemistry* **14**, 243-253 (2017).

9. A. Drott, E. Bjorn, S. Bouchet, U. Skyllberg, Refining thermodynamic constants for mercury (II)-sulfides in equilibrium with metacinnabar at sub-micromolar aqueous sulfide concentrations. *Environmental science & technology* **47**, 4197-4203 (2013).

10. H. Hsu-Kim, K. H. Kucharzyk, T. Zhang, M. A. Deshusses, Mechanisms regulating mercury bioavailability for methylating microorganisms in the aquatic environment: a critical review. *Environ Sci Technol* **47**, 2441-2456 (2013).

11. P. Dranguet, V. I. Slaveykova, S. Le Faucheur, *Kinetics of mercury accumulation by freshwater biofilms*. (2018), vol. 14.

12. J. B. Fein, Q. Yu, J. Nam, N. Yee, Bacterial cell envelope and extracellular sulfhydryl binding s: Their roles in metal binding and bioavailability. *Chemical Geology*, (2019).

13. S. Han *et al.*, Sulfide and iron control on mercury speciation in anoxic estuarine sediment slurries. *Marine Chemistry* **111**, 214-220 (2008).

14. Y. Si, Y. Zou, X. Liu, X. Si, J. Mao, Mercury methylation coupled to iron reduction by dissimilatory iron-reducing bacteria. *Chemosphere* **122**, 206-212 (2015).

15. M. Ganguly, S. Dib, P. A. Ariya, Fast, Cost-effective and Energy Efficient Mercury Removal-Recycling Technology. *Scientific Reports* **8**, 16255 (2018).

16. K. H. Johannesson, K. Neumann, Geochemical cycling of mercury in a deep, confined aquifer: Insights from biogeochemical reactive transport modeling. *Geochimica et Cosmochimica Acta* **106**, 25-43 (2013).

17. W. Stumm, & Morgan, J. J., *Aquatic Chemistry: Chemical Equilibria and Rates in Natural Waters*. (Wiley, New York, ed. 3rd, 1996).

18. S. Guedron, S. Grangeon, B. Lanson, M. Grimaldi, Mercury speciation in a tropical soil association; Consequence of gold mining on Hg distribution in French Guiana. *Geoderma* **153**, 331-346 (2009).

19. G. Liu, Y. Li, Y. Cai, in *Environmental Chemistry and Toxicology of Mercury*. (2011), pp. 367-387.

20. J. Harris-Hellal, M. Grimaldi, E. Garnier-Zarli, N. Bousserrhine, Mercury mobilization by chemical and microbial iron oxide reduction in soils of French Guyana. *Biogeochemistry* **103**, 223-234 (2011).

21. J. Hellal *et al.*, Mercury mobilization and speciation linked to bacterial iron oxide and sulfate reduction: A column study to mimic reactive transfer in an anoxic aquifer. *Journal of Contaminant Hydrology* **180**, 56-68 (2015).

22. H. A. Wiatrowski *et al.*, Reduction of Hg(II) to Hg(0) by Magnetite. *Environmental Science & Technology* **43**, 5307-5313 (2009).

23. S. Sah, R. Singh, in *Agriculture (Polnohospodárstvo)*. (2015), vol. 61, pp. 97.

24. E. Ahmed, S. J. M. Holmström, Siderophores in environmental research: roles and applications. *Microbial Biotechnology* **7**, 196-208 (2014).

25. R. Saha, N. Saha, R. S. Donofrio, L. L. Bestervelt, Microbial siderophores: a mini review. *J Basic Microbiol* **53**, 303-317 (2013).

26. J. Kramer, Ö. Özkaya, R. Kümmerli, Bacterial siderophores in community and host interactions. *Nature Reviews Microbiology*, (2019).

27. S. M. Kraemer, O. W. Duckworth, J. M. Harrington, W. D. C. Schenkeveld, Metallophores and Trace Metal Biogeochemistry. *Aquatic Geochemistry* **21**, 159-195 (2015).

28. T. C. Johnstone, E. M. Nolan, Beyond iron: non-classical biological functions of bacterial siderophores. *Dalton Trans* **44**, 6320-6339 (2015).

29. M. Hofmann, G. Retamal-Morales, D. Tischler, Metal binding ability of microbial natural metal chelators and potential applications. *Natural Product Reports* **37**, 1262-1283 (2020).

30. J. D. Semrau, B. Gu, "Final Technical Report: Methanotrophic-Mediated Methylmercury Transformation: Characterization of Products, Mechanism, and Environmental Significance," (University of Michigan, 2020).

31. X. Yin *et al.*, Synergistic Effects of a Chalkophore, Methanobactin, on Microbial Methylation of Mercury. *Applied and Environmental Microbiology* **86**, e00122-00120 (2020).

32. A. Szczuka, F. M. M. Morel, J. K. Schaefer, Effect of Thiols, Zinc, and Redox Conditions on Hg Uptake in Shewanella oneidensis. *Environmental Science and Technology* **49**, 7432-7438 (2015).

33. J. K. Schaefer, A. Szczuka, F. M. M. Morel, Effect of Divalent Metals on Hg(II) Uptake and Methylation by Bacteria. *Environmental Science & Technology* **48**, 3007-3013 (2014).

34. J. K. Schaefer *et al.*, Active transport, substrate specificity, and methylation of Hg(II) in anaerobic bacteria. *Proceedings of the National Academy of Sciences* **108**, 8714-8719 (2011).

35. U. Ndu *et al.*, The use of a mercury biosensor to evaluate the bioavailability of mercury-thiol complexes and mechanisms of mercury uptake in bacteria. *PLoS One* **10**, e0138333 (2015).

36. B. R. Stenzler, A. Hinz, M. O. Ruuskanen, A. J. Poulain, Ionic strength differentially affects the bioavailability of neutral and negatively charged inorganic Hg complexes. *Environ Sci Technol*, (2017).

37. S. A. Thomas, T. Tong, J.-F. Gaillard, Hg(ii) bacterial biouptake: the role of anthropogenic and biogenic ligands present in solution and spectroscopic evidence of ligand exchange reactions at the cell surface. *Metallomics* **6**, 2213-2222 (2014).

38. Y. Wang, J. K. Schaefer, B. Mishra, N. Yee, Intracellular Hg(0) Oxidation in Desulfovibrio desulfuricans ND132. *Environmental Science & Technology* **50**, 11049-11056 (2016).

39. M. J. Colombo, J. Ha, J. R. Reinfelder, T. Barkay, N. Yee, Anaerobic oxidation of Hg(0) and methylmercury formation by Desulfovibrio desulfuricans ND132. *Geochimica et Cosmochimica Acta* **112**, 166-177 (2013).

40. H. Hu *et al.*, Oxidation and methylation of dissolved elemental mercury by anaerobic bacteria. *Nature Geoscience* **6**, 751-754 (2013).

41. M. J. Colombo, J. Ha, J. R. Reinfelder, T. Barkay, N. Yee, Oxidation of Hg(0) to Hg(II) by diverse anaerobic bacteria. *Chemical Geology* **363**, 334-340 (2014).

42. Z. Zhang *et al.*, Effects of Extracellular Polymeric Substances on the Formation and Methylation of Mercury Sulfide Nanoparticles. *Environmental Science & Technology* **54**, 8061-8071 (2020).

43. A. M. Graham, G. R. Aiken, C. C. Gilmour, Dissolved Organic Matter Enhances Microbial Mercury Methylation Under Sulfidic Conditions. *Environmental Science & Technology* **46**, 2715-2723 (2012).

44. A. M. Graham, G. R. Aiken, C. C. Gilmour, Effect of Dissolved Organic Matter Source and Character on Microbial Hg Methylation in Hg–S–DOM Solutions. *Environmental Science & Technology* **47**, 5746-5754 (2013).

45. Nashaat M. Mazrui *et al.*, The precipitation, growth and stability of mercury sulfide nanoparticles formed in the presence of marine dissolved organic matter. *Environmental Science: Processes & Impacts* **20**, 642-656 (2018).

46. L. Tian *et al.*, Microbial methylation potential of mercury sulfide particles dictated by surface structure. *Nature Geoscience* **14**, 409-416 (2021).

47. S. A. Thomas, K. E. Rodby, E. W. Roth, J. Wu, J. F. Gaillard, Spectroscopic and Microscopic Evidence of Biomediated HgS Species Formation from Hg(II)-Cysteine Complexes: Implications for Hg(II) Bioavailability. *Environ Sci Technol* **52**, 10030-10039 (2018).

48. J. An *et al.*, Mercury Uptake by Desulfovibrio desulfuricans ND132: Passive or Active? *Environmental Science & Technology* **53**, 6264-6272 (2019).

49. S. A. Thomas, P. Catty, J.-L. Hazemann, I. Michaud-Soret, J.-F. Gaillard, The role of cysteine and sulfide in the interplay between microbial Hg(ii) uptake and sulfur metabolism. *Metallomics* **11**, 1219-1229 (2019).

50. S. A. Thomas, J.-F. Gaillard, Cysteine Addition Promotes Sulfide Production and 4-Fold Hg(II)–S Coordination in Actively Metabolizing Escherichia coli. *Environmental Science & Technology* **51**, 4642-4651 (2017).

51. R. Hider, X. Kong, Chemistry and biology of siderophores. *Natural product reports* **27**, 637 (2010).

52. T. Kobayashi, T. Nozoye, N. K. Nishizawa, Iron transport and its regulation in plants. *Free Radical Biology and Medicine* **133**, 11-20 (2019).

53. C. Laffont, P. Arnoux, The ancient roots of nicotianamine: diversity, role, regulation and evolution of nicotianamine-like metallophores. *Metallomics* **12**, 1480-1493 (2020).

54. A. Santos-Zavaleta *et al.*, RegulonDB v 10.5: tackling challenges to unify classic and high throughput knowledge of gene regulation in E. coli K-12. *Nucleic Acids Research* **47**, D212-D220 (2018).

55. N. A. Beauchene *et al.*, O₂ availability impacts iron homeostasis in Escherichia coli. *Proceedings of the National Academy of Sciences* **114**, 12261-12266 (2017).

56. O. Kwon, M. E. Hudspeth, R. Meganathan, Anaerobic biosynthesis of enterobactin Escherichia coli: regulation of entC gene expression and evidence against its involvement in menaquinone (vitamin K2) biosynthesis. *Journal of Bacteriology* **178**, 3252-3259 (1996).

57. A. E. Fazary, Y.-H. Ju, A. S. Al-Shihri, M. Y. Alfaifi, M. A. Alshehri, Biodegradable siderophores: survey on their production, chelating and complexing properties. *Reviews in Inorganic Chemistry* **36**, 153-181 (2016).

58. I. J. Schalk, M. Hannauer, A. Braud, New roles for bacterial siderophores in metal transport and tolerance. *Environ Microbiol* **13**, 2844-2854 (2011).

59. A. Braud, M. Hannauer, L. A. Mislin Gaëtan, J. Schalk Isabelle, The Pseudomonas aeruginosa Pyochelin-Iron Uptake Pathway and Its Metal Specificity. *Journal of Bacteriology* **191**, 3517-3525 (2009).

60. K. T. Schiessl, E. M.-L. Janssen, S. M. Kraemer, K. McNeill, M. Ackermann, Magnitude and Mechanism of Siderophore-Mediated Competition at Low Iron Solubility in the Pseudomonas aeruginosa Pyochelin System. *Frontiers in Microbiology* **8**, (2017).

61. D. Visaggio *et al.*, A Highly Sensitive Luminescent Biosensor for the Microvolumetric Detection of the Pseudomonas aeruginosa Siderophore Pyochelin. *ACS Sensors* **6**, 3273-3283 (2021).

62. L. J. Liermann, B. E. Kalinowski, S. L. Brantley, J. G. Ferry, Role of bacterial siderophores in dissolution of hornblende. *Geochimica et Cosmochimica Acta* **64**, 587-602 (2000).

63. E. A. Barka *et al.*, Taxonomy, Physiology, and Natural Products of Actinobacteria. *Microbiol Mol Biol Rev* **80**, 1-43 (2015).

64. D. Bellotti, M. Remelli, Deferoxamine B: A Natural, Excellent and Versatile Metal Chelator. *Molecules* **26**, 3255 (2021).

65. D. Eto *et al.*, Divergent effects of desferrioxamine on bacterial growth and characteristics. *The Journal of Antibiotics* **66**, 199-203 (2013).

66. A. A. Roberts, A. W. Schultz, R. D. Kersten, P. C. Dorrestein, B. S. Moore, Iron acquisition in the marine actinomycete genus Salinispora is controlled by the desferrioxamine family of siderophores. *FEMS Microbiology Letters* **335**, 95-103 (2012).

67. H.-S. Lee *et al.*, Cyclic Peptides of the Nocardamine Class from a Marine-Derived Bacterium of the Genus Streptomyces. *Journal of Natural Products* **68**, 623-625 (2005).

68. J. Meiwes, H. P. Fiedler, H. Zähner, S. Konetschny-Rapp, G. Jung, Production of desferrioxamine E and new analogues by directed fermentation and feeding fermentation. *Appl Microbiol Biotechnol* **32**, 505-510 (1990).

69. H.-P. Fiedler, P. Krastel, J. Müller, K. Gebhardt, A. Zeeck, Enterobactin: the characteristic catecholate siderophore of Enterobacteriaceae is produced by Streptomyces species. *FEMS Microbiology Letters* **196**, 147-151 (2001).

70. C. Ferret *et al.*, Siderophore-promoted dissolution of smectite by fluorescent Pseudomonas. *Environ Microbiol Rep* **6**, 459-467 (2014).

71. J. L. Ramos, *Virulence and Gene Regulation*. (Springer US, 2012).

72. P. Visca, in *Virulence and Gene Regulation*, J.-L. Ramos, Ed. (Springer US, Boston, MA, 2004), pp. 69-123.

73. A. Braud, F. Hoegy, K. Jezequel, T. Lebeau, I. J. Schalk, New insights into the metal specificity of the Pseudomonas aeruginosa pyoverdine–iron uptake pathway. *Environ Microbiol* **11**, 1079-1091 (2009).

74. E. Ahmed, S. J. Holmström, The effect of soil horizon and mineral type on the distribution of siderophores in soil. *Geochimica et Cosmochimica Acta* **131**, 184-195 (2014).

75. M. Valdebenito, A. L. Crumbliss, G. Winkelmann, K. Hantke, Environmental factors influence the production of enterobactin, salmochelin, aerobactin, and yersiniabactin in Escherichia coli strain Nissle 1917. *International Journal of Medical Microbiology* **296**, 513-520 (2006).

76. C. Adler *et al.*, The Alternative Role of Enterobactin as an Oxidative Stress Protector Allows Escherichia coli Colony Development. *PLOS ONE* **9**, e84734 (2014).

77. D. R. Peralta *et al.*, Enterobactin as Part of the Oxidative Stress Response Repertoire. *PLOS ONE* **11**, e0157799 (2016).

78. T. Nozoye, The Nicotianamine Synthase Gene Is a Useful Candidate for Improving the Nutritional Qualities and Fe-Deficiency Tolerance of Various Crops. *Frontiers in plant science* **9**, 340-340 (2018).

79. R. M. Boiteau, J. B. Shaw, L. Pasa-Tolic, D. W. Koppenaal, J. K. Jansson, Micronutrient metal speciation is controlled by competitive organic chelation in grassland soils. *Soil Biology and Biochemistry* **120**, 283-291 (2018).

80. B. Stenzler, J. Gaudet, A. J. Poulain, An Anaerobic Biosensor Assay for the Detection of Mercury and Cadmium. *JoVE*, e58324 (2018).

81. Z. Ma, F. E. Jacobsen, D. P. Giedroc, Metal Transporters and Metal Sensors: How Coordination Chemistry Controls Bacterial Metal Homeostasis. *Chemical reviews* **109**, 4644-4681 (2009).

82. G. Porcheron, A. Garénaux, J. Proulx, M. Sabri, C. M. Dozois, Iron, copper, zinc, and manganese transport and regulation in pathogenic Enterobacteria: correlations between strains, site of infection and the relative importance of the different metal transport systems for virulence. *Frontiers in Cellular and Infection Microbiology* **3**, 90 (2013).

83. S. Octavia, R. Lan, in *The Prokaryotes: Gammaproteobacteria*, E. Rosenberg, E. F. DeLong, S. Lory, E. Stackebrandt, F. Thompson, Eds. (Springer Berlin Heidelberg, Berlin, Heidelberg, 2014), pp. 225-286.

84. R. M. Boiteau *et al.*, Siderophore profiling of co-habitating soil bacteria by ultra-high resolution mass spectrometry. *Metallomics* **11**, 166-175 (2019).

85. V. Rai, N. Fisher, O. W. Duckworth, O. Baars, Extraction and Detection of Structurally Diverse Siderophores in Soil. *Frontiers in Microbiology* **11**, (2020).

86. D. İ. Kurtböke, in *Biology and Biotechnology of Actinobacteria*, J. Wink, F. Mohammadipanah, J. Hamedi, Eds. (Springer International Publishing, Cham, 2017), pp. 123-149.

87. K. Choon-Mee, P. Yong-Jin, S. Sung-Heui, A Widespread Deferoxamine-Mediated Iron-Uptake System in Vibrio vulnificus. *The Journal of Infectious Diseases* **196**, 1537-1545 (2007).

88. F. Jalilehvand, N. S. Sisombath, A. C. Schell, G. A. Facey, Lead(II) complex formation with L-cysteine in aqueous solution. *Inorganic chemistry* **54**, 2160-2170 (2015).

89. F. Jalilehvand, B. O. Leung, V. Mah, Cadmium(II) complex formation with cysteine and penicillamine. *Inorganic chemistry* **48**, 5758-5771 (2009).

90. D. L. a. Parkhurst, *Description of input and examples for PHREEQC version 3--a computer program for speciation, batch-reaction, one-dimensional transport, and inverse geochemical calculations*. (Reston, Virginia : U.S. Department of the Interior, U.S. Geological Survey, 2013., 2013).

91. Y. Song *et al.*, Toward an Internally Consistent Model for Hg(II) Chemical Speciation Calculations in Bacterium–Natural Organic Matter–Low Molecular Mass Thiol Systems. *Environmental Science & Technology* **54**, 8094-8103 (2020).

92. R. Banakar *et al.*, Phytosiderophores determine thresholds for iron and zinc accumulation in biofortified rice endosperm while inhibiting the accumulation of cadmium. *J Exp Bot* **68**, 4983-4995 (2017).

93. M. T. Ringel, T. Brüser, The biosynthesis of pyoverdines. *Microb Cell* **5**, 424-437 (2018).

94. M. Petrik *et al.*, Imaging of Pseudomonas aeruginosa infection with Ga-68 labelled pyoverdine for positron emission tomography. *Scientific reports* **8**, 1-9 (2018).

95. I. L. Lamont, P. A. Beare, U. Ochsner, A. I. Vasil, M. L. Vasil, Siderophore-mediated signaling regulates virulence factor production in Pseudomonasaeruginosa. *Proc Natl Acad Sci U S A* **99**, 7072-7077 (2002).

96. E. Banin, M. L. Vasil, E. P. Greenberg, Iron and Pseudomonas aeruginosa biofilm formation. *Proc Natl Acad Sci U S A* **102**, 11076-11081 (2005).

97. C. Adler *et al.*, Catecholate siderophores protect bacteria from pyochelin toxicity. (2012).

98. E. Butaitė, J. Kramer, S. Wyder, R. Kümmerli, Environmental determinants of pyoverdine production, exploitation and competition in natural Pseudomonas communities. *Environ Microbiol* **20**, 3629-3642 (2018).

99. L. Semenec *et al.*, Adaptive Evolution of Geobacter sulfurreducens in Coculture with Pseudomonas aeruginosa. *mBio* **11**, e02875-02819 (2020).

100. L. Semenec *et al.*, Deciphering the electric code of Geobacter sulfurreducens in cocultures with Pseudomonas aeruginosa via SWATH-MS proteomics. *Bioelectrochemistry* **119**, 150-160 (2018).

101. M. S. Cortese *et al.*, Metal chelating properties of pyridine-2,6-bis(thiocarboxylic acid) produced by Pseudomonas spp. and the biological activities of the formed complexes. *Biometals* **15**, 103-120 (2002).

102. C. S. Eckley *et al.*, The assessment and remediation of mercury contaminated sites: A review of current approaches. *Sci Total Environ* **707**, 136031-136031 (2020).

103. R. Dixit *et al.*, Bioremediation of Heavy Metals from Soil and Aquatic Environment: An Overview of Principles and Criteria of Fundamental Processes. *Sustainability* **7**, 2189-2212 (2015).

104. P. Bararunyeretse, Y. Zhang, H. Ji, Molecular Biology-Based Analysis of the Interactive Effect of Nickel and Xanthates on Soil Bacterial Community Diversity and Structure. *Sustainability* **11**, (2019).

105. J. Labuda, M. Skatulokova, M. Nemeth, S. Gergely, Formation and stability of diethyldithiocarbamate complexes. *Chem. zvesti* **38**, 597 (1984).

106. T. Y. a. M. Nanjo, Studies of Xanthate Complexes by Solubility Method. *Science reports of the Research Institutes, Tohoku University* **21**, 45-62 (1969).

107. J. M. Lo, J. C. Yu, F. I. Hutchison, C. M. Wai, Solvent extraction of dithiocarbamate complexes and back-extraction with mercury(II) for determination of trace metals in seawater by atomic absorption spectrometry. *Analytical Chemistry* **54**, 2536-2539 (1982).

108. V. S. Sastri, K. I. Aspila, C. L. Chakrabarti, Studies on the solvent extraction of metal dithiocarbamates. *Can J Chem* **47**, 2320-2323 (1969).

109. J. A. Gideon, The separation of ionic and organic mercury from water using milk proteins, xanthates and keratin. **Master's Thesis, Virginia Polytechnic Institute and State University**, (1971).

110. X. Liang *et al.*, Stepwise Reduction Approach Reveals Mercury Competitive Binding and Exchange Reactions within Natural Organic Matter and Mixed Organic Ligands. *Environmental Science & Technology* **53**, 10685-10694 (2019).

111. L. Zhao *et al.*, Contrasting Effects of Dissolved Organic Matter on Mercury Methylation by Geobacter sulfurreducens PCA and Desulfovibrio desulfuricans ND132. **51**, 10468-10475 (2017).

112. Y.-R. Liu *et al.*, Effects of Cellular Sorption on Mercury Bioavailability and Methylmercury Production by Desulfovibrio desulfuricans ND132. *Environmental Science & Technology* **50**, 13335-13341 (2016).

113. L. Gerhardsson, G. Kazantzis, in *Handbook on the Toxicology of Metals (Fourth Edition)*, G. F. Nordberg, B. A. Fowler, M. Nordberg, Eds. (Academic Press, San Diego, 2015), pp. 487-505.

114. A. Oskarsson, Dithiocarbamate-induced redistribution and increased brain uptake of lead in rats. *Neurotoxicology* **5**, 283-293 (1984).

115. Y. Peng *et al.*, Nanoscale Copper(II)–Diethyldithiocarbamate Coordination Polymer as a Drug Self-Delivery System for Highly Robust and Specific Cancer Therapy. *Molecular Pharmaceutics* **17**, 2864-2873 (2020).

7.6 Acknowledgments

Funding:

This work was funded by an NSERC discovery grant, an Early Researcher Award from the

Province of Ontario, and an NSERC Accelerator Grant funding to AJP.

Author contributions:

A.J.P. supervised the project. B.R.S., R.Z, and A.J.P. designed the research and methodologies.

B.R.S and R.Z performed the experiments. B.R.S and A.J.P. performed analyses on the data.

B.R.S and A.J.P wrote the paper.

Competing interests:

The authors declare that they have no known competing interests.

Chapter 8: Synthesis

8.1 Summary of Research contributions

My thesis expands the framework of mechanisms governing Hg^{II} bioavailability to anaerobic microbes. I accomplished this by designing an anaerobic microbial biosensor that can detect Hg. When Hg^{II} transitions to anoxic conditions where it is methylated, it can be subject to ligand exchanges with ligands that have subsequential higher affinities to Hg^{II} unless Hg speciation is reset (through reduction to Hg^0) along the way. Creating a biosensor that did not require oxygen either for biosensor growth or to produce a signal opened up the possibility of addressing Hg bioavailability under various redox conditions that are relevant for Hg transformations.

The objective of **chapter 2** was to develop a microbial Hg-biosensor that functions independent of the presence of oxygen. I achieved this by fusing a gene encoding the flavin-based fluorescent protein to the transcriptional regulator of the *mer* operon (*merR*) on a plasmid and transforming it into *E. coli*.

Some of the first ligands to control Hg speciation are halides. Hg^0 is oxidized to Hg^{II} by halides through Atmospheric Mercury Depletion Events (AMDE) (*1, 2*) or in marine waters (*3*), which brings them into an aquatic system. Hg is methylated in conditions where halides will control speciation, such as polar snow (*4*), Antarctic sea ice (*5*), or in the open ocean water column (*6-8*). These post-oxic zones exhibit low oxygen/sulfide concentrations and host anaerobic metabolisms (*9*). Hg^{II} halide species and conditions such as pH have already been tested aerobically with Hg-biosensors, making them ideal to see if I can replicate previously published data under anaerobic conditions (NO_3^- respiration).

In **chapter 2**, I validated the biosensor with Hg^{II} species and conditions found in the oxic/pot-oxic zones of the water. One hypothesis I addressed was that negatively charged Hg^{II} species were unavailable to microbes (e.g., $HgCl_3^-$ and $HgCl_4^{2-}$). Aerobically I replicated the results of previous studies and demonstrated that they were not bioavailable. However, when tested anaerobically, $HgCl_4^{2-}$ was highly bioavailable to the biosensor. Here I provide evidence for the hypothesis that different transport pathways for Hg can exist in an organism based on its metabolism; aerobic or anaerobic. Evidently, some negatively charged Hg^{II} species are bioavailable.

I further attempted to tease apart the pathways $HgCl_4^{2-}$ of Hg bioavailability and that of other negatively charged inorganic Hg^{II} species. I provide evidence of distinct transport pathways for neutral Hg^{II} species ($Hg(OH)_2$) and negatively charged Hg species ($HgCl_4^{2-}$) by performing metal competition experiments. I provide evidence that compression of the negatively charged double layer of a cell surface through changes in ionic strength and pH, limited anionic exclusion and may allow negatively charged Hg^{II} species to access the membrane for transport. Lastly, my results also support the hypothesis that increasing reversible sorption of Hg^{II} onto the cell membrane is a necessary step in Hg^{II} bioavailability.

There are plenty of studies showing the interactions between cell membranes and metal species based on changes in ionic strength. However, my research is unique as, to date, it is the only study that incorporates changes in ionic strength and the bioavailability of various inorganic Hg^{II} species. This research demonstrates a potential pathway to explain Hg methylation in environments such as marine systems such as the oxygen-deficient zone in the oceanic water column, sea ice, or polar snow. This pathway may become more prominent with climate change.

With a melting arctic, this is poised to release thousands of years of accumulated Hg^{II} bound up in halides from AMDE into the environment (*10*).

One key observation that I did not address in this chapter was the comparative bioavailability of Hg(II)-halides. There was a notable decrease in bioavailability for all halides when increasing halide (X) concentrations to change Hg^{II} speciation from HgX_2 to HgX_3^-. However, when increasing halide concentration to change Hg speciation from HgX_3^- to HgX_4^{2-} only the halides Cl and I increased Hg^{II} bioavailability, Br did not. It would be reasonable to assume that going down periodic table periods with increasing sizes of complexes (Cl<Br<I) would produce a trend. The fact that this skips a period is perplexing. I would be curious to investigate this further, but negatively charged Hg(II)-Br/I complexes are not environmentally relevant.

After publishing **chapter 2,** I was invited by an editor of the Journal of Visualized Experiments to write a more detailed methods paper describing how to utilize the biosensor I developed. In **chapter 3,** I give a more detailed methodological approach on how to use the Hg-biosensor. I further expand on the biosensor's capabilities by showing it can detect Cd in addition to Hg. Due to the limitations and scope of a methods paper, I could not discuss specific results. In this paper, I showed that increasing concentrations of Mg^{2+} would lower Hg^{II} bioavailability until it reached a plateau at 1 mM. Mg^{2+} is an essential nutrient for microbes but also stabilizes cell membranes. Cell membranes are polyanionic surfaces. Ca^{2+} and Mg^{2+} stabilize it by cross-linking carboxylated and phosphorylated head groups of lipids (*11*). A previous study from our lab using Hg-biosensors has demonstrated that divalent cations can limit Hg^{II} bioavailability (*12*) but are unlikely to compete for transport sites (*13*). These results indicate that stabilized cell membranes, through the addition of divalent cations, are less permeable to Hg^{II}. Therefore,

restricting pathways to reach the transport sites on the inner membrane may lower Hg^{II} bioavailability.

The next step was to determine how dissolved organic matter (DOM) affects Hg bioavailability. Halides may initially complex Hg^{II} entering a system, but DOM will outcompete them for Hg speciation (*14-16*). There are a lot of studies addressing DOM and Hg^{II} bioavailability. Still, the relationship between microbial Hg uptake and algal DOM remains largely unexplored. Algal primary producers generate the substrate of the oxic/anoxic interface that incorporates Hg methylating microbes such as in biofilms (*17, 18*). They directly impact Hg methylating microbes by supplying labile DOM that affects community structure and methylation rates (*19-29*). Therefore, in **Chapter 4**, I take a reductionist approach to understand how primary algal producers affect Hg bioavailability. This was done in collaboration with Vaughn Mangal during his Ph.D. at Trent University.

In chapter 4, I obtained DOM freshly harvested from a diverse set of primary producers of the divisions Chlorophyta (*Scenedesmus obliquus, Chlorella vulgaris, Chlamydomonas reinhardtii*) and Euglenozoa (*Euglena gracilis* and *Euglena mutabilis*). These algal species are common in various aquatic systems, including biofilms associated with high Hg methylation rates (*30-32*). Using the biosensor aerobically and anaerobically, I show that as little as 0.1 ppm decreased Hg^{II} uptake by 50–90% depending on the DOM source. The exception was DOM from *E. gracillis* that did not inhibit Hg^{II} bioavailability with increasing DOM concentrations. These results demonstrate how specific algal species in an ecosystem can directly affect Hg^{II} bioavailability to organisms. Algal species in an ecosystem are poised to change with a changing world that can affect Hg^{II} bioavailability in an ecosystem. Rising ocean temperatures and eutrophication will alter algal community structures, changing labile DOM pools (*33-35*).

The next objective was to identify the DOM's specific parts and functional groups that affected Hg^{II} bioavailability. We used asymmetrical flow field-flow fractionation (AF4) to separate DOM based on molecular weight. While 1 ppm of unfractionated DOM from all algae significantly inhibited Hg^{II} bioavailability ($p < 0.05$) (except *E. gracillis)*, the process of fractionating the DOM led to an overall increase in Hg uptake in all algae tested. Therefore it is likely that processes leading to fractionation of algal DOM in the environment, such as photo/microbial degradation, may trigger periods of increased microbial Hg^{II} uptake.

We then combined the biosensor data with high-resolution mass spectrometry (Fourier transform ion cyclotron resonance mass spectrometry) to gather DOM compositional information. We show that glutamine/serine transformations were positively correlated (R^2 = 0.68, p = 0.001/R^2 = 0.45, p = 0.01) with Hg bioavailability aerobically. Anaerobically, Hg uptake was positively corelated to Polyamine (R^2 = 0.60, p = 0.001), cytosine (R^2 = 0.45, p = 0.01), and glutamine (R^2 = 0.40, p = 0.001), transformations. Carboxylic (COOH) transformations were exponentially but negatively correlated (R^2 = 0.57, p = 0.001) with anaerobic Hg^{II} uptake.

This study highlights an emergent property of DOM, where different biomolecules that comprise the complex DOM pool interact to affect metal uptake. The DOM components alone of may not have the same inhibition effect on bioavailability we observe. To the best of our knowledge, the role of such emergent properties of DOM on Hg^{II} bioavailability remains poorly understood.

The biosensor up until **chapter 4** was limited to detecting Hg^{II} using aerobic respiration and anaerobic metabolism using NO_3^- as a terminal electron acceptor. These are redox conditions at the oxic/post-oxic interface but not representative of the metabolisms conducive to Hg

methylation. These conditions are conducive for inorganic ligands like DOM and halides, but because of thermodynamics, the most stable form of sulfur is oxidized (e.g., SO_4^{2-}), limiting potential thiol concentrations. Thiols will be found under all redox conditions, but working under thermodynamically relevant conditions is ideal. Hg methylation is performed by iron and sulfate-reducing microbes and methanogenic archaea, which occupy more reducing conditions in the post-oxic, sulfidic and methanic zones. In **chapter 5**, I delve deeper into more reduced conditions and thoroughly expand the genetic and metabolic capabilities of the biosensor.

In **chapter 5**, together with my colleague Aaron Hinz, we developed an efficient molecular biology method to rapidly generate biosensor constructs in *E. coli* based on Golden Gate assembly (*36*). Here we produced constitutive, Hg inducible and As inducible genetic constructs fused to various reporter sequences; yellow fluorescent protein, mCherry, bacterial luciferase, and an anaerobically active flavin-based fluorescent protein. I subsequentially validated and optimized each of these biosensors. I was able to expand the metabolic capabilities of the biosensors to produce a signal from flavin-based fluorescent proteins while respiring on fumarate. This is a metabolism common among microorganisms that carry out environmental mercury methylation (37-39). In addition, I developed the first anaerobic biosensor for the detection of arsenic. Going forward, I am now able to address the bioavailability of Hg^{II} with ligands under metabolisms that will persist in highly reduced environments.

In **Chapter 6**, I followed Hg^{II} into highly reduced environments characteristic of low molecular weight thiols and cryptic H_2S cycling. Hg^{II} has a high affinity for reduced sulfur (S) moieties (e.g., thiols and sulfide), and their role on Hg^{II} bioavailability has been largely explored (*40, 41*). However, studies that explore Hg^{II} bioavailability typically focus on single ligand systems. Using simple ligand systems to understand Hg^{II} bioavailability is essential for building

conceptual models, but Hg^{II} speciation is dynamic with constant series of ligand exchanges. When some Hg^{II} thiol species are bioavailable and others are not, the mechanism governing Hg^{II} bioavailability is unclear. The objective was to test if a dynamic equilibrium of competing thiols can facilitate Hg^{II} bioavailability. Where the change in Hg speciation can facilitate Hg bioavailability.

First I determined which thiols enhanced or inhibited Hg^{II} bioavailability. My results support that Hg^{II} bioavailability is highly dependent on speciation. They also indicate that Hg^{II} complexation with the cell membrane is necessary for bioavailability. From here, I identified both non-bioavailable and bioavailable species to perform ligand exchanges. Continuing in **chapter 6**, I tested my hypothesis that ligand exchanges would promote Hg^{II} bioavailability. I altered Hg^{II} speciation from a non-bioavailable Hg(II)-thiol species to form a bioavailable Hg(II)-thiol species by performing ligand exchanges (e.g., $Hg(GSH)_2 \rightarrow Hg(Pen)_2$). Interestingly, changing the Hg^{II} speciation could not rescue bioavailability. My results indicate that Hg^{II} is not achieving the thermodynamic equilibrium predicted by models. The system likely has emergent properties that prevent changing Hg^{II} speciation to affect bioavailability. This phenomenon may also be a result of the limitations to modeling parameters. However, by performing these experiments, I serendipitously discovered the role of H_2S diffusion on Hg^{II} bioavailability.

As I am writing this, this is the first study to address the role of H_2S diffusion on Hg^{II} bioavailability. I demonstrated how the biosensor could cleave cysteine to H_2S, rapidly diffusing away from the production site in a 96 well microplate and affecting Hg^{II} speciation in remote wells. The diffusion was rapid and made otherwise completely non-bioavailable Hg^{II} species in the other wells highly bioavailable within minutes. In real-time, I observe H_2S diffusion, altering

Hg^{II} speciation and the immediate effect this process has on Hg^{II} bioavailability. H_2S is highly volatile, and in my research, I show how microbes can use it to access inaccessible/sequestered Hg^{II} locally and in neighboring redox zones. This experimental design demonstrates specific advantages to measuring bioavailability using Hg biosensors. The biosensor can detect Hg^{II} bioavailability within minutes. I provide a unique perspective of how fast these Hg^{II} transformations are occurring to make it bioavailable.

One of the reoccurring messages from my thesis is how microbes can control Hg^{II} bioavailability to each other; algal DOM in **Chapter 4**, or biogenic H_2S production and cryptic H_2S cycling in **Chapter 6**. However, I also gained insight into the effect of cryptic methane cycling on Hg^{II} bioavailability. Methane generated through methanogenesis will diffuse to other redox zones where microbes subsequentially oxidize it (*42*). While methane itself is unlikely to interact with Hg^{II}, the methanotrophs that use methane as their carbon/electron source will. One of the thiols tested in **Chapter 6** was the chalcophore methanobactin (MB) from the methanotroph *Methylosinus trichosporium* OB3b. I demonstrated how MB can sequester Hg^{II} and how only diffuse H_2S was able to liberate it. MB is secreted by methanotrophs to acquire copper (43) but is not specific to copper, and Hg^{II} can be internalized through MB transport systems (*44*). There are many metal acquisition pathways in nature, and like MB, not entirely specific to the metal they are trying to access. These complex microbial/ligand interactions demonstrating the interplay of post-oxic, sulfidic, and methanic zones on Hg^{II} bioavailability are summarized in Figure 8.1.

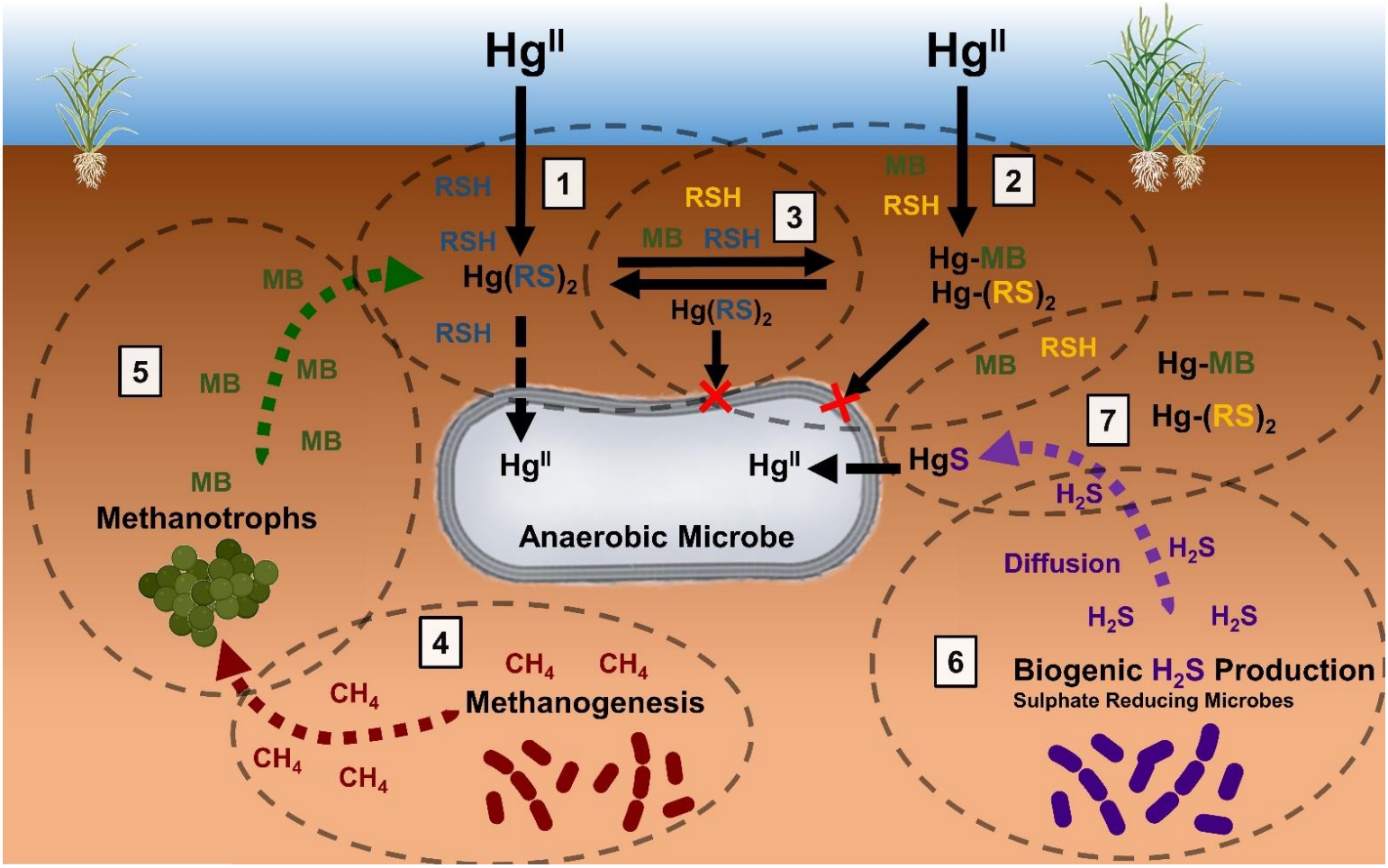

Figure 8.1: Thiolated ligand and microbial interactions control Hg^{II} bioavailability to anaerobic microbes. In microbial communities where Hg methylation occurs, many different ligands compete for Hg^{II} speciation that controls bioavailability indicative of different redox zones. Each circle contains different ligands/metabolites: RSH (thiols), MB (the chalcophore, methanobactin), CH_4 (methane), and H_2S (hydrogen sulfide). **1)** Hg^{II} binds to thiols, forming a Hg(II)-thiol complex ($Hg(RS)_2$) that is bioavailable to an anaerobic microbe. These thiols include cysteine and penicillamine. **2)** Hg^{II} may also form non-bioavailable $Hg(RS)_2$ species with thiols such as MB or glutathione. **3)** Thiols constantly exchange Hg^{II} in a dynamic equilibrium, where both bioavailable and non-bioavailable Hg^{II} species are present. However, this dynamic equilibrium does not facilitate bioavailability from non-bioavailable $Hg(RS)_2$ complexes. However, processes facilitated by microbial communities will affect Hg^{II} bioavailability. **4)** Methanogens will generate CH_4 from methanogenesis **5**) which is used as a substrate used by methanotrophic bacteria. These bacteria secrete MB to acquire copper, but MB will also form complexes with Hg^{II} (**5 to 1 to 3)**. These Hg-MB complexes are not always bioavailable to other microbes. **6)** Microbes, particularly sulfate-reducing bacteria, will generate biogenic H_2S that can diffuse into other ligand systems. **7)** H_2S will rapidly outcompete other thiols for Hg^{II} to form highly bioavailable Hg(II)-sulphides (HgS). H_2S ligand exchange makes an otherwise non-bioavailable Hg^{II} species immediately accessible to microbes.

In Chapter 7, I demonstrated how pathways associated with iron acquisition could be a potential mechanism for microbes to access Hg^{II}. Hg^{II} is not only sequestered by DOM in post-oxic conditions but is easily sorbed and incorporated into the structures of iron-oxide minerals (*39, 45-51*). Iron-oxide minerals have a multifaceted role in Hg bioavailability to Hg-methylating microbes. i) they readily sorb and incorporate Hg preventing bioavailability (*39, 47-51*), and ii) provide a necessary substrate and TEM for Hg-methylating microbes (*39, 46, 52*). Several processes can release Hg^{II} from these structures, typically involving the reductive dissolution of the mineral, Hg^{II} reduction, or mineral leaching. These processes usually require reducing agents, microbial metabolisms, or sulfidic conditions (*39, 45, 46, 53, 54*). Iron, however, is an essential metal but is not bioavailable as an insoluble oxide. Microbes have developed strategies to acquire iron from insoluble oxides by secreting siderophores. These chelate and solubilize ferric iron (Fe^{III}). The Fe^{III}-siderophore complex is then transported into the cell via siderophore-specific transport pathways (*55-58*). The objective of this study was to determine if this strategy to acquire iron would inadvertently affect Hg^{II} bioavailability to the biosensor. I tested siderophores widely found in nature and siderophores compatible with *E. coli*'s transport pathways. The transport machinery in *E. coli* is well-documented, allowing me to test potential Hg^{II} transport through these systems.

My results demonstrated that almost every siderophore tested affected Hg^{II} bioavailability. First, I tested siderophores *E. coli* had known transport systems for; enterobactin (Ent), desferrioxamine B (DFOB), citrate and ferrichrome. Both Ent and DFOB affected Hg^{II} bioavailability to the biosensor. 1 nM Ent increased bioavailability by 50%, and increasing concentrations of both siderophores reduced bioavailability. It is possible that Hg^{II} can hijack these transport systems, providing alternate pathways for Hg^{II} bioavailability in *E. coli*. This

hypothesis needs to be further tested by determining if these siderophore complexes have an affinity to the siderophore transporter. Some siderophores, ferrichrome, and citrate, did not have an impact on Hg^{II} bioavailability.

I then tested siderophores *E. coli* did not have transport pathways for; nicotianamine (NA), pyochelin (Pch), desferrithiocin (DFT), and pyoverdines (Pyo). There was no cut and dry contrast between siderophores *E. coli* had transport systems for and other siderophores. Ent, NA, Pch, and DFT will enhance Hg^{II} bioavailability at low concentrations of siderophore. However, increasing Ent, NA, DFOB, DFT, and Pyo concentrations will limit Hg^{II} bioavailability. The effect of Pyo was fascinating. Low concentrations inhibited Hg^{II} bioavailability and exhibited toxic effects on the biosensor.

The siderophores that affected Hg^{II} bioavailability are produced predominantly by Enterobacteriaceae, *Pseudomonas*, and *Streptomyces.* These are found everywhere in the environment and likely have a role in the Hg cycle. Each siderophore and the microbes that produce them have unique roles in ecology. This work opens up the possibility for Hg^{II} acquisition through siderophore-specific transport pathways and how microbes can influence Hg^{II} bioavailability to each other. Iron homeostasis is essential in all living organisms, and microbes may use processes associated with iron acquisition to inadvertently incorporate Hg^{II} and control its bioavailability.

For the second objective of **chapter 7**, I investigated how the two emerging contaminants, ethyl xanthate and diethyldithiocarbamate (DDTC) affected Hg^{II} bioavailability. These two compounds are extensively used in the mining industry as a floatation agent but are regularly discharged into the environment and have become an ecological and health concern

(*59*). These compounds make Hg^{II} bioavailable to the biosensor. They also form bioavailable species regardless of ligand concentration. In **Chapter 6,** I covered Hg^{II} bioavailability in the presence of two other anthropogenic ligands, BAL and DMSA. Both are dithiols that bind Hg^{II} with the same coordination (*60, 61*). Hg^{II} bound to BAL was highly bioavailable, which directly contrasted with DMSA that completely inhibited Hg^{II} bioavailability (in almost equimolar concentrations to Hg^{II}). Similar to ethyl xanthate and DDTC, BAL is highly lipophilic and can diffuse through membranes, while DMSA is not due to its negative charge at neutral pH (*62-65*). It is unclear if these Hg^{II} species are bioavailable through passive diffusion, but the data suggest so. It is theoretically possible for neutrally charged, low molecular weight, inorganic/non-sulfide Hg^{II} species to diffuse through a membrane passively. However, there is limited evidence supporting this process being significant (*66*). Ligands that form lipophilic Hg^{II} species capable of diffusing into a microbial cell may be problematic. These ligands are not naturally occurring and can provide alternate pathways for Hg^{II} bioavailability that might overwise not be present.

8.2 Limitation and recommendations

In my thesis, I develop conceptual models describing Hg^{II} bioavailability to *E. coli.* While Hg-methylation is a process that occurs over multiple domains of life (*41*), *E. coli* is exceptionally useful as a model organism. *E. coli* do not methylate Hg, limiting environmental implications. Developing biosensors in Hg-methylating microbes was the initial goal when starting my thesis. However, the technology to use anaerobic biosensing circuits was not established when I started my thesis. Initially, I was able to get the biosensor to produce a signal on aerobic and nitrate respiration. It took a while, in **chapter 5**, to be able to figure out how to get the biosensor to produce a signal when respiring fumarate—simultaneously developing a framework to build

biosensor constructs rapidly. Fumarate is a highly reduced terminal electron acceptor commonly by Hg-methylating microbes (sulfate and iron-reducing bacteria and methanogens) (37-39). Genetic systems for Hg-methylating microbes to potentially make biosensors have recently been developed. Particularly for the sulfate-reducing bacteria *Geobacter sulfurreducens (67, 68). These systems also have potential in archaea too and are being developed for archaea* (*69*). My thesis provides the framework and proof of concept to build Hg-biosensors in these organisms.

In my thesis, I noticed a phenomenon that alters Hg^{II} bioavailability based on microbial metabolism. I did not directly address this over the progression of my thesis but instead focused on ligands that would be present under each redox condition. In **chapter 2**, I show that $HgCl_4^{2-}$ is not bioavailable to *E. coli* respiring aerobically but is highly bioavailable when respiring on nitrate. In **chapter 6,** I found that increasing concentrations of Pen and Cys could not inhibit Hg^{II} bioavailability to the biosensor respiring on fumarate. Contrasting this observation, increasing concentrations of Cys completely inhibited Hg^{II} bioavailability to the biosensor when respiring on nitrate (*70*). A previous study demonstrated increasing concentrations of Pen inhibited Hg^{II} bioavailability to an *E. coli* biosensor aerobically (*71*). Alternate transporters may be expressed under various microbial metabolisms that can differentially affect Hg^{II} bioavailability. Hg^{II} enters the cell through non-specific metal ion transporters when bound to thiols (*13, 37*). There are also many different metal ion transporters in *E.* coli, a lot of which are controlled by different metabolisms and redox conditions (*72, 73*). It is unclear which transporters Hg^{II} is using to enter the cell or if it is even using a metal transporter. It is possible that *E. coli* expresses transporters (or transport machinery) that are more effective at competing for Hg^{II} through ligand exchange under more reducing conditions.

This phenomenon might also be explained by the increased expression of thiol sites on the cell membrane. Reversible sorption of Hg^{II} to thiols on the membrane is likely an essential step in the Hg^{II} bioavailability process (*71, 74-76*). The expression of thiols on the cell membrane is an intrinsic property of bacterial membranes (gram-negative and gram-positive) (*75*). Different factors will alter the expression of thiols concentrations on a cell membrane of microbes. Membrane thiol concentrations will increase when the bacteria are given more electron donors (i.e., glucose), or its metabolism uses a more reduced electron acceptor (*77, 78*). While fumarate reduction will increase concentrations of membrane thiols as opposed to nitrate reduction and aerobic respiration for *Shewanella oneidensis* (*76*), very little is still known about how metabolism using different substrates can affect the expression of membrane thiols. Differential metabolisms based on carbon sources and redox conditions will likely affect the expression of thiols sites on a membrane that may alter Hg^{II} bioavailability in the same organism. As of writing this, this has yet to be addressed, especially in Hg-methylating microbes. These microbes are metabolically diverse, and different environmental conditions may alter Hg^{II} to the same organism by changing their physiology.

One of the limitations in my thesis is the extent to which thermodynamic modeling can accurately predict speciation. I used many of these to tease apart mechanisms regarding the bioavailability of various Hg^{II} species. Without a doubt, calculating Hg^{II} species is essential to develop conceptual models and hypotheses, but these need to be taken with a grain of salt. As David Rickard put phrases elegantly in his book, *Sulfidic Sediments and sedimentary rocks*, "It is all too easy to run a computer-based equilibrium computation engine and get what appears to be a meaningful result. In fact, the acronym GIGO of the early computing business applies directly to this area of science: Garbage In, Garbage Out." (*79*). The understanding of Hg speciation in

solution has come a long way over decades of research, of which there is an extensive history of refining these equilibrium constants (*80*). The typical approach to developing constants for a new chemical species is to first 'imagine' the species and then provide evidence that it exists. This system is problematic since it requires the burden of proof, and it is very difficult to prove something does not exist. Science can only falsify hypotheses and in this process, approach understanding the "truth". For instance, recent research has identified that the free sulfide anion (S^{2-}) that has been widely used in calculations determining aqueous metal speciation for decades does not exist (*81*). Even though the speciation and calculations are 'wrong' does not mean the phenomenon they are measuring is not. One can plug in the numbers for the free sulfide anion and get the right mineral solubilities, gas exchanges and have some reliable metric of what is going on.

Modern methodologies have advanced considerably over the years to refine equilibrium constants, making thermodynamic modeling a much more reliable tool. These studies combine in silico approaches such as quantum computing and density functional theory with liquid chromatography, mass spectrometry, and EXAFS spectroscopy measurements (*74*, *82-86*). There are still many ligands with non-refined equilibrium constants, and modeling Hg^{II} speciation using them is not inherently useful. Their uncertainty can skew Hg^{II} speciation distributions over orders of magnitude of ligand concentration (80, 86). Hg^{II} speciation is dynamic and in a constant state of ligand exchanges where equilibrium is seldom reached—modeling these mixed ligands is challenging. Novel ligands are also constantly being revealed and can potentially influence Hg^{II} speciation, bioavailability, and the Hg cycle. Isolating these compounds and testing interactions that may not exist is rather gratuitous when in silico approaches can warrant

their investigation. Going forward, thermodynamic modeling has a long way to go, but the potential to advance the field is limitless.

8.3 References

1. T. A. Douglas *et al.*, The fate of mercury in Arctic terrestrial and aquatic ecosystems, a review. *Environmental Chemistry* **9**, 321-355 (2012).

2. S. E. Lindberg *et al.*, Dynamic Oxidation of Gaseous Mercury in the Arctic Troposphere at Polar Sunrise. *Environmental Science & Technology* **36**, 1245-1256 (2002).

3. M. Yamamoto, Stimulation of elemental mercury oxidation in the presence of chloride ion in aquatic environments. *Chemosphere* **32**, 1217-1224 (1996).

4. C. Larose *et al.*, Springtime changes in snow chemistry lead to new insights into mercury methylation in the Arctic. *Geochimica et Cosmochimica Acta* **74**, 6263-6275 (2010).

5. C. M. Gionfriddo, M. T. Tate, R. R. Wick, Microbial mercury methylation in Antarctic sea ice. **1**, 16127 (2016).

6. D. Cossa *et al.*, The open sea as the main source of methylmercury in the water column of the Gulf of Lions (Northwestern Mediterranean margin). *Geochimica et Cosmochimica Acta* **199**, 222-237 (2017).

7. C. T. Driscoll, R. P. Mason, H. M. Chan, D. J. Jacob, N. Pirrone, Mercury as a Global Pollutant: Sources, Pathways, and Effects. *Environmental Science & Technology* **47**, 4967-4983 (2013).

8. B. Braune *et al.*, Mercury in the marine environment of the Canadian Arctic: Review of recent findings. *Science of The Total Environment* **509–510**, 67-90 (2015).

9. C. C. Gilmour *et al.*, Mercury Methylation by Novel Microorganisms from New Environments. *Environmental Science & Technology* **47**, 11810-11820 (2013).

10. P. F. Schuster *et al.*, Permafrost Stores a Globally Significant Amount of Mercury. *Geophysical Research Letters* **45**, 1463-1471 (2018).

11. L. A. Clifton *et al.*, Effect of Divalent Cation Removal on the Structure of Gram-Negative Bacterial Outer Membrane Models. *Langmuir* **31**, 404-412 (2015).

12. V. Daguené *et al.*, Divalent Base Cations Hamper HgII Uptake. *Environmental Science & Technology* **46**, 6645-6653 (2012).

13. J. K. Schaefer, A. Szczuka, F. M. M. Morel, Effect of Divalent Metals on Hg(II) Uptake and Methylation by Bacteria. *Environmental Science & Technology* **48**, 3007-3013 (2014).

14. H. Zhong, W.-X. Wang, Controls of Dissolved Organic Matter and Chloride on Mercury Uptake by a Marine Diatom. *Environmental Science & Technology* **43**, 8998-9003 (2009).

15. U. Skyllberg, Chemical speciation of mercury in soil and sediment. *Environmental chemistry and toxicology of mercury*, 219-258 (2012).

16. S. Han *et al.*, Mercury Speciation in Marine Sediments under Sulfate-Limited Conditions. *Environmental Science & Technology* **44**, 3752-3757 (2010).

17. P. Dranguet, V. I. Slaveykova, S. Le Faucheur, *Kinetics of mercury accumulation by freshwater biofilms*. (2018), vol. 14.

18. T. A. Olsen, C. C. Brandt, S. C. Brooks, Periphyton biofilms influence net methylmercury production in an industrially contaminated system. *Environmental Science & Technology* **50**, 10843-10850 (2016).

19. K. Toming *et al.*, Contributions of autochthonous and allochthonous sources to dissolved organic matter in a large, shallow, eutrophic lake with a highly calcareous catchment. *Limnology and Oceanography* **58**, 1259-1270 (2013).

20. L. Lambertsson, M. Nilsson, Organic material: the primary control on mercury methylation and ambient methyl mercury concentrations in estuarine sediments. *Environmental science & technology* **40**, 1822-1829 (2006).

21. V. Liem-Nguyen *et al.*, Effects of Nutrient Loading and Mercury Chemical Speciation on the Formation and Degradation of Methylmercury in Estuarine Sediment. *Environmental Science and Technology* **50**, 6983-6990 (2016).

22. A. Drott, L. Lambertsson, E. Björn, U. Skyllberg, Importance of Dissolved Neutral Mercury Sulfides for Methyl Mercury Production in Contaminated Sediments. *Environmental Science & Technology* **41**, 2270-2276 (2007).

23. M. Kim, S. Han, J. Gieskes, D. D. Deheyn, Importance of organic matter lability for monomethylmercury production in sulfate-rich marine sediments. *Science of The Total Environment* **409**, 778-784 (2011).

24. W. L. Lázaro, J. R. D. Guimarães, A. R. Ignácio, C. J. Da Silva, S. Díez, Cyanobacteria enhance methylmercury production: a hypothesis tested in the periphyton of two lakes in the Pantanal floodplain, Brazil. *Science of the Total Environment* **456**, 231-238 (2013).

25. W. L. Lázaro, S. Díez, C. J. da Silva, Á. R. A. Ignácio, J. R. D. Guimarães, Seasonal changes in peryphytic microbial metabolism determining mercury methylation in a tropical wetland. *Science of The Total Environment* **627**, 1345-1352 (2018).

26. S. Gentès, J. Taupiac, Y. Colin, J.-M. André, R. Guyoneaud, Bacterial periphytic communities related to mercury methylation within aquatic plant roots from a temperate

freshwater lake (South-Western France). *Environmental Science and Pollution Research* **24**, 19223-19233 (2017).

27. E. B. Graham *et al.*, Oligotrophic wetland sediments susceptible to shifts in microbiomes and mercury cycling with dissolved organic matter addition. *PeerJ* **6**, e4575-e4575 (2018).

28. A. G. Bravo *et al.*, Molecular composition of organic matter controls methylmercury formation in boreal lakes. *Nature Communications* **8**, 1-9 (2017).

29. G. A. Christensen *et al.*, Carbon Amendments Alter Microbial Community Structure and Net Mercury Methylation Potential in Sediments. *Applied and environmental microbiology* **84**, e01049-01017 (2018).

30. M. Leclerc, D. Planas, M. Amyot, Relationship between Extracellular Low-Molecular-Weight Thiols and Mercury Species in Natural Lake Periphytic Biofilms. *Environ Sci Technol* **49**, 7709-7716 (2015).

31. S. Dasgupta, J. Fang, S. S. Brake, S. T. Hasiotis, L. Zhang, Biosynthesis of sterols and wax esters by Euglena of acid mine drainage biofilms: Implications for eukaryotic evolution and the early Earth. *Chemical Geology* **306-307**, 139-145 (2012).

32. I. Krohn-Molt *et al.*, Metagenome survey of a multispecies and alga-associated biofilm revealed key elements of bacterial-algal interactions in photobioreactors. *Applied and environmental microbiology* **79**, 6196-6206 (2013).

33. I. E. Huertas, M. Rouco, V. López-Rodas, E. Costas, Warming will affect phytoplankton differently: evidence through a mechanistic approach. *Proceedings of the Royal Society B: Biological Sciences* **278**, 3534-3543 (2011).

34. L. Bopp, O. Aumont, P. Cadule, S. Alvain, M. Gehlen, Response of diatoms distribution to global warming and potential implications: A global model study. *Geophysical Research Letters* **32**, (2005).

35. H. W. Paerl *et al.*, Mitigating cyanobacterial harmful algal blooms in aquatic ecosystems impacted by climate change and anthropogenic nutrients. *Harmful Algae* **54**, 213-222 (2016).

36. A. J. Hinz, B. Stenzler, A. J. Poulain, A. Bose, Golden Gate Assembly of Aerobic and Anaerobic Microbial Bioreporters. *Applied and Environmental Microbiology* **88**, e01485-01421 (2022).

37. J. K. Schaefer *et al.*, Active transport, substrate specificity, and methylation of Hg(II) in anaerobic bacteria. *Proceedings of the National Academy of Sciences* **108**, 8714-8719 (2011).

38. R.-Q. Yu, J. R. Reinfelder, M. E. Hines, T. Barkay, Mercury Methylation by the Methanogen Methanospirillum hungatei. *Applied and Environmental Microbiology* **79**, 6325-6330 (2013).

39. Y. Si, Y. Zou, X. Liu, X. Si, J. Mao, Mercury methylation coupled to iron reduction by dissimilatory iron-reducing bacteria. *Chemosphere* **122**, 206-212 (2015).

40. O. Regnell, C. J. Watras, Microbial Mercury Methylation in Aquatic Environments: A Critical Review of Published Field and Laboratory Studies. *Environmental Science & Technology* **53**, 4-19 (2019).

41. H. Hsu-Kim, K. H. Kucharzyk, T. Zhang, M. A. Deshusses, Mechanisms regulating mercury bioavailability for methylating microorganisms in the aquatic environment: a critical review. *Environ Sci Technol* **47**, 2441-2456 (2013).

42. S. Guerrero-Cruz *et al.*, Methanotrophs: Discoveries, Environmental Relevance, and a Perspective on Current and Future Applications. *Frontiers in Microbiology* **12**, (2021).

43. J. D. Semrau, A. A. DiSpirito, S. Yoon, Methanotrophs and copper. *FEMS Microbiology Reviews* **34**, 496-531 (2010).

44. A. Vorobev *et al.*, Detoxification of Mercury by Methanobactin from Methylosinus trichosporium OB3b. *Applied and Environmental Microbiology* **79**, 5918-5926 (2013).

45. J. Harris-Hellal, M. Grimaldi, E. Garnier-Zarli, N. Bousserrhine, Mercury mobilization by chemical and microbial iron oxide reduction in soils of French Guyana. *Biogeochemistry* **103**, DOI 10.1007/s 10533-10010-19457-y (2010).

46. J. Hellal *et al.*, Mercury mobilization and speciation linked to bacterial iron oxide and sulfate reduction: A column study to mimic reactive transfer in an anoxic aquifer. *Journal of Contaminant Hydrology* **180**, 56-68 (2015).

47. M. Ganguly, S. Dib, P. A. Ariya, Fast, Cost-effective and Energy Efficient Mercury Removal-Recycling Technology. *Scientific Reports* **8**, 16255 (2018).

48. K. H. Johannesson, K. Neumann, Geochemical cycling of mercury in a deep, confined aquifer: Insights from biogeochemical reactive transport modeling. *Geochimica et Cosmochimica Acta* **106**, 25-43 (2013).

49. W. Stumm, & Morgan, J. J., *Aquatic Chemistry: Chemical Equilibria and Rates in Natural Waters*. (Wiley, New York, ed. 3rd, 1996).

50. S. Guedron, S. Grangeon, B. Lanson, M. Grimaldi, Mercury speciation in a tropical soil association; Consequence of gold mining on Hg distribution in French Guiana. *Geoderma* **153**, 331-346 (2009).

51. G. Liu, Y. Li, Y. Cai, in *Environmental Chemistry and Toxicology of Mercury*. (2011), pp. 367-387.

52. S. Han *et al.*, Sulfide and iron control on mercury speciation in anoxic estuarine sediment slurries. *Marine Chemistry* **111**, 214-220 (2008).

53. J. Harris-Hellal, M. Grimaldi, E. Garnier-Zarli, N. Bousserrhine, Mercury mobilization by chemical and microbial iron oxide reduction in soils of French Guyana. *Biogeochemistry* **103**, 223-234 (2011).

54. H. A. Wiatrowski *et al.*, Reduction of Hg(II) to Hg(0) by Magnetite. *Environmental Science & Technology* **43**, 5307-5313 (2009).

55. S. Sah, R. Singh, in *Agriculture (Polnohospodárstvo)*. (2015), vol. 61, pp. 97.

56. E. Ahmed, S. J. M. Holmström, Siderophores in environmental research: roles and applications. *Microbial Biotechnology* **7**, 196-208 (2014).

57. R. Saha, N. Saha, R. S. Donofrio, L. L. Bestervelt, Microbial siderophores: a mini review. *J Basic Microbiol* **53**, 303-317 (2013).

58. J. Kramer, Ö. Özkaya, R. Kümmerli, Bacterial siderophores in community and host interactions. *Nature Reviews Microbiology*, (2019).

59. R. Dixit *et al.*, Bioremediation of Heavy Metals from Soil and Aquatic Environment: An Overview of Principles and Criteria of Fundamental Processes. *Sustainability* **7**, 2189-2212 (2015).

60. G. Bjørklund *et al.*, A Review on Coordination Properties of Thiol-Containing Chelating Agents Towards Mercury, Cadmium, and Lead. *Molecules* **24**, (2019).

61. E. Chekmeneva, J. M. Díaz-Cruz, C. Ariño, M. Esteban, Study of the Hg2+ binding with chelation therapy agents by differential pulse voltammetry on rotating Au-disk electrode and electrospray ionization mass-spectrometry. *Analytica chimica acta* **653**, 77-85 (2009).

62. L. Gerhardsson, G. Kazantzis, in *Handbook on the Toxicology of Metals (Fourth Edition)*, G. F. Nordberg, B. A. Fowler, M. Nordberg, Eds. (Academic Press, San Diego, 2015), pp. 487-505.

63. A. Oskarsson, Dithiocarbamate-induced redistribution and increased brain uptake of lead in rats. *Neurotoxicology* **5**, 283-293 (1984).

64. Y. Peng *et al.*, Nanoscale Copper(II)–Diethyldithiocarbamate Coordination Polymer as a Drug Self-Delivery System for Highly Robust and Specific Cancer Therapy. *Molecular Pharmaceutics* **17**, 2864-2873 (2020).

65. M. Berlin, S. Ullrebg, Increased Uptake of Mercury in Mouse Brain caused by 2,3-Dimercaptopropanol. *Nature* **197**, 84-85 (1963).

66. J. Zhou *et al.*, Modeling of the Passive Permeation of Mercury and Methylmercury Complexes Through a Bacterial Cytoplasmic Membrane. *Environmental Science & Technology* **51**, 10595-10604 (2017).

67. M. V. Coppi, C. Leang, S. J. Sandler, D. R. Lovley, Development of a Genetic System for Geobacter sulfurreducens. *Applied and Environmental Microbiology* **67**, 3180-3187 (2001).

68. C. H. Chan *et al.*, Scarless Genome Editing and Stable Inducible Expression Vectors for Geobacter sulfurreducens. *Applied and Environmental Microbiology* **81**, 7178-7186 (2015).

69. H. Wang, N. Peng, S. A. Shah, L. Huang, Q. She, Archaeal extrachromosomal genetic elements. *Microbiology and Molecular Biology Reviews* **79**, 117-152 (2015).

70. N. C. Lavoie, D. S. Grégoire, B. R. Stenzler, A. J. Poulain, Reduced sulphur sources favour HgII reduction during anoxygenic photosynthesis by Heliobacteria. *Geobiology*, (2019).

71. S. A. Thomas, T. Tong, J.-F. Gaillard, Hg(ii) bacterial biouptake: the role of anthropogenic and biogenic ligands present in solution and spectroscopic evidence of ligand exchange reactions at the cell surface. *Metallomics* **6**, 2213-2222 (2014).

72. Z. Ma, F. E. Jacobsen, D. P. Giedroc, Metal Transporters and Metal Sensors: How Coordination Chemistry Controls Bacterial Metal Homeostasis. *Chemical reviews* **109**, 4644-4681 (2009).

73. G. Porcheron, A. Garénaux, J. Proulx, M. Sabri, C. M. Dozois, Iron, copper, zinc, and manganese transport and regulation in pathogenic Enterobacteria: correlations between strains, site of infection and the relative importance of the different metal transport systems for virulence. *Frontiers in Cellular and Infection Microbiology* **3**, 90 (2013).

74. Y. Song *et al.*, Toward an Internally Consistent Model for Hg(II) Chemical Speciation Calculations in Bacterium–Natural Organic Matter–Low Molecular Mass Thiol Systems. *Environmental Science & Technology* **54**, 8094-8103 (2020).

75. J. B. Fein, Q. Yu, J. Nam, N. Yee, Bacterial cell envelope and extracellular sulfhydryl binding sites: Their roles in metal binding and bioavailability. *Chemical Geology* **521**, 28-38 (2019).

76. B. Mishra *et al.*, Stoichiometry of mercury-thiol complexes on bacterial cell envelopes. *Chemical Geology*, (2017).

77. Q. Yu, J. B. Fein, Controls on Bacterial Cell Envelope Sulfhydryl Site Concentrations: The Effect of Glucose Concentration During Growth. *Environmental Science & Technology* **51**, 7395-7402 (2017).

78. M. L. Butzen, J. B. Fein, Electron Donor Effects on Bacterial Surface Sulfhydryl Site Concentrations. *Geomicrobiology Journal* **38**, 294-303 (2021).

79. D. Rickard, *Sulfidic sediments and sedimentary rocks*. (Newnes, 2012).

80. L. Guo, S. L. Painter, S. C. Brooks, J. M. Parks, J. C. Smith, A probabilistic perspective on thermodynamic parameter uncertainties: Understanding aqueous speciation of mercury. *Geochimica et Cosmochimica Acta* **263**, 108-121 (2019).

81. P. May, D. Batka, G. Hefter, E. Königsberger, D. Rowland, Goodbye to S 2− in aqueous solution. *Chemical communications* **54**, 1980-1983 (2018).

82. A. Drott, E. Bjorn, S. Bouchet, U. Skyllberg, Refining thermodynamic constants for mercury (II)-sulfides in equilibrium with metacinnabar at sub-micromolar aqueous sulfide concentrations. *Environmental science & technology* **47**, 4197-4203 (2013).

83. Y. Song *et al.*, Thermodynamics of Hg(II) Bonding to Thiol Groups in Suwannee River Natural Organic Matter Resolved by Competitive Ligand Exchange, Hg LIII-Edge EXAFS and 1H NMR Spectroscopy. *Environmental Science & Technology* **52**, 8292-8301 (2018).

84. V. Liem-Nguyen, U. Skyllberg, E. Björn, Thermodynamic Modeling of the Solubility and Chemical Speciation of Mercury and Methylmercury Driven by Organic Thiols and Micromolar Sulfide Concentrations in Boreal Wetland Soils. *Environmental Science & Technology* **51**, 3678-3686 (2017).

85. V. Liem-Nguyen, U. Skyllberg, K. Nam, E. Björn, Thermodynamic stability of mercury(II) complexes formed with environmentally relevant low-molecular-mass thiols studied by competing ligand exchange and density functional theory. *Environmental Chemistry* **14**, 243-253 (2017).

86. A. Asaduzzaman *et al.*, Environmental Mercury Chemistry – In Silico. *Accounts of Chemical Research* **52**, 379-388 (2019).

Appendix A: Supporting information from chapter 2.

Benjamin Stenzler, Aaron Hinz, Matti Ruuskanen & Alexandre J. Poulain*

Biology Department, University of Ottawa, 30 Marie Curie, Ottawa, ON, K1N 6N5, Canada.

*Corresponding author: Alexandre J. Poulain

E-mail address: apoulain@uottawa.ca

Telephone: 1-613-562-5800 ext. 2373

A modified version of this chapter was originally published as: Stenzler, B., Hinz, A., Ruuskanen, M., & Poulain, A. J. (2017). Ionic strength differentially affects the bioavailability of neutral and negatively charged inorganic Hg complexes. *Environmental science & technology*, *51*(17), 9653-9662.

List of Supporting information

Supporting Methods and Data

A, Media Recipes:

200 mL of Growth Media Contained 34.8 mL of Disco M9 Minimal Salts (5x), 2 mL of 2M Glucose, 12 µL of 0.225M $FeSO_4$ in 0.2M H_2SO_4 (stored anaerobically), 100 µL of 2M $MgSO_4$, 960 µL of 0.6M Thiamine HCl from a frozen (-20˚C) aliquot, 1 mL of 4M $NaNO_3$, 610 µL of 0.075M l-leucine/ l-isoleucine/ valine, 200 µL trace elements #1, 200 µL of trace element #2 and 200 µL of 0.01M EDTA sodium salt.

Trace elements #1 solution consisted of 1.5×10^{-3} M Na_2MoO_4, 6.5×10^{-4} M Na_2SeO_4, 5×10^{-3} M H_3BO_3, and 0.1M NaOH.

Trace elements #2 solution consisted of 0.01M $MnSO_4$, 5×10^{-4} M $ZnSO_4$, 3.25×10^{-3} M $CoCl_2$, 6.25×10^{-3} M $NiCl_2$ and 0.1M H_2SO_4.

100 mL of BMMA exposure media contained 5Beta-Gylcerophosphate from a frozen (-20˚C) aliquot, 4 mL of 1M Mops free acid, 100 µL of 1M $(NH_4)_2SO_4$, 250 µL of 2M Glucose, 600 µL of 2.5M KOH, 200 µL of 2.5M NaOH, and 94 mL of Milli-Q water. The measured pH of this exposure media always measured 7.00 ± 0.02 at 25˚C regardless of the presence of NaCl or remaking of standards. This media was always made the day of exposure. (All standards were stored anaerobically). We report that no pH adjustments were made and reducing agents were not added.

100 mL of exposure media developed in this study contained 700 µL of 1M Sodium Beta-Gylcerophosphate from a frozen (-20˚C) aliquot, 4 mL of 1M Mops free acid, 100 µL of 1M

$(NH_4)_2SO_4$, 250 µL of 2M Glucose, 600 µL of 2.5M KOH, 200 µL of 2.5M NaOH, and 94 mL of Milli-Q water. The measured pH of this exposure media always measured 7.00 ± 0.02 at 25˚C regardless of the presence of NaCl or remaking of standards. This media was always made the day of exposure following the manufacturer's information for 1M Sodium Beta-Gylcerophosphate to ensure its stability. (All standards were stored anaerobically) We report that no pH adjustments were made and reducing agents were not added.

A, Growth Protocols:

Growth protocol for *E. coli* NEB 5α harbouring the vectors pUC57merR-Pp and pUC19AH206-Pp prior to the aerobic bioreporter assay:

1. Plate cultures from cryostock onto LB plate containing 120ug/ml amp
2. Take one colony from the plate (120ug/ml amp) in 10 mL LB (210ug/mL amp) at 11-noon and grow over day at +37˚C with shaking at 220 RPM.
3. At 6-7pm transfer (100 uL) of LB culture into 10 mL of SGM (1% inoculum) (210ug/mL amp, SGM is stored anaerobically and must be vortexed to be aerobic) and grow overnight at + 37˚C with shaking at 220 RPM.
4. At 8-9 am (OD will be approximately 5.5-6.5) resuspend (9.5RCF for 90 seconds) 2mL of the culture into SGM and add to 8mL SGM (20% inoculum) (210ug/mL amp) and grow over at +37˚C with shaking at 220 RPM.
5. Stop the growth when the culture reaches an OD_{600} of 0.64 ±0.01. (around noon).
6. Resuspend (9.5RCF for 90 seconds) 6 mL culture into exposure media and transfer into 3x2 mL ependorf tubes and the cells were left to acclimate for 1 hour.

7. Resuspend (9.5RCF for 90 seconds) all the cells into exposure media and allocate the 6 mL into a 7 mL scintillation vial as a **cell stock solution**. Wait 1 hour before 1/20 dilution.
8. Distribute 100uL of cells to a total of 2000uL of assay media (1/20 dilution) in Teflon.
9. Shake well (orbitally) and transfer everything into a 96 well plate.

Note: Balch tubes were also used to grow *E. coli* aerobically but were given a yellow test tube cap instead of a rubber stopper.

Growth protocol for *E. coli* NEB 5α harbouring the vectors pUC57merR-Pp and pUC19AH206-Pp prior to the anaerobic bioreporter assay:

1. Plate cultures from cryostock onto LB plate containing 120ug/ml amp
2. Take one colony from the plate (120ug/ml amp) and add to 10 mL LB (210ug/mL amp) at 5-6 pm at night and grow over night at +37˚C with shaking at 220 RPM.
3. The next morning at 9-10 am, resuspend (9.5RCF for 90 seconds) 4 mL of the culture in anaerobic chamber into anaerobic SGM and add to 6mL of SGM (40% inoculum) (210ug/mL amp) in a balch tube and grow over day at +37˚C with shaking at 220 RPM.
4. At 5-6 pm resuspend (9.5RCF for 90 seconds) 2mL of the culture in the anaerobic chamber into SGM and add to 8mL SGM (20% inoculum) (210ug/mL amp) in a balch tube and grow over night at +37˚C with shaking at 220 RPM.
5. Stop the growth when the culture reaches an OD_{600} of 0.64 ±0.01. (around 9am the next day, if overgrown we diluted with 67mM PI buffer at pH 6.8) (as anaerobic dilution are ‘difficult’ we recommend not allowing to overgrow).

6. Resuspend (9.5RCF for 90 seconds) 6 mL culture into exposure media and transfer into 3x2 mL ependorf tubes and the cells were left to acclimate for 1 hour. This step was performed in an anaerobic chamber.
7. Resuspend (9.5RCF for 90 seconds) all the cells into exposure media and allocate the 6 mL into a 7 mL scintillation vial as a **cell stock solution**. Wait 1 hour before 1/20 dilution. This step was performed in an anaerobic chamber.
8. Distribute 100uL of cells to a total of 2000uL of assay media (1/20 dilution) in Teflon.
9. Shake well (orbitally) and transfer everything into a 96 well plate.

A, Sorption of to the cell surface:

The amount of Hg sorbed to the surface of the bacteria was determined using a method modified from Hu et al., (2013) (1). Cells were added to the teflon vials in concentrations 10x higher than the original assay conditions with 100nM Hg with the corresponding salt treatment (Na_2SO_4 or NaCl) under anaerobic conditions. Cells were allowed to equilibrate with Hg for 1 hour before filtered being filtered (Sasdedt Filtropur S 0.2). Filtered and non-filtered cell fractions were immediately preserved using 30% BrCl. Sorbed fraction was determined through mass balance using EPA method 245.7.

A, Fluorescence Calculations:

To appropriately blank the fluorescence measurements, each time point for fluorescence of the mercury inducible strain induced with Hg was blanked using the fluorescence of the same strain but without mercury. The constitutive strain was blanked to that of the same treatment without cells and mercury. Because the constitutive reporter already expresses fluorescence prior

to the start of the experiment, all constitutive data are substracted by the fluorescence value observed at t=0.

$$\text{Normalized Fluorescence} = \frac{Fluorescence\ from\ Mercury\ Addition\ to\ the\ Mercury\ Inducible\ Strain}{Fluorescence\ Emmitted\ from\ the\ constitutive\ Strain} =$$

$$\frac{(Fluorescence\ of\ Mercury\ inducible\ with\ Mercury)-(Fluorescence\ of\ Mercury\ Inducible\ without\ mercury\ )}{((Fluorescence\ Emitted\ by\ Constitutive\ Reporter\ with\ Mercury)-(Fluorescence\ of\ sample\ without\ cells))-Inital\ Fluorescence\ V}$$

A, Genetic Constructs:

The complete nucleotide sequences of pUC57merR-Pp construct on the vector pUC57 in *E. coli* NEB 5α.

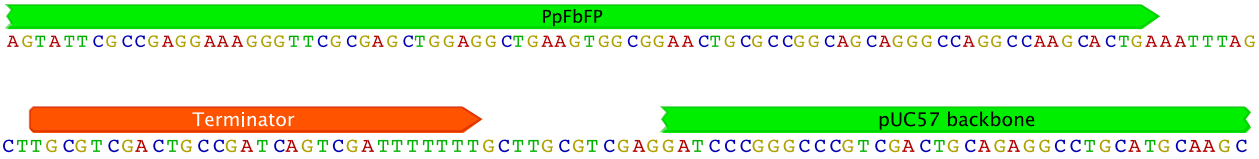

The complete nucleotide sequences of pUC19AH206-Pp construct on the vector pUC19 in *E. coli* NEB 5α.

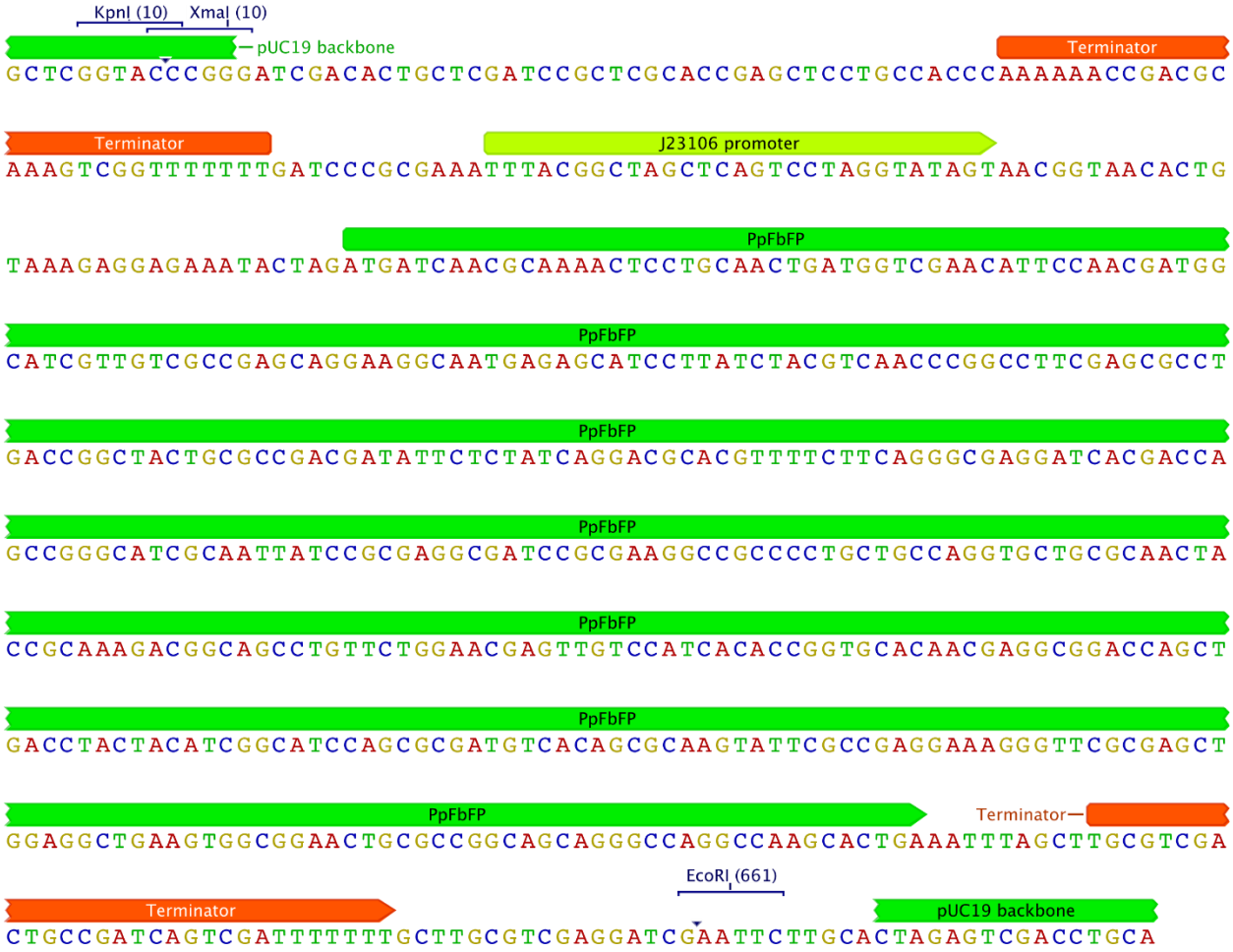

Supporting Tables and Figures

A, Thermodynamic Modeling:

Table A1: Equilibrium formation constants ($log_{10}K$, T = 37°C) for all aqueous species considered in the speciation calculations. Activity corrections for ionic strength were made using the B-dot Equation if the ion-specific hard core diameter (å) was present, otherwise activity corrections were made according to the Davies equation. Temperature corrections to $log_{10}K$ were made using the Van't Hoff equation but if a temperature dependent analytical expression was present, $log_{10}K$ was calculated using the expression from Parkhurst et al., (2013)[(2)] with values A_1, A_2, A_3, A_4, A_5, A_6 and temperature in kelvin:

Formula	å	$log_{10}K$	ΔH(KJ/mol)	A_1, A_2, A_3, A_4, A_5, A_6	Reference
$Hg^{2+} + 2H_2O = Hg(OH)_2 + 2H^+$	3.4		39.72	2.9718996E+2, 4.0967002E-2, -1.7978768E+4, -1.0663825E+2, 7.7240765E+5, 0	(3) ΔH (4)
$Hg^{2+} + NH_3 = HgNH_3^{2+}$		8.8	-12.28		$log_{10}K$ (4) ΔH (5)
$Hg^{2+} + 2NH_3 = Hg(NH_3)_2^{2+}$		17.8	-311		(4)
$Hg^{2+} + 3NH3 = Hg(NH_3)_3^{2+}$		18.156	-429		(4)
$Hg^{2+} + 4NH_3 = Hg(NH_3)_4^{2+}$		19.3	-548		(4)
$Hg^{2+} + Cl^- = HgCl^+$	4.1		-23	8.3901966E+2, 1.3660176E-1, -4.524016E+4, -3.0460641E+2, 2.9270363E+6, 0	(6) ΔH (4)
$2Cl^- + Hg^{2+} = HgCl_2$	3.4		-52.7	1.628757E+3, 2.6423967E-1, -8.7765028E+4, -5.9148558E+2, 5.7245444E+6, 0	(6) ΔH (4)
$3Cl^- + Hg^{2+} = HgCl_3^-$	3.6		-54.3	1.7509172E+3, 2.8619069E-1, -9.6316803E+4, -6.3530984E+2, 6.5688689E+6, 0	(6) ΔH (4)
$4Cl^- + Hg^{2+} = HgCl_4^{2-}$	4.7		-61	1.6653929E+3, 2.7781643E-1, -9.2970913E+4, -6.0481699E+2, 6.7205484E+6, 0	(6) ΔH (4)
$Hg^{2+} + Br^- = HgBr^+$		9.609	-42.2		(4)
$2Br^- + Hg^{2+} = HgBr_2$		18.0785	-87.4		(4)
$3Br^- + Hg^{2+} = HgBr_3^-$		20.5085	-99.1		(4)
$4Br^- + Hg^{2+} = HgBr_4^{2-}$		21.739	-114		(4)
$Hg^{2+} + Br^- + H_2O = HgOHBr + H^+$		6.239			(4)
$Hg^{2+} + I^- = HgI^+$		13.409	-71.5		(4)
$2I^- + Hg^{2+} = HgI_2$		24.6285	-143		(4)
$3I^- + Hg^{2+} = HgI_3^-$		28.4085	-154.5		(4)
$4I^- + Hg^{2+} = HgI_4^{2-}$		30.339	-181		(4)
$Hg^{2+} + H_2PO4^- = HgHPO_4 + H^+$	3.4	1.587			(3)
$Hg^{2+} + Cl^- + H_2O = HgOHCl + H^+$	3.4		-42.72	9.6186636E+2, 1.481468E-1, -5.1533988E+4, -3.4834456E+2, 2.9178749E+6, 0	(7) ΔH (4)
$2Hg^{2+} + H_2O = Hg_2(OH)^{+3} + H^+$	8.2			6.0697961E+2, 9.0888386E-2, -3.2328536E+4, -2.2128295E+2, 1.6509003E+6, 0	(3)
$Hg^{2+} + H_2O = HgOH^+ + H^+$	4.1			2.7850062E+2, 4.2312059E-2, -1.7809314E+4, -9.9689226E+1, 1.0569647E+6, 0	(8)
$Hg^{2+} + H_2PO_4^- = HgPO_4^- + 2H^+$	3.6	-3.962			(3)
$Hg^{2+} + SO_4^{2-} = HgSO_4$		2.535			(4)
$Hg^{2+} + NO_3^- = HgNO_3^+$		-0.3157			(4)
$Hg^{2+} + 2NO_3^- = Hg(NO_3)_2$		-0.697			(4)
$MOPS^- + H^+ = HMOPS$		7.184	-21.1		(9)

β-Gylcerophosphate^{2-} + H^+ = Hβ-Gylcerophosphate$^-$	6.65	1.85		(9)
Hβ-Gylcerophosphate$^-$ + H^+ = H_2β-Gylcerophosphate	1.329	12.2		(9)

Table A2: Calculated solubility of several divalent metals in the assay media described in PI exposure media (68mM phosphate) at 37˚C and the associated mineral phase that will precipitate at higher concentrations of metal than listed in the table. Solubility was calculated assuming all possible species in solution with the only the limiting phase being reported. All calculations were performed using PHREEQC using the thermoddem database (10).

Metal	Solubility (Molal)	Limiting Mineral Phase	Formula	$log_{10}K$ (37˚C)
Ca	5.29E-05	Whitlockite(low)	$Ca_3(PO_4)_2 + 4H^+ = 3Ca^{2+} + 2H_2PO_4^-$	7.6016
Cd	2.57E-03	Cd3(PO4)2	$Cd_3(PO_4)_2 + 4H^+ = 3Cd^{2+} + 2H_2PO_4^-$	7.5565
Cu	1.22E-10	Cu3(PO4)2	$Cu_3(PO_4)_2 + 4H^+ = 3Cu^{2+} + 2H_2PO_4^-$	-13.4071
Fe	5.65E-08	Vivianite	$Fe_3(PO_4)_{2:}\ 8H_2O + 4H^+ = 3Fe^{2+} + 2H_2PO_4^- + 8H_2O$	-3.272 (no temperature correction available)
Zn	4.98E-11	Hopeite(alpha)	$Zn_3(PO_4)_{2:}\ 4H_2O + 4H^+ = 2H_2PO_4^- + 3Zn^{2+} + 4H_2O$	-11.3287
Mg	1.67E-10	$MgHPO_4$	$MgHPO_4 + H^+ = Mg^{2+} + H_2PO_4^-$	-5.815 (no temperature correction available)
Mn	2.00E-08	$MnHPO_4$	$MnHPO_4 + H^+ = Mn^{2+} + H_2PO_4^-$	-4.119 (no temperature correction available)
Ni	3.09E-04	$Ni_3(PO_4)_2$	$Ni_3(PO_4)_2 = 3Ni^{2+} + 2PO_4^{3-}$	-31.3 (no temperature correction available)
Sr	2.52E-07	$Sr_5(PO4)_3(OH)$	$Sr_5(PO_4)_3(OH) + 7H^+ = 3H_2PO_4^- + 5Sr^{2+} + H_2O$	5.3794
Pb	2.58E-11	Pyromorphite	$Pb_5(PO_4)_3OH + 7H^+ = 3H_2PO_4^- + 5Pb^{2+} + H_2O$	-18.119 (no temperature correction available)
Hg	6.30E-04	$Hg_3(OH)_3PO_4$	$Hg_3(OH)_3PO_4 + 5H^+ = 3Hg^{2+} + H_2PO_4^- + 3H_2O$	-2.185 (no temperature correction available)

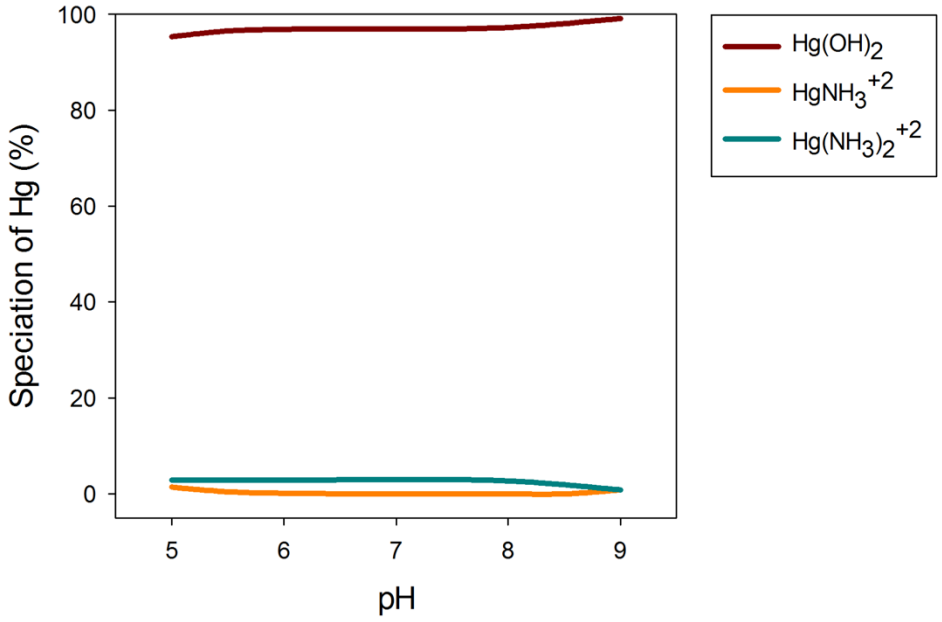

Figure A1: Modeling of Hg speciation across a pH gradient. Thermodynamic model of mercury speciation (%) over a gradient of pH (5-9) in exposure media. [Hg^{2+}] was set to of 5nM and temperature was set to 37˚C. Species representing less than 1% of the total mercury species were excluded from this figure. All calculations were performed using PHREEQC.

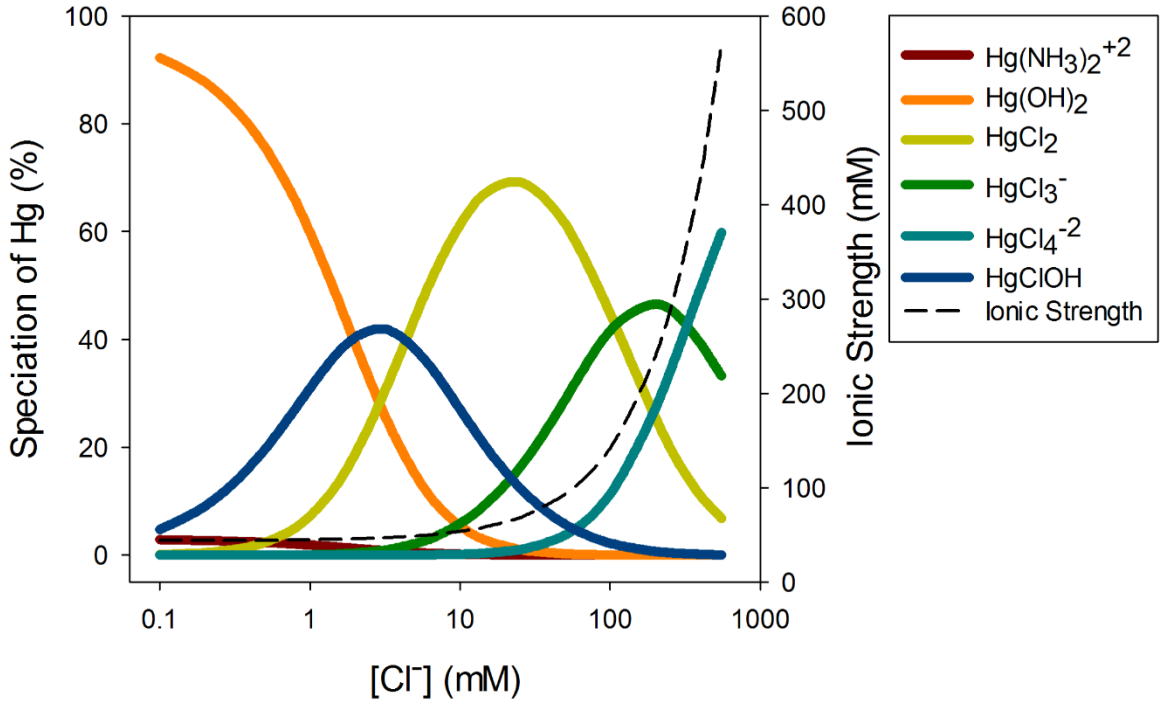

Figure A2: Modeling of Hg speciation across a chloride gradient. Thermodynamic model of mercury speciation (%) over a gradient of chloride (0.1-550mM) in exposure media at a pH of 7. $[Hg^{2+}]$ was set to of 5nM and temperature was set to 37˚C. Chloride concentrations were modified through the addition of NaCl in the model to properly account for changes in pH and ionic strength. Species representing less than 1% of the total mercury species were excluded from this figure. The changes in NaCl and temperature did not influence the pH and were verified empirically using a pH probe. All calculations were performed using PHREEQC.

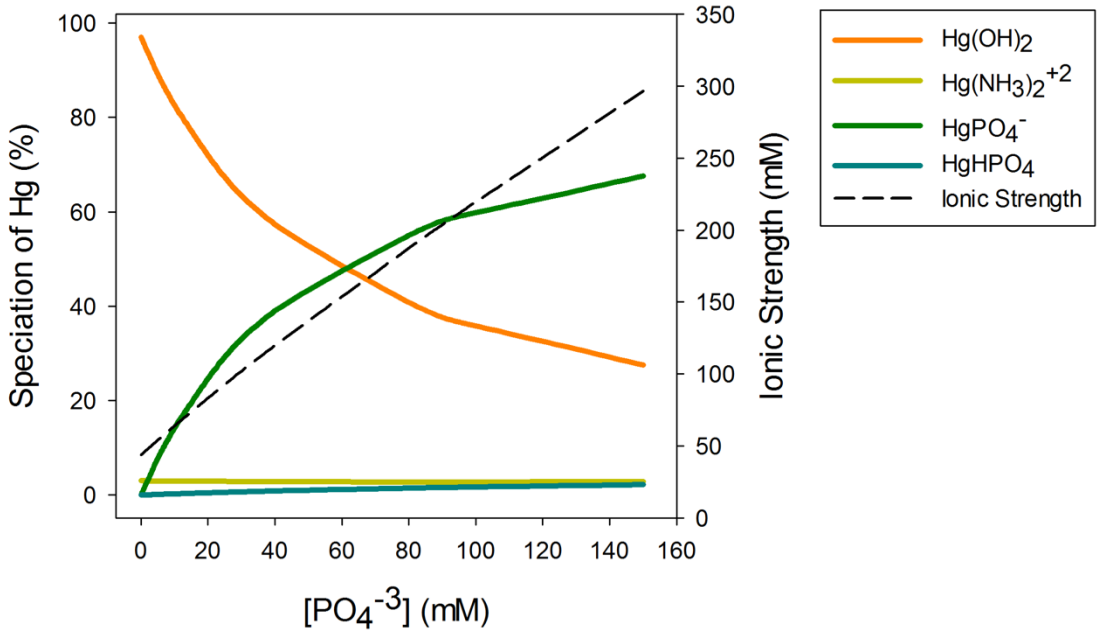

Figure A3: Modeling of Hg speciation across a phosphate gradient. Thermodynamic model of mercury speciation (%) over a gradient of phosphate (0-150mM) in buffered exposure media at a pH of 7. [Hg^{2+}] was set to of 5nM and temperature was set to 37˚C. Phosphate concentrations were modified through the addition of Sodium Phosphate with a ratio of 1.61 M Na^{+}: 1 M PO_4^{3-} in the model to properly account for changes in pH and ionic strength. Species representing less than 1% of the total mercury species were excluded from this figure. The changes in phosphate and temperature did not influence the pH and were verified empirically using a pH probe. All calculations were performed using PHREEQC.

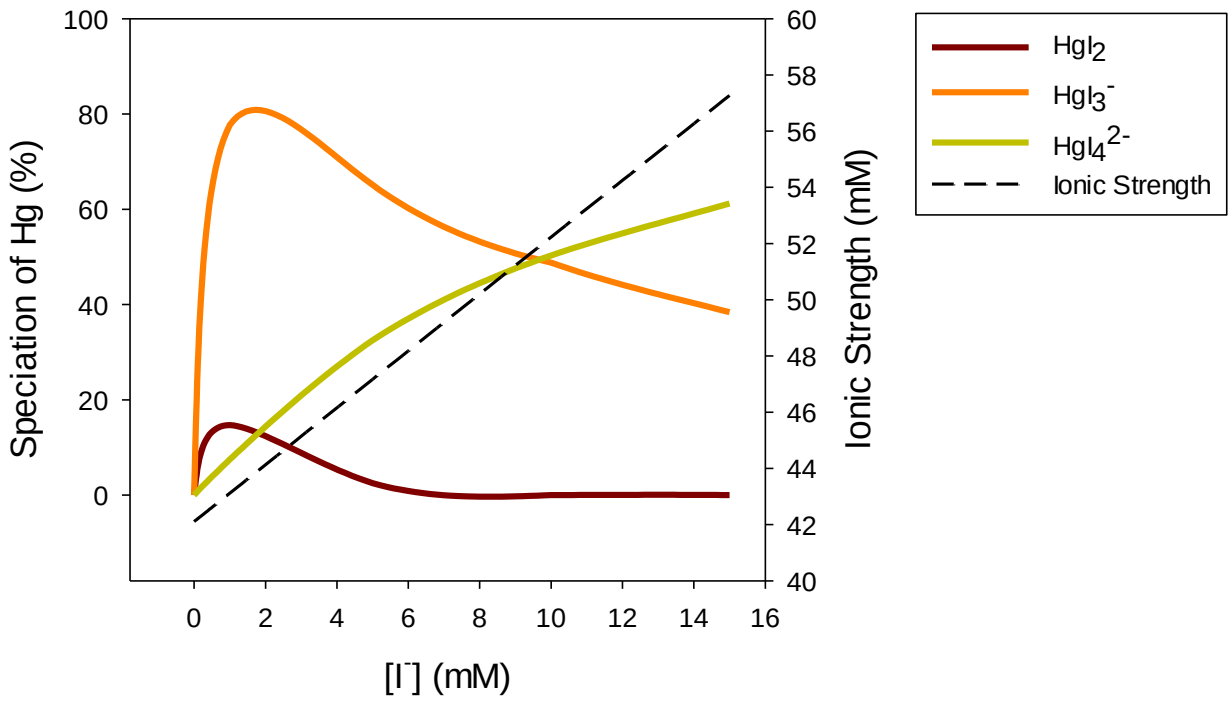

Figure A4: Modeling of Hg speciation across an Iodide gradient. Thermodynamic model of mercury speciation (%) over a gradient of iodide (0-15mM) in buffered exposure media at a pH of 7. [Hg^{2+}] was set to of 5nM and temperature was set to 37˚C. Iodide concentrations were modified through the addition of NaI in the model to properly account for changes in pH and ionic strength. Species representing less than 1% of the total mercury species and species at 0 mM iodide were excluded from this figure. The changes in NaI and temperature did not influence the pH and were verified empirically using a pH probe. All calculations were performed using PHREEQC.

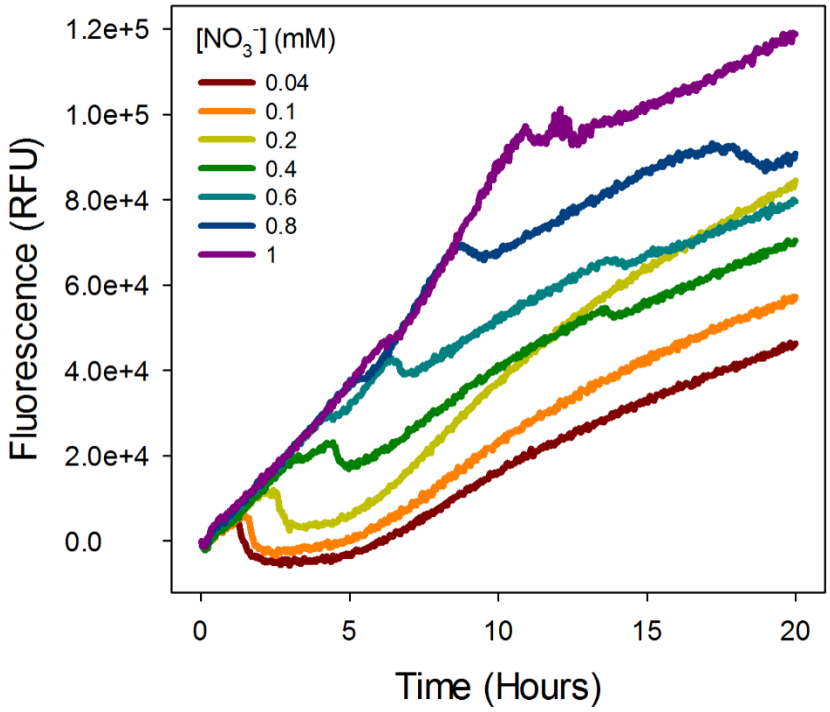

Figure A5: Determination of the nitrate concentration to achieve optimal fluorescence. Fluorescence measured as relative fluorescence units (RFU) emitted by constitutive *E. coli* NEB5α harbouring the pUC19AH206-Pp with the addition of NO_3^- (0.04-1mM) under anaerobic conditions. Experiments were analyzed as the average of technical replicates of 3 at 37˚C in exposure media

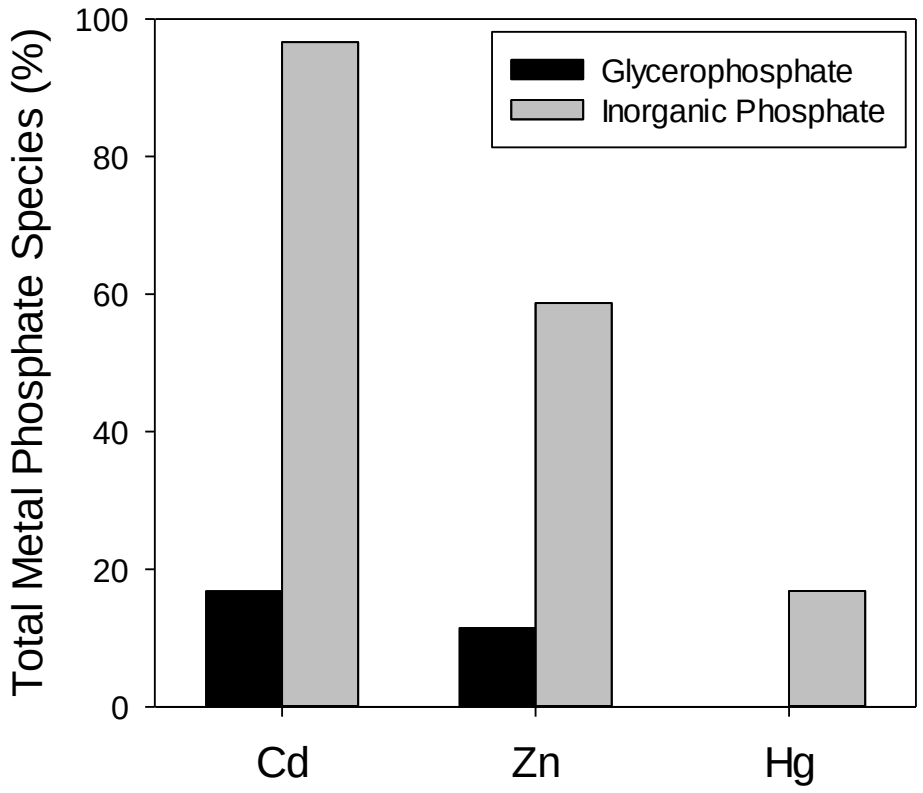

Figure A6: Prediction of Hg species with B-Glycerophosphate. Thermodynamic model of Hg, Cd and Zn speciation as a percent bound to Inorganic phosphate (grey bars) or Glycerosphosphate (black bars) in buffered exposure media at a pH of 7. Hg, Cd and Zn concentrations were set to of 5nM and temperature was set to 37˚C. All phosphate species were set to 7mM. Glycerophosphate stability constants for Zn and Cd were incorporated from the IUPAC SC database (11). All calculations were performed using PHREEQC.

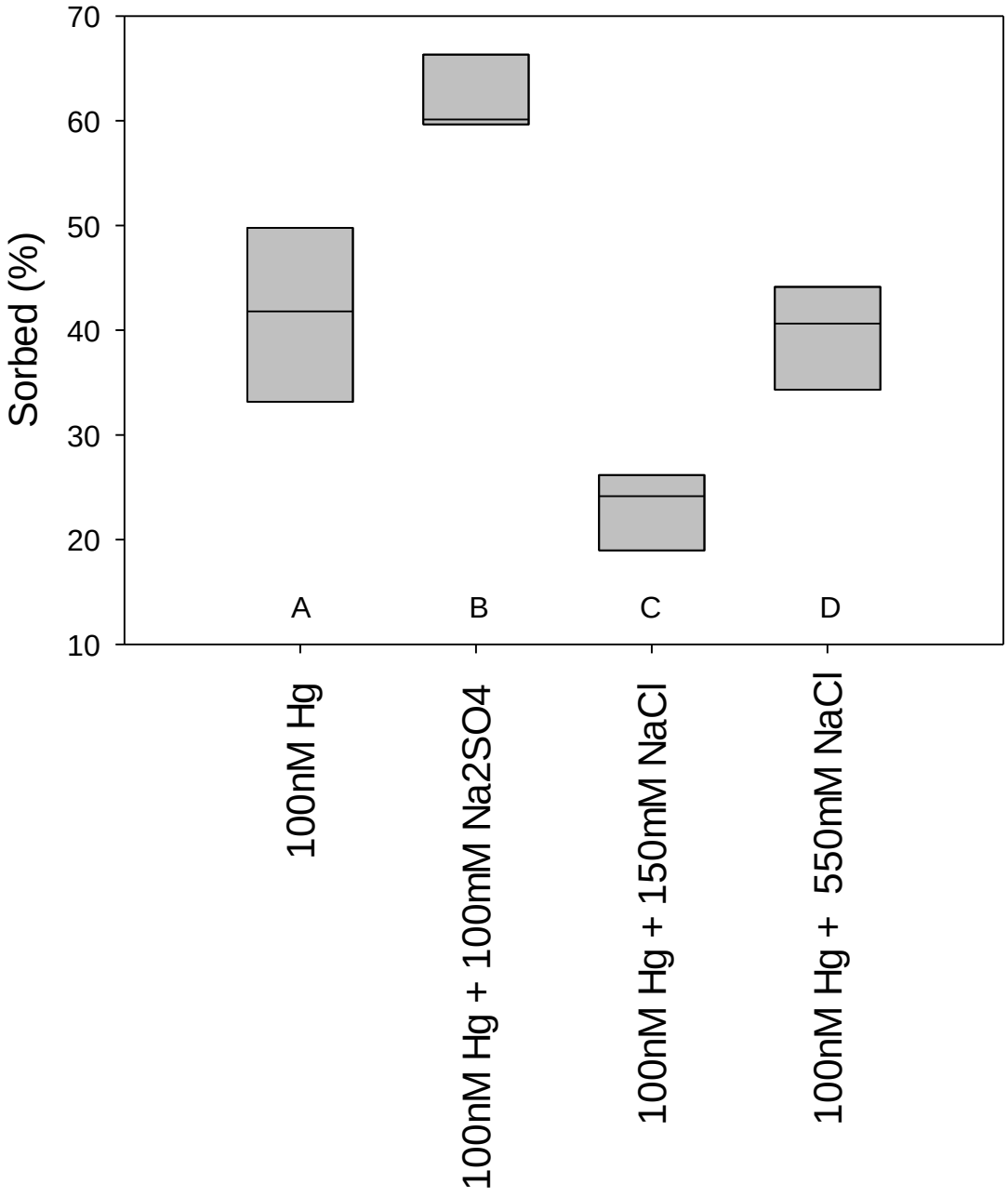

Figure A7: Hg Sorption to *E. Coli*. Sorption (%) of 100nM Hg to *E. coli* NEB5α harbouring pUC57merR-Pp in exposure media under anaerobic conditions. Treatments represent A) 100nM Hg control, B) 100nM Hg + 100 mM Na_2SO_4, C) 100nM Hg + 150 mM NaCl and D) 100nM Hg + 550 mM NaCl. Data is represented as a box plot of 3 biological replicates. Multiple comparison results from Tukeys PHT are as follows: A-B (diff = 20.44, p = 0.0082), A-C (diff = 18.49, p = 0.014), A-D (diff = 1.89, p = 0.97), B-C (diff = 38.93, p = 0.0001), B-D (diff = 22.33, p = 0.005), and C-D (diff = 16.59, p = 0.025)

Supporting References

1. Hu, H.; Lin, H.; Zheng, W.; Rao, B.; Feng, X.; Liang, L.; Elias, D. A.; Gu, B., Mercury reduction and cell-surface adsorption by Geobacter sulfurreducens PCA. *Environmental science & technology* **2013,** *47*, (19), 10922-10930.

2. Parkhurst, D. L. a., *Description of input and examples for PHREEQC version 3--a computer program for speciation, batch-reaction, one-dimensional transport, and inverse geochemical calculations*. Reston, Virginia : U.S. Department of the Interior, U.S. Geological Survey, 2013.: 2013.

3. Blanc, P., Mercury associated physical and chemical constants: updating of the THERMODDEM database. *IMaHg project* **2012,** *rapport BRGM RP-61299-FR*, 32p.

4. Smith, R.; Martell, A.; Motekaitis, R., NIST standard reference database 46. *NIST Critically Selected Stability Constants of Metal Complexes Database Ver* **2004,** *2*.

5. Herndon, V., MINTEQA2/PRODEFA2, A Geochemical Assessment Model for Environmental Systems: User Manual Supplement for Version 4.0. **1998**.

6. Sverjensky, D.; Shock, E.; Helgeson, H., Prediction of the thermodynamic properties of aqueous metal complexes to 1000 C and 5 kb. *Geochimica et Cosmochimica Acta* **1997,** *61*, (7), 1359-1412.

7. Baes Jr, C.; Mesmer, R., T he Hydrolysis of Cations. In Wiley, New York: 1976.

8. Shock, E. L.; Sassani, D. C.; Willis, M.; Sverjensky, D. A., Inorganic species in geologic fluids: correlations among standard molal thermodynamic properties of aqueous ions and hydroxide complexes. *Geochimica et Cosmochimica Acta* **1997,** *61*, (5), 907-950.

9. Goldberg, R. N.; Kishore, N.; Lennen, R. M., Thermodynamic quantities for the ionization reactions of buffers. *Journal of physical and chemical reference data* **2002,** *31*, (2), 231-370.

10. Blanc, P.; Lassin, A.; Piantone, P.; Azaroual, M.; Jacquemet, N.; Fabbri, A.; Gaucher, E. C., Thermoddem: A geochemical database focused on low temperature water/rock interactions and waste materials. *Applied Geochemistry* **2012,** *27*, (10), 2107-2116.

11. Pettit, L. D.; Powell, K., The IUPAC stability constants database. *Chemistry international* **2006**.

Appendix B: Supporting information from chapter 4.

Mangal V[a$]., Stenzler B.R.[b$]., Poulain A.J.[b*]., Guéguen C[c*].

[a] Environmental and Life Sciences Graduate program, Trent University, 1600 West Bank Drive Peterborough ON, Canada, K9J 7B8

[b] Biology Department, University of Ottawa, 30 Marie Curie, Ottawa ON, Canada, K1N 6N5

[c] Chemistry Department, Trent University, 1600 West Bank Drive Peterborough ON, Canada, K9J 7B8

[*] Corresponding authors; **celinegueguen@trentu.ca**; **apoulain@uottawa.ca**

[$]authors contributed equally to this work

A modified version of this chapter was originally published as V. Mangal, B. R. Stenzler, A. J. Poulain, C. Guéguen, Aerobic and Anaerobic Bacterial Mercury Uptake is Driven by Algal Organic Matter Composition and Molecular Weight. *Environmental Science & Technology* 53, 157-165 (2019).

Supporting Figures

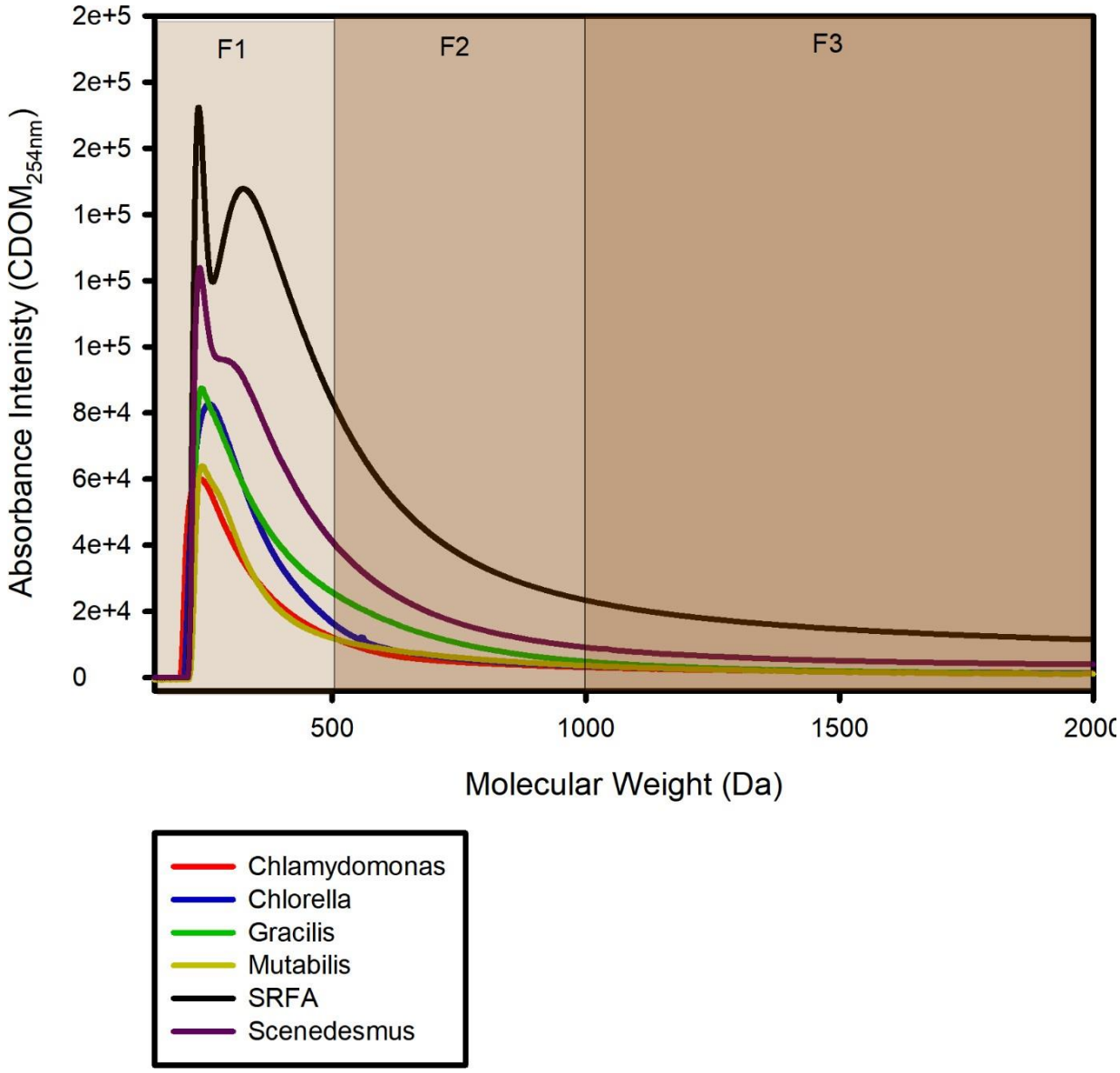

Figure B1: AF4 fractogram outlining overall molecular weight distributions for SRFA DOM and algal derived organic matter from *S. Obliquus*, *C. reinhardtii*, *C. vulgaris*, *E. mutabilis* and *E. gracilis*. Fractionswere collected based on 1-minute retention time intervals corresponding to molecular weight ranging fromF1 (300-500Da), F2 (500-1000Da) and F3 (1000-20000Da).

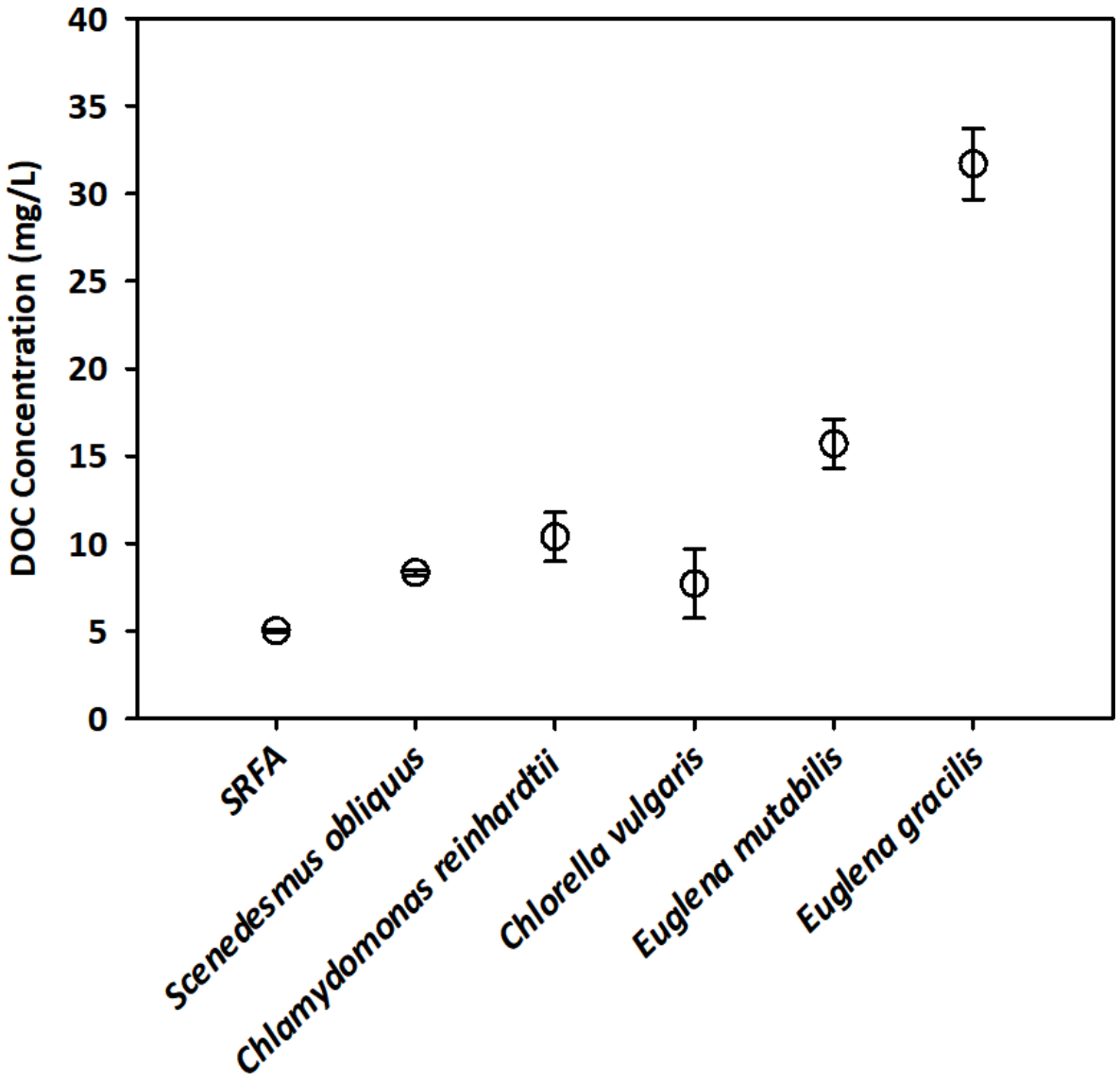

Figure B2: Dissolved organic carbon (DOC) analysis outlining SRFA, and algal DOM concentrations ofunfractionated samples.

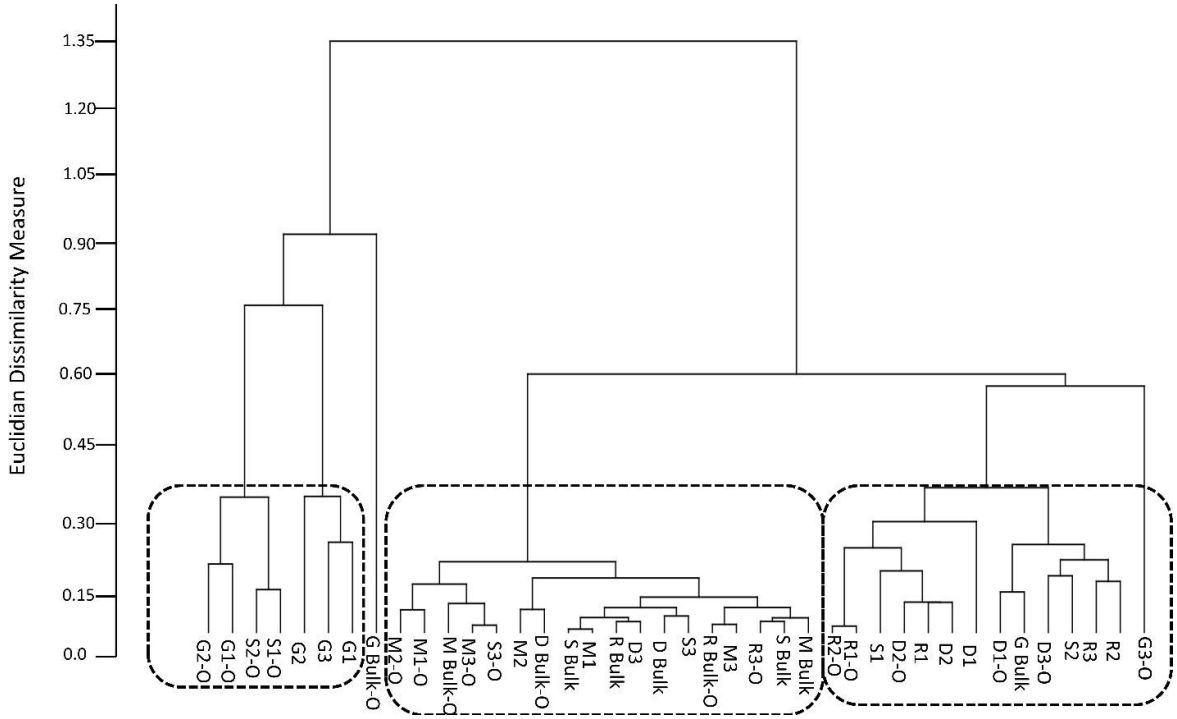

Figure B3: The effect of fractionation on algal DOM composition portrayed by a hierarchical cluster analysis using a Euclidian dissimilarity measure. Based on their composition, three distinct clusters based on a 0.35 dissimilarity where found and outlined by dashed lines.

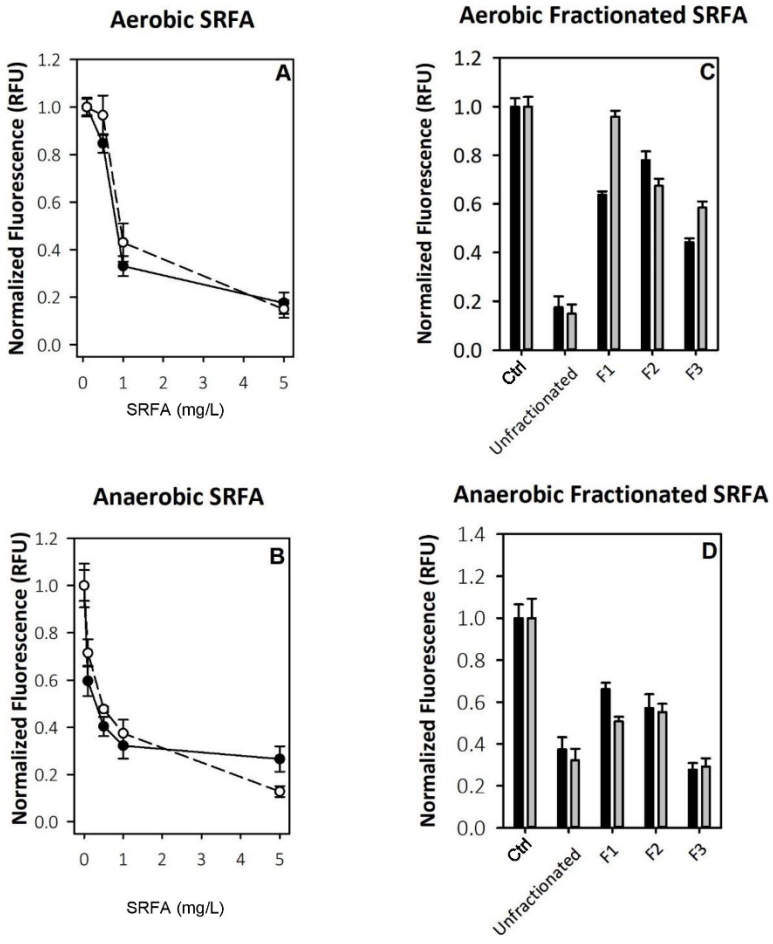

Figure B4: Aerobic and anaerobic Hg bioavailability with fractionated and unfractionated SRFA. Normalized fluorescence (RFU) with increasing concentrations of SRFA (0-5mg/L) (A, B, respectively). Normalized fluorescence (RFU) with fractionated SRFA (1mg/L) for F1, F2, F3, unfractionated, and no SRFA (Ctrl) (C, D). [Hg] was set to 2 nM. The experiment was performed at 37 ˚C in an anaerobic exposure medium (pH 7).

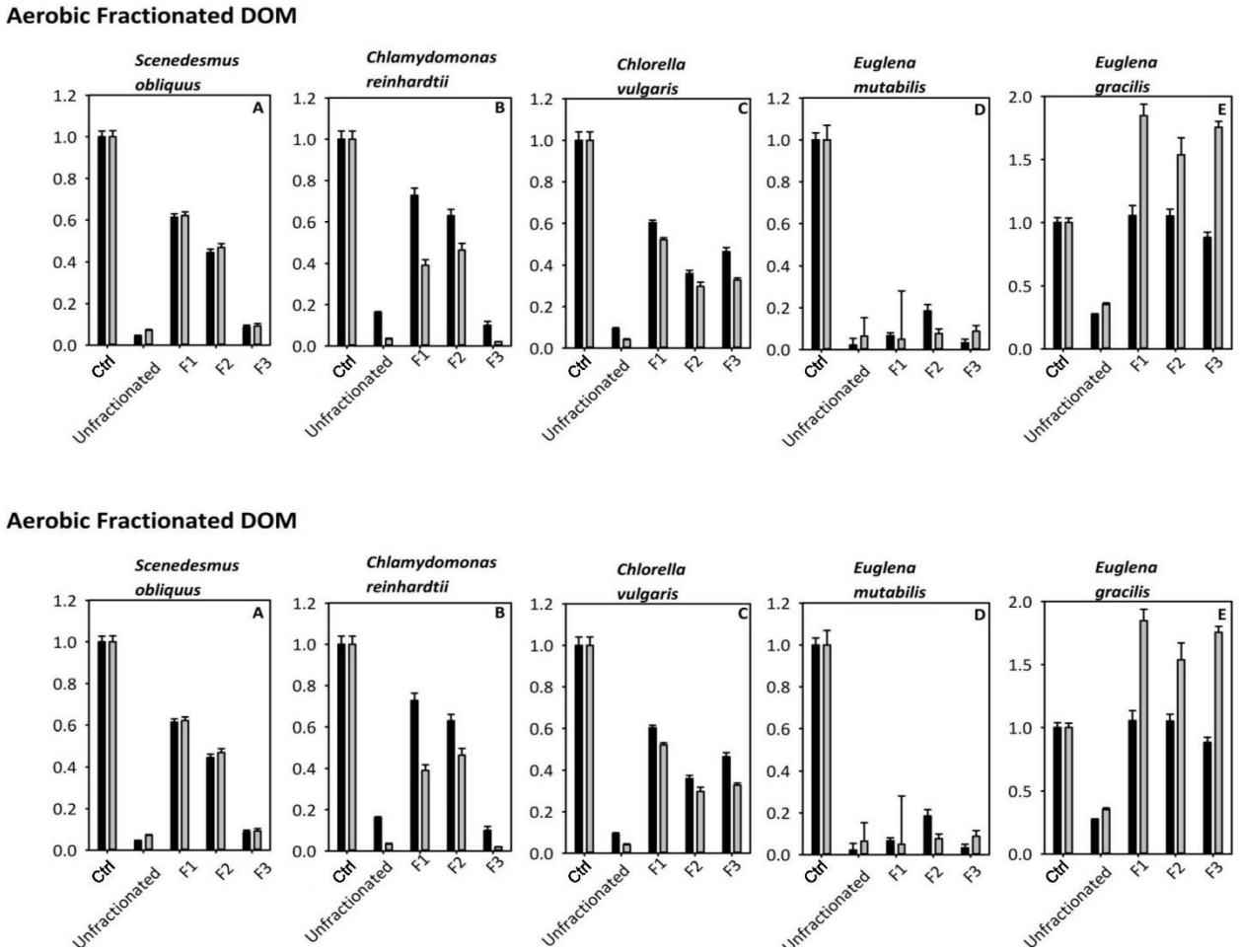

Figure B5: Aerobic and anaerobic Hg bioavailability with fractionated and unfractionated algal DOM. Normalized fluorescence (RFU) with increasing concentrations of algal DOM Aerobic (A-E) and anaerobic (F-J) bioassays of fractionated organic matter from *S. obliquus* (A, F), *C. reinhardtii* (B, G), *C. vulgaris* (C, H), *E. mutabilis* (D, I) and *E. gracilis* (E, J) (n=3). DOM was set to 1mg/L for F1, F2, F3, unfractionated, and no SRFA (Ctrl) (C, D). [Hg] was set to 2 nM. The experiment was performed at 37 ˚C in an anaerobic exposure medium (pH 7).

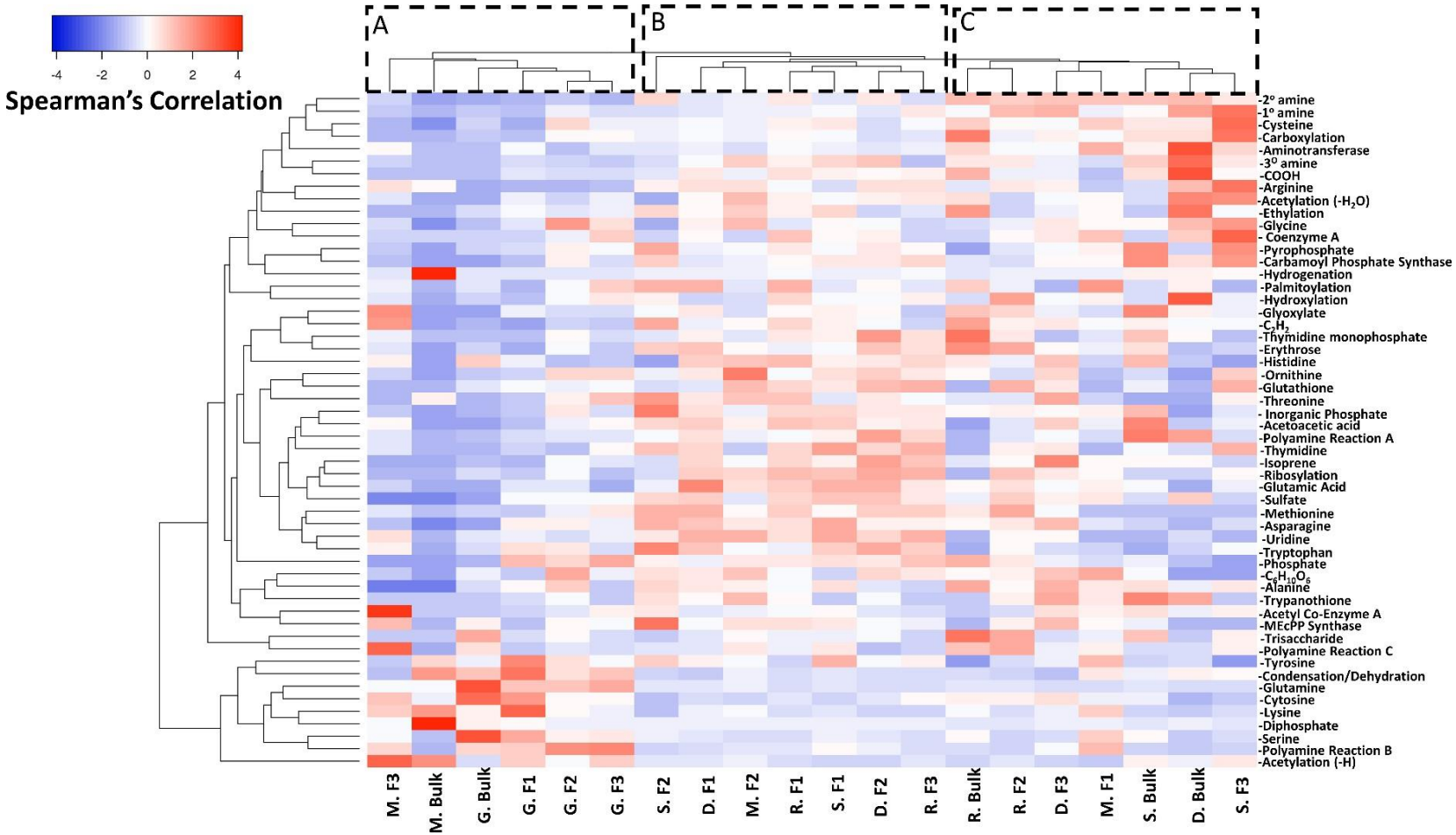

Figure B6: Correlations between FT ICR MS derived biomolecules for all algae. Heatmap Spearman's correlation matrix outlining correlations between FT ICR MS derived biomolecules for all algae encompassing both unfractionated and fractionated material (n=2). Red colours indicate a stronger relationship between the molecular transformations (y axis) andthe algae sample (x-axis) whereas blue indicates a weaker correlation. Samples within distinct groups emphasize significant differences between samples based on molecular composition. Three distinct clusters of algal DOM were observed where the (A) comprised of Euglenoid DOM, (B) of mainly Chlorophyta F1 and F2 fractions and (C) of Chlorophyta unfractionated material.

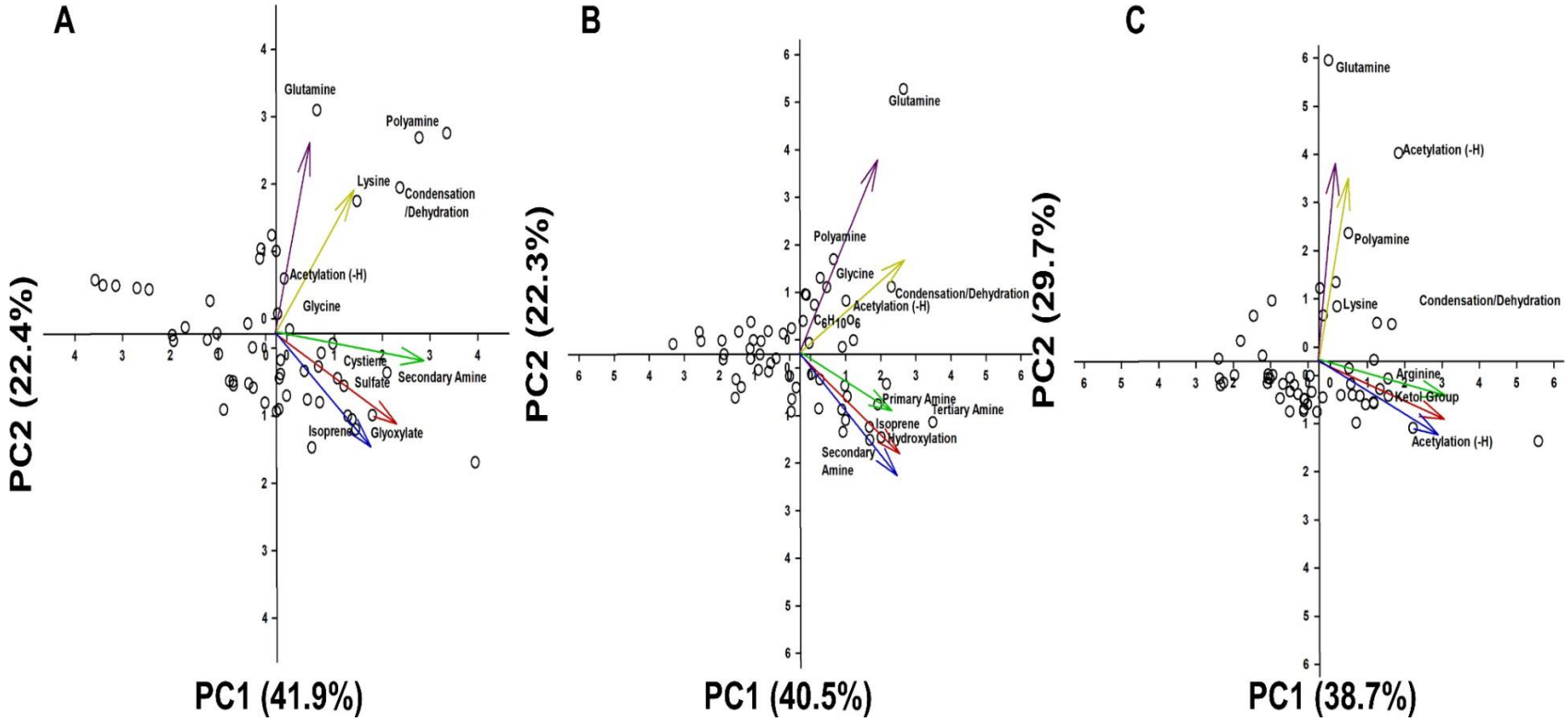

Figure B7: PCA outline outlining the main transformation across all algal DOM. Principal component analysis (PCA) outlining the main transformation across all F1 (A), F2 (B) and F3 (C) algal DOM samples. Blackcircles indicate transformations and named circles represent significant contributions. Arrows indicate the five algae where purple is *E. gracilis*, yellow is *E. mutabilis*, green is *S. obliquus*, red is *C. reinhardtii* and blue is *C. vulgaris.*

Appendix C: Supporting information from chapter 5.

Aaron Hinz[a], Benjamin Stenzler[a], & Alexandre J. Poulain[a#]

[a]Department of Biology, University of Ottawa, Ottawa, Ontario, Canada

[#]**Correspondence:**

Dr. Alexandre Poulain

E-mail address: apoulain@uottawa.ca

Running title: Assembly of Microbial Bioreporters

A modified version of this chapter was originally published as: Hinz, A. J., Stenzler, B., & Poulain, A. J. (2021). Golden Gate Assembly of Aerobic and Anaerobic Microbial Bioreporters. *Applied and environmental microbiology*, AEM0148521. Advance online publication. https://doi.org/10.1128/AEM.01485-21

Supporting MATERIAL

Supplemental Tables

Table C1. Description and construction details of vectors featured in this study.

Table C2. Amplicons used for assembly of destination vectors and inserts.

Supplemental Figures

Fig. C1. Genetic maps of destination vectors.

Fig. C2. Sequence of BsaI-*lacZ* Golden Gate assembly site.

Fig. C3. Time-course of light production for constitutive and mercury-inducible luciferase bioreporters.

Fig. C4. Constitutive fluorescence of PpFbFp under anaerobic conditions.

Supplemental References

Supporting Tables

Table C1. Description and construction details of vectors featured in this study.

Plasmid	Description	Genotype or relevant features	Reference or construction details
Golden Gate destination vectors			
pR6KT-SacB	Allelic exchange vector	*oriR6K*, *oriT*, *bla(T720C)*(Amp^R), **BsaI-*lacZ***, *sacB*, *tet*(Tet^R)	BsaI-*lacZ* site (amplified from pUC19) cloned into BglII and SpeI sites of pAH385
pAH1-Tn7	Mini-Tn7 vector	pMB1, **BbsI-AmpR**, mini-Tn7T-Gm, **BsaI-*lacZ***	BsaI-*lacZ* site (amplified from pR6KT-SacB) cloned into BamHI and XhoI sites of pIN1-Tn7
pAH1T-Tn7	Conjugative mini-Tn7 vector	pMB1, **BbsI-AmpR**, mini-Tn7T-Gm, **BsaI-*lacZ***, *oriT*	BsaI-*lacZ* site (amplified from pR6KT-SacB) cloned into BamHI and XhoI sites of pIN1T-Tn7
pAH1T-Tn7-Tet	Tet^R conjugative mini-Tn7 vector	pMB1, TetR, mini-Tn7T-Gm, **BsaI-*lacZ***, *oriT*	Tetracycline resistance gene cloned into BbsI-AmpR site of pAH1T-Tn7
pAH1	*E. coli* vector	pMB1, **BbsI-AmpR**, T0-T1 Term, **BsaI-*lacZ***, T1-T2 Term	BsaI-*lacZ* site (ApaI, NsiI fragment from pAH1T-Tn7-Tet) cloned into ApaI and NsiI sites of pIN1
pAH1T	Conjugative *E. coli* vector	pMB1, **BbsI-AmpR**, T0-T1 Term, **BsaI-*lacZ***, T1-T2 Term, *oriT*	BsaI-*lacZ* site (ApaI, NsiI fragment from pAH1T-Tn7-Tet) cloned into ApaI and NsiI sites of pIN1T
pAH1-SacB	Counterselectable *E. coli* vector	pMB1, *sacB*, **BbsI-AmpR**, T0-T1 Term, **BsaI-*lacZ***, T1-T2 Term	pMB1-*sacB* (AscI, FseI digested amplicon) cloned into AscI and FseI sites of pAH1
pAH1T-SacB	Conjugative counterselectable *E. coli* vector	pMB1, *sacB*, **BbsI-AmpR**, T0-T1 Term, **BsaI-*lacZ***, T1-T2 Term, *oriT*	pMB1-*sacB* (AscI, FseI digested amplicon) cloned into AscI and FseI sites of pAH1T
Intermediate vectors			

pAH385	Allelic exchange vector with *bla(T720C)* mutation	*oriR6K*, *oriT*, *bla(T720C)* (Amp^R), BglII-SpeI cloning site, *sacB*, *tet*(Tet^R)	*bla(T720C)* amplicon (BsaI, EcoRI digested) ligated with pAH79 fragment (BsaI, EcoRI digested)
pAB97	pUC19 with *bla(T720C)* mutation	pMB1, *bla(T720C)* (Amp^R), pUC19 *lacZα*	*bla(T720C)* amplicon (BsaI, XmaI digested) ligated with pUC19 fragment (BsaI, XmaI digested)
pIN19	pUC19 marker exchange vector	pMB1, **BbsI-AmpR**, pUC19 *lacZα*	BsaI assembly of three PCR amplicons (see Table S3)
pIN1-Tn7	Intermediate mini-Tn7 destination vector	pMB1, **BbsI-AmpR**, mini-Tn7T-Gm	BsaI assembly of three PCR amplicons (see Table S3)
pIN1T-Tn7	Intermediate conjugative mini-Tn7 vector	pMB1, **BbsI-AmpR**, mini-Tn7T-Gm-*oriT*	BsaI assembly of three PCR amplicons (see Table S3)
pIN1	Intermediate *E. coli* destination vector	pMB1, **BbsI-AmpR**, T0-T1 Term, T1-T2 Term, Spacer	BsaI assembly of five PCR amplicons (see Table S3)
pIN1T	Intermediate conjugative *E. coli* destination vector	pMB1, **BbsI-AmpR**, T0-T1 Term, T1-T2 Term, *oriT*	BsaI assembly of five PCR amplicons (see Table S3)

Source vectors

pUC19	High-copy *E. coli* vector	Source of pMB1 origin, *bla*(Amp^R), and *lacZ*a	(1)
pAH79	Allelic exchange vector	*oriR6K*, *oriT*, *bla*(Amp^R), BglII-SpeI cloning site, *sacB*, *tet*(Tet^R)	(2)
pUC18-mini-Tn7T-Gm	Mini-Tn7T vector	Source of mini-Tn7T-Gm element lacking adjacent *oriT*	(3)
pUC18T-mini-Tn7T-Gm	Conjugative mini-Tn7T vector	Source of *oriT*, mini-Tn7T-Gm element with adjacent *oriT*, and T0-T1 Term	(3)
pUC18T-mini-Tn7T-Gm-gfpmut3	Conjugative mini-Tn7T-GFP vector	Source of P_{rrnB} promoter	(4)
pUC18T-mini-Tn7T-Gm-eyfp	Conjugative mini-Tn7T-YFP vector	Source of *eyfp* and $P_{A1/04/03}$ promoter	(4)
pUC18-mini-Tn7T-Gm-lux	Mini-Tn7T-lux vector	Source of *luxCDABE* luciferase operon	(3)
pEX18Gm	Counterselectable vector	Source of *aacC1*(Gen^R) and T1-T2 Term	(5)
pEX18Tc	Counterselectable vector	Source of *tet*(Tet^R)	(5)
pIDTSmart-Kan:cons-mCherry	Constitutive mCherry vector	Source of *neo*(Kan^R), *mCherry*, and P_{cons} promoter	Custom Gene Synthesis Product (IDT)
pMA7SacB	Counterselectable λ Red vector	Source of *sacB*-pMB1	(6)
pMQ72	*E. coli*-yeast shuttle vector	Source of *araC*-P_{BAD} promoter	(7)
pUC57Pp	Mercury-PpFbFP vector	Source of PpFbFP and *merR*-P_{mer} promoter	(8)

pUCP19-ArsRBS2-mCherry	Arsenic-mCherry vector	Source of *arsR*-P_{ars} promoter	(9)

Table C2. Amplicons used for assembly of destination vectors and inserts.

Amplicon name *	Description	Primer 1	Primer 2	Template plasmid
BsaI-lacZ cloning site				
BsaI-*lacZ* site (pUC19)	Cloning BsaI-flanked *lacZ*α gene into pAH385	F2-pUC19-BsaI	R2-pUC19-BsaI	pUC19
BsaI-*lacZ* site (pR6KT-SacB)	Transferring BsaI-*lacZ* site from pR6KT-SacB to mini-Tn7 polylinker	F-MCS	R-MCS	pR6KT-SacB
Site-directed mutagenesis of bla(T720C)				
bla(T720C) amplicon (pUC19)	pUC19 fragment with introduced *bla(T720C)* mutation	F-pUIC3-bla	R2-pUC19-BsaI	pUC19
bla(T720C) amplicon (pAH385)	pAH79 fragment with introduced *bla(T720C)* mutation	F-pUIC3-bla	R-pUIC3-EcoRI	pAH79
Destination vector segments				
pMB1	High-copy pMB1 replicon from pUC19	F-pMB1	R-pMB1	pUC19
BbsI-AmpR	BbsI-flanked *bla(T720C)* ampicillin resistance gene	F-Marker	R-Marker	pAB97
T0-T1 Terminators	Phage Lambda terminator T0 and *E. coli rrnB* terminator T1	F-termT0T1	R-termT0T1	pUC18T-mini-Tn7T-Gm
T1-T2 Terminators	E. coli *rrnB* transcriptional terminators T1 and T2	F-termT1T2	R-termT1T2	pEX18Gm
Spacer	pUC19 spacer sequence	F-oriT	R-oriT	pUC19
oriT	Origin of transfer	F-oriT	R-oriT	pUC18T-mini-Tn7T-Gm
mini-Tn7T-Gm	Mini-Tn7T-Gm element	F-oriT	R-lacZalpha	pUC18-mini-Tn7T-Gm
mini-Tn7T-Gm-*oriT*	Mini-Tn7T-Gm element and origin of transfer	F-oriT	R-lacZalpha	pUC18T-mini-Tn7T-Gm
pMB1-*sacB*	High-copy pMB1 replicon and *sacB* marker gene	F-sacB-pMB1	R-pMB1	pMA7SacB

pUC19 *lacZα*	pUC19 *lacZ*a gene with polylinker	F-oriT	R-lacZalpha	pUC19

Promoter inserts

P_{rrnB}	*E. coli* constitutive rRNA promoter	F-PrrnB	R-PA10403	pUC18T-mini-Tn7T-Gm-gfpmut3
$P_{A1/04/03}$	Strong constitutive modified *lac* promoter	F-PA10403	R-PA10403	pUC18T-mini-Tn7T-Gm-eyfp
P_{cons}	Synthetic constitutive promoter	F-Pconst-term	R-Pcont	pIDTSmart-Kan:cons-mCherry
araC-P_{BAD}	*E. coli* arabinose-inducible promoter	F2-Pbad	R2-Pbad	pMQ72
arsR-P_{ars}	*E. coli* arsenite-inducible promoter	F-arsRbs2	R-arsRbs2	pUCP19-ArsRbs2-mCherry
merR-P_{mer}	*E. coli* mercury-inducible promoter	F-merR	R-merR	pUC57Pp

Reporter inserts

eYFP	Enhanced yellow fluorescent protein	F-yfp	R-gfpmut3	pUC18T-mini-Tn7T-Gm-eyfp
mCherry	mCherry fluorescent protein (contains 6X His tag and G456A mutation)	F-mCherry/R-mCherry-Syn	F-mCherry-Syn/R-mCherry	pIDTSmart-Kan:cons-mCherry
PpFbFP	Flavin-based fluorescent protein (derived from *Pseudomonas putida*)	F-PpFbFP	R-PpFbFP	pUC57Pp
Luciferase	*luxCDABE* operon (contains *luxC(A1312C)* mutation)	F1-lux/R1-lux	F2-lux/R3-lux	pUC18-mini-Tn7T-Gm-lux

Selectable marker inserts

AmpR	Ampicillin resistance gene; *bla(T720C)*	F-AmpR	R-AmpR	pAB97
GenR	Gentamicin resistance; *aacC1*	F-AmpR	R-AmpR	pEX18Gm
KanR	Kanamycin resistance; *neo*	F-KanR	R-KanR	pIDTSmart-Kan:cons-mCherry
TetR	Tetracycline resistance gene; *tet(C654G)*	F-AmpR/R-TetR-Syn	F-TetR-Syn/R-AmpR	pEX18Tc

***** Nucleotide sequences for the promoter, reporter, and selectable marker inserts listed here are deposited at GenBank under the following accession numbers: OK148695-OK148700 (promoter inserts), OK165501-OK165504 (reporter inserts), OK165505-OK165508 (selectable marker inserts).

Supporting Figures

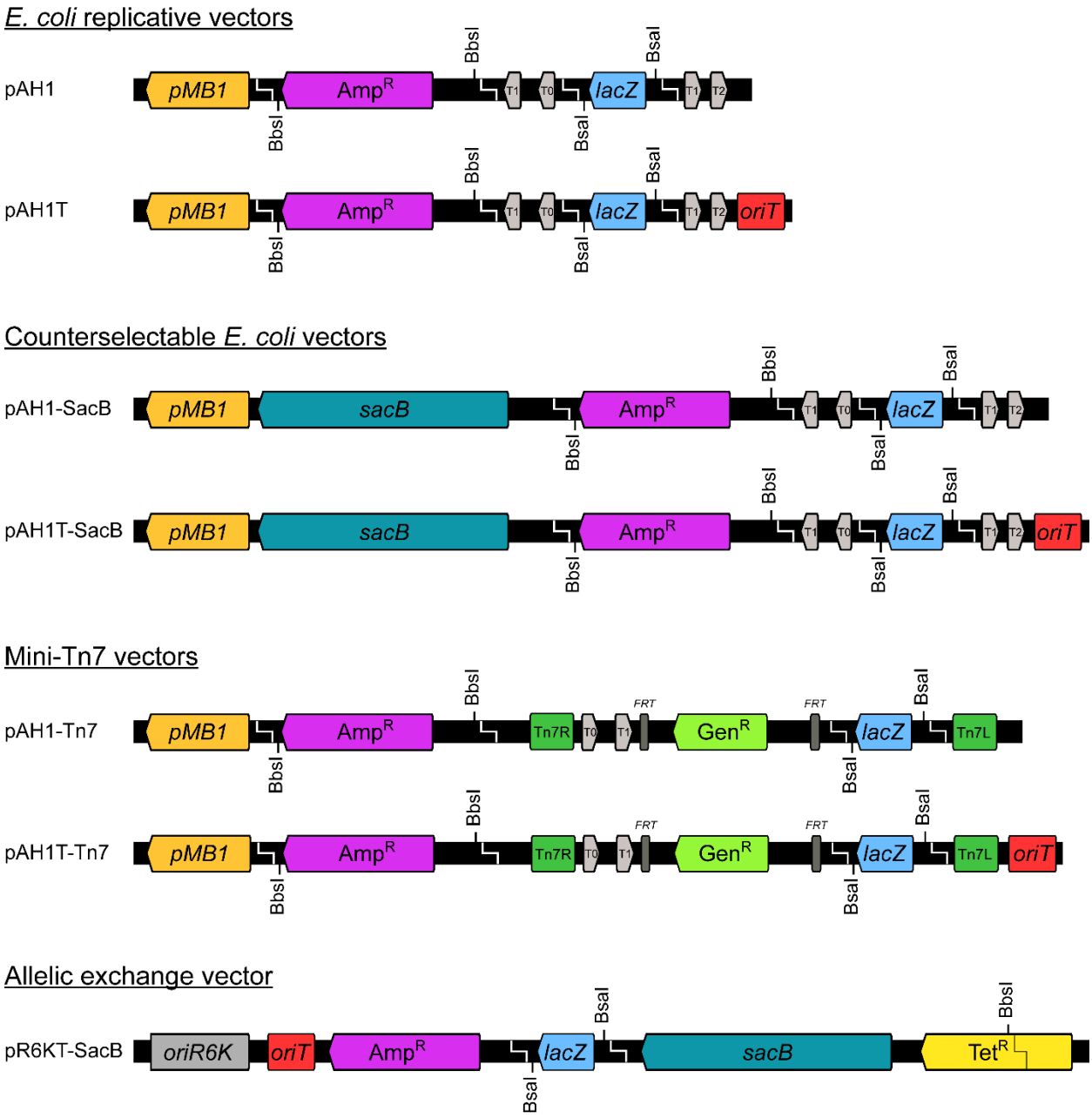

Fig. C1. Genetic maps of destination vectors. The position and orientation of genetic elements and Type IIS restriction sites are depicted for Golden Gate destination vectors. Cleavage locations of BsaI and BbsI sites are indicated by white lines. Vectors replicate in *E. coli* via the pMB1 origin of replication (1). Counterselectable vectors encode the *sacB* gene conferring sucrose sensitivity (10). Mini-Tn7 vectors encode the site-specific transposon mini-Tn7T-Gm (3), modified to incorporate a Golden Gate cloning site. Following transposition in susceptible

hosts, sequences between the transposon ends (Tn7R and Tn7L) become stably integrated at the *attTn7* genomic site. The allelic exchange vector pR6KT-SacB replicates in hosts expressing the *pir* gene (eg, DH5α λpir or SM10 λpir) (11), and can be used as a suicide plasmid in all other recipients. Additional vector elements include: Amp^R, ampicillin-resistance gene with a synonymous mutation *bla (T720C)* altering an internal BsaI recognition sequence; *lacZ*, pUC19 *lacZ*α fragment for blue-white screening; T0, lambda phage transcriptional terminator; T1 and T2, *E. coli rrnB* operon terminators; *oriT*, RP4-based origin of conjugative transfer; Tet^R, tetracycline-resistance gene; Gen^R, gentamicin-resistance gene (*aacC1*); *FRT*, FLP-recombinase target for Gen^R marker removal. Construction details and sequence sources are described in the Materials and Methods, Table 2, and Tables S1-S2. The sequences of the BsaI cloning site are presented in Fig. S2. Nucleotide sequences for each destination vector are deposited at GenBank under the following accession numbers: OK148689 (pAH1), OK148690 (pAH1T), OK148691 (pAH1-SacB), OK148692 (pAH1T-SacB), OK148693 (pAH1-Tn7), OK148694 (pAH1T-Tn7), and OK165509 (pR6KT-SacB). Complete sequences were deposited, except for pR6KT-SacB, in which a partial sequence containing the Golden Gate assembly site was deposited, as the source sequences of the vector backbone are unknown.

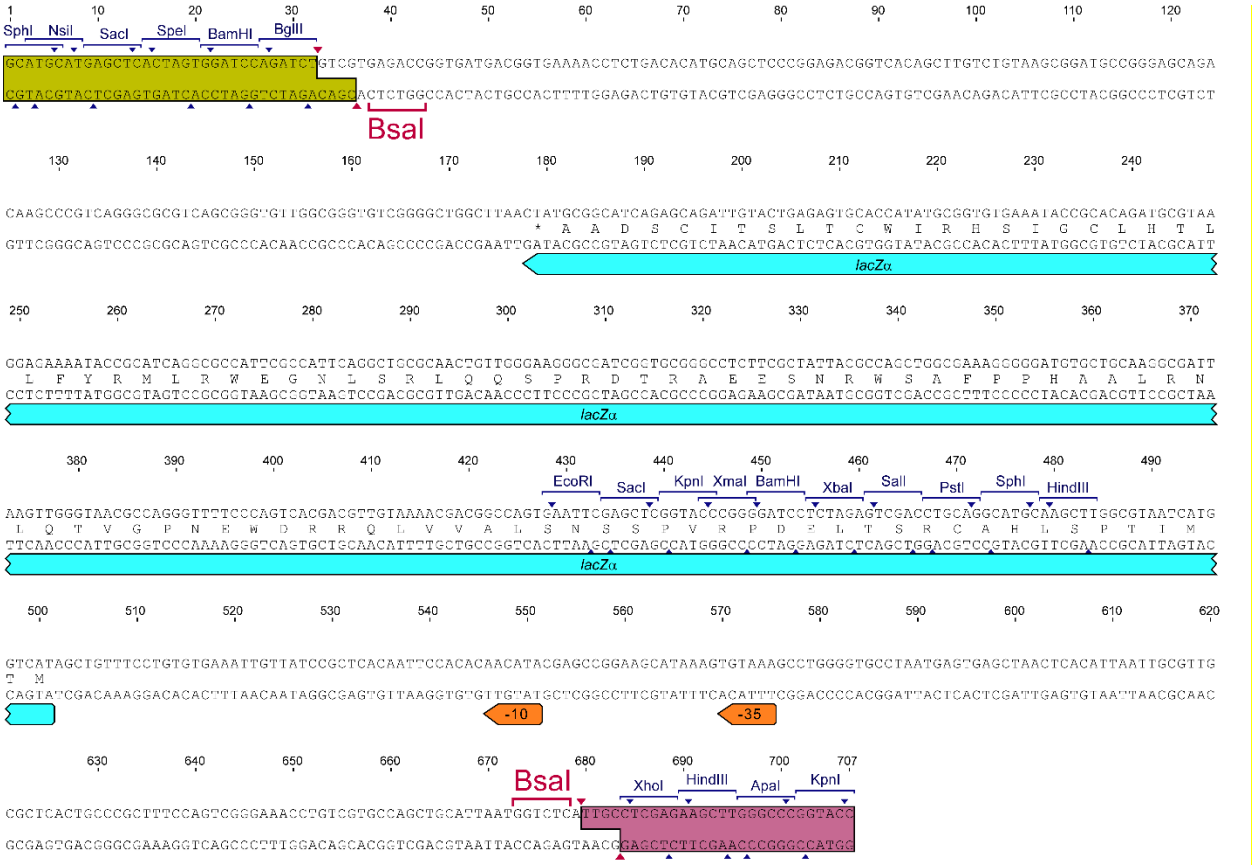

Fig. C2. Sequence of BsaI-*lacZ* Golden Gate assembly site. The *lacZα* gene and promoter (-10 and -35) elements are derived from pUC19 (1). The positions of BsaI recognition sequences (5'-GGTCTC-3') and cleavage sites (triangles) are shown. All Golden Gate destination vectors, with the exception of pR6KT-SacB, contain polylinkers derived from mini-Tn7T-Gm (3) outside of the BsaI assembly site (shaded yellow and purple regions). Nucleotide sequences of the BsaI-*lacZ* cloning site of all destination vectors can be accessed at GenBank under the accession numbers listed in Fig. C1.

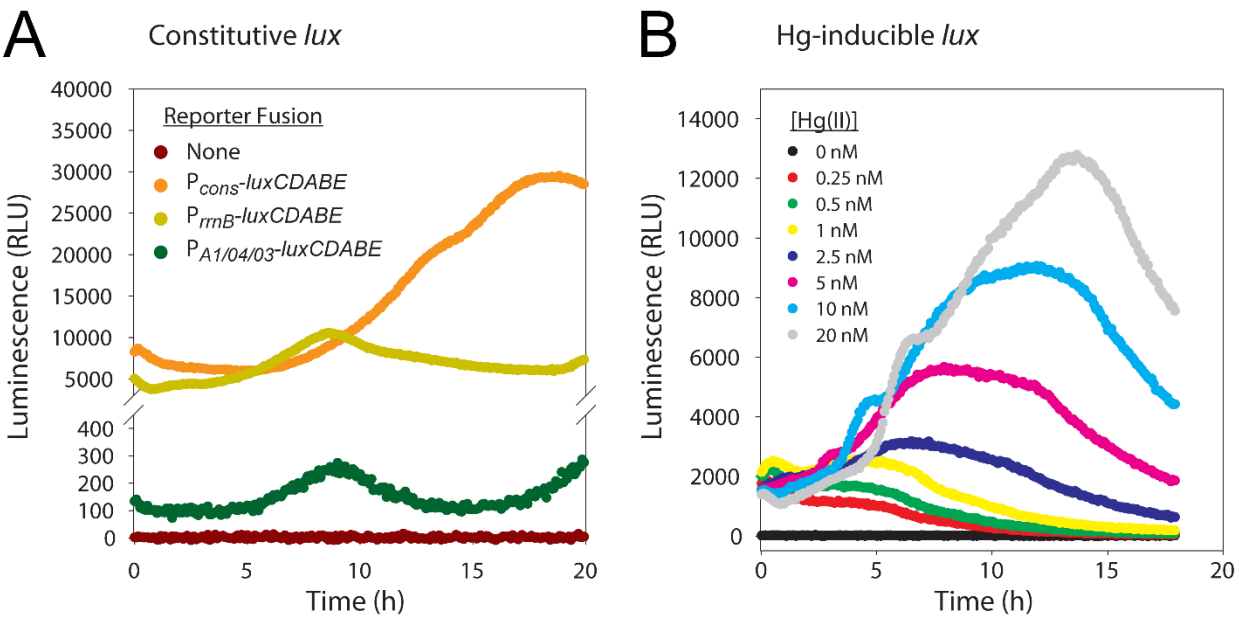

Fig. C3. Time-course of light production for constitutive and mercury-inducible luciferase bioreporters. Suspension assays were prepared for *E. coli* bioreporters containing (A) constitutive and (B) mercury-inducible promoters fused to the *Photorhabdus luminescens* luciferase operon on the pAH1T vector. The time-course of light production, plotted as relative luminescence units (RLU), illustrates the non-linear induction response with peak luminescence occurring at different time points depending on the promoter identity or Hg(II) concentration. The unexpectedly low signal production for the $P_{A1/04/03}$-*lux* construct was explained by an IS1-like transposable element within the promoter that was identified by DNA sequencing. The insertion was likely selected to compensate for the high cost of light production. For each strain or treatment, the mean of triplicate assays prepared from a single representative assay is shown.

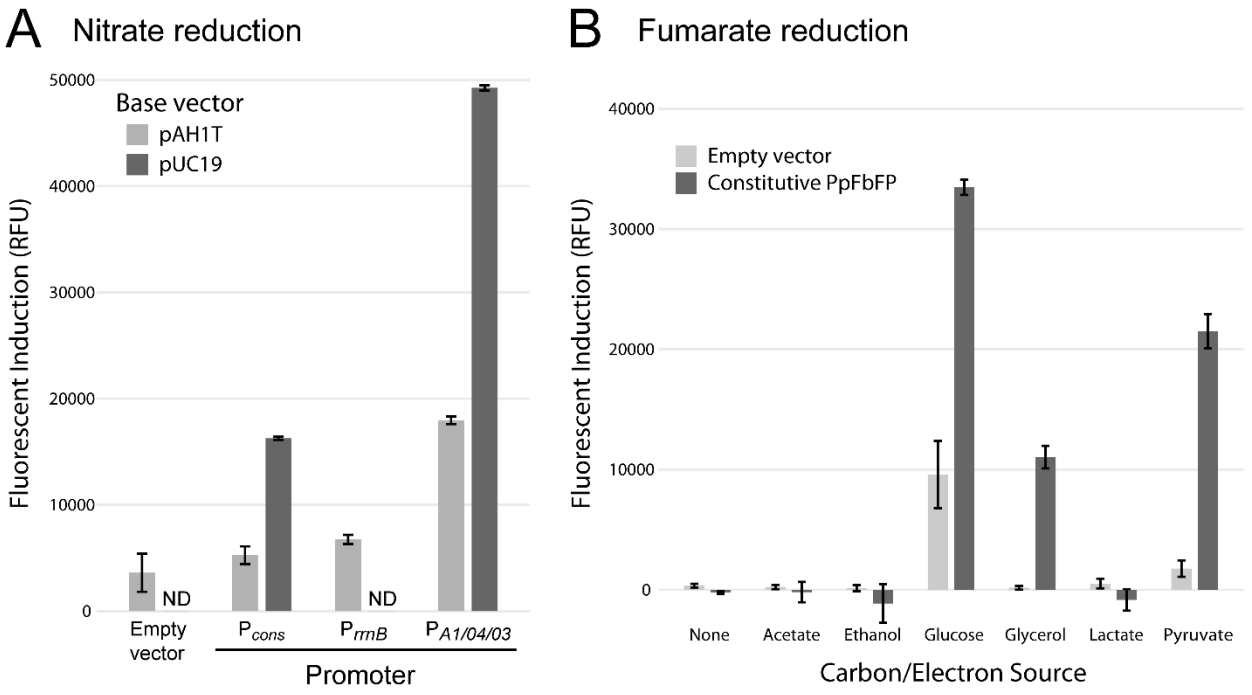

Fig. C4. Constitutive fluorescence of PpFbFp under anaerobic conditions Fluorescence was quantified as fluorescent induction in relative fluorescence units (RFU) at 4 hours (Nitrate reduction) or at 10 hours (Fumarate reduction) in anaerobic cell suspension assays of *E. coli* NEB5-α with the reporter PpFbFP. (A) Comparison of signal production among bioreporters with different promoters and base vectors undergoing nitrate reduction. (B) Fluorescence from the pUC19-$P_{A1/O4/O3}$-PpFbFP construct using 10 mM of different carbon/electron donors on fumarate reduction. Each treatment including "None" contains beta-glycerophosphate. The mean fluorescent induction and standard error is shown for three independent suspension assays (each assayed in triplicate).

Supporting References

1. Yanisch-Perron C, Vieira J, Messing J. 1985. Improved M13 phage cloning vectors and host strains: nucleotide sequences of the M13mpl8 and pUC19 vectors. Gene 33:103–119.

2. Bailey SF, Hinz A, Kassen R. 2014. Adaptive synonymous mutations in an experimentally evolved Pseudomonas fluorescens population. Nat Commun 5:1–7.

3. Choi K-H, Gaynor JB, White KG, Lopez C, Bosio CM, Karkhoff-Schweizer RR, Schweizer HP. 2005. A Tn*7*-based broad-range bacterial cloning and expression system. Nat Methods 2:443–448.

4. Choi K-H, Schweizer HP. 2006. mini-Tn*7* insertion in bacteria with single *att*Tn*7* sites: example *Pseudomonas aeruginosa*. Nat Protoc 1:153–161.

5. Hoang TT, Karkhoff-Schweizer RR, Kutchma AJ, Schweizer HP. 1998. A broad-host-range Flp-*FRT* recombination system for site-specific excision of chromosomally-located DNA sequences: application for isolation of unmarked *Pseudomonas aeruginosa* mutants. Gene 212:77–86.

6. Lennen RM, Nilsson Wallin AI, Pedersen M, Bonde M, Luo H, Herrgård MJ, Sommer MOA. 2016. Transient overexpression of DNA adenine methylase enables efficient and mobile genome engineering with reduced off-target effects. Nucleic Acids Res 44:e36.

7. Shanks RMQ, Caiazza NC, Hinsa SM, Toutain CM, O'Toole GA. 2006. *Saccharomyces cerevisiae*-based molecular tool kit for manipulation of genes from gram-negative bacteria. Appl Environ Microbiol 72:5027–5036.

8. Stenzler B, Hinz A, Ruuskanen M, Poulain AJ. 2017. Ionic strength differentially affects the bioavailability of neutral and negatively charged inorganic Hg complexes. Environ Sci Technol 51:9653–9662.

9. Pothier MP, Hinz AJ, Poulain AJ. 2018. Insights into arsenite and arsenate uptake pathways using a whole cell biosensor. Front Microbiol 9:2310.

10. Blomfield IC, Vaughn V, Rest RF, Eisenstein BI. 1991. Allelic exchange in *Escherichia coli* using the *Bacillus subtilis sacB* gene and a temperature-sensitive pSC101 replicon. Molecular Microbiology 5:1447–1457.

11. Rakowski SA, Filutowicz M. 2013. Plasmid R6K replication control. Plasmid 69:231–242.

Appendix D: Supporting information from chapter 6.

Diffusion of H_2S from anaerobic thiolated ligand biodegradation rapidly generates bioavailable mercury

Benjamin R. Stenzler[1], Rui Zhang[1], Jeremy D. Semrau[3], Alan A. DiSpirito[2], and Alexandre J. Poulain[1]*†

* Alexandre Poulain[1]. Email: apoulain@uottawa.ca

This includes:

Supporting Text

Recipes for Growth and Exposure Media

Fumarate reduction plates were made as follows: 191mL of milli-Q water was autoclaved with 3.75 grams of bacto agar for 1 hour in a borosilicate bottle. Once finished, 43.5mL of Difcto™ M9 salts(5x). 250 µL of Trace elements #1 and 250 µL of Trace elements #2 solution as described in (*1*), 250 µL of 10mM EDTA. 125 uL of 2M $MgSO_4$, 10mL of 1M Na_2Fumarate,15 µL of 0.225M FeSO4 in 0.1M H2SO4, 0.5 mL of 500mM Thiamine HCl, 1.5 mL of amino acids (75mM Leucine, 75 mM Isoleucine and 75 mM Valine), 5 mL of 1M glucose and 250µL of 100mg/mL ampicillin sodium salt. The plates were poured in an Coy Vinyl Anaerobic chamber (98% N_2, 1.5% H_2) (The cap of the borosilicate bottle was tightly screwed on before placing in the airlock to prevent unnecessary and violent explosions). Plates were used the day they were prepared.

Growth Media (250 mL) consisted of 43.5mL of Difcto™ M9 salts(5x), 20 mM Glucose, 15 µL of 0.225M $FeSO_4$ in 0.2M H_2SO_4 (stored anaerobically), 125 µL of 2M $MgSO_4$, 0.5 mL of 0.5M Thiamine HCl from a frozen (-20˚C) aliquot, 10 mL of 1M Na_2Fumarate, 1.5 mL of 75mM l-leucine/ l-isoleucine/ valine, 250 µL of Trace elements #1 and 250 µL of Trace elements #2 solution as described in (81), and 250 µL of 0.01M EDTA sodium salt. Bubbled under N2 gas to make anaerobic. Growth media was not stored longer than 1 week.

Exposure media (100 mL) developed in this study contained 700 µL of 1M Sodium Beta-Gylcerophosphate from a frozen (-20˚C) aliquot, 4 mL of 1M Mops free acid, 200 µL of 0.5M $(NH_4)_2SO_4$, 2 mL of 1M Glucose, and 620-660 µL of (1.725M KOH and 0.775M NaOH) to

adjust pH to 7. All reagents, except Sodium Beta-Gylcerophosphate, were stored anaerobically in the anaerobic chamber. Exposure media was prepared the day it was used.

Supporting Tables and Figures

Table D1. Raw data for Figure 6.1 (A, B, C, D, E, and F), and Figure 6.2 (A and B), including the number of biologic replicates (n). Average Normalized Fluorescence measured as relative fluorescence units (RFU) ± 1SD at 10 hours by the Hg-Inducible biosensor (*E. coli* NEB5α harboring the pUC57merR-Pp plasmid) and the Constitutive biosensor (*E. coli* NEB5α harboring pUC19AH206-Pp plasmid). Fluorescence at 10 hours was normalized to the control (0 µM) at 10 hours for each biological replicate. [Hg] was set to 2 nM. These experiments were performed at 37 ˚C in anaerobic exposure medium (pH 7).

Figure 6.1A

Glutathione (uM)	Hg-Inducible Fluorescence (RFU)	SD	n	Constitutive Fluorescence (RFU)	SD	n
0	1	0	6	1		3
0.001	0.953	0.054	3	1.075	0.035	3
0.01	0.914	0.084	2	1.092	0.066	3
0.1	0.850	0.139	6	1.127	0.049	3
0.5	0.082	0.012	3	1.206	0.049	3
1	0.026	0.036	6	1.459	0.141	3
5	0.019	0.059	6	1.764	0.374	3

Figure 6.1B

MethanobactinOB3b (uM)	Hg-Inducible Fluorescence (RFU)	SD	n	Constitutive Fluorescence (RFU)	SD	n
0	1		4	1		3
0.001	1.022	0.124	4	1.129	0.069	3
0.01	1.054	0.064	4	1.120	0.085	3
0.1	1.254	0.084	4	1.116	0.094	3
0.5	0.780	0.050	4	1.100	0.137	3
1	0.123	0.043	4	1.288	0.184	3
5	-0.096	0.019	4	2.292	0.205	3

Figure 6.1C

DMSA (uM)	Hg-Inducible Fluorescence (RFU)	SD	n	Constitutive Fluorescence (RFU)	SD	n
0	1		13	1		9
0.001	0.618	0.580	5	1.125	0.048	5
0.005	0.077	0.109	5	1.086	0.066	5

0.01	0.117	0.058	5	0.936	0.060	3
0.1	-0.003	0.095	7	1.120	0.088	4
1	-0.030	0.066	7	0.635	0.110	8

Figure 6.1D

Penicillamine (uM)	Hg-Inducible Fluorescence (RFU)	SD	n	Constitutive Fluorescence (RFU)	SD	n
0	1		4	1		4
50	5.133	1.094	4	1.160	0.031	4
500	1.076	0.499	4	0.984	0.070	4
1000	0.481	0.227	4	0.789	0.026	4
4000	0.331	0.123	4	0.516	0.084	4

Figure 6.1E

Cysteine (uM)	Hg-Inducible Fluorescence (RFU)	SD	n	Constitutive Fluorescence (RFU)		n
0	1		9	1		8
50	1.272	0.427	4	0.668	0.056	3
500	1.530	0.595	4	0.678	0.027	3
1000	0.689	0.472	3	0.889	0.143	3
4000	0.295	0.103	3	0.515	0.059	3

Figure 6.1F

BAL (uM)	Hg-Inducible Fluorescence (RFU)	SD	n	Constitutive Fluorescence (RFU)	SD	n
0	1		16	1		4
0.001	1.740	0.848	3	1.078	0.088	3
0.005	1.887	0.037	2	1.029	0.097	3
0.01	2.399	0.751	5	0.793	0.045	3
0.1	2.971	0.704	71	1.003	0.125573	3
1	1.447	0.311	11	1.092	0.089	3

Figure 6.3A

Treatment	Hg-Inducible Fluorescence (RFU)	SD	n	Constitutive Fluorescence (RFU)	SD	n
0 uM Pen	1		9	1		6
50 uM Pen	5.133	1.094	4	1.160	0.031	4
500 uM Pen	1.076	0.499	4	0.984	0.070	4
5 uM GSH	0.038	0.046	5	1.878	0.248	2

5 uM GSH + 50 uM Pen	0.044	0.035	5	1.942	0.006	5
5 uM GSH + 500 uM Pen	-0.019	0.028	5	1.672	0.023	2
5 uM Mtb	-0.042	0.029	5	2.348	0.202	5
5 uM Mtb + 50 uM Pen	-0.062	0.049	5	2.271	0.193	2
5 uM Mtb + 500 uM Pen	-0.036	0.024	5	1.925	0.121	2

Figure 6.3B

Treatment	Hg-Inducible Fluorescence (RFU)	SD	n	Constitutive Fluorescence (RFU)		n
0 uM Cys	1		4	1		4
50 uM Cys	1.272	0.427	4	0.668	0.056	3
500 uM Cys	1.530	0.595	4	0.678	0.027	3
5 uM GSH	2.431	0.311	4	1.031	0.055	4
5 uM GSH + 50 uM Cys	4.196	0.426	4	1.033	0.059	4
5 uM GSH + 500 uM Cys	3.797	0.498	4	0.822	0.087	4
5 uM Mtb	1.993	0.424	4	1.612	0.108	4
5 uM Mtb + 50 uM Cys	2.813	1.221	4	1.462	0.084	4
5 uM Mtb + 500 uM Cys	2.391	0.308	4	1.133	0.082	4

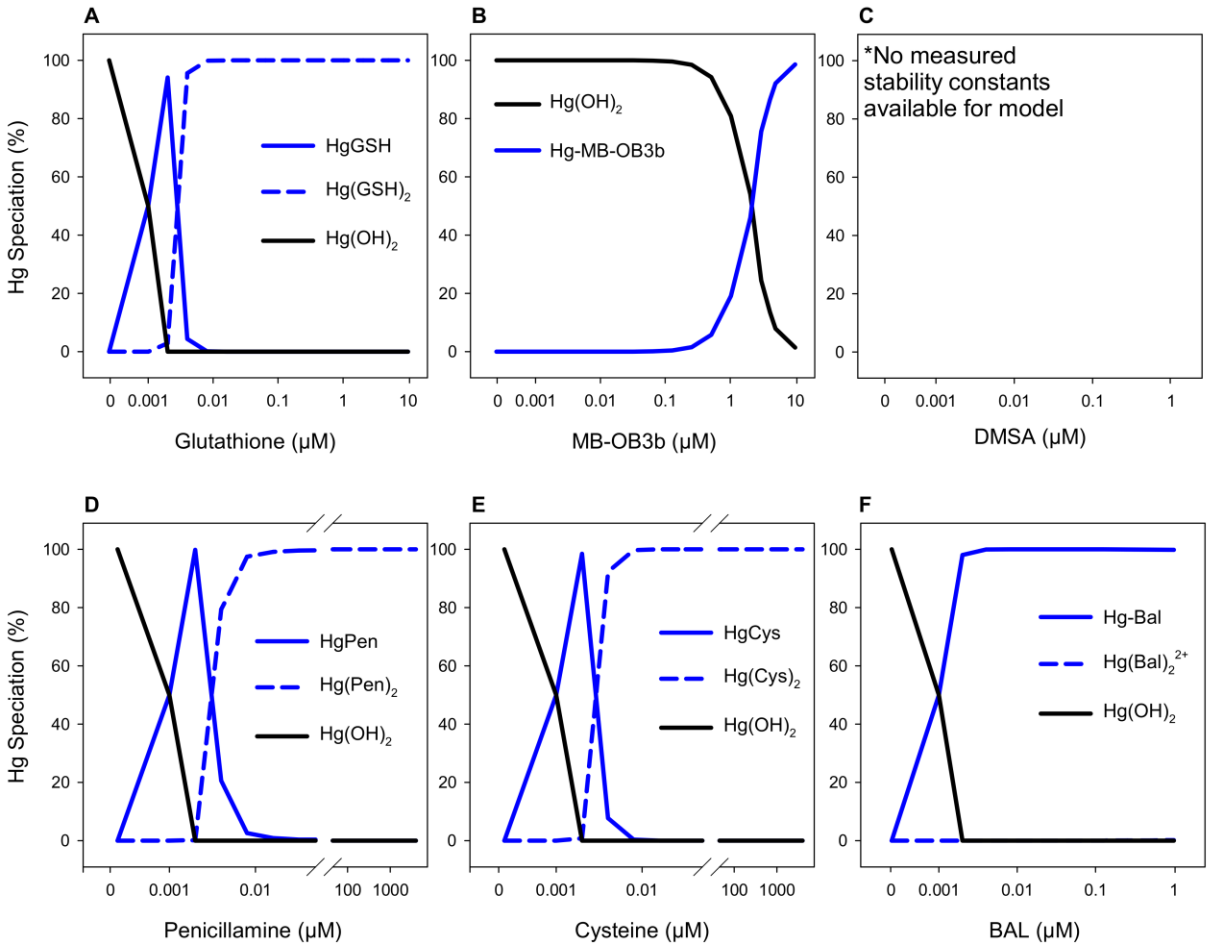

Figure D1: Hg(II) species with the addition of various thiols without membrane thiols. Thermodynamic model predicting the Hg speciation (%) with the addition **A)** glutathione (0-10 μM) **B** methanobactin from *M trichosporium* OB3b (MB-OB3b) (0-10 μM), **C)** DMSA (0-4000 μM), **D)** penicillamine (0, 7.5-4000 μM), **E)** cysteine (0, 7.5-4000 μM) and **F)** BAL (0-1 μM). Models were performed in anaerobic exposure medium (pH 7) and [Hg(II)] was set to 2 nM. The models performed at 25˚C due to the availability of thermodynamic data. Stability constants were altered for HgGSH, HgPen and HgCys from (*2*). No stability constants were available to construct a model with DMSA.

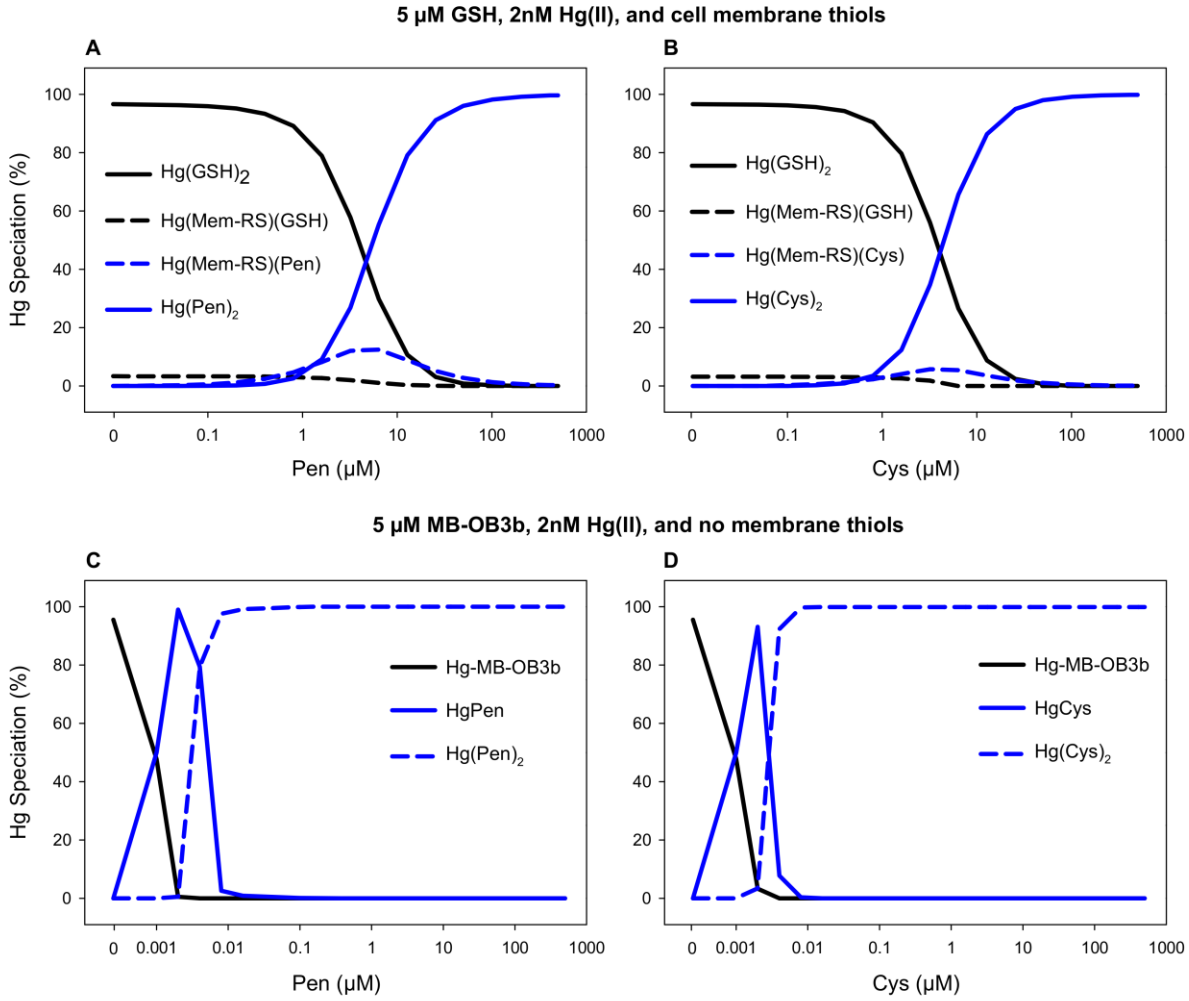

Figure D2. Hg(II) species with thiol ligand exchanges. Thermodynamic model predicting the Hg speciation (%) with the addition penicillamine (Pen) and cysteine (Cys) (0-500 µM). **A and B)** Models were done with 5 µM glutathione (GSH) at equilibrium with the cell membrane thiols. **C and D)** Models were done with 5 µM methanobactin from *M trichosporium* OB3b (MB-OB3b) with equilibrium of the cell membrane excluded. Models were performed in anaerobic exposure medium (pH 7), and [Hg(II)] was set to 2 nM. The models performed at 25˚C due to the availability of thermodynamic data.

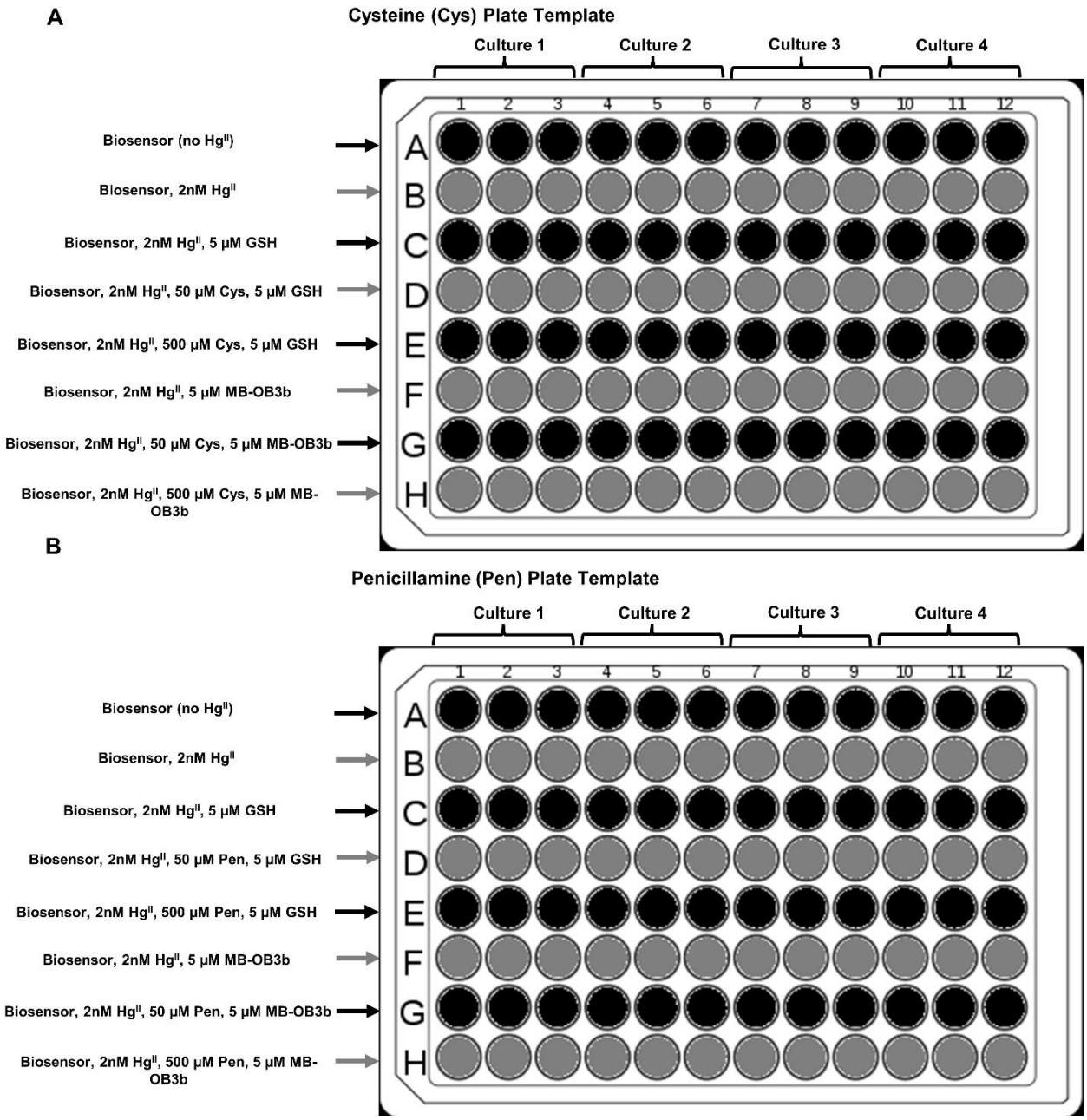

Figure D3: Plate templates with ligand exchanges using Penicillamine (Pen) and Cysteine (Cys). Experimental plate templates for **A)** Figure 2a and **B)** Figure 2b. In this experiment Hg(II) had already equilibrated with 5 uM glutathione (GSH) or 5 uM methanobactin from *Methylosinus trichosporium* OB3b (MB-OB3b). 50, 500 µM Cys/Pen were added to these treatments to investigate ligand exchange. Each row represents a different treatment and each column (into sections of 3) consisted of different biological replicates (separate cultures). Experiments with 50, 500 µM Cys/Pen with 2 nM Hg^{II} were performed in separate 96 well plates and are the same data of Fig 1D and E.

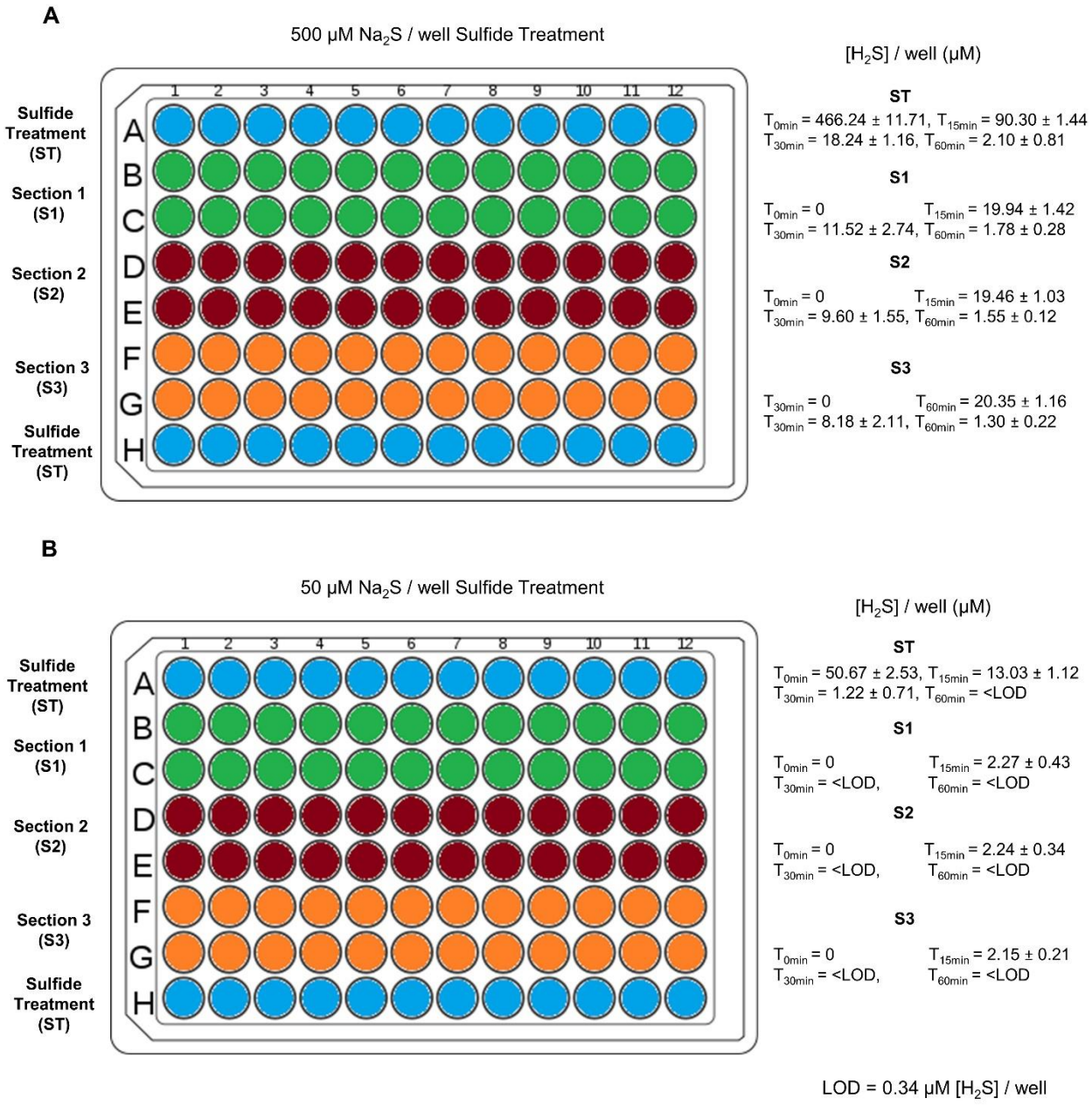

Figure D4: Sulfide Migration in the 96 well microplate experimental design and raw data. H_2S concentration per well measured as ([H_2S]/well) (µM) ± 1SD in the 96 well microplate containing **A)** 500 or **B)** 50 µM Na_2S (in exposure medium, (pH 7)) in the Sulfide Treatment wells (ST) (wells A1-A12 and H1-H12). Average H_2S was measured after 0, 15, 30, and 60 minutes in the microplate reader for ST, section 1 (S1) (wells B1-B12 and C1-C12), section 2 (S2) (wells D1-D12 and E1-E12), and section 3 (S3) (wells F1-F12 and G1-G12). Sections 1-3 contained only 200 µL of exposure medium/well. Measurements for each time point were measured in triplicate (3 separate 96 well microplates). The detection limit for S^{2-} (0.34 µM [[H_2S]/well]).

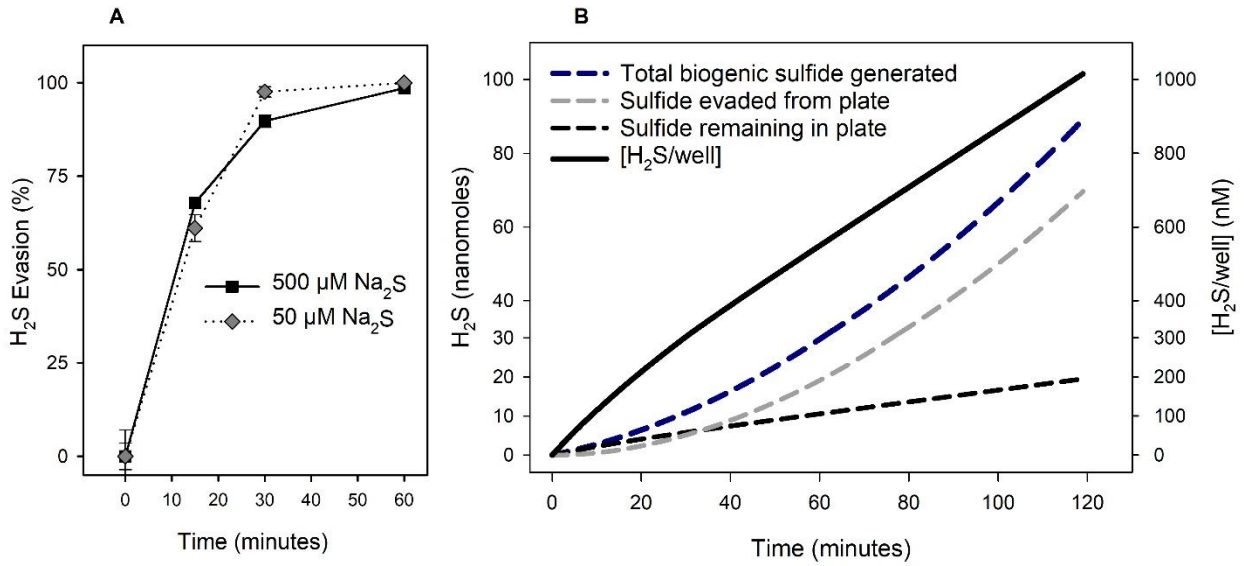

Figure D5: Predicted biogenic H_2S concentrations in a 96 well microplate. **A)** H_2S (%) that evaded from the 96 well microplates over time (minutes) containing 500 or 50 µM Na_2S from Fig D4. A half-life of about 11-12.5 minutes was determined. **B)** Estimated quantity of biogenic H_2S (nanomoles) (left axis) generated by the biosensor over time in the 96 well microplate and predicted quantity of sulfide that will evade or remain in the microplate. The estimated maximum concentration of sulfide in each well ([H_2S/well] (nM)) (right axis) over time. This model assumes that all the sulfide remaining in the plate is evenly distributed across all wells and in the liquid phase. Biosensor H_2S production rates are based on the biosensor metabolizing 500 µM cysteine in ¼ of the plate wells from Fig 6.5.

Table D2: H_2S produced by *E. coli* with added thiols. Hydrogen sulfide (H_2S) (µM) produced by the Hg-Inducible biosensor over time (hours) in the presence of no added thiol (control), 5 µM GSH, 5 µM MB-OB3b, 1 µM DMSA, or 1 µM BAL. The experiment was performed at 37 ˚C in an anaerobic exposure medium (pH 7), 100 serum bottles, and triplicate. Values with concentrations below the detection limit for H_2S (0.34 µM) are reported as zero.

	Biosensor H_2S production (µM)				
Time (hours)	Control	5 µM GSH	5 µM MB-OB3b	1 µM DMSA	1 µM BAL
0	0	0	0	0	0
1	0	0	0	0	0
2	0	0	0	0	0
3	0	0	0	0	0
4	0	0	0	0	0
24	0	0	0	0	0

Table D3. Stability constants ($log_{10}K$) for all aqueous Hg(II)-species considered in the speciation calculations. Molar enthalpy changes (ΔH(KJ/mol)) are reported if available. Constants are reported for 25°C at an ionic strength of 0 M. Some values were not measured specifically (i.e, for heterothiol complexes (HgGshCysteine) and one-coordinated thiols ($HgGsh^+$)) and were approximated based on the recommendation of the study (Liem-Nguyen et al., 2017) to maintain internal consistency for the modelling data. One coordinated complexes are a mix complex with one thiol and one or more O/N functional groups. Hg(Mem-RSRO) complex is composed of a mixture of Mem-R^ISH and neighboring O/N functional groups.. The stability constants for hetero complexes were determined to be at least 1.5 log units smaller than the average stability constant for the corresponding $Hg(SR)_2$ complexes (Liem-Nguyen et al., 2017).

Formula	$log_{10}K$	ΔH(KJ/mol)	Reference
$Hg^{2+} + 2H_2O = Hg(OH)_2 + 2H^+$	-5.98 ± 0.06	51.5 ± 1.8	(Powell et al., 2005)
$NH_3 + H^+ = NH_4^+$	-9.244		(NIST, 2015)
$Hg^{2+} + NH_3 = HgNH_3^{2+}$	8.8		(NIST, 2015)
$Hg^{2+} + 2NH_3 = Hg(NH_3)_2^{2+}$	17.8	-311	(NIST, 2015)
$Hg^{2+} + 3NH3 = Hg(NH_3)_3^{2+}$	18.156	-429	(NIST, 2015)
$Hg^{2+} + 4NH_3 = Hg(NH_3)_4^{2+}$	19.3	-548	(NIST, 2015)
$Hg^{2+} + H_2O = HgOH^+ + H^+$	2.797	-18.91	(Powell et al., 2005)
$Hg^{2+} + SO_4^{2-} = HgSO_4$	2.535		(NIST, 2015)
$MOPS^- + H^+ = HMOPS$	7.184	-21.1	(Goldberg et al., 2002)
$H^+ + Cysteine^- = HCysteine$	8.6		(Liem-Nguyen et al., 2017)
$H^+ + Penicillamine^- = HPenicillamine$	8.3		(Liem-Nguyen et al., 2017)
$H^+ + Gsh^- = HGsh$	9.3		(Liem-Nguyen et al., 2017)
$Hg^{2+} + 2Cysteine^- = Hg(Cysteine)_2$	37.5 ± 0.2		(Liem-Nguyen et al., 2017)

$Hg^{2+} + 2Gsh^{-} = Hg(Gsh)_2$	38.8 ± 0.2	(Liem-Nguyen et al., 2017)
$Hg^{2+} + 2Penicillamine^{-} = Hg(Penicillamine)_2$	36.9 ± 0.2	(Liem-Nguyen et al., 2017)
$Hg^{2+} + Cysteine^{-} = HgCysteine^{+}$	25 ± 0.5	(Song et al., 2018)
$Hg^{2+} + Gsh^{-} = HgGsh^{+}$	25 ± 0.5	(Song et al., 2018)
$Hg^{2+} + Penicillamine^{-} = HgPenicillamine^{+}$	25.5 ± 0.5 aproximated from study	(Song et al., 2018)
$Hg^{2+} + Cysteine^{-} = HgCysteine^{+}$	30.75 ± 0.25 aproximated from study	(Liem-Nguyen et al., 2017)
$Hg^{2+} + Gsh^{-} = HgGsh^{+}$	30.75 ± 0.25 aproximated from study	(Liem-Nguyen et al., 2017)
$Hg^{2+} + Penicillamine^{-} = HgPenicillamine^{+}$	30.75 ± 0.25 aproximated from study	(Liem-Nguyen et al., 2017)
$Hg^{2+} + Cysteine^{-} + Gsh^{-} = HgGshCysteine$	36.65 aproximated from study	(Liem-Nguyen et al., 2017)
$Hg^{2+} + Gsh^{-} + Penicillamine^{-} = HgGshPenicillamine$	36.35 aproximated from study	(Liem-Nguyen et al., 2017)
$H^{+} + Mem\text{-}R^{I}S = H\ Mem\text{-}R^{I}S$	9.5	(Song et al., 2020)
$H^{+} + Mem\text{-}R^{II}S^{-} = HMem\text{-}R^{II}S$	9.5	
$Hg^{2+} + Mem\text{-}R^{II}S^{-} = Hg(Mem\text{-}R^{II}S)_2$	39.1 ±0.2	
$Hg^{2+} + Mem\text{-}R^{I}S^{-} + Cysteine\text{-} = Hg(Mem\text{-}R^{I}S)Cysteine$	38.1 ±0.1	
$Hg^{2+} + Mem\text{-}R^{II}S^{-} + Cysteine\text{-} = Hg(Mem\text{-}R^{II}S)Cysteine$	38.1 ±0.1	
$Hg^{2+} + Mem\text{-}R^{I}S^{-} + Penicillamine^{-} = Hg(Mem\text{-}R^{I}S)$ Penicillamine	38.1 Assumed for mdelling (not measured)	
$Hg^{2+} + Mem\text{-}R^{II}S^{-} + Penicillamine^{-} = Hg(Mem\text{-}R^{II}S)$ Penicillamine	38.1 Assumed for mdelling (not measured)	
$Hg^{2+} + Mem\text{-}R^{I}S^{-} + Gsh^{-} = Hg(Mem\text{-}R^{I}S)Gsh$	38.1	

	Assumed for mdelling (not measured)	
Hg^{2+} + Mem-$R^{II}S^-$ + Gsh^-= Hg(Mem-R^{II}S)Gsh	38.1 Assumed for mdelling (not measured)	
Hg^{2+} + Mem-$RSRO^{2-}$ = Hg(Mem-RSRO)	25.6	(Pettit and Powell, 2006)
H^+ + BAL^{2-} = $HBAL^-$	8.62	(Pettit and Powell, 2006)
$2H^+$ + BAL^{2-} = H_2BAL	19.87	(Pettit and Powell, 2006)
BAL^{2-} + Hg^{2+} = HgBAL	44.8 ± 0.45	(Coates and Jones, 1977)
BAL^{2-} + HgBAL = $HgBAL_2^{2-}$	7.11 ± 0.1	(Coates and Jones, 1977)
H^+ + $DMPS^{3-}$ = $HDMPS^{2-}$	12.38	(Pettit and Powell, 2006)
$2H^+$ + BAL^{3-} = H_2DMPS^-	21.97	(Pettit and Powell, 2006)
$DMPS^{3-}$ + Hg^{2+} = $HgDMPS^-$	43.49	(Pettit and Powell, 2006)
$2DMPS^{3-}$ + Hg^{2+} = $Hg(DMPS)_2^{4-}$	55.40	(Pettit and Powell, 2006)
HS^- + H^+ = H_2S	7.02	(Smith et al., 2004)
Hg^{2+} + $1HS^-$ = $HgHS^+$	20.01 ± 0.431	(Drott et al., 2013)
Hg^{2+} + $2HS^-$ = $HgS(HS)^-$ + $1.000H^+$	32.5 ± 0.806	(Drott et al., 2013)
Hg^{2+} + $2HS^-$ = HgS_2^{2-} + $2.000H^+$	23.2 ± 0.806	(Drott et al., 2013)

$Hg^{2+} + 2HS^{-} = Hg(HS)_2$	39.1± 0.806	(Drott et al., 2013)
β-HgS(Metacinnabar) + $H^{+} = Hg^{2+} + HS^{-}$	-36.8 ± 0.447	(Drott et al., 2013)
$Hg^{2+} + S_2O_3^{2-} = Hg(S_2O_3)_2^{2-}$	29.18	(Nyman and Salazar, 1961)
$Hg^{2+} + 3S_2O_3^{2-} = Hg(S_2O_3)_3^{4-}$	30.3	(Nyman and Salazar, 1961)
$S_2O_3^{2-} + 2H^{+} = H_2S_2O_3$	2.320	(Shock et al., 1997)
$S_2O_3^{2-} + H^{+} = HS_2O_3^{-}$	1.720	(Shock et al., 1997)
$Na^{+} + S_2O_3^{2-} = NaS_2O_3^{-}$	0.608	(Shock et al., 1997)
Mb-OB3b $^{-}$(site 1) + Hg^{2+} = Hg(Mb-OB3b)(site 1)$^{+}$	$\log K_1$= 7 ± 0.13	(Choi et al., 2006)
Hg Mb-OB3b(site 1)$^{+}$ + Mb-OB3b $^{-}$(site 2)= Hg(Mb-OB3b)(sites 1 + 2)	log K_2= 5.954 ± 0.000048	(Choi et al., 2006)

Supporting References

1. B. Stenzler, J. Gaudet, A. J. Poulain, An Anaerobic Biosensor Assay for the Detection of Mercury and Cadmium. *JoVE*, e58324 (2018).
2. V. Liem-Nguyen, U. Skyllberg, K. Nam, E. Björn, Thermodynamic stability of mercury(II) complexes formed with environmentally relevant low-molecular-mass thiols studied by competing ligand exchange and density functional theory. *Environmental Chemistry* **14**, 243-253 (2017).
3. K. J. Powell *et al.*, Chemical speciation of environmentally significant heavy metals with inorganic ligands. Part 1: The Hg2+–Cl–, OH–, CO32–, SO42–, and PO43–aqueous systems (IUPAC Technical Report). *Pure and applied chemistry* **77**, 739-800 (2005).
4. NIST. (P.J. Linstrom and W.G. Mallard, National Institute of Standards and Technology,, Gaithersburg MD, 2015).
5. R. N. Goldberg, N. Kishore, R. M. Lennen, Thermodynamic quantities for the ionization reactions of buffers. *Journal of physical and chemical reference data* **31**, 231-370 (2002).
6. Y. Song *et al.*, Thermodynamics of Hg(II) Bonding to Thiol Groups in Suwannee River Natural Organic Matter Resolved by Competitive Ligand Exchange, Hg LIII-Edge

EXAFS and 1H NMR Spectroscopy. *Environmental Science & Technology* **52**, 8292-8301 (2018).

7. Y. Song *et al.*, Toward an Internally Consistent Model for Hg(II) Chemical Speciation Calculations in Bacterium–Natural Organic Matter–Low Molecular Mass Thiol Systems. *Environmental Science & Technology* **54**, 8094-8103 (2020).

8. L. D. Pettit, K. Powell, The IUPAC stability constants database. *Chemistry international*, (2006).

9. R. L. Coates, M. M. Jones, Stability constants of the Hg2+-BAL complexes. *Journal of Inorganic and Nuclear Chemistry* **39**, 677-678 (1977).

10. R. Smith, A. Martell, R. Motekaitis, NIST standard reference database 46. *NIST Critically Selected Stability Constants of Metal Complexes Database Ver* **2**, (2004).

11. A. Drott, E. Bjorn, S. Bouchet, U. Skyllberg, Refining thermodynamic constants for mercury (II)-sulfides in equilibrium with metacinnabar at sub-micromolar aqueous sulfide concentrations. *Environmental science & technology* **47**, 4197-4203 (2013).

12. C. Nyman, T. Salazar, Complex ion formation of mercury (II) and thiosulfate ion. *Analytical Chemistry* **33**, 1467-1469 (1961).

13. E. L. Shock, D. C. Sassani, M. Willis, D. A. Sverjensky, Inorganic species in geologic fluids: correlations among standard molal thermodynamic properties of aqueous ions and hydroxide complexes. *Geochimica et Cosmochimica Acta* **61**, 907-950 (1997).

14. D. W. Choi *et al.*, Spectral and thermodynamic properties of Ag(I), Au(III), Cd(II), Co(II), Fe(III), Hg(II), Mn(II), Ni(II), Pb(II), U(IV), and Zn(II) binding by methanobactin from Methylosinus trichosporium OB3b. *Journal of Inorganic Biochemistry* **100**, 2150-2161 (2006).

Appendix E: Supporting information from chapter 7.

Iron acquisition pathways and Hg bioavailability

Authors

Benjamin R. Stenzler[1], Rui Zhang[1] and Alexandre J. Poulain[1]*†

Affiliations

[1]Biology Department, University of Ottawa, 30 Marie Curie, Ottawa, ON K1N 6N5, Canada

*Corresponding author. Email: apoulain@uottawa.ca

This PDF file includes:

Tables E1

Supporting Tables

Table E1: Raw data for Figure 7.2 (A, B, C, and D) Figure 7.3 (A, B, C, and D), and Figure 7.4(A and B), including the number of biologic replicates (n). Average Normalized Fluorescence measured as relative fluorescence units (RFU) ± 1SD at 10 hours by the Hg-Inducible biosensor (*E. coli* NEB5α harboring the pUC57merR-Pp plasmid) and the Constitutive biosensor (*E. coli* NEB5α harboring pUC19AH206-Pp plasmid). Fluorescence at 10 hours was normalized to the control (0 µM) at 10 hours for each biological replicate. [Hg] was set to 2 nM. These experiments were performed at 37 ˚C in an anaerobic exposure medium (pH 7).

Figure 7.2 A

Enterobactin (uM)	Hg-Inducible Fluorescence (RFU)	SD	n	Constitutive Fluorescence (RFU)	SD	n
0.000	1.000			1.000		
0.001	1.532	0.360	3	1.232	0.195	3
0.100	1.233	0.173	5	1.282	0.223	3
0.500	1.009	0.309	3	1.737	0.176	2
1.000	0.293	0.033	3	1.564	0.245	3
5.000	0.639	0.125	4	1.770	0.200	3

Figure 7.2 B

Desferoxamine E (uM)	Hg-Inducible Fluorescence (RFU)	SD	n	Constitutive Fluorescence (RFU)	SD	n
0.000	1.000			1.000	0.000	
0.001	0.843	0.252	5	1.142	0.005	3
0.100	0.510	0.147	5	1.271	0.245	3
0.500	0.235	0.291	5	1.223	0.233	3
1.000	0.507	0.082	4	1.464	0.312	3
5.000	0.459	0.046	3	1.125	0.098	3

Figure 7.2 C

Ferrichrome (uM)	Hg-Inducible Fluorescence (RFU)	SD	n	Constitutive Fluorescence (RFU)	SD	n
0.000	1.000			1.000	0.000	
0.001	1.095	0.256	5	1.146	0.133	3
0.100	1.069	0.548	5	0.900	0.301	3
1.000	0.930	0.309	5	1.369	0.101	3
5.000	0.834	0.391	3	1.384	0.083	3
						n

Figure 7.2 D

Citrate (uM)	Hg-Inducible Fluorescence (RFU)	SD	n	Constitutive Fluorescence (RFU)	SD	n

0.000		1.000			1.000	0.000	
0.001		1.429	0.371	3	1.187	0.048	3
0.010		1.248	0.633	6	1.259	0.098	3
0.100		1.197	0.697	6	1.340	0.068	3
1.000		1.413	0.783	6	1.324	0.078	3
5.000		1.238	0.117	3	1.320	0.075	3

Figure 7.3 A

Pyochelin (uM)	Hg-Inducible Fluorescence (RFU)	SD	n	Constitutive Fluorescence (RFU)	SD	n
0.000	1.000	0.000		1.000	0.000	
0.001	0.970	0.087	4	1.160	0.082	3
0.100	1.285	0.181	3	1.923	0.343	3
0.500	0.868	0.269	4	2.154	0.514	3
1.000	1.334	0.769	3	2.323	0.660	3
5.000	2.305	0.451	5	2.583	1.017	3

Figure 7.3 B

Desferrithiocin (uM)	Hg-Inducible Fluorescence (RFU)	SD	n	Constitutive Fluorescence (RFU)	SD	n
0.000	1.000			1.000	0.000	
0.001	0.852	0.162	3	1.126	0.203	3
0.100	1.315	0.054	3	1.318	0.145	3
1.000	2.580	0.164	3	1.491	0.153	3
5.000	0.212	0.078	4	1.851	0.104	3

Figure 7.3 C

Nicotianamine (uM)	Hg-Inducible Fluorescence (RFU)	SD	n	Constitutive Fluorescence (RFU)	SD	n
0.000	1.000	0.000		1.000	0.000	
0.001	2.210	0.549	4	1.102	0.190	3
0.010	1.358	0.504	3	1.145	0.107	3
0.100	0.545	0.132	4	1.320	0.085	3
1.000	0.229	0.190	3	1.514	0.167	3
5	0.3619	0.173	5	1.589736	0.178	3

Figure 7.3 D

Pyoverdines (uM)	Hg-Inducible Fluorescence (RFU)	SD	n	Constitutive Fluorescence (RFU)	SD	n
0.000	1.000			1.000	0.000	
0.001	0.856	0.038	3	1.294	0.295	7
0.100	0.351	0.183	3	1.104	0.498	4
0.500	0.115	0.495	5	0.584	0.515	4
1.000	0.030	0.273	3	-0.552	0.158	4
5.000	-0.531	0.414	3	-1.134	0.882	4

Figure 7.4 A

Ethylxanthate (uM)	Hg-Inducible Fluorescence (RFU)	SD	n	Constitutive Fluorescence (RFU)	SD	n
0	1.000			1.000		
0.1	1.271	0.330	5	1.050	0.063	4
1	0.360	0.158	6	0.839	0.097	7
10	0.143	0.083	4	0.983	0.065	4
100	0.213	0.044	3	0.775	0.014	3
250	0.132	0.048	4	0.646	0.100	3

Figure 7.4 B

DDTC (uM)	Hg-Inducible Fluorescence (RFU)	SD	n	Constitutive Fluorescence (RFU)	SD	n
0.000	1.000			1.000		
0.100	0.946	0.414	8	1.012	0.090	5
1.000	0.370	0.150	8	0.995	0.046	4
10.000	0.493	0.171	6	0.840	0.117	4
100.000	0.171	0.018	3	0.515	0.050	3
250.000	0.156	0.107	4	0.336	0.062	7